UNIVERSITY OF SOUTHAMPTON

Faculty of Engineering, Science & Mathematics

School of Civil and Environmental Engineering

Predictive Methods for the Fire Resistance of Single Skin and Sandwich Composite Materials

by

Philip Anthony Cutter

Thesis for the degree of Doctor of Philosophy

November 2008

UNIVERSITY OF SOUTHAMPTON

ABSTRACT

Faculty of Engineering, Science & Mathematics

School of Civil and Environmental Engineering

Doctor of Philosophy

Predictive Methods for the Fire Resistance of Single Skin and Sandwich Composite Materials

by Philip Anthony Cutter

Polymer composite materials are becoming increasingly popular in many engineering structures in the civil, aerospace, marine and automotive industries. The increased strength and stiffness to weight ratios which are possible with certain types of composites make them particularly attractive to many high performance applications such as military aircraft, offshore lifeboats and formula one racing cars.

One aspect of composite materials which is preventing more widespread use is the perceived poor performance in fire. The perception is due to the fact that organic compounds used in polymer composites are combustible. The loss of the Norwegian Navy's composite mine hunter vessel *Orkla* in 2002 to a fire did much to prevent further widespread use of such materials.

The work presented here describes the research that has been conducted into assessing and predicting the performance of single skin and sandwich composite materials subjected to fire and mechanical load. The materials that were investigated were representative of the materials used in the construction of Royal National Lifeboat Institution (RNLI) lifeboats.

A new method has been developed to assess the response both thermally and mechanically of single skin and sandwich panels subjected to combined fire and mechanical load. This has been done by the construction of a small scale fire and load testing apparatus. An empirical relationship was developed to predict the stiffness of single skin and sandwich panels during a fire and load test.

Numerical models have also been generated to predict the thermo-mechanical response of single skin and sandwich panels to fire and load. Testing of single skin and sandwich panels on the newly developed apparatus has been conducted to verify the numerical models.

The numerical models and the empirical relationship were used to predict the response of a full scale composite sandwich panel, representative of a lifeboat deck, to a standard cellulosic fire and mechanical load.

Contents

List of Figures

List of Tables

Acknowledgements

Firstly I would like to thank the Royal National Lifeboat Institution (RNLI) who provided the funding for this project as part of the Advanced Technology Partnership (ATP). It has been a great experience to work for such a worthy organisation that put so much back into the world of engineering and technology as well as carrying out their invaluable role in marine search and rescue.

I am particularly indebted to my supervisory team throughout this work. Firstly Professor Ajit Shenoi, for his support, guidance and motivation and for making me feel very welcome within the Fluid Structure Interaction Research Group. To Dr Holly Phillips of the RNLI who has always been at the end of the phone when needed to offer advice and motivation. To Professor Stuart Moy who has provided me with thorough and useful feedback on all the work I have completed. Finally I would like to thank Professor Bob Cripps for helping start this research project and for his guidance in the early stages.

I also would like to thank my colleagues who helped with the initial design and construction of the apparatus used in this research when it was an undergraduate design project; Nikolas Mitsotakis, Gudmundur Hilmarsson and Adrian Gillitt. There have been various French undergraduate students who have provided me with vital man power when needed in the laboratory and their help has also been very much appreciated.

I owe a great deal of debt to the technical staff at the University who have helped me out of many seemingly insurmountable technical problems as well as putting up with me burning bits of lifeboats on a regular basis. To Erik Roszkowiak for his constant help, support and inspiration all matters technical. To James Rabbetts and Clive Stafford for their frequent help in all things electrical. And to all the staff in the EDMC who have helped with this project.

I am grateful to the research staff within the Fluid Structure Interaction research group for their help and the support in the office and the laboratory, in particular I would like to thank Steve, James and Ajaya. Also thanks to Janice for her support and in particular her help when my experiments seemed in danger of being halted. Also thanks to all the

postgrads in the department for making me feel welcome and listening to my frequent tales of woe.

Finally I would like to thank my family for their support, reassurance and motivation during my time here. I am also indebted to Becks for her loving support and understanding and for making me switch off when not at work.

Abbreviations

FRP	Fibre reinforced plastic
IMO	International Maritime Organization
CSM	Chopped strand mat
FTP	Fire Test Procedures
MCA	Maritime and Coastguard Agency
WR	Woven rovings
TGA	Thermogravimetric analysis
RNoN	Royal Navy of Norway
RNLI	Royal National Lifeboat Institution
PVC	Polyvinyl chloride

1 Introduction

Polymer composite materials are becoming increasingly popular in many engineering structures in the civil, aerospace, marine and automotive industries. The increased strength and stiffness to weight ratios which are possible with certain types of composites make them particularly attractive to many high performance applications such as military aircraft, offshore lifeboats and formula one racing cars. In the marine sector composites have been used extensively in the small boat market where it is rare to find a modern boat that is not constructed from a glass reinforced plastic of some variety. The excellent corrosion properties coupled with the light weight are what drives the selection. There is also a huge potential for composites to be used in many commercial transport applications as the economics of using such light weight materials can lead to reduced fuel costs. This could outweigh the potentially higher build costs in some applications especially in the current climate of rising oil prices. There is also a growing pressure to provide greener solutions to many current modes of transport and decreasing weight by careful material selection is a logical step in the right direction.

One aspect of composite materials which is preventing more widespread use is the perceived poor performance in fire. The perception is due to the fact that organic compounds used in polymer composites are combustible. The loss of the Norwegian Navy's composite mine hunter vessel *Orkla* in 2002 [RNoN TEG Report 2003] to a fire did much to prevent further widespread use of such materials. In fact in the case of the *Orkla* the reasons given for the spread of the fire in the accident report [RNoN TEG Report 2003] were not principally down to the structural materials used.

This perceived weakness of composite materials in fire is largely down to a lack of understanding about the materials in question. Thick single skin composites can in fact be very good insulators at high temperatures. The work done by the research groups in Newcastle University by Gibson et al. [Gibson, Wu et al. 1995; Looyeh, Bettess et al. 1997; Dodds, Gibson et al. 2000; Gibson, Wright et al. 2004; Gibson 2005; Mouritz, Mathys et al. 2005] and in Manchester University by Davies et al. [Dodds, Gibson et al. 2000; Davies 2001; Davies, Wang et al. 2005] has done much to help increase the level of understanding in this complex subject area.

When ‘performance in fire’ is mentioned it must be made clear to what this refers as there are many aspects to how materials react to fire that are relevant in different applications. In this thesis the properties have been studied in two different categories, which are highly coupled. First, the effects of the fire on the temperature of the given materials, which is highly important when relating to particular applications. For example in a building with a fire, a wall that is highly thermally conductive could conduct enough heat through it to set off a fire in an adjacent room. Similarly in a boat with a fire below a deck, a deck material that is a good thermal conductor could be too hot for passengers to walk across.

The second property that is of interest is the strength and stiffness of materials subjected to fire. A structure could contain a fire successfully and be sufficiently insulating, but if the structure is load bearing then there will be a danger of collapse as the stiffness and strength decreases, as would be expected with most materials at elevated temperatures.

The motivation for the research reported in this thesis has come from the Royal National Lifeboat Institution (RNLI). This is a charity that provides a search and rescue service up to 100 nautical miles from the coast of the United Kingdom and Republic of Ireland. The RNLI operates a series of all weather lifeboats; Figure 1.1 shows a Severn class lifeboat in the kind of conditions which the vessels are required to operate. Since the Arun class lifeboat was developed in 1971 using glass reinforced plastics (GRP) the RNLI lifeboats have been constructed from polymer composite materials using a combination of single skin and sandwich type constructions [Hudson, Hicks et al. 1993].

Figure 1.1: Severn class lifeboat in rough seas

Materials for use in marine vessels have to pass specific standards set by the industry's governing bodies. In terms of the performance in fire, it is necessary to go through what can be an expensive and time-consuming test programme. This has the effect of limiting designers in their choice of materials to those that have already passed the tests. There is therefore a need to be able to predict the fire performance of materials in these tests from small scale, low cost testing and numerical modelling.

The aim of much of the research discussed in this thesis is to reach a point where just the specific properties of the materials need to be measured and input into a numerical model in order to predict the performance in one of the test standards. This would give designers the chance of experimenting with different materials in a more economical manner.

Looking further ahead it should be possible to use these numerical models to perform more comprehensive risk assessments of structures in given fire situations. This will require computational fluid dynamic modelling of fire in conjunction with multi-dimensional fire response models.

The aim of this thesis is to develop a method for assessing the thermal and mechanical effects of fire on single skin and sandwich composite structures.

The specific objectives are:

1. To understand the behaviour of single skin and sandwich structures under fire and mechanical loading.
2. To outline approaches to allow for scaling of experimental results from laboratory bench to full scale panels.
3. To develop predictive models for predicting the behaviour of single skin and sandwich panels under fire and mechanical loading.

2 Literature Review

2.1 Introduction

This chapter highlights the current state of the art regarding composite materials and fire. It explains why this research is necessary, highlighting recent fire accidents involving composite structures. An overview is given of the current state of knowledge regarding the modelling and testing of composites in fire and the areas requiring further work are highlighted.

2.2 Fire Mechanics

For a fire to occur three elements are needed to combine in sufficient quantities; namely fuel, oxygen and energy. The fire triangle shown in Figure 2.1 as described by Quintiere [1998] displays the interaction between the elements.

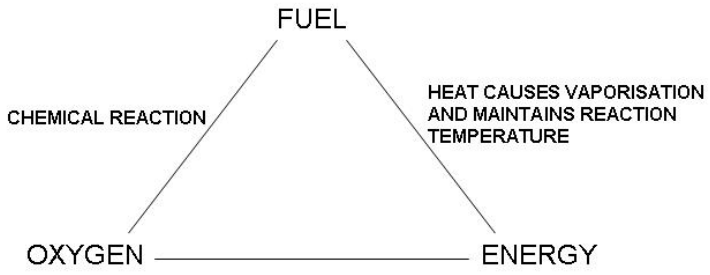

Figure 2.1: The fire triangle [Quintiere 1998]

The fuel combines with the oxygen in a chemical reaction to produce energy. The energy heats the fuel, which aids the combustion process further. If one of the elements can be removed then the fire will be put out.

The development of a fire will be dependent on the elements described above, which themselves will be a product of many different factors. There is however an accepted generalised model for the development of a fire in an enclosed volume or compartment. Drysdale [1999] indicates the following three stages in the development of a ‘compartment fire’:

Stage 1 the growth or pre flashover stage in which the average compartment temperature is relatively low and the fire is localised in the vicinity of its origin;

Stage 2 the fully developed or flashover fire, during which all combustible items in the compartment are involved and flames appear to fill the entire volume; and

Stage 3 the decay period, often identified as that stage of the fire after the average temperature has fallen to 80% of its peak value.

Figure 2.2 shows the heat release rate of a typical compartment fire as a function of time. The average temperature of the compartment is often plotted against time as in Davies [2001] with a similar form.

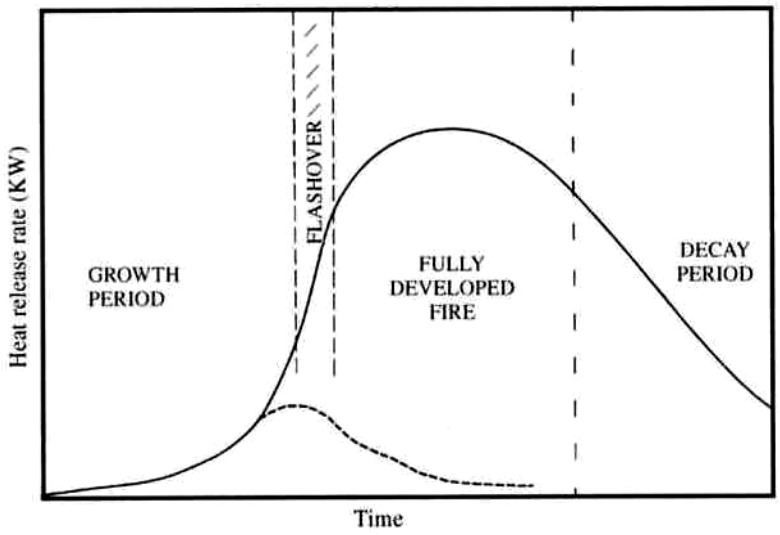

Figure 2.2: The course of a well- ventilated compartment fire expressed as the rate of heat release as a function of time. The broken line represents depletion of fuel before flashover has occurred [Drysdale 1999].

2.3 Fire in Marine Structures

Uncontrolled fire in enclosed spaces can have devastating effects on structures, often resulting in costly damage and sometimes even fatalities. Recent fires such as that aboard the Star Princess cruise ship in March 2006, which resulted in one fatality, have again shown the need to keep fire safety in mind in every aspect of design and operation.

An area of high fire risk aboard a ship is the engine room, due to the presence of inflammable liquids, a search through the Marine Accident Investigation Branch (MAIB) reports [MAIB 2000a; MAIB 2000b; MAIB 2000c; MAIB 2003] show some recent instances of such fires on merchant vessels. These fires had all been started by fuel or oil leaks resulting from seal failures. The ignition of the fuel had been started by the leaking fluids coming into contact with hot surfaces such as exhaust manifolds. In each of the cases described, fires were eventually contained and none were fatal. It is also worth noting that no structural damage was caused by any of the fires and that none of the vessels were reported to be constructed from composites.

There have however been numerous fatalities due to fires, the Scandinavian Star disaster in 1992 was one of the worst in recent times where a deliberately started fire caused the loss of 158 lives.

2.4 The Orkla Disaster

The Royal Navy of Norway composite mine hunter "Orkla" fire in 2002 did much to publicise the perceived weaknesses of composite boats. The vessel was largely constructed using sandwich materials with PVC cores and glass reinforced plastic skins. The fire, which started due to an oil leak resulting from a shaft failure, burnt for 24 hours before the boat capsized. The official report into the accident [RNoN TEG Report 2003] and Høyning [2003] give an insight into the causes of the fire, this is summarised in Appendix A.1.

The causes of the fire according to the report [RNoN TEG Report 2003] are numerous and involve design flaws, inadequate training, lack of risk assessments and a poor culture of safety within the organisation.

The fire and eventual loss of the Orkla cannot be put down to one single cause. The use of composite materials alone was not to blame for the loss of the vessel. The root cause of the fire was a general lack of regard for safety in all stages of design and operation within the organisation.

It can be concluded from the report that composite boats are not intrinsically unsafe and should be able to withstand a fire given the correct preventative measures. Careful risk

assessment and a culture of reporting problems and acting on them is needed to ensure the safety of any vessel. The fact that the Orkla was a military vessel meant that it did not have to comply with the IMO fire regulations. If it had followed these regulations it could have reduced the severity of the fire and prevented the loss of the vessel.

2.5 Fire Response Modelling

2.5.1 Composites in Fire Phenomena

In the context of this research composite materials refer to:

i. single skin fibre reinforced plastic (FRP) and
ii. sandwich structures with polymer cores and FRP skins.

Single skin composites react to fire in a manner similar to that of a common natural composite; wood. A thick (>10mm) piece of polymer composite material will slowly char as it is heated to high temperatures(>300°C). The volatile gasses emitted from a material will aid the combustion process on the surface of the material.

Initially, during heating, pure conduction will occur through a composite material. The resin then undergoes an instantaneous charring reaction, known as pyrolysis, at around 200°C-400°C depending on the material. This reaction produces a carbonaceous char, which is less thermally conductive than the original material. Volatile gases are also produced by the reaction, which are initially trapped within the composite due to the low porosity. This can cause a degree of expansion within the resin. As the pressure of the volatiles increase and the porosity decreases they begin to flow back through the material towards the heat source. This has a cooling effect on the composite as a whole and results in a contraction of the composite. The layer of char progresses through the thickness of the material at a decreasing rate. This is due to the endothermic nature of the reaction, the cooling provided by the volatile gasses and the fact that the char material is less thermally conductive than the virgin composite. At temperatures of over 1000°C the char can react with the silica in glass fibres to decompose further and release more volatiles. Eventually the char material will be totally consumed, leaving just the fibres, which melt at around 1400°C (glass). The fibres aid in holding the material together but as mentioned in Gibson et al. [1995] the type of fibre used has little overall affect on the thermal performance of a composite in fire. In terms of resisting the flow of heat through the thickness of the material, single skin composites

around 10mm thick or more perform exceptionally well when compared with other commonly used engineering materials. This is due to the low conductivity of the virgin material, the even lower conductivity of the char material and the endothermic pyrolysis reaction. The temperatures at which all of the above processes occur are highly dependent on heating rate, with higher heating rates causing the reactions to occur at higher temperatures.

The strength of single skin composites is strongly related to the temperature within the laminate. By the time the pyrolysis reaction has occurred the strength of the composite in that region will have negligible strength and stiffness.

In sandwich structures the skins will react to high temperature in the same manner as single skin composites. Foam cores have low thermal conductivities and the large (>20mm) thicknesses typically used mean that sandwich structures tend to be very good insulators at lower temperatures. Little work has been done on the performance of foams at elevated temperatures, but there is a small amount of expansion at temperatures of around 100°C before decomposition occurs between 150°C and 300°C [Grenier, Dembsey et al. 1998]. The decomposition of the foam causes it to recede and the adhesion between the faces is then lost [Davies 1995a; 1995b; Grenier, Dembsey et al. 1998]. The mechanical performance of a sandwich structure exposed to fire is very much reliant on the performance of the fire-exposed face. Once a face of a sandwich structure loses its strength then the mechanical advantage gained by the sandwich structure is lost.

2.6 Fire Resistance Modelling

The first paper of great significance in this area was published by Henderson et al. [1985] and used the principles of a model proposed by Bamford et al. [1946] and applied them to a phenolic/glass composite. The model predicted the heat transfer using the one dimensional transient heat conduction equation with extra terms to account for the decomposition reaction and the cooling effect of the decomposition gasses flowing back through the charred material.

The decomposition reaction was modelled using a n^{th} order Arrhenius equation and temperature and mass dependant thermal material properties were used. These material

properties were calculated in previous works by the same authors [Henderson, Tant et al. 1981; 1982; 1983]. The decomposition term also took account of carbon silica reactions at higher temperatures and the equations were solved using a finite difference method. The boundary conditions used were a prescribed heat flux on one side and a fully insulated unexposed side. In Henderson and Wiecek [1987] an attempt was made to model the thermo-chemical expansion as well as the expansion due to the trapped pyrolysis gasses inside decomposing composites.

Gibson et al. [1995] developed a model similar to the model presented by Henderson et al. [1985]. Constant material properties were used with a first order decomposition equation to model the pyrolysis reaction. The model was verified by comparison with furnace testing of glass/polyester panels from 10mm-22mm thick under the hydrocarbon fire curve [BS476-20 1987]. The hot face temperature was used as the input condition to the model and on the cold face free convection was assumed to the surrounding air. It was found however that in the absence of forced air currents the heat transfer coefficient from the cold face could be modelled as being zero. The results presented indicate that the model is underestimating the temperature profile within the composites in general. It is also evident that the predictions for the WR panels are much closer to the experimental results than in the CSM panels.

Davies and Wang [1996] used a finite difference model based on the Henderson [1985] approach. They found that the term in the general equation, which modelled the volatile gas convection, could be neglected. It was stated that the cooling effect of the decomposition gas was negligible when compared to the powerful incident heat flux. In their furnace testing on glass/polyester composites using hydrocarbon and cellulosic fire curves [BS476-20 1987] they found a much greater degree of variation than Henderson et al. [1985] had reported. This was said to be due to the very controlled testing method used by Henderson et al. as well as the low heat flux and the particular material used. Another key factor could be the radiant heat source used by Henderson et al., which one would expect to deliver a much more constant thermal load than a flame.

Looyeh et al. [1998] present a model for the two-dimensional thermal response of composite panels. The same principles that were applied to the Looyeh and Bettes model [1998] are used for the geometry shown in Figure 2.3.

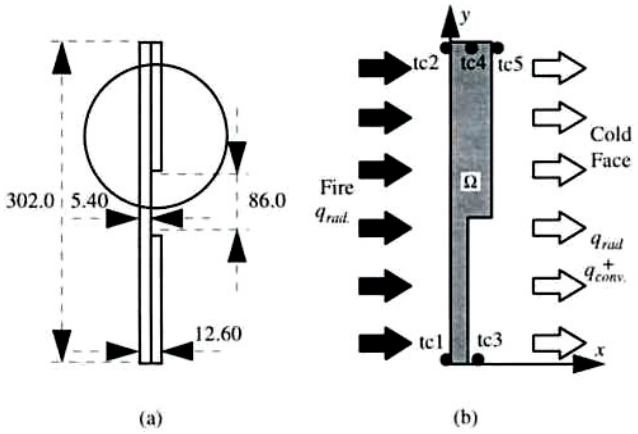

Figure 2.3: 2-D heat transfer model for stepped single skin panel. source [Looyeh, Bettes et al. 1998]

In the image on the left the whole structure is shown and the image on the right shows the direction of heat flow and the location of the thermocouples. The temperature variations are modelled in the through thickness direction, x and longitudinal direction, y and it is assumed that there is no temperature variation in the transverse direction, z. It is also assumed that the decomposition gas diffuses through the composite in the x direction only. The panel is exposed to a hydrocarbon curve on one side and ambient conditions on the cold face, which is stepped, as shown in Figure 2.3. Different temperature dependent material properties are used for heat transfer in the x and y directions for the glass/polyester composite. The results from the two-dimensional model and a one-dimensional model were compared. It was stated that the average difference from the recorded temperatures during experimentation and the predictions was 22°C for the two-dimensional model, which is very similar to the quoted values from Looyeh and Bettes [1998]. The difference between the two dimensional model and the one-dimensional model was reported to be 8.6°C. This shows that temperature gradients are larger in the through thickness direction than the longitudinal direction. It must be borne in mind that the values of average temperature difference are dependent on the position of the thermocouples. Figure 2.3 shows the position of the thermocouples (tc1 to tc5) but do not seem to indicate that any measurement was taken in the region of the step, which is the region of most interest.

Thermal response of sandwich panels to fire seems to have started with Davies et al. [1995a; 1995b] where a numerical model is reported upon but details are not given. The results of a series of tests on sandwich materials with GRP faces and a range of cores are reported. The fire resistance of the cores increases with thickness as would be

expected but it is made clear that this does not increase the safety of a structure. The strength of a sandwich structure will be effectively lost once one of the faces has fully charred. Results of a furnace test on a sandwich panel with GRP faces and a Vermiculux (calcium silicate) core are given. It is shown that the predictions match the measured cold face temperatures well during a test for over two hours. The Vermiculux core does not however, degrade and it is expected that since the core is 60 mm thick and the faces are thin that the problem is a relatively simple one.

Looyeh et al. [2001] present a one-dimensional model for the heat transfer through a sandwich panel with GRP faces and a Vermiculux core. The work concentrates, in particular, on the interface between the faces and the core. Voids, which can occur at the interface due to poor processing, can cause areas of relative insulation due to the low thermal conductivity of the trapped gasses. The effect of the voids is accounted for by calculating the ratio of the total area of the panel to the void area. Knowledge of the thermal conductivity of the trapped gas is also needed. It is expected that these values would be difficult to measure or predict. The authors claim that the fire resistance of the panel was predicted to within 17 minutes without taking into account the effect of the voids and that taking account of the voids increased the precision further.

Krysl et al. [2004] produced a one-dimensional finite element model to predict the heat transfer through composite sandwich panels. The model assumes a decomposing fire-exposed face and a non-decomposing core and unexposed face. The model is validated using results from Wu et al. [1993] for a single skin composite. It is stated that this could represent a sandwich panel with a lightweight core, but without modelling the decomposition of the core it is unclear how this could be the case. Lightweight cores are known to decompose at relatively low temperatures [1995a; 1995b; Davies 2001] and the change in properties would have a significant affect on the sandwich as a whole. An element of this paper, which will aid other investigators in subsequent models, is the parametric study of input variables. This work was followed by others in a similar area [Ramroth, Krysl et al. 2005; Key and Lua 2006] who looked at the relative affects of the different material properties as inputs to the numerical models and is discussed further in section 2.8.3 Determination of Material Properties.

The boundary conditions applied to the models discussed above have a significant bearing on the outputs generated. On the fire exposed boundary some authors have

stated that the hot face temperature was taken as the input to the model. The method of measurement of the hot face temperature was not discussed in any of the literature and is an area that should be clarified since the adhesion of thermocouples to composites at high temperatures is very difficult to achieve [Davies, Dewhurst et al. 2000]. In other cases [Henderson, Wiebelt et al. 1985] a heat flux meter has been used to measure the incident heat flux experienced by the samples during heating.

On the unexposed surface of the composites there have been two approaches in the modelling of the boundary conditions. The first is to assume a fully insulated boundary where no heat escapes. This is the simplest method and has been used by a number of authors [Henderson, Wiebelt et al. 1985; Henderson and Wiecek 1987; Gibson, Wright et al. 2004]. As previously mentioned Gibson et al. [1995] state that the heat transfer coefficient has very little influence over the results when there are no forced air currents over the cold surface. It is generally accepted that there are two processes taking place however, namely convection and radiation. Looyeh and Bettes [Looyeh and Bettes 1998] simplify this by assuming that radiation heat transfer is an equivalent convection boundary condition where the non-linearity is represented by a temperature-dependant convection coefficient. It is unclear from any the models reported upon as to which method proves the most effective. One method that has not been mentioned in any of the literature is the approach of measuring the unexposed surface temperature. This is discussed further in Section 2.8.2 Experimental Test Methods.

The combustion of volatile gasses released at the fire exposed surface of composites is an area that has not been mentioned thus far. None of the models discussed above have accounted for this and it is claimed that in small furnace tests the heat created by this effect is small when compared to the high incident heat flux [Davies and Wang 1996]. In large scale tests and in an actual fire the contribution could be significant especially after the removal of the heat source. The heat release rate is the single most important fire reaction property of combustible materials according to certain authors [Babrauskas and Peacock 1992; Mouritz, Mathys et al. 2006].

Table 2.1 shows the evolution of the numerical models to predict heat transfer through degrading composites. The general equation, which is now common among all models published in the last 10 years, has not changed since it was proposed by Henderson et al. [1985].

The hydrocarbon and cellulosic curves refer to temperature time curves used in standard fire resistance tests and are described in BS476 Fire tests on building materials and structures [BS476-20 1987].

Author	General equation	Material	Modelled heat source	Dimensions	Material properties
[Bamford, Crank et al. 1946]	$K\frac{\partial^2 T}{\partial x^2} - q\frac{\partial m}{\partial t} = C_p \rho \frac{\partial T}{\partial t}$	Wood	Non-standard temperature-time curve approximately 545°C	1D	Constant
[Pering, Farrell et al. 1980]	$\frac{\partial \rho C_p T}{\partial t} = \frac{\partial}{\partial x} k \frac{\partial T}{\partial x} + \dot{m} L$	Graphite/ epoxy	Const surface temps 540°C, 760°C, 980°C	1D	Constant
[Springer 1984]	$\frac{\partial \left(\rho_v C_p T\right)}{\partial t} = \frac{\partial}{\partial x} k_x \frac{\partial T}{\partial x} + \frac{\partial}{\partial y} k_y \frac{\partial T}{\partial y} + \frac{\partial \rho_c}{\partial t} Q$	Graphite/ epoxy & Wood	Const surface temps 540°C, 760°C, 980°C	2D	Constant
[Henderson, Wiebelt et al. 1985]	$\rho C_p \frac{\partial T}{\partial t} = k\frac{\partial^2 T}{\partial x^2} - \dot{m}_g C_{pg} \frac{\partial T}{\partial x} - \frac{\partial \rho}{\partial t}\left(Q + h - h_g\right)$	Glass/ phenolic	279.7kW/m^2	1D	TD
[Chen, Sun et al. 1985]	$\rho C_p \frac{\partial T}{\partial t} = k\frac{\partial^2 T}{\partial \overline{z}'^2} - \rho C_p \frac{\partial T}{\partial \overline{z}'} \frac{\partial \overline{z}_b}{dt}$	Graphite/ epoxy	800kW/m^2- 24500kW/m^2	1D	TD
[Fanucci 1987]	Not reported	Kevlar graphite/ epoxy	833kW/m^2- 4186 kW/m^2	1D	TD
[McManus and Springer 1992]	$\rho C_p \frac{\partial T}{\partial t} = k\frac{\partial^2 T}{\partial x^2} - \dot{m}_g C_{pg} \frac{\partial T}{\partial x} - \frac{\partial \rho}{\partial t}\left(Q + h - h_g\right)$	Carbon/ phenolic	600kW/m^2	1D	TD

[Gibson, Wu et al. 1995]	$\rho C_p \frac{\partial T}{\partial t} = k \frac{\partial^2 T}{\partial x^2} - \dot{m}_g C_{pg} \frac{\partial T}{\partial x} - \frac{\partial \rho}{\partial t}\left(Q + h - h_g\right)$	Glass/ polyester	Hydrocarbon curve	1D	Constant
[Davies and Wang 1996]	$\frac{\partial}{\partial t}(\rho h) = \frac{\partial}{\partial x}\left(k \frac{\partial T}{\partial x}\right) - \frac{\partial}{\partial x}\left(\dot{m}_g h_g\right) - Q \frac{\partial \rho}{\partial t}$	Glass/ polyester	Hydrocarbon and cellulosic curve	1D	TD
[Looyeh, Bettess et al. 1997]	$\rho C_p \frac{\partial T}{\partial t} = k \frac{\partial^2 T}{\partial x^2} - \dot{m}_g C_{pg} \frac{\partial T}{\partial x} - \frac{\partial \rho}{\partial t}\left(Q + h - h_g\right)$	Glass/ polyester	Hydrocarbon curve	1D	Constant
[Looyeh, Bettes et al. 1998]	$\rho C_p \frac{\partial T}{\partial t} = k_x \frac{\partial^2 T}{\partial x^2} + k_y \frac{\partial^2 T}{\partial x^2} - \dot{m}_g C_{pg} \frac{\partial T}{\partial x} - \frac{\partial \rho}{\partial t}\left(Q + h - h_g\right)$	Glass/ polyester	Cellulosic curve	2D	TD
[Looyeh and Bettes 1998]	$\rho C_p \frac{\partial T}{\partial t} = k \frac{\partial^2 T}{\partial x^2} - \dot{m}_g C_{pg} \frac{\partial T}{\partial x} - \frac{\partial \rho}{\partial t}\left(Q + h - h_g\right)$	Glass/ polyester	Hydrocarbon curve	1D	TD
[Dodds, Gibson et al. 2000]	$\rho C_p \frac{\partial T}{\partial t} = k \frac{\partial^2 T}{\partial x^2} - \dot{m}_g C_{pg} \frac{\partial T}{\partial x} - \frac{\partial \rho}{\partial t}\left(Q + h - h_g\right)$	Glass/ polyester, glass/epoxy, glass/ phenolic	Hydrocarbon curve	1D	Constant
[Krysl, Ramroth et al. 2004]	$\rho C_p \frac{\partial T}{\partial t} = k \frac{\partial^2 T}{\partial x^2} - \dot{m}_g C_{pg} \frac{\partial T}{\partial x} - \frac{\partial \rho}{\partial t}\left(Q + h - h_g\right)$	Glass/ polyester + sandwich	Hydrocarbon curve	1D	Constant

Table 2.1: Numerical models to predict the heat transfer through fire exposed composites. TD refers to temperature dependent properties.

A range of different single skin materials have been tested in each of the different publications and seem to behave in a similar manner. A number of the more recent models [Looyeh, Bettess et al. 1997; Looyeh and Bettes 1998; Krysl, Ramroth et al. 2004] have all been verified using the same experimental data from Wu et al. [1993]. Whilst this is an economical method to verify improvements in the numerical models it does not necessarily create a comprehensive proof of the predictions.

Most of the models have concentrated on predicting the response during a hydrocarbon fire or at heat fluxes that correspond to similar temperatures. This is a standard test for materials to be used in offshore applications and is a much more severe temperature curve than specified for buildings and maritime applications. Only constant heat flux and smooth temperature curves have been reported on and it remains to be seen whether the models can predict the response during real fires where the temperatures would be expected to fluctuate.

Only one model has been published which takes into account and verifies two-dimensional heat transfer [Looyeh, Bettes et al. 1998]. The particular application in this instance was a relatively simple case and there is scope for much more work to be done in this area.

Many of the authors mentioned above have commented on the lack of accurate material properties as the main source of error within the models. Manufacturers do not tend to publish data on the thermal properties of their materials above certain temperatures and consequently testing needs to be carried out in order to calculate the properties of each different resin.

2.7 Thermo- Mechanical Modelling

The aims of the thermo-mechanical modelling techniques are to predict the change in strength and stiffness of a structure exposed to a given fire source and the post fire strength of a structure.

Research into the effects on the mechanical properties of composites exposed to high temperature and fire has been reported since the early 1980s. Pering et al. [1980] used

tensile and 3 point bending tests to measure the change in strength and modulus of samples which had been subjected to fire. They found that even after very short fire exposure times, 15-30 seconds, all shear strength was lost in the 2-4mm thick samples and after 30-60 seconds all tensile strength was lost. A correlation was found between the relative mass loss and the ultimate tensile strength of the samples. For the ultimate shear strength tests, failure was related to the thickness of the layer in which 5% of the mass had volatized. Both the thickness of the char layer and the mass loss could be predicted using the thermal model for given fire exposure times. Whilst the data showed a large degree of scatter it was clear those trends were present and further work needed to be done in acquiring more accurate material properties.

In Chen et al. [1985] tensile tests were performed on graphite/epoxy laminates whilst being heated by irradiation. The rectangular specimens were subjected to an intensive heat source over a circular region in the centre of the specimen. A finite element model was created of the sample and the moduli of the plies were related to the temperature in the circular region. The relationship was derived from knowledge of the glass transition temperature of the epoxy and the moduli of the fibres at elevated temperatures. The temperature dependant strength was taken from open literature for temperatures up to 200°C and was then assumed to decrease linearly to zero at the temperature at which the resin was completely burnt out. The predictions of the temperatures within the sample were combined with the finite element model to predict failure times at various temperatures. The model was said to slightly underestimate the failure times, a phenomenon that was due to the fibres running in the load-bearing direction still retaining some strength. In Griffis et al. [1986] the same experimental method as Chen et al. [1985] was adopted. A finite element model of the test sample was created and the failure of the sample was predicted using two different methods; maximum stress criterion and Tsai-Wu theory [Tsai and Hahn 1980]. The maximum stress criterion states that lamina failure occurs when the stresses along the material axes exceed the prescribed critical temperature-dependant strengths. The thermal model proposed is linked to the strength and modulus of each lamina through use of temperature dependant strength and moduli relationships taken from other sources. It was found that in general the maximum stress criterion predictions were closer to the experimental results than the Tsai-Wu method. The predictions in general underestimated the failure times, which could be due to the

fibres retaining strength after the resin had been depleted to some extent. The authors gave the following possible explanations for this difference in results; firstly the accuracy of the temperature predictions through the samples, the lack of accurate temperature dependant strength properties and lastly the limitation of the classical plate theory to deal with the non-linear in plane strain.

Both Griffis et al. [1986] and Chen et al. [1985] used very intensive heat sources in their testing programmes and it is not necessarily representative of the temperatures a structure that would be subjected to during a compartment fire.

Dao and Asaro [1999] used a master degradation curve as shown in Figure 2.4 to relate the strength and modulus of a laminate to the temperature at certain points through the thickness.

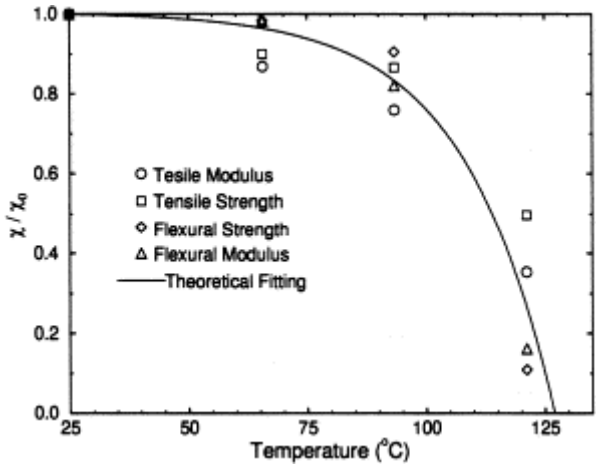

Figure 2.4: Master degradation curve, X and X_o represent the properties shown on the graph as they depend on temperature and their initial state respectively [Dao and Asaro 1999]

The overall modulus and strength of the laminate was then calculated by a rule of mixtures approach. The testing was conducted at relatively low temperatures, with the exposed face of the panels reaching 100°C after one hour. The thermal model used to predict the temperature profile is the one dimensional transient heat conduction equation, without any terms to model the effects of pyrolysis. The loading used was compressive as this was expected to be the worst case scenario for the failure of the samples. The ultimate strength was predicted using the Euler critical buckling load and the modulus value calculated using the rule of mixtures approach.

Mouritz and Mathys [1999] developed a technique whereby the length of time and intensity of heating was related to the thickness of the char layer that develops within the composite. The mechanical properties were then modelled as if the composite was a bi-layer material such that the uncharred layer had the properties of the virgin material and the charred layer had properties that could be determined by tests on fully charred samples. In this instance it was the post-fire strength that was being assessed.

In Mouritz and Gardiner [2002] a two layer modelling approach was adapted to look at the compressive properties of sandwich composites. The first proposed model was used to determine the core shear failure. In this model it was assumed that the charred layer had no compressive stiffness and the structure was modelled as having skins of unequal thickness. It was also assumed that the fire damage was confined to the exposed skin and had no affect on the core material. For failure due to global buckling three instances were covered (i) fire damage restricted to one face, (ii) fire damage occurs through one skin and into the core and (iii) fire damage occurs through one skin and core and extends partway into the other face skin. They found that the assumption that any charred region has zero mechanical properties generally agreed well with the test results except in the case where a phenolic foam core was used. In this instance the core was reported to retain some mechanical properties after charring.

Gibson et al. [2004] looked at the post fire mechanical properties as well as those of single skin composites during a fire. Having performed a series of experiments, involving tensile and compressive testing of coupon samples exposed to fire, the authors produced an empirical model to predict the changes in strength.

They found that the 'two-layer' model proposed by Mouritz and Mathys [1999] gave failure times longer than the measured times when samples were being loaded during a fire. The method they then proposed was to assume that the boundary layer between depleted resin with zero mechanical properties and the uncharred resin with virgin properties occurred at a temperature of 170^{o}C. This was said to be the case for a range of thermosetting resin systems. This prediction however was only true for the case of

compressive loading, in tensile loading the predictions underestimated the failure times as the fibres were still able to carry load after the resin had degraded.

Asaro et al. [2005] extend the theory from their earlier work [Dao and Asaro 1999] using the same temperature degradation curve in a finite element model. The model was stated to be generic and applicable to sandwich and single skin composites in any loading condition. Experimental verification is now needed for a range of thermal and mechanical loading situations.

Feih et al [2005] proposed two separate methods for determining the failure times of composite samples under tension and compression. A series of tests were conducted to ASTM 3039 to determine the effects of temperature on Young's modulus and failure strength. This produced a temperature-dependant relationship for tensile and compressive strengths. It was found that the tensile strengths were an order of magnitude higher than the compressive strengths for a given heat flux and normalised load. Tensile testing was also conducted on dry glass fibres during exposure to a heat flux of 50 kW/m^2. It was found the failure times were very similar to the laminates, which shows that failure can occur after pyrolysis of the matrix and is dependent on the softening of the fibres to a large extent.

In compression the following relationship was given to model the strength at any temperature:

$$\sigma_c(T) = \left[\frac{\sigma_0 + \sigma_R}{2} - \frac{\sigma_0 - \sigma_R}{2} \tanh\left(k\left(T - T_k\right)\right) \right] R(T) \qquad (2.1)$$

Where:

σ_0 = compressive failure stress of the laminate at room temperature, (Pa)

σ_R = minimum failure stress at elevated temperature, (Pa)

T = temperature, (K)

T_k = temperature at which composite strength begins to decline (K)

k = material constant.

The values were found by curve fitting to the temperature dependant strength relationship. R is a scaling function to account for the normalised mass loss during

pyrolysis and is a value between 0 and 1. The residual strength was calculated at individual points throughout the laminate using Equation (2.1) and the bulk strength was determined by integration of these values. Thermogravimetric analysis (TGA) data was used to calculate the value of R using two different methods. The first method was to conduct the TGA tests in air to account for the processes which occur on and near the surface of the composite and the second method was to conduct the tests in an atmosphere of nitrogen to account for the processes which occur deeper inside the composite. From these two results a curve for a hypothetical air / nitrogen mix was extrapolated. It was found that relating the value of R to data from the air / nitrogen mix produced the best fit to the experimental data.

For the prediction of tensile strengths, the two layer method proposed by Mouritz and Mathys [2001] was used. In order to determine the instantaneous thickness of the layer with zero mechanical properties four different temperatures were tried:

i. Heat distortion temperature (105^{o}C)
ii. Glass transition temperature (118^{o}C)
iii. Decomposition start temperature (350^{o}C)
iv. Decomposition end temperature (450^{o}C)

It was found that the experimental results fell in between the predictions for the decomposition start temperature and the decomposition end temperatures. The prediction did however underestimate the times to failure even using the decomposition end temperature for low tensile stresses.

Table 2.2 gives an overview of the models that have been published which aim to predict the failure or loss of stiffness of composites exposed to fire or high temperature.

From the table it can be seen that a wide range of single skin composites have been tested and used to verify the range of models proposed. Also, a wide range of heat sources have been used in the testing. The form of loading employed has solely involved the use of coupon samples in simple tensile, compressive or bending tests. There has been no reported analysis of more complex loading scenarios. Looking at

the strength analysis it is clear that no generally accepted method has evolved to link the thermal and mechanical models. It is also evident, looking at Table 2.2, that there has been no testing of sandwich composites during fire and little using different core materials.

In the collected papers of Mouritz et al. [Mouritz and Mathys 1999; Mouritz and Mathys 2001; Mouritz and Gardiner 2002; Mouritz 2003] a simple method has been created and tested for a wide range of materials and conditions. The basis of that method seems a logical way of assessing the strength and also provides a means for assessing the strength of full-scale structures with fire damage.

The method used by Feih et al. [2005] combines the mass loss and temperature dependence of strength. However one possible drawback with this method is the use of two different models to predict the compressive and tensile strength. This may be difficult to implement on structures where both tensile and compressive loads are in action.

The crucial aspect of thermo-mechanical modelling is the link between the models that can predict temperature, mass loss, char layer thickness and resin content within heat exposed composites and a mechanical model. Each of these methods has been employed by one of the models discussed above. The most recent models have employed the char layer method and used an instantaneous temperature to define the thickness of this layer. The results have shown reasonable correlation but may prove less successful when different heating rates are used. The decomposition reactions will occur at higher temperatures with higher heating rates. Most of the models presented have concentrated on the change in properties of the materials due to ablation of the resin matrix. It has been claimed that the thermal stresses induced in the composite during an intense fire are insignificant [Chen, Sun et al. 1985] when compared to the effects of the resin ablation.

Reference	During or post fire	Material	Modelled heat source	Mode of loading	Strength analysis
[Pering, Farrell et al. 1980]	Post fire	Graphite/epoxy	Const surface temps 540°C, 760°C, 980°C	Tensile and shear	Mass loss and char thickness
[Chen, Sun et al. 1985]	During fire	Graphite/epoxy	800kW/m^2-24500kW/m^2	Tensile	Temperature dependant strength and moduli
[Griffis, Nemes et al. 1986]	During fire	Graphite/epoxy	50000kW/m^2 – 25000kW/m^2	Tensile	Temperature dependant strength and moduli
[Dao and Asaro 1999]	During fire	Glass/vinyl-ester	ASTM E119 fire curve (dampened)	Compressive	Temperature defined master degradation curve
[Mouritz and Mathys 1999; Mouritz and Mathys 2001; Mouritz and Gardiner 2002; Mouritz 2003]	Post fire	Glass/polyester, vinyl-ester, phenolic, glass/epoxy Sandwich with PVC and phenolic cores	10-100kW/m^2	Compressive, tensile and shear	Char thickness in two-layer model
[Gibson, Wright et al. 2004]	During fire	Glass/polyester, vinyl-ester, phenolic	800^{o}C or 75kW/m^2	Compressive	Temperature defined two-layer model
[Feih, Mathys et al. 2005]	During fire	Glass/ vinyl ester	10-75kW/m^2	Compressive and tensile	Temperature and mass loss defined two-layer model

Table 2.2: Summary of models to predict failure of composites during or after fire damage

2.8 Fire Testing

2.8.1 Regulations and Standard Test Methods

There are many standard tests relating to the properties of materials and structures when subjected to fire. These tests are essentially broken down into two areas as described by Davies [2001]. The first area is relevant for the initial phase of a fire, shown in Figure 2.2, and is labelled reaction to fire. These tests are described in Appendix A.3. The second area is relevant in determining properties in the fully developed phase of a fire and is referred to as resistance to fire. This thesis is principally concerned with fire resistance and the following section will give an overview of these tests.

The resistance to fire tests are carried out in a furnace and involve subjecting samples to specific temperature-time curves such as the cellulosic curve described in BS 476-20 shown in Figure 2.5. This curve was developed in the 1930s using data collected from fires in residential, office and commercial buildings. The curve was developed such that it models the temperatures experienced over the potential course of a fire in most modern buildings. Fire tests have shown, however that the maximum temperature of a natural fire exceeds that of the standard curve, but afterwards the temperature decreases whereas the standard curve rises continuously [Zehfuss and Hosser 2007]. The curve described in ASTM E119 is also used in many fire resistance tests and is very similar to the British, European and ISO standards. There are three properties of a sample that can be measured in a fire resistance test:

i. the ability of a sample to resist a mechanical load during exposure to a heat source from one side.
ii. the ability of a sample to resist penetration of flames and hot gasses when exposed to a heat source from one side.
iii. the thermal insulation provided by a sample when exposed to a heat source from one side.

Different regulatory bodies or classification societies in the aerospace, automotive, maritime, offshore and building industries all identify the specific requirements for the materials that can be used in various applications. In the maritime industry the Fire Test

Procedures Code (FTP) [IMO 1998] published by the International Maritime Organization (IMO) specifies the allowances for the fire resistance of items such as bulkhead and deck materials on all vessels carrying 12 or more passengers or greater than 500 gross tons. For smaller vessels in the United Kingdom the Maritime and Coastguard Agency (MCA) specify a separate test whereby a material must stop the passage of smoke and flame for 15 minutes whilst being subjected to a flame at a temperature of 843^{o}C.

The IMO classify materials for fire resistance by the period of time before a certain temperature is reached on the unexposed surface of the material, whilst being subjected to the cellulosic fire curve from the other side. If the material is to form part of a load bearing structure then a static load is defined for either decks or bulkheads, which must be supported for the set period of time for the material rating. Failure is determined by the amount or rate of deflection. The integrity of a material is defined by the length of time before flames penetrate through the material during exposure to a cellulosic fire curve.

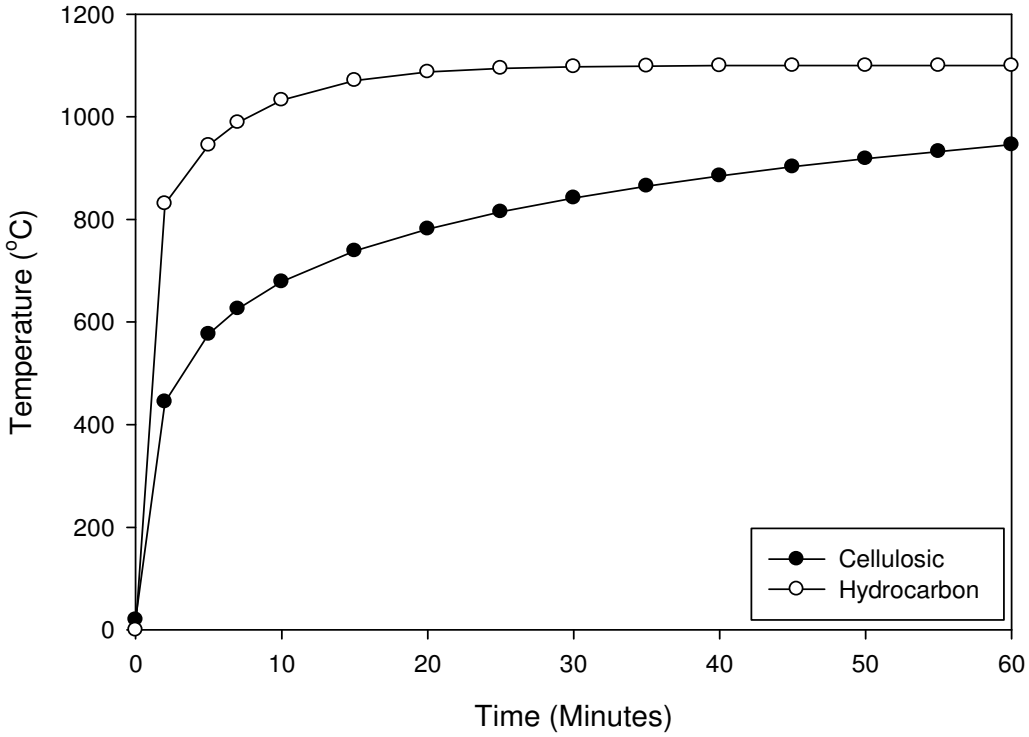

Figure 2.5: Standard temperature -time curves, Source [BS476-20 1987]

In the offshore industry, test procedures use a more severe curve known as the hydrocarbon curve displayed in Figure 2.5 along with the cellulosic curve. This seeks to model the flashover and fully developed phase of a fire with a hydrocarbon fuel. Barnett [2007] gives an overview of each of the different temperature/time curves in use.

2.8.2 Experimental Test Methods

The apparatus used to verify the modelling conducted in a number of the papers reviewed in this thesis seems to be broadly similar. Dao and Asaro [1999] and the collected papers of Davies et al. [Dodds, Gibson et al. 2000; Davies, Wang et al. 2005] and Gibson et al. [Gibson, Wu et al. 1995; Looyeh, Bettess et al. 1997; Dodds, Gibson et al. 2000; Gibson, Wright et al. 2004; Gibson 2005] have all used apparatus similar to that specified in ASTM E119 or BS 476, which are two versions of a fire resistance test. In these experiments a sample in the form of a flat and rectangular panel is exposed to a fire source from one side and the unexposed side is left exposed to ambient conditions. This would seem like a logical method to test the fire resistance of walls, doors and deck materials for a range of uses. The tests that have been documented have used panels ranging from 300 mm × 300 mm up to around 3 m × 3 m. Other investigators, such as Henderson et al. [1985] and McManus and Springer [1992a; 1992b] have conducted experiments on a smaller scale in order to verify their models.

Henderson et al.'s approach to experimentation is a more efficient way of verifying one dimensional heat transfer through a composite from a purely scientific point of view and where simple material comparisons are required. The larger scale experiments do however allow for the addition of mechanical loads to be applied to panels and for testing to be conducted of full scale structures. Davies and Wang [1996] claim however that the test methods adopted by Henderson et al. are too precise and give results that are not necessarily representative of a real fire. Another factor, which has been mentioned, is the contribution to the fire from the volatiles released by the composite. In a small scale test these contributions will be insignificant compared to the incident heat flux and as such it is not necessarily representative of a real fire.

As mentioned previously there have been two approaches to the mechanical testing of samples subjected to fire; first by subjecting the samples to a combined fire and mechanical load, and secondly, by subjecting samples to fire and then testing them

mechanically afterwards. The scale of testing has ranged from panels up to 3 m × 3 m to coupons 100 mm in length.

The merits of testing on small scale as described by Gibson et al. [2004] and Lui et al. [2005] are more akin to proving thermo-mechanical relationships. The larger scale experiments allow more complex mechanical loading scenarios and are more suitable for testing actual structures. The IMO regulations require that large-scale testing is needed in order for materials to be classified.

Measuring the internal and surface temperatures of the test specimens is a subject that needs careful consideration. There is little mention in much of the literature reviewed here of the exact methods used.

The measurement of the hot surface temperature poses a particular problem as some of the testing is conducted at temperatures around 1000°C. In Henderson et al. [1985] and Gibson et al. [2005] a heat flux meter has been positioned in place of the test sample to record the heat flux the sample would be subjected to during a test. The exposed surface heat flux or temperature is the boundary condition which is needed in the Henderson model as the input to calculate the heat flow through a specimen. Some investigators have tried to adhere thermocouples onto the hot surface of test samples, but in many cases they have found that once the temperatures reach sufficient values the adhesive does not hold the thermocouples [Davies, Dewhurst et al. 2000]. This therefore leads to a problem in the measurement of the hot surface temperature in many cases. A possible solution to this problem is to follow the method used by Urbas and Parker [1993] whereby two small diameter holes are drilled through a sample no more than 10mm apart. Through each hole a thermocouple wire is inserted so that the hot junction of the thermocouple is located in between the two holes on the exposed surface of the sample. The wires are then held in tension so that the hot junction is tight against the exposed surface and will remain so even when the material recedes.

Temperatures within samples have been measured by thermocouples that are laminated in the sample in the manufacturing process as described in Davies and Wang [1996] and also by inserting thermocouples into holes drilled into samples after manufacture as in Henderson et al. [1985].

The drawback with the first method is that during the laminating process it is difficult to position the wires effectively and some manufacturing processes, which involve vacuum bagging, become difficult and can lead to poor seals and inferior samples being produced. The benefit of this method, however, is that there is a lower chance that the hot junction of the thermocouple is in an air pocket within the sample. Henderson et al. [1985] went to the lengths of filling the holes made to insert the thermocouples with a ground powder obtained from the same material as the test samples to eliminate air space around the wires. It is unclear exactly how this was done however, when considering the holes were only 0.66mm in diameter. The positions of the thermocouples were determined by x-ray in this instance, which is an extreme to which no other investigator has reported to have gone.

It is important to be clear about what needs to be measured on the unexposed face of a sample. There are a number of boundary conditions that could occur and the measurement needs to match the modelling that is taking place. The test standards such as ASTM E119 and BS 476 stipulate that the unexposed surface is to be open to ambient conditions and that copper disc type thermocouples are attached to the surface. The recommended means of attachment is by securing an insulating pad over the back of the thermocouple onto the surface of the sample. It is stated that no adhesive is to be applied to the thermocouple on either side of the disc. Similar methods have been reported in Dodds et al. [2000] but it is unclear how the unexposed surface of the material was modelled. This method of attaching thermocouples provides an unnecessarily complicated boundary condition on the unexposed surface, where the measuring device is insulated but the rest of the face is not. It is also questionable how good a contact can be made between the thermocouple plate and the usually rough surface of a composite panel.

The simplest boundary condition to model would be to fully insulate the unexposed surface of the sample so that the heat flux from the surface can be neglected. This has been done in some cases [Gibson, Wright et al. 2004] and whilst it would present the simplest way to model the unexposed face, it does not however represent the vast majority of real-life scenarios.

2.8.3 Determination of Material Properties

With the development of the one dimensional model for heat transfer reaching a plateau investigators have turned to a more thorough look at the material properties needed for the thermal modelling [Krysl, Ramroth et al. 2004; Lattimer and Ouellette 2006; Lua, O'Brien et al. 2006; Ramroth, Krysl et al. 2006].

In Lua et al. [2006] there is an in depth investigation into the temperature dependent nature of the various material properties needed to predict the heat flow through a decomposing solid. Specific apparatus has been developed to measure the thermo-physical properties of samples and an accompanying finite element program to compute the properties of a woven fabric composite. On a similar theme Ramroth et al. [2006] have expanded on the work published in Krysl et al. [2004] to look at the sensitivity of the material properties on the results of the thermal model. For the modelling of fire resistance of composites the specific material properties are of utmost importance. Further discussion in this area is given in Appendix A.4. The following properties are needed to model the heat transfer through a decomposing composite using the model initially proposed by Henderson et al. [1985]:

Specific heat capacity, Cp	J/kg-K
Thermal conductivity, k	W/m-K
Activation energy, Ea	J/Kg-mole
Heat of decomposition, Q	J/kg
Pre-exponential factor, A	sec^{-1}
Order of reaction, n	
Density, ρ	kg/m^3
Enthalpy, h	J/kg

The specific heat capacity, thermal conductivities and densities are required for both virgin and char states. The enthalpies and specific heat capacities are also required for the gas evolved during the reaction.

In addition to these properties, depending on the boundary conditions, the following properties may also be required:

Surface heat transfer coefficient, h W/m^2-K

Emissivity, ε

Time period	Positive effect	Neutral effect	Negative effect
Early stages	E_a, K_v		C_{pv}, ρ_v
Mid stage	C_{pg}, ρ_v	E_a	K_{ch}, ρ_{ch}
Later stages	C_{pg}, E_a, ρ_v		K_{ch}, k_v, ρ_{ch}

Table 2.3: Summary of effects of input parameters from Ramroth et al. [2006]

Table 2.3 shows which properties have a significant impact on the output at different stages of the simulation conducted by Ramroth et al. [2006]. A, C_{pch}, n and Q have very little effect on the output during any period of this simulation and have been omitted from the table. During the mid-stage of the simulation the effect of E_a starts off having a positive effect and then switches to a negative one. This analysis has limitations since it is specific to this particular test on a 10.9mm thick glass/polyester laminate subjected to a hydrocarbon fire curve. Other limiting factors are that the properties used in this instance are not temperature dependant. If temperature dependant properties were used it is expected that the results may be different. It must also be borne in mind that the output to which the effects are judged is the temperature of the cold face. If one were to link a thermal and mechanical model by means of the temperatures within the composite or the thickness of the char layer then these results may not be relevant.

There are various standards in place to measure the material properties required for the modelling of composites. However these standards are not always appropriate for the materials in question and at the temperatures required. The following sections outline some of the methods which have been used and applied to fire resistance modelling.

2.9 Conclusion

Much was learned from the fire aboard the "Orkla" and the accident report showed that it was not the materials themselves that were unsafe, more the lack of a safety culture

within the organisation. Specifically looking at the design and operation of a composite vessel the following recommendations were made:

- The need for structural redundancy; possibly from internal stiffeners.
- Sandwich structures to be self supporting in the case of the failure of one of the faces.
- Intumescent coatings on all interior surfaces.
- Comprehensive testing of insulation materials to ensure non-combustibility.
- Decks and bulkheads rated to the appropriate fire class.
- Sprinkler systems installed in all internal rooms onboard.
- Testing of fire water systems on a regular basis.

These recommendations were specific to the "Orlka", but do provide generalised advice for all composite boats. It was stated in the report [RNoN TEG Report 2003] that if the RNoN had been required to adhere to IMO regulations many of the design faults would have been addressed prior to construction.

In its current form the numerical models used to predict heat transfer through thermally degrading composites have not moved forwards a great deal since they were first produced [Henderson, Wiebelt et al. 1985]. They have however been verified using a number of materials and using different temperature curves for single skin materials. Authors claim that it is now possible to predict the following for single skin materials in fires from 25kW/m^2 to at least the hydrocarbon curve in terms of fire intensity:

- temperature-time history throughout the thickness of a single skin composite.
- thickness of the layer of char within a composite with respect to temperature and time.
- density of a composite with respect to temperature and time.

It is claimed that this can be done to a precision of around 20^{o}C difference on average when compared to experimental results. A large factor in this precision is obtaining accurate material properties. A number of papers have been published recently that highlight the properties having the largest affect on the results of these simulations.

This provides useful information as to where efforts should be concentrated in determining the properties of materials for future research.

The initial aim of the numerical modelling was to be able to predict the performance of materials in standard fire tests without having to conduct the tests themselves. The next stage in the development of these models will, however, seek to replicate the response of more complex structures in more realistic fire scenarios. This begins with the development of multi-dimensional models [Looyeh, Bettes et al. 1998]. The example presented by Looyeh et al. [1998] was relatively simple and there is room for more work in this area to develop more complex modelling tools.

Sandwich structures have been tested fairly extensively [Davies 1995; Davies, Dewhurst et al. 1995; Grenier, Dembsey et al. 1998] where by certain panels with non-combustible core materials have been modelled and tested [Looyeh, Rados et al. 2001; Davies, Wang et al. 2006]. A finite element model for the heat transfer through a generic sandwich panel has also been created [Krysl, Ramroth et al. 2004] but again this does not account for any decomposition of the core.

Thermo-mechanical modelling of composites has been evident since the early 1980s and there has been a range of predictive models reported upon, modelling a variety of different loading scenarios. Purely mechanical modelling of composites is a well researched subject and there are numerous methods available to predict the response in any given loading situation. Likewise the modelling of the thermal response of single skin composites in one dimension is reaching a similar point. The crucial area then, which defines each thermo-mechanical model, is the link between the output from the thermal models and the input to the mechanical models. The following methods have been used to link the two models:

- temperature dependant values of moduli and strengths.
- relating overall mass loss to a change in strength or moduli.
- assuming the char layer thickness to be a region with zero mechanical properties.
- relating the boundary of the region with zero mechanical properties to a temperature.

- relating the boundary of the region with zero mechanical properties to a temperature and using the percentage mass loss as a scaling function.

Using temperature dependant relationships for the instantaneous strength of composites is a common method, which has been used in the more recent publications. What is not clear is how these relationships have been obtained and whether they can be applied at different heating rates.

So far mainly simple methods have been produced, which aim to model the response of coupon samples subjected to intense heating and simple loading. It has been concluded that in these instances the effect of thermal stresses is negligible when compared to the effects of material ablation. However, if one wanted to predict the response of a more complex structure, the thermal stresses to which some parts of the, directly unexposed, structure may be subjected to could have a significant effect on the structure as a whole.

There has been very little in the way of modelling the thermo-mechanical response of sandwich composites. Mouritz and Gardener [2002] looked at the post fire compression properties of sandwich beams with lightweight cores and related the mechanical performance to the thickness of the char layer. There seems to be no research in the area of mechanical performance of sandwich materials during fire exposure.

The very small scale testing conducted by Henderson et al. [1985] can give an economical representation of how a material may react in a full scale fire test. The level of control achievable in that scale of testing helped to verify the predictive models proposed by the authors. This effectiveness of the scale of testing is limited since the effect of the burning volatiles will be small when compared with the effect experienced in a full scale fire. The larger scale panel tests conducted by many of the authors discussed in this chapter can possibly provide a method that is more representative of a full scale fire.

The determination of material properties is the area of most development in recent years. The numerical models have now reached a plateau in their development where any improvements in the modelling are insignificant compared to the importance of obtaining accurate material properties. For most of the properties needed there are

standard test methods which can be applied to composites at the temperatures required. The areas of contention seem to be in determining the temperature-dependant thermal conductivity at high temperatures and determining the temperature dependant values of the surface heat transfer coefficient. It is also evident that there is very little mention in any of the literature reviewed on the determination of the specific heat capacity of the evolved gas.

From the point of view of a naval architect wishing to construct a vessel from composite materials one of the most crucial aspects with regards to fire is passing the relevant regulatory tests. There is currently no published work seeking to find a method of predicting how a given structure will fare in the tests. The testing can be very expensive, which prohibits extensive trialling of different solutions.

3 Methodology

The purpose of this chapter is to outline how the objectives of this research have been implemented.

The literature review highlighted the need for the ability to predict the effects of fire on composite materials for two reasons. First to predict the effect of fire on structures exposed to fire in order to mitigate against that risk and, secondly, to predict the results of the fire tests required by regulatory bodies.

There are two aspects to fire resistance; namely the effects of fire on the temperature of a structure and the effects of fire on the strength and stiffness of a structure. In order to be able to predict and compare these effects two different routes have been proposed for each aspect and this thesis will look at each one in order to find the most viable. Each route is outlined in the form of a flow chart shown in Figures 3.1 and 3.2.

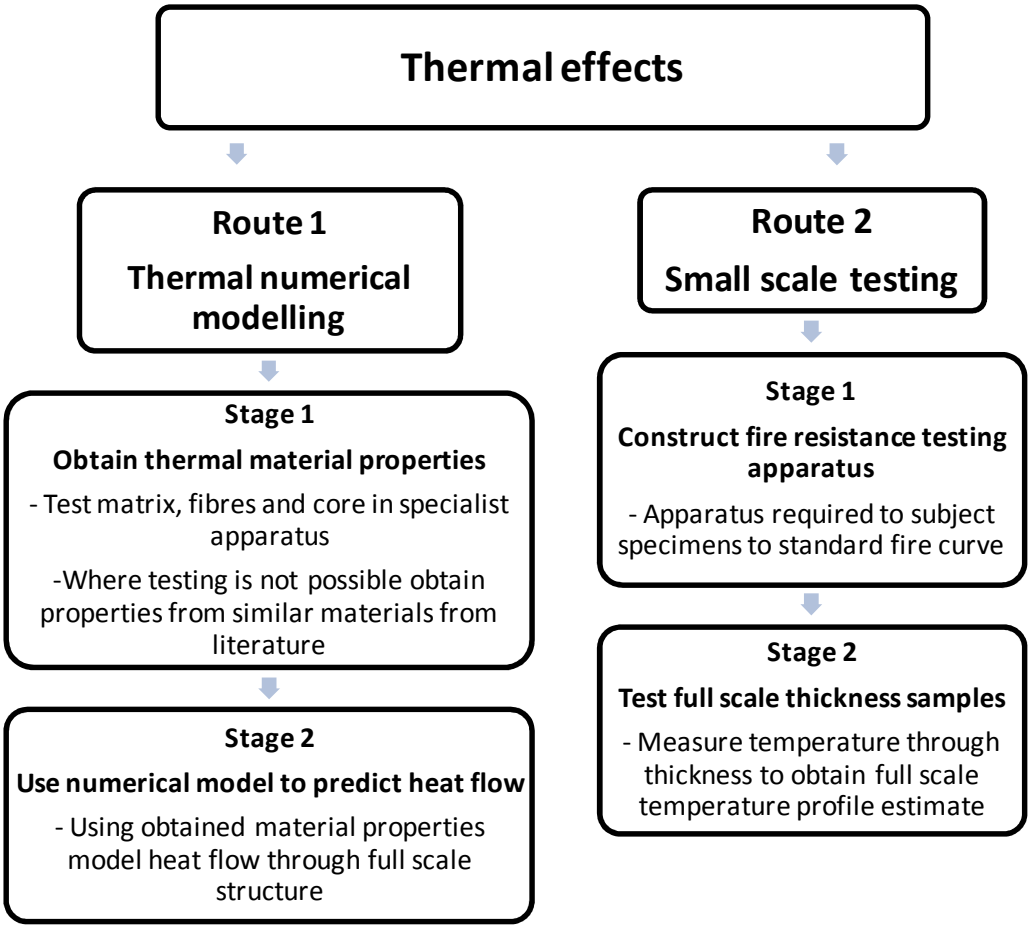

Figure 3.1: Flow chart methodology for thermal effects of fire on composite structures

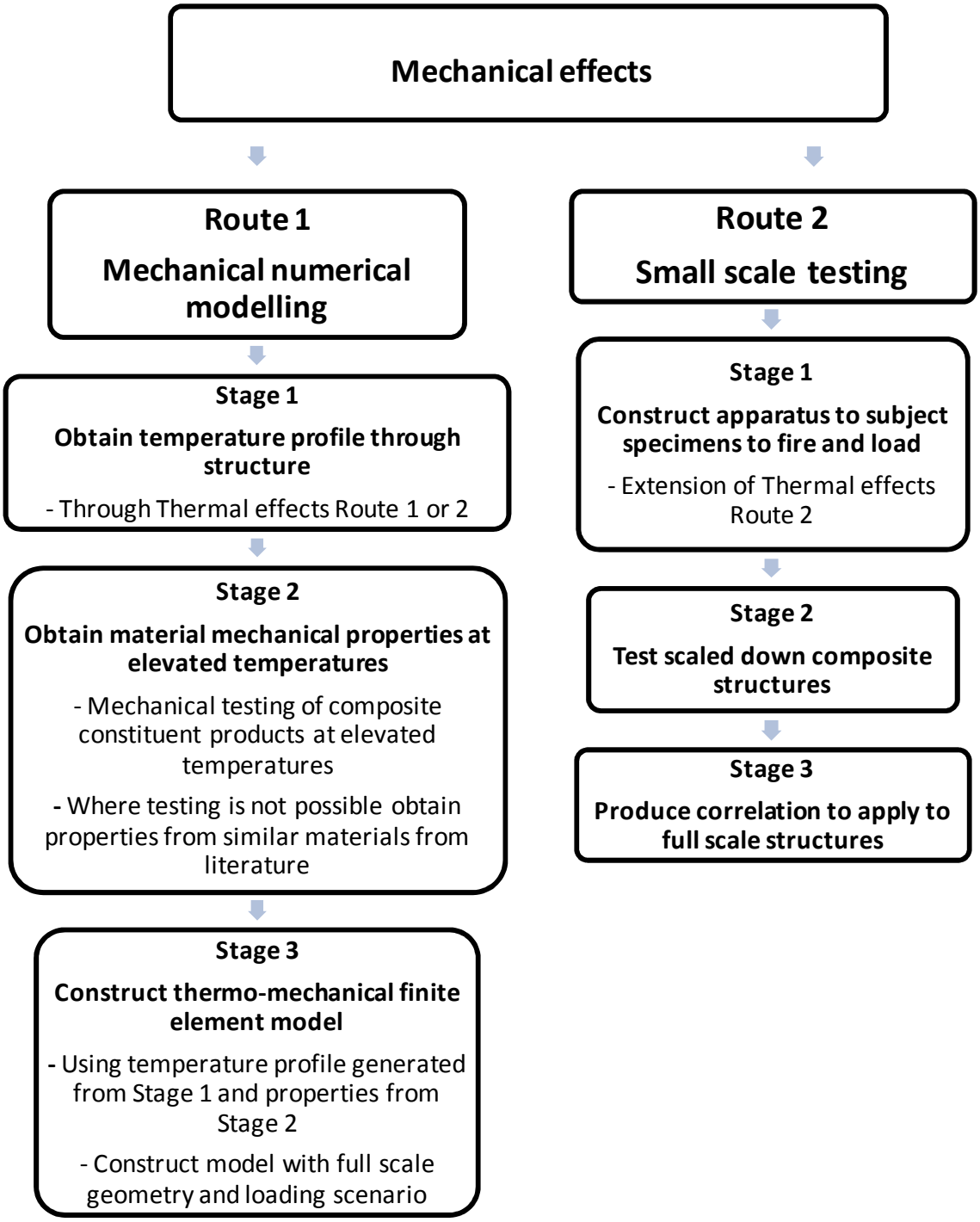

Figure 3.2: Flow chart of methodology for mechanical effects of fire on composite structures

The thermal effects of fire will be looked at first and the two routes proposed are tackled together in Chapter 4. The chapter describes a heat transfer finite element model, which has been obtained and utilised to predict the temperature profile through single skin and

sandwich panels which are tested in the apparatus. The properties required as inputs for the model are obtained by experiment and from literature where necessary.

The construction of a new small scale fire resistance testing apparatus is detailed. This is able to test single skin and sandwich composite panels using the standard cellulosic fire curve required by the IMO regulatory tests. A series of single skin and sandwich panels are tested at full and reduced scale thickness in order to generate full scale thickness temperature profiles to be used in Mechanical modelling, Route 1, Stage 1 as described in Figure 3.2. The testing was also used to verify the heat transfer numerical model.

Chapter 5 details the methods by which the mechanical properties at elevated temperatures of the constituent products of the single skin and sandwich panels are obtained. This fits in to the methodology in Mechanical modelling, Route 1, Stage 2 in Figure 3.2. In this case the core and matrix are tested experimentally while data for the reinforcements is taken from literature. This data provides the link between the thermal and mechanical models to produce the thermo-mechanical model. Previous research has often assumed the properties to vary linearly within matrix materials and this provides a more authoritative approach to obtaining the data. The mechanical properties of PVC foam core materials at elevated temperatures has not been investigated previously and this chapter trials a method for doing so and presents the data obtained. The properties of single skin and sandwich composites at elevated temperatures are then derived combining the properties obtained in Chapter 5 by the rule of mixtures method.

A new thermo-mechanical model shown in Figure 3.2 under Mechanical effects, Route 1, Stage 3 is described in Chapter 6. The model requires a temperature profile, which has been generated by the results taken from Chapter 4 and the properties generated in Chapter 5 in order to predict the response of a composite panel subjected to fire and load simultaneously. The construction of a new small scale fire and load testing apparatus is described. This is an extension of the apparatus illustrated in Chapter 4. A series of single skin and sandwich panels are subjected to the cellulosic fire curve as well as an out-of-plane load. The results are compared to predictions made by the thermo-mechanical model. A relationship is also derived in order to predict the response of composite panels in large scale fire and load tests.

In Chapter 7 two of the objectives of this thesis are realised. A large scale fire resistance test is carried out at a commercial test facility in order to verify the predictions made in Chapters 4 and 6. A large sandwich panel representative of a lifeboat deck is tested under combined fire and load. The measured temperatures and deflections are compared with numerically and experimentally predicted values. The merits of each of the proposed methods are discussed and recommendations made for further research.

4 Heat Transfer Through Single Skin and Sandwich Panels Subjected to Fire

4.1 Introduction

This chapter sets out to predict and compare the thermal effects of fire on composite structures as outlined in Chapter 3, Figure 3.1.

In this chapter the reader is introduced to a new small scale fire resistance test, representative of the full scale test required by the IMO for fire restricting divisions aboard ships, subjecting composite panels to fire only. Experiments have been carried out using single skin and sandwich composite test specimens and the results have been predicted using a heat transfer finite element model. The Henderson equation, [Henderson, Wiebelt et al. 1985] which has been used to predict the results, is explained and the methods of obtaining the material properties required for the equation are described.

A series of tests were also carried out in order to establish the temperature profile across the surface of the test specimens. This was done, first, to assess how evenly the panels were being heated and, secondly to provide 2 dimensional temperature profiles for thermo-mechanical models which are described in Chapter 6.

As was discussed in the literature review there is a generally accepted method for modelling the heat transfer and decomposition of composites, which has been developed over the last 3 decades. What has not been looked into to any great extent is the heat transfer through sandwich structures, which will be discussed in this chapter.

As indicated in Chapter 3 Methodology the experimentally generated and predicted temperature profiles from this chapter will be used to form a thermo-mechanical model in Chapter 6.

4.2 Theoretical Models

The particular heat transfer model used in this case was written by Krysl et al. [2004] in MATLAB. This model, which is based on the Henderson equation [Henderson, Wiebelt et al. 1985], has been developed from the transient heat conduction equation to account for the effects of a pyrolysis reaction and also the effects of the decomposition gas.

$$\rho C_p \frac{\partial T}{\partial t} = \underbrace{k\frac{\partial^2 T}{\partial x^2}}_{\text{Pure heat conduction}} - \underbrace{\dot{m}_g C_{pg}\frac{\partial T}{\partial x}}_{\text{Cooling effect of volatiles}} - \underbrace{\frac{\partial \rho}{\partial t}\left(Q + h - h_g\right)}_{\text{Decomposition endotherm}} \tag{4.1}$$

Where:

ρ	= density (kg/m^3)	C_p	= specific heat capacity (kJ/kg-K)
T	= temperature (K)	k	= thermal conductivity (W/mK)
$\dot{m}_g$	= mass flux of gas (kg/s)	C_{pg}	= specific heat capacity of gas (kJ/kg-K)
h	= enthalpy (J)	h_g	= enthalpy of gas (J)
t	= time (s)	Q	= heat of decomposition (J/kg)

The decomposition is modelled by the Arrhenius equation as shown in Equation (4.2).

$$\frac{\partial \rho}{\partial t} = A\rho_v \left(\frac{\rho - \rho_{ch}}{\rho_v}\right)^n e^{\left(-\frac{E_a}{RT}\right)} \tag{4.2}$$

Where:

A	= pre-exponential factor (s^{-1})	ρ_v	= density of virgin material (kg/m^3)
n	= order of reaction	R	= gas constant (J/kg-mol)
E_a	= activation energy (J/kg)	ρ_{ch}	= density of charred material (kg/m^3)

Assuming that no mass is lost it can be said that the mass flux of gas is equal to the rate of change of density.

$$\frac{\partial \dot{m}_g}{\partial x} = -\frac{\partial \rho}{\partial t} \tag{4.3}$$

It is also assumed that the enthalpies of solid and gas can be given by:

$$h = C_p T \tag{4.4}$$

The initial conditions are:

$$\begin{aligned} \rho(0) &= \rho_v \\ T(0) &= T_{ini} \end{aligned} \tag{4.5}$$

Where:

T_{ini} = initial temperature (K)

The boundary conditions are taken as the recorded temperature on the fire exposed face of the panel and on the unexposed face of the panel the following condition is used:

$$q(t,l) = k_{s,cold}\left(T(t,l) - T_a(t)\right) \tag{4.6}$$

Where:

$k_{s,cold}$ = surface heat transfer coefficient (W/m^2-K)

l = thickness of the panel (m)

In its original form the program is used with $k_{s,cold} = 1$ to simulate an insulated face.

It is assumed that all the gas produced will flow back through the material and exit through the fire exposed face. Therefore the following can be assumed:

$$\dot{m}_g(t,l) = 0 \tag{4.7}$$

It is now possible to eliminate gas mass flux from Equation (4.1) by integrating:

$$\dot{m}_g(l) - \dot{m}_g(x) = \int_x^l \frac{\partial \dot{m}_g}{\partial x} = -\int_x^l \frac{\partial \rho}{\partial t}\partial x = \int_l^x \frac{\partial \rho}{\partial t}\partial x \tag{4.8}$$

With Eq (4.4) and inserting in Eq (4.1) gives:

$$\rho C_p \frac{\partial T}{\partial t} = \frac{\partial}{\partial x}\left(k \frac{\partial T}{\partial x}\right) - \frac{\partial \rho}{\partial t}\left(C_p - C_{pg}\right)T + \left(\int_l^x \frac{\partial \rho}{\partial t}\partial x\right) C_{pg} \frac{\partial T}{\partial t} - Q \frac{\partial \rho}{\partial t} \tag{4.9}$$

This equation is solved for the unknown function T in terms of x and t. The density is given in terms of T and is found using Equation (4.2). The derivation of the finite element model is given in full in Krysl et al. [2004] and will not be repeated here.

There were some errors within the Krysl program, when run initially, which needed changing. The model showed that the density of the material was nearly constant throughout the time period and at a value very close to the charred density for this duration. This also affected the temperature profile generated by the program. It was found that the density from the final step in one iteration was being used as the density for the first step in the subsequent iteration. By clearing the current density matrix after each iteration this problem was resolved.

4.3 Experimental Apparatus

The testing was conducted in the Vulcan fire test rig at the University of Southampton [Cutter, Gillitt et al. 2004]. Figure 4.1 shows the apparatus including the loading system which was not used in his chapter.

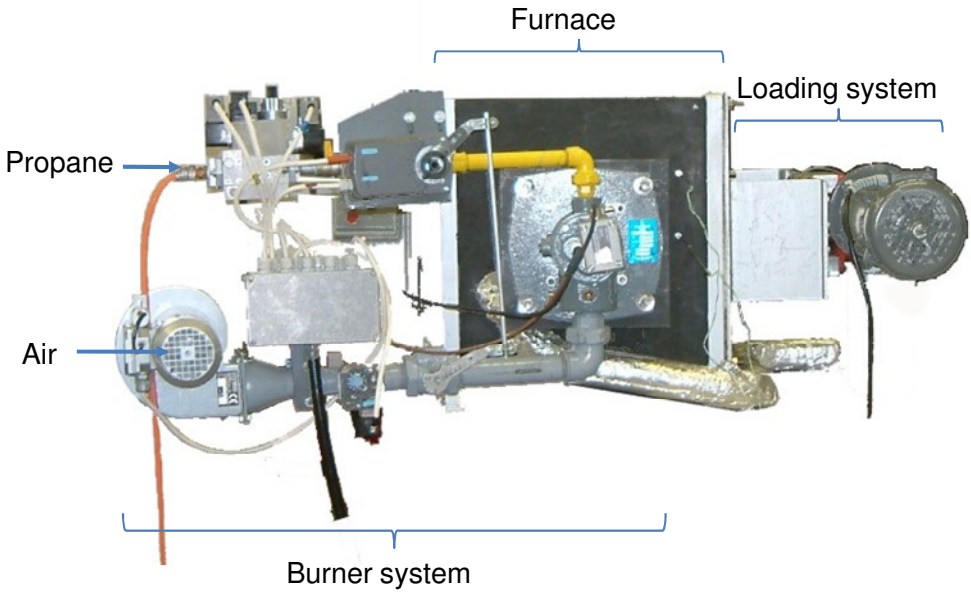

Figure 4.1: Vulcan Fire testing apparatus

This has been built and developed at the University of Southampton and consists of a Maxon Kinemax MVG 70 30kW propane burner, which fires into a cubic furnace with outer dimensions approximately 500mm × 500 mm × 500mm and an active volume of 0.064m^3. One face of the furnace is detachable and houses the test sample. This arrangement is shown in Figure 4.2 and Figure 4.3.

Figure 4.2: Detachable front plate holding test sample

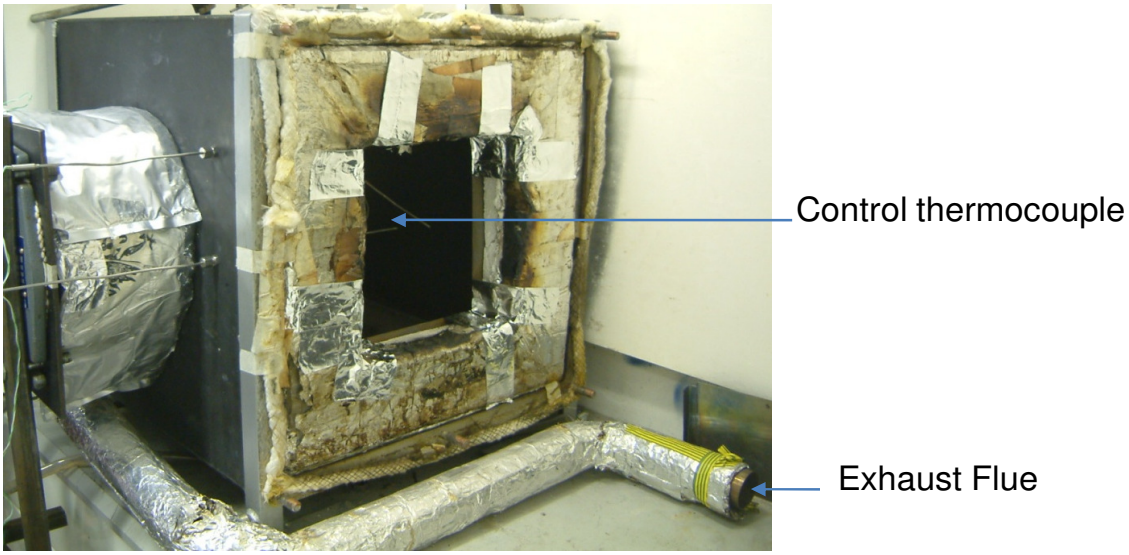

Figure 4.3: Furnace with front plate removed

The flame fires onto the wall adjacent to the panel in order that the apparatus can fit inside a laboratory fume cupboard. This is essential to vent the exhaust fumes and any fumes emitted from the unexposed face of the test sample. The flame has to therefore be deflected by 90° so that it fires directly on to the sample. This has been carried out by placing a stainless steel dairy tube with a 90° bend in line with the opening in the refractory block. The centre of the tube is lined up with the centre of the sample in order to gain an even a temperature distribution across the panel surface. The temperature inside the furnace is controlled using an Omron Digital Controller E5CK. A detailed specification of the burner and control system is given in Cutter et al. [2004]. The temperature feedback to the controller is provided by a stainless steel sheathed thermocouple, which was located in line with the flame and the centre of the panel as shown in Figure 4.3.

The sample is bolted into the front plate with 8 off M12 bolts and a square frame as shown in Figure 4.4. The sample is therefore exposed to the fire on one side and ambient conditions on the other side. The samples measure 240mm × 240mm with an area exposed to the fire of 200 mm × 200 mm. Heat loss from the edge of the panels has been minimised by the insulation around the edges which is 150mm thick WDS® ULTRA Fibre Board. This has a thermal conductivity of less than 0.05 W/m-K even at 800°C.

Figure 4.4: Clamping arrangement for test samples

4.3.1 Temperature Measurements

Three types of thermocouple were used in order to measure the temperature at various locations throughout the experiments. Two stainless steel sheathed thermocouples measured the temperature of the flame inside the furnace. One was used as a control feedback and one was used to measure the temperature for analysis. As mentioned in the previous section these were located in line with the centre of the panel and the centre of the flame source approximately 100mm from the exposed side of the front plate. This varied by up to 20 mm depending on the thickness of the samples that was being tested. In BS 476, which gives details of the procedure and apparatus to be used in the IMO tests the control thermocouples are required to be 100 mm from the hot surface of the panel at the start of the test and no more than 50mm to 150mm during the test.

In order to measure the temperature through the thickness of the panels, thermocouples were laminated into the panels during manufacture. This did cause some problems with manufacture, however, as the edges where the thermocouples protruded from the panels were difficult to cut. There was also a difficulty in getting a good seal around the panel during vacuum bagging with the wires coming out of the bag and in some cases the resin flowed along the wires causing them to become brittle and snap off.

On the unexposed face of the sample a stainless steel leaf k type thermocouple was used, measuring 10mm × 20mm × 1mm. Two methods were trialled in order to attach the thermocouple. The first method was to secure the thermocouple with insulating board as required in the standard fire resistance tests [BS476-20 1987]. Using this method, it was not clear how good a contact the thermocouple had with the surface of the panel and the insulating board was prone to falling off the panel during the tests. In the second method a thin layer of high temperature epoxy was applied to the thermocouple in order to achieve good contact with the sample surface. The back face of the leaf thermocouple was sprayed matt black in order to attain a closer match to the emissivity of the composite surface than would be achieved with the polished surface of the thermocouple. It was found that the difference in measured temperature was very small on the cold surface with the two different methods and fixing the thermocouples with an adhesive was preferred for reasons of practicality.

Initially the exposed face temperature was measured by inserting a thermocouple through the centre of the sample from the back face and bending it round onto the front on the sample. Testing gave inconsistent results using this method as it was not possible to be sure that the thermocouple was in good contact with the surface

The second method was to attach a leaf type thermocouple to the exposed face with a thin layer of epoxy and then secure the ‘leaf’ to the surface with fire cement over the back face. After the test the thermocouple was no longer attached to the surface but it was unclear from the results at what point it had fallen off.

On the same panel another method was tried, which was used by Urbas and Parker [1993] in the surface temperature measurements of burning wood samples. In this method two small holes were drilled from the unexposed side of the sample 10mm apart through to the exposed face. The wires of a thermocouple were inserted through the holes so the hot junction was in contact with the exposed surface in between the holes. The thermocouple cable was then put in tension so that the hot junction was kept in contact with the surface on the exposed side and any temperature gradient was eliminated which would conduct heat toward or away from the surface. With this method it was possible to be sure that the hot junction of the thermocouple was in good contact with the surface, even when the surface was receding.

A Pico Technology TC-08 unit was used to record and log thermocouple readings directly into a PC. This allowed a maximum of 8 thermocouples to be used for data acquisition in each test.

4.3.2 Heating Rates

The following temperature curves show the flame temperatures recorded by the furnace thermocouples for the two heating rates used in the testing. The two standard curves shown are given by the following equations:

Cellulosic Curve:

$$T = 345log_{10}(8t + 1) + 20 \quad (4.10)$$

Hydrocarbon curve:

$$T = 20 + 1080\left(-0.325\exp(-0.167\text{t}) - 0.675\exp(-2.5\text{t})\right) \quad (4.11)$$

Where:

T = temperature (^{o}C) t = time (Minutes)

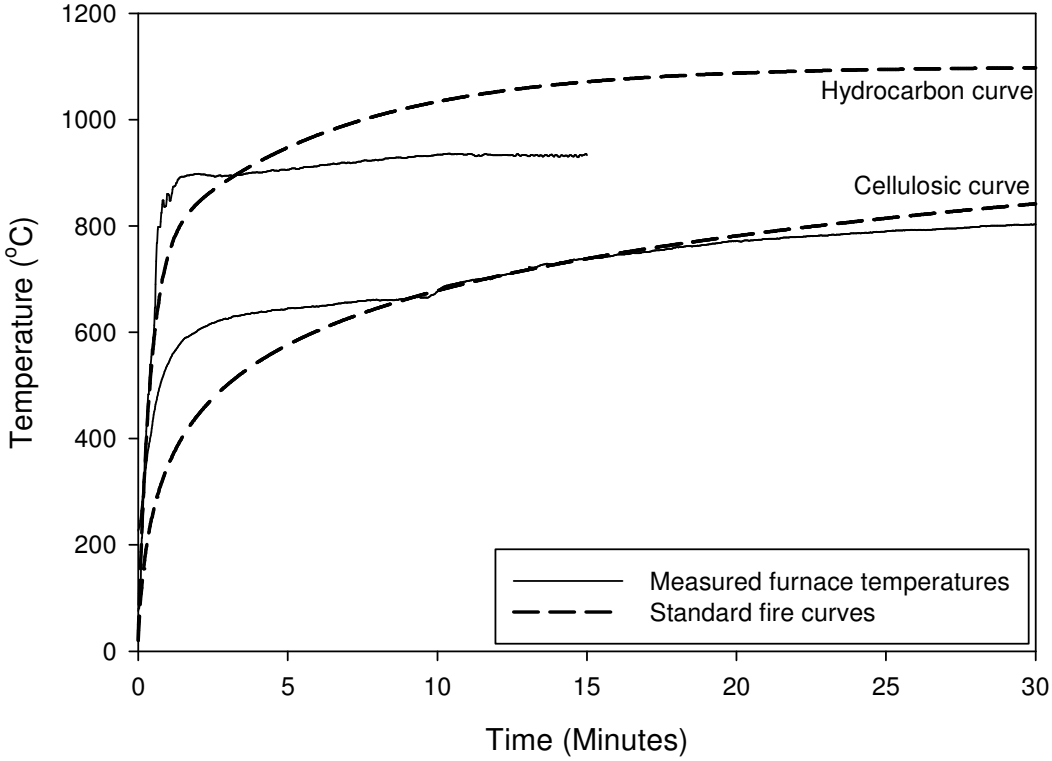

Figure 4.5: Recorded furnace temperatures measured at 100 mm from sample hot surface compared with standard fire curves

For the cellulosic fire curve the recorded temperatures which are shown in Figure 4.5 fall within the allowances given in BS 476 for a standard fire test for the first 30 minutes of the test, the calculation of this is shown in Appendix B.1. The figure shows that the hydrocarbon standard curve exceeds the maximum furnace temperature after three minutes and consequently the recorded curve will be describe as heating rate A.

4.4 Experimental Procedure and Test Matrix

4.4.1 Materials

The materials used in the test programme are of particular interest to the sponsors of this research and are typical of those found in all weather RNLI lifeboats. They are glass reinforced epoxy resin single skin panels and sandwich panels with PVC foam cores and glass and epoxy skins. There is also little published data on the performance of these materials in fire resistance tests as was highlighted in the literature review.

The different lay ups used are detailed in Table 4.1. All of the panels were made by wet lay-up technique and vacuum consolidation, which is a method used in lifeboat construction. The resin used in each case was Ampreg 22 (A22) manufactured by Gurit, which is a resin that has been optimised for open mould laminating of large structures. The reinforcements used were all stitched e-glass fibres and supplied by Gurit. They consisted of UTE 800, which is a low-crimp uni-directional e-glass fabric with a stated weight of 800g/m^2, when measured it was found that the average weight of the fabric was actually 758g/m^2. XE 900 is a stitched e-glass fabric with a weight of 900g/m^2 with the fibres running at ±45^o. QE1200 and QE 600 are both stitched quadriaxial e-glass fabrics with the fibres running at -45^o,0^o,90^o,+45^o the weights of each fabric are 1231g/m^2 and 643g/m^2 respectively. The PVC foam core is manufactured by Diab and is Divinycell H100 with a density of 100kg/m^3. The sandwich panels and the XE900 panels were made by Green Marine Offshore Composites and the other single skin panels were manufactured at the University of Southampton.

Panel	Reinforcement and core	Lay up	Density (kg/m^3)	Thickness (mm)	V_f
SS1	UTE 800	$[0]_{16}$	1783	11.8	0.35
SS2	UTE 800	$[0/90]_{8S}$	1715	11.2	0.40
SS3	UTE 800	$[\pm45]_{8S}$	1882	11.0	0.25
SS4	UTE 800	$[0]_{12}$	1675	9.1	0.31
SS5	UTE 800	$[0/90]_{6S}$	1675	8.8	0.39
SS6	XE 900	$XE900_{13}$	1794	8.9	0.57
SW1	QE600, QE1200, 25mm thick H100 Divinycell	QE600 QE1200 H100 QE1200 QE600	280	27.9	0.51
SW2	QE600, QE1200, 15mm thick H100 Divinycell	QE600 QE1200 H100 QE1200 QE600	431	19.07	0.51

Table 4.1: Test material details

The thicknesses of the panels were measured with digital verniers to a precision of 0.01 mm at each side and an average was taken for each panel. To calculate the volume fraction of the fibres the resin density was measured at 1046 kg/m^3, from a resin casting and the weight of each of the fabrics was measured in g/m^2. The volume fraction was then calculated from the following equation:

$$V_f = \frac{V - \frac{W_P - A f_w N_P}{\rho_r}}{V} \tag{4.12}$$

Where:

W_P = weight of the panel (kg)
A = area of the panel (m^2)
N_P = number plies
f_w = fibre weight (kg/m^2)
ρ_r = resin density (kg/m^3)
V = panel volume (m^3)

4.4.2 Thermal Properties

As indicated in the previous section it was necessary to know a number of specific material properties in order to predict the behaviour of degrading materials subjected to fire. Where possible properties were determined by experimentation and where the resources were not available to conduct appropriate testing, data from literature for similar materials and data from manufacturers were used in the modelling process. The following section will outline each property and the process by which the values were obtained.

4.4.2.1 Thermophysical Properties

The specific heat capacities used in the modelling were given by the relevant manufactures for the foam and resin. For Divinycell H100 the specific heat capacity was taken as 1700 J/kg-K. For the Ampreg 22 resin the specific heat capacity was taken as 1000 J/kg-K. For e glass fibres the values were taken to be 1300 J/kg-K [Lattimer and Ouellette 2006]. The specific heat of the gas produced was taken as 2386.5 J/kg-K from Krysl et al. [2004] for polyester resin as no values could be found for any epoxy resins.

The specific heat capacity of the composite was calculated using a rule of mixtures approach with the weight fraction of fibre and resin as used in Dodds et al. and Lua et al. [2000; 2006]:

$$C_{PV} = W_f C_{Pf} + W_r C_{Pr} \tag{4.13}$$

Where:

C_{PV} = specific heat capacity of virgin composite (J/kg-K)

C_{Pf} = specific heat capacity of fibre (J/kg-K)

C_{Pr} = specific heat capacity of resin (J/kg-K)

W_f = weight fraction of fibres

W_r = weight fraction of resin

The specific heat capacity of the charred materials were estimated using Equation (4.13) with the glass fibre specific heat capacity taken from Lattimer and Ouellette [2006] as 1400 J/kg-K. The specific heat of the Ampreg 22 resin char was estimated using the ratio of virgin specific heat to char specific heat of polyester given in Dodds et al.

[2000] since no values for epoxy could be found. This made the char specific heat $1.0847 \times Cp_v$ where Cp_v is the virgin specific heat of the resin. The weight fractions used took account of the reduced density of the resin. The specific heat capacity of the charred core was estimated using the same ratio given above as no data was available.

The foam thermal conductivity was measured by Gearing Scientific using a LaserComp Fox200HT following the BS 874 standard. The guarded hot plate method was used and the foam was tested at 50°C, 80°C, 100 °C, 120 °C and 140 °C. In each case the hot plate was held at T+9°C and the cold plate at T-9°C for a test temperature of T°C to a precision of ±0.03°C.

The thermal conductivity of the resin and fibres were conducted together as a composite panel. The testing was conducted on a complimentary basis and it was not possible to measure the fibre conductivity separately. With the limited testing available it was decided that testing the composite was more beneficial than testing a resin casting.
The tests were conducted to the BS 874 standard using the LaserComp Fox50 at the following temperatures: 0 ºC, 25 ºC, 50 ºC, 75 ºC and 100ºC.

Using the equation below taken from Staggs [2002] for a solid with fibres running perpendicular to the direction of heat flow the conductivities of the resin and fibres were estimated from the composite results provided by the thermal conductivity testing. The thermal conductivity of glass fibre was taken to be 1.04 W/m-K [Krysl, Ramroth et al. 2004]:

$$K_V = K_r \left(1 + \frac{2V_f}{(k_r + k_f)/(k_f - k_r) - V_f} \right) \tag{4.14}$$

Where:

K_V = thermal conductivity of virgin composite (W/m-K)

K_r = thermal conductivity of resin (W/m-K)

K_f = thermal conductivity of fibre (W/m-K)

V_f = fibre volume fraction

The thermal conductivity of the char composite material was estimated using the following equation given in Krysl et al. [2004] and Jakob [1959] for a solid with parallel planar fissures (gas pockets) parallel to the direction of heat flow:

$$K_{ch} = K_f \left(\frac{1}{1 - V_f + \left(K_{air}/K_f V_f + 4\sigma T^3 \, x/K_f \right)^{-1}} \right) \tag{4.15}$$

Where:

K_{ch} = char material thermal conductivity (W/m-K)

K_{air} = thermal conductivity of air (W/m-K)

σ = Stefan-Boltzmann constant, 5.67×10^{-8} W/m^2-K^4

x = panel thickness (m)

T = temperature (K)

The heat of decomposition was taken from Davies et al. [2006] as -30,000 J/kg for an epoxy resin.

The density of the resin, the composite panels and the foam was measured and the density of the e glass fibre was taken from Callister [2000]. The charred density was calculated using a rule of mixtures method and assuming the density of the fibres did not change and the charred density of the resin was inferred from the results of the thermogravimetric analysis.

4.4.2.2 Kinetic Properties

The kinetic properties were measured using the Polymer Laboratories STA-1500 thermogravimetric analyser (TGA). Resin casts were made and filed into a powder for testing. The foam was also tested but it was not possible to file this into a powder. Instead a small fragment of the foam was used. To ensure that no other material contaminated the samples a new file was used and care was taken to ensure no finger prints were left on the samples before filing and that the environment was as dirt free as possible.

Friedman's method [Henderson, Tant et al. 1981] was followed in order to calculate the kinetic parameters for the resins and the core materials. The Ampreg 22 samples were subjected to heating rates of 10^{o}C/minute and 30^{o}C/minute in an atmosphere of

nitrogen, to prevent combustion. The foam samples were tested to heating rates of 10°C/minute, 20°C/minute and 30°C/minute.

4.4.3 Test Matrix

The first set of tests conducted in the furnace were used to determine the temperature profile across the surface of the panels, rather than through the thickness. A series of tests were conducted, using the cellulosic fire curve, to determine the temperature distribution across the hot and cold surfaces of the panels as it was suspected that there may be some variation in this.

Thermocouples were attached on to the hot face of single skin e glass panels with Ampreg 22 resin in the locations shown in Figure 4.11a. The thermocouples were located at radii of 30mm, 60mm, 90mm and 120mm from the panel centre. The gaps in the figure below are due to thermocouples giving erroneous readings.

The temperature variation over the cold surface was also measured to assess how evenly the heat transferred through the panel. Again using the cellulosic fire curve thermocouples were placed in the locations shown in Figures 4.8b-c for the 16 and 12 ply panels described in Table 4.1 and the sandwich panel with 15mm core; SW2.

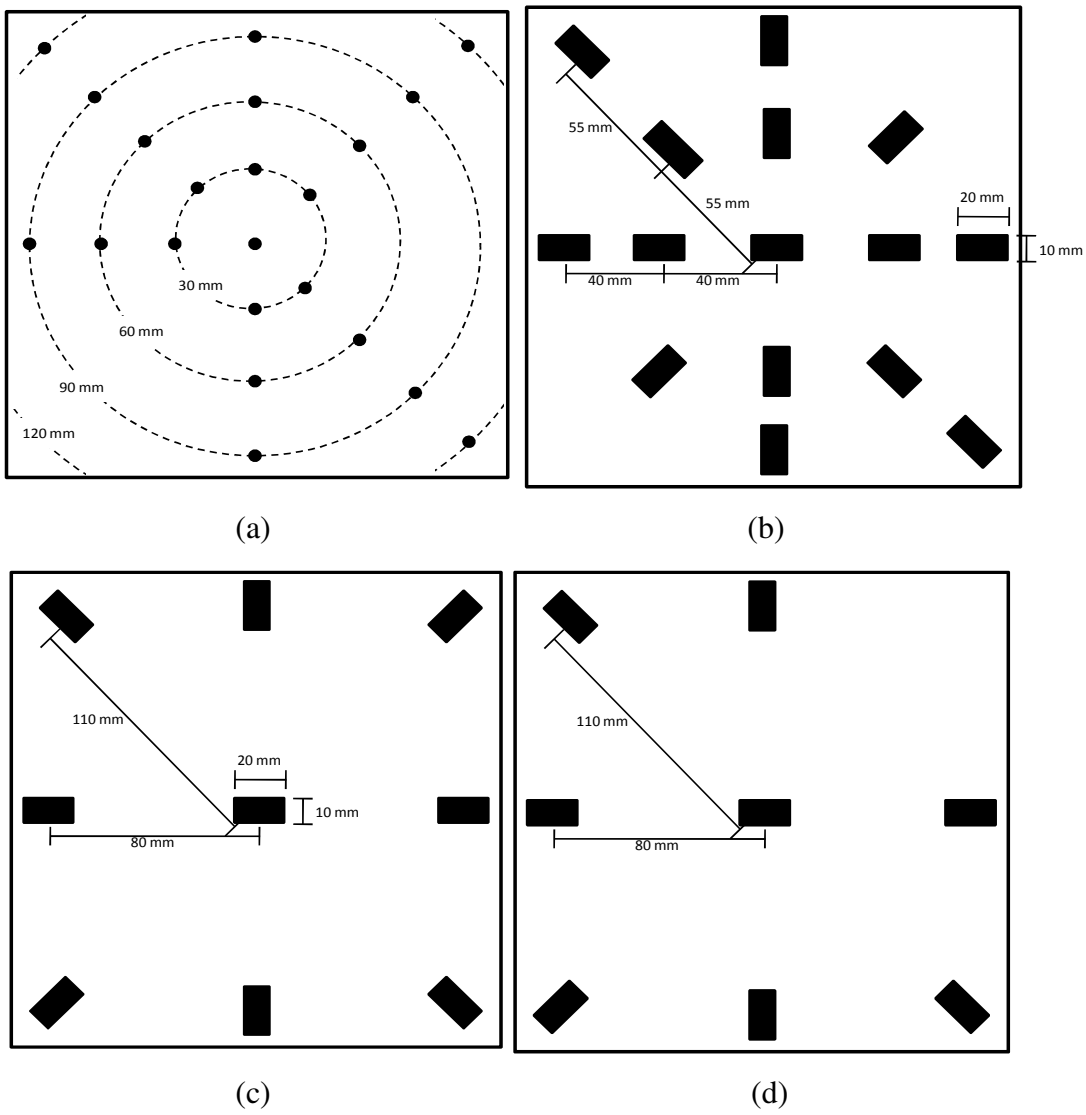

Figure 4.6: Location of thermocouples on hot surface of panels (a) and cold surface of SS1 (b), SS4 (c), SW2 (d)

The second stage of testing looked at the heat transfer through the thickness of the panels. Thermocouples were located in the centre of the panels at various locations through the thickness. The test samples used in the fire resistance tests are listed in Table 4.2 along with the locations of thermocouples and the heating rates and durations that they were exposed.

Sample id	V_f	Thickness (mm)	Thermocouple locations	Heating rate
SS 1.C.1	0.27	11.84	HF, CF	Cellulosic
SS 1.C.2	0.41	10.72	HF, CF	Cellulosic
SS 2.C.1	0.45	10.85	HF, CF	Cellulosic
SS 2.C.2	0.35	11.61	HF, $^1/_3$, $^2/_3$, CF	Cellulosic
SS 3.C.1	0.55	11.1	HF,CF	Cellulosic
SS 4.C.1	0.27	8.82	HF, CF	Cellulosic
SS 4.C.2	0.35	9.12	HF, CF	Cellulosic
SS 5.C.1	0.39	8.8	HF, CF	Cellulosic
SS 6.C.1	0.55	9.1	HF, $^1/_3$, $^2/_3$, CF	Cellulosic
SS 6.A.1	0.50	8.9	HF, C, CF	A
SS 6.A.2	0.49	8.9	HF, C, CF	A
SS 6.A.3	0.52	8.8	HF, C, CF	A
SS 6.A.4	0.50	8.8	HF, C, CF	A

Table 4.2: Single skin panels fire resistance test matrix

Where:

HF = hot face

CF = cold face

C = centre of panel (through thickness)

$^1/_3$ = 1/3 thickness from the hot face

$^2/_3$ = 2/3 thickness from the hot face

Sample id	Thermocouple locations	Heating rate	Duration (Minutes)
SW 1.A.1	HF, HS,C,CS,CF	A	21:06
SW 1.A.2	HF, HS,C,CS,CF	A	05:00
SW 1.C.1	HF,HS, C,CF	Cellulosic	09:36
SW 1.C.2	HS, C, CS CF	Cellulosic	08:36
SW 2.C.1	HF, CF	Cellulosic	13:12
SW 2.C.2	HS, $^1/_3$C , $^2/_3$C, CS, CF	Cellulosic	10:18

Table 4.3: Sandwich panels fire resistance test matrix

Where:

HS = hot skin to core interface

C = core mid thickness

CS = cold skin to core interface

$^1/_3$C = 1/3 core thickness from hot skin to core interface

$^2/_3$C = 2/3 core thickness from hot skin to core interface

In panels SW 1.C.2 and SW 2.C.2 the hot face thermocouple failed and the temperature input into the heat transfer model was taken as the hot skin temperature. The panel was then modelled as having a nominally thin hot skin so that the temperature at the hot skin to core interface was the same as the hot face temperature.

In two of the tests strain gauges were attached to the cold face of the panels at 0^o and 90^o to ascertain the level of thermal strain induced by the heating process. So that the effects of the temperature could be accounted for, a reference strain gauge was used in each orientation, which was not bonded to the sample. The strain measuring gauges were bonded to the panel surface with Micro-measurements M-bond 600. This is a high temperature epoxy strain gauge adhesive and has operating temperatures from -269^{o}C to 175^{o}C and up to 370^{o}C for short periods. The other two gauges were kept in contact with the sample using flash tape over the top of the gauges. The response from the reference gauges would only be due to temperature effects and could therefore be subtracted from the response measured from the bonded gauges to give the true strain.

4.5 Results and Discussion

4.5.1 Material Properties

The results from the thermal conductivity testing conducted on the Divinycell H100 PVC foam and the Ampreg 22/ e glass epoxy panel are shown in Table 4.4. The foam density was calculated to be 98.6kg/m^3. The composite panel used was made by wet lay-up with vacuum bagging and consisted of 13 plies of XE 900. The fibre volume fraction, V_f = 0.49. At 140^{o}C the foam was reported to give off a pungent odour and changed in appearance from yellow to a deep purple.

Sample	thickness (mm)	Thermal conductivity (W/m-K)						
		0°C	20 °C	50 °C	80 °C	100 °C	120 °C	140 °C
H100 Foam	12.15		0.038	.042	.046	.049	0.052	0.055
A22 /e glass	9.12	0.30	0.32	0.33	0.35	0.37		

Table 4.4: Calculated thermal conductivities of H100 foam and an A22/e-glass panel.

The values of the foam conductivity compare reasonably well with the manufacturer's stated values of 0.03W/m-K at 10°C and 0.032 W/m-K at 37°C. Using Equation (4.14) and a value of fibre conductivity of 1.04 W/m-K [Krysl, Ramroth et al. 2004], the resin conductivity was estimated at 0.17 W/m-K. This was done using a value of 0.35 W/m-K for the composite conductivity. This is slightly lower than the value given by Gibson and Mouritz [2006] of 0.2 W/m-K for a typical epoxy.

From the thermogravimetric analysis a mass loss curve was produced, which can be seen in Figure 4.7. This shows for the Ampreg 22 epoxy resin that the decomposition reaction is very sudden and starts at around 350°C but continues until around 800°C. The reaction is a single-step type reaction which leaves around 10% of the original mass remaining at the end. The higher heating rate has the effect of increasing the temperature at which a reaction occurs. In Figure 4.8 it can be seen that the PVC foam reacts in a two stages. The first stage of the reaction occurs at around 250°C and during this stage around 30% of the original mass is lost. The second stage is much slower and seems to finish between 600°C and 700°C when there is about 10% of the original mass left. Again the lower heating rates caused reactions to occur at lower temperatures.

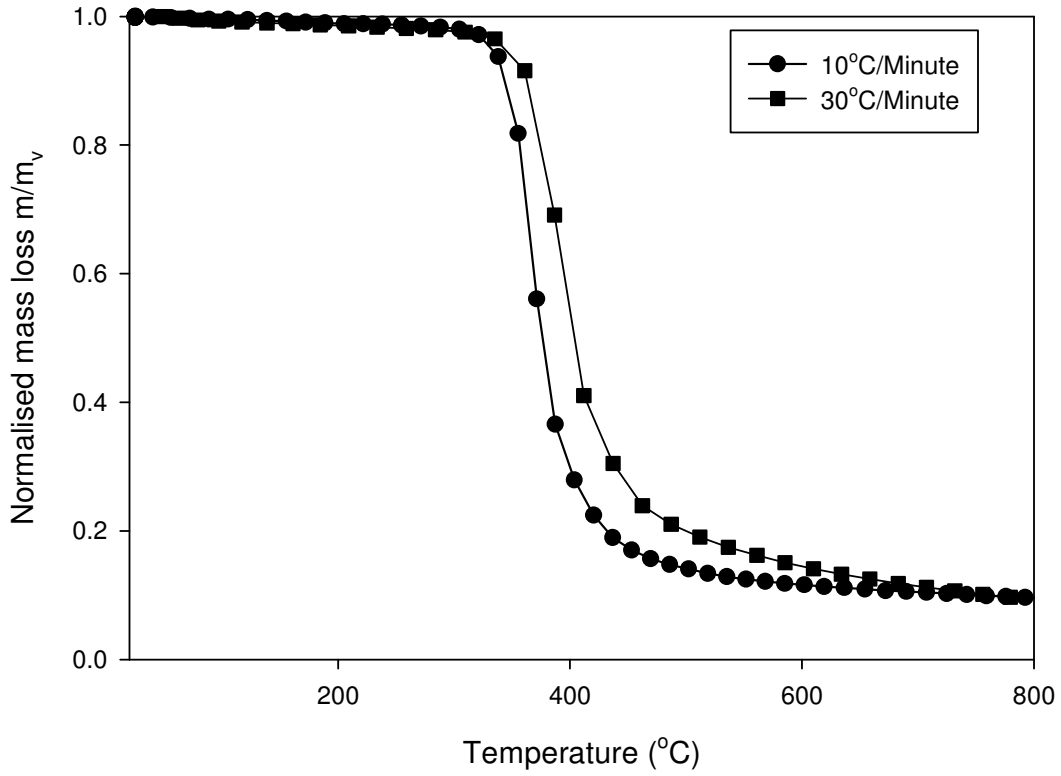

Figure 4.7: Mass loss curves for Ampreg 22 epoxy resin in a nitrogen atmosphere

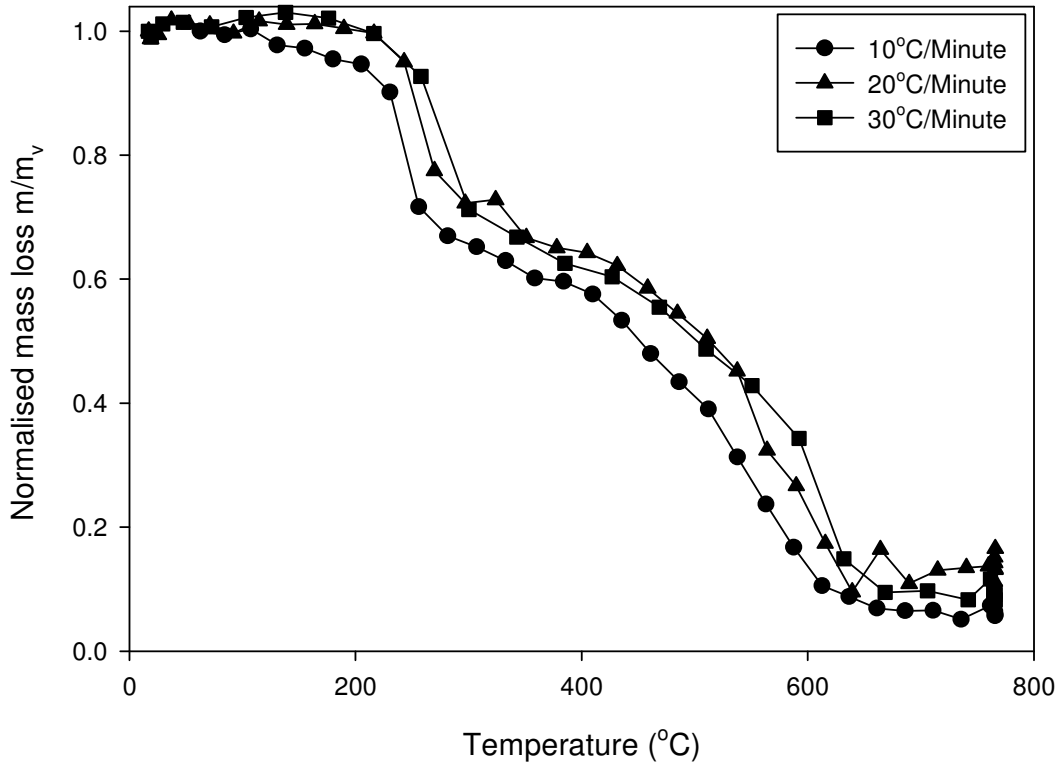

Figure 4.8: Mass loss curves for Divinycell H100 PVC foam in a nitrogen atmosphere

Table 4.5 shows the kinetic properties calculated in the TGA experiments using Friedman's method [Henderson, Tant et al. 1981]. The details of the calculations are given in Appendix B.2.

Material	**E_a (kJ/kg-mol)**	**N**	**A (s^{-1})**
Ampreg 22	4.06×10^4	2.78	115
Divinycell H100	0.997×10^5	0.626	1.15×10^6

Table 4.5: Kinetic constants determined from TGA experiments

For the kinetic properties of the foam the values refer to the first stage in the reaction. It was not possible to extrapolate the data required from the second stage of the reaction, due to the non-linear nature of the curves.

It was not possible to find any value for the kinetic properties of PVC foam to compare with these results. In the case of epoxy resins, all other literature that was found gave the values of activation energy between 56 kJ/mol and 490 kJ/mol with most authors giving values between 56 kJ/mol and 76 kJ/mol [Costa, Rezende et al. 2006; Davies, Wang et al. 2006; Ho, Leu et al. 2006]. In Krysl et al. [2004] the activation energy for a polyester resin is given as 5.0×10^4 kJ/kg-mol.

It is suspected that the units used by the authors given above have been misleading and that they should in fact be kJ/g-mol. This brings them in the same order of magnitude as the polyester value used by Krysl et al. [2004] and the value calculated by the author.

4.5.2 In-Plane Temperature Profile

The first objective in determining the temperature distribution across the hot and cold surfaces of the panels was to establish if there was a significant temperature difference between the top and bottom of the panels.

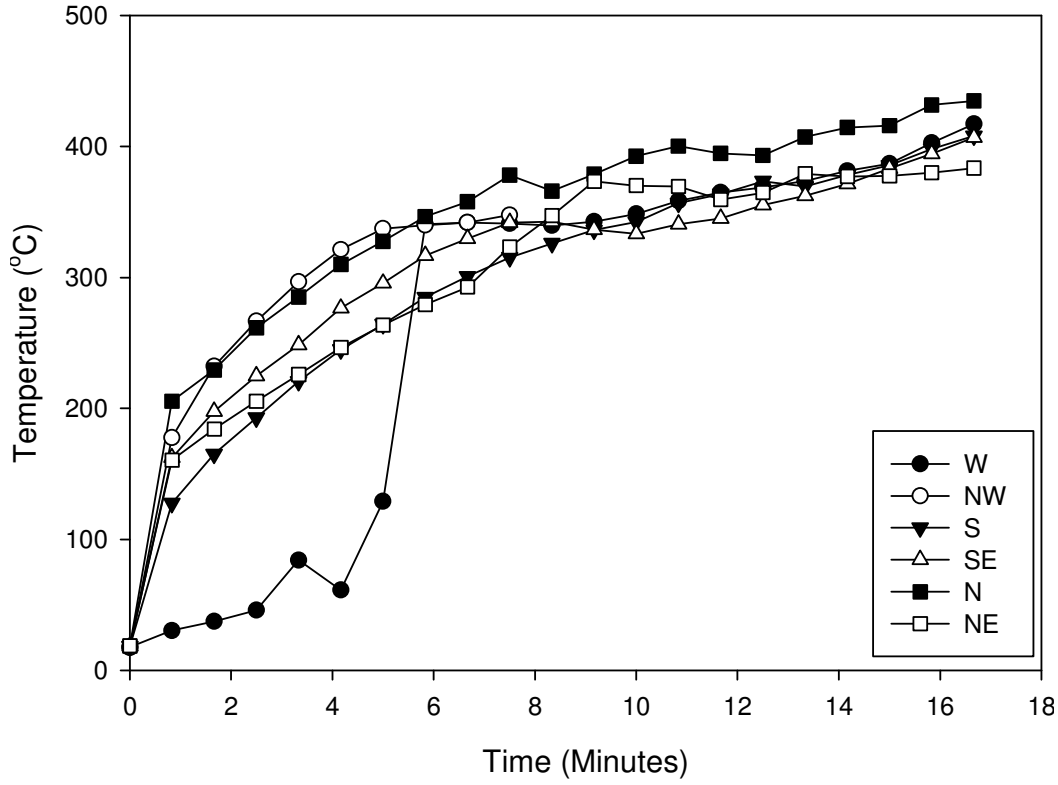

Figure 4.9: Temperature measurements taken from the hot surface at 90mm from the panel centre under the cellulosic fire curve. Legend refers to the location of the recording as a compass bearing.

Figure 4.9 shows there is a small amount of variation from the temperatures recorded at the edge of the panels. The reading taken at the top of the panel (N) is generally higher than the rest as would be expected due to the convection of hot gasses upwards. It can also be seen that there is an irregularity with the initial reading up to 6 minutes from the W thermocouple. These values were not used in determining the temperature spread over the panel. The average range of temperature readings was calculated to be 60.3°C with a standard deviation of 22.4°C. It was expected that the S and SE readings would be the lowest as they are at the bottom of the panel. The fact they are not consistently lower than the others indicates that there is a relatively even spread of temperature at 90mm from the centre of the panel and the variations are due to a natural fluctuations of

the flame. The same analysis was carried out with the thermocouples placed at 120 mm from the panel centre in the NW and SE positions and age range of the data was 11.4°C with a standard deviation of 8°C. Full results are given in Appendix B.4.

The above results have established that there is a degree of variation in the temperatures at equal distances from the panel centre but that the variation is random and does not appear to show a temperature gradient in any one direction.

In order to model the panel effectively in the thermo-mechanical model, to be presented in Chapter 6, it was necessary to know how the temperature varies from the centre outwards during a standard fire test. The following figure was produced by taking the average temperature from the readings at each of the set distances measured. These values were then subtracted from the average centre temperature and normalised with respect to the centre temperature.

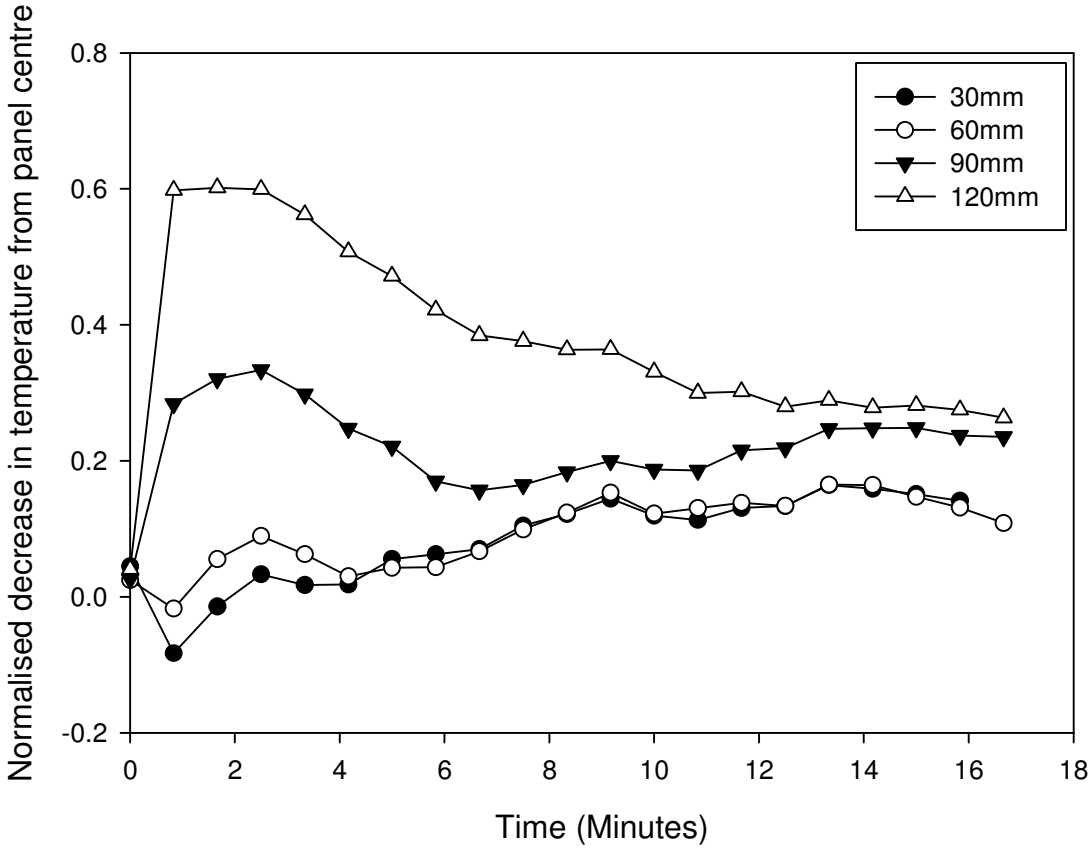

Figure 4.10: Normalised decrease in hot face temperature at set distances from the panel centre under cellulosic fire curve.

Figure 4.10 shows that initially there is a large decrease in temperature at the edges of the panel; up to 60% lower in the corners than at the centre. The variation appears to be non-linear until about 13 minutes at which point the temperature gradient is fairly even from the centre to the edges. The amount of variation is also decreasing with time as the panel temperature becomes more uniform. The graph also indicates that the temperature is relatively even between 30mm and 60mm from the centre.

This data will be used in creating a thermo-mechanical model of a panel subjected to fire and load, regions of equal temperature in the plane of the panels will be divided up as shown in Table 4.6

	Location	Temperature
Region 1	Central square 60mm × 60mm	T
Region 2	Square ring around region 1 140mm × 140mm	0.75T
Region 3	Area outside Region 2	0.5T

Table 4.6: Assumed regions of constant temperature in the plane of the test panels

4.5.3 Fire Resistance

One of the limitations of the apparatus set up was that it was not possible to directly observe the panels during the experiments. The panel faced the side of the fume cupboard housing and left little room to view the panels' cold faces. A mirror was positioned to view as much as possible, but the large amount of smoke generated often obscured the panel.

There was very little audible above the noise of the extraction system and the burner system throughout the tests. During the initial period of the tests there was a small amount of white smoke, emitted from the exhaust of the furnace, gradually becoming denser until about 50 seconds in to each test. By this point the smoke had become very dense and filled the fume cupboard. As the tests progressed smoke was escaping from the edge of the front plate of the furnace and from around the edges of the test panel. The extraction system inside the fume cupboard worked effectively and prevented any smoke from escaping into the laboratory. The smoke was, however, a problem after it had been emitted from the extraction system outside the laboratory building. It had a very strong odour and caused mild nausea in those who became exposed to it. This

caused some problems in the experimental programme and prevented a full series of experiments from being carried out. A scrubber system has been recommended to be built into the fume cupboard to reduce the effects of the fumes.

Once each test was completed it was possible to examine the panels and the apparatus. A sticky and viscous black liquid was left on the inside of furnace around the area where the test panel was secured. The odour of the burnt panels lingered around the apparatus after the panels had been disposed and it was necessary to seal the apparatus with a plastic sheet in between testing.

After each test, on the hot face of the panels, the resin had completely charred in every instance. The resin formed small clusters of a black char, which stuck to the fibres. The first few layers of fibres had become delaminated from the rest of the panel and were covered in the black char residue. Figure 4.11 shows the degradation, which occurred in the panels. For the longer duration test shown there was a small amount of decolouring of the cold side of the panel, which was not evident in the shorter duration test. It was also possible to see where the black liquid, previously mentioned, had flowed from the holes in the centre of the panel through which the thermocouple wires passed.

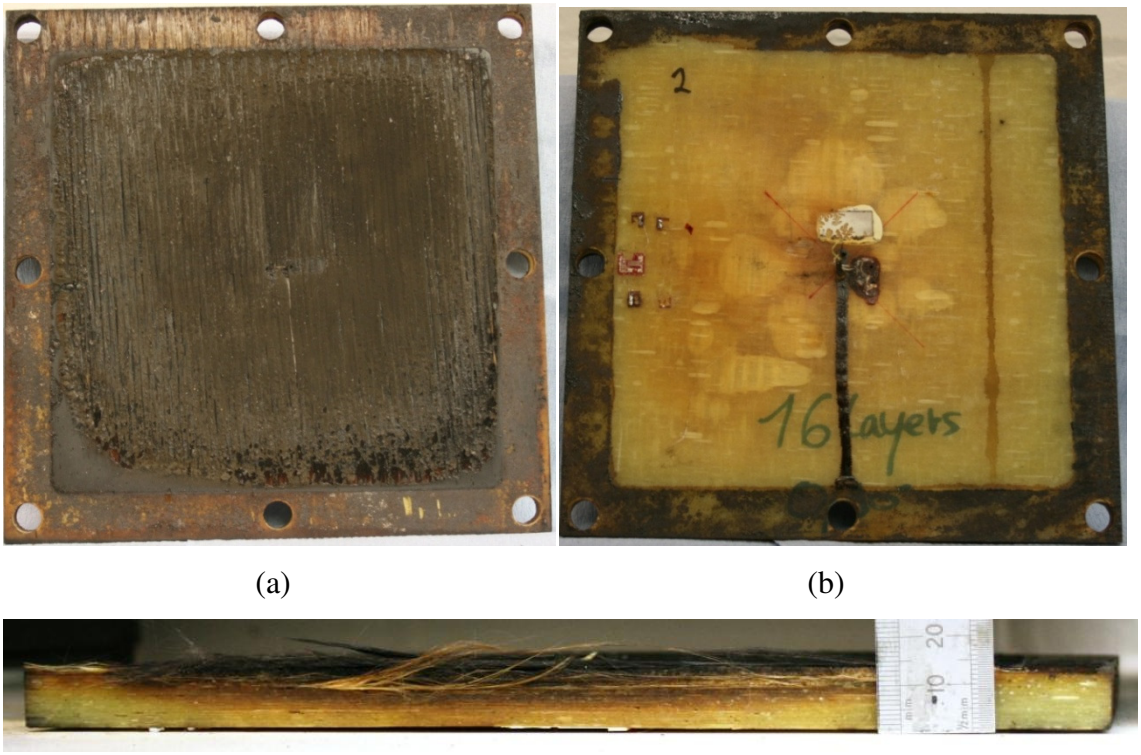

(a) (b)

(c)

Figure 4.11: Hot(a) and cold(b) face and cross-section(c) from panel SS.1C.1 after exposure to cellulosic fire curve for 20 minutes

On the sandwich panels the core appeared to undergo three stages of decomposition as shown in Figure 4.12. There is a black char region nearest to the heat source followed by a golden-brown band and then again by a black band of char at the cold side. It is also possible to see the delamination caused in the skins and a large cavity on the right hand side of the cross section.

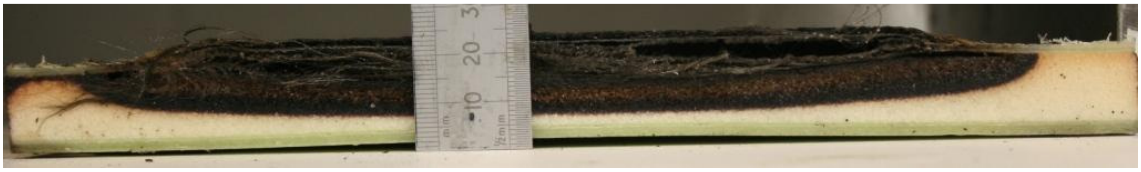

Figure 4.12: Cross section through sandwich panel SW.2.C.2 after exposure to cellulosic fire curve for 13 minutes.

In both single skin and sandwich panels the heat transfer appears to be mainly through the thickness. It can be seen in Figures 4.11 and 4.12 that the edges where the panels have been clamped have not charred. This indicates that the heat flow in the plane of the panels is minimal compared with the heat flow through the thickness.

The temperature readings from the single skin and sandwich fire resistance tests were compared with results predicted using the Krysl et al. [2004] MATLAB program. The sandwich panel results were also compared to the adapted program, which modelled the core decomposition as well as the skins. Table 4.7 shows the values that were input into the heat transfer models and the source of those values.

Property	Value	Source
A 22 epoxy resin thermal conductivity (W/m-K)-virgin state	0.17	Experimentation
e glass fibre thermal conductivity (W/m-K)-virgin state	1.04	[Looyeh, Bettess et al. 1997]
Divinycell H100 foam thermal conductivity (W/m-K)	0.05	Experimentation
A 22 /e glass fibre composite thermal conductivity (W/m-K)- charred state	V_f dependent Eq. (4.15)	[Jakob 1959; Krysl, Ramroth et al. 2004]
A22 specific heat capacity (J/kg-K)- virgin state	1000	[Davies, Wang et al. 2006; Gurit 2006]
e glass fibre specific heat capacity (J/kg-K)- virgin state	1300	[Lattimer and Ouellette 2006]
A 22 /e glass fibre composite specific heat capacity (J/kg-K)- virgin state	V_f dependent Eq. (4.13)	[Dodds, Gibson et al. 2000; Lua, O'Brien et al. 2006]
H100 specific heat capacity (J/kg-K)	1700	[DIAB 2007]
A22 specific heat capacity (J/kg-K)-charred state	$1.085 \times C_{pv}$	Ratio of C_{pv}:C_{pch} as for polyester [Dodds, Gibson et al.]
e glass fibre specific heat capacity (J/kg-K)- high temperature	1400	[Lattimer and Ouellette 2006]
Composite char specific heat capacity (J/kg-K)	V_f dependent Eq. (4.13)	[Krysl, Ramroth et al. 2004]
A22 density (kg/m^3)-virgin state	1046	Measurement
e glass density (kg/m^3)-virgin state	2580	[Callister 2000]
H100 density (kg/m^3)	98	Measurement
Composite density (kg/m^3)-charred state	V_f dependent	Measurement
A22 Activation energy (J/kg-mol)	0.406×10^5	Measurement
Pre-exponential factor (s^{-1})	115	Measurement
Order of reaction	2.78	Measurement
Heat of decomposition (J/kg)	-30000	[Davies, Wang et al. 2006]

Table 4.7: Material properties used in fire resistance modelling.

Taking the results from the panels tested at the higher temperature fire curve, rate A, it was noted that there was a degree of scatter in the experimental results.

Figure 4.13 shows the recorded temperatures from four single skin panels each with the same thickness ±0.05mm and the same weight ± 11g. The panel with the highest recorded hot face temperature does not have the highest mid-thickness or cold face temperature as would be expected. Therefore the input hot face temperatures taken to validate the heat transfer model were the highest and lowest hot face temperatures of the four tests, taken as SS6.A.2 and SS6.A.1. It should be noted that on panel SS6.A.3 the cold face thermocouple fell off after two minutes.

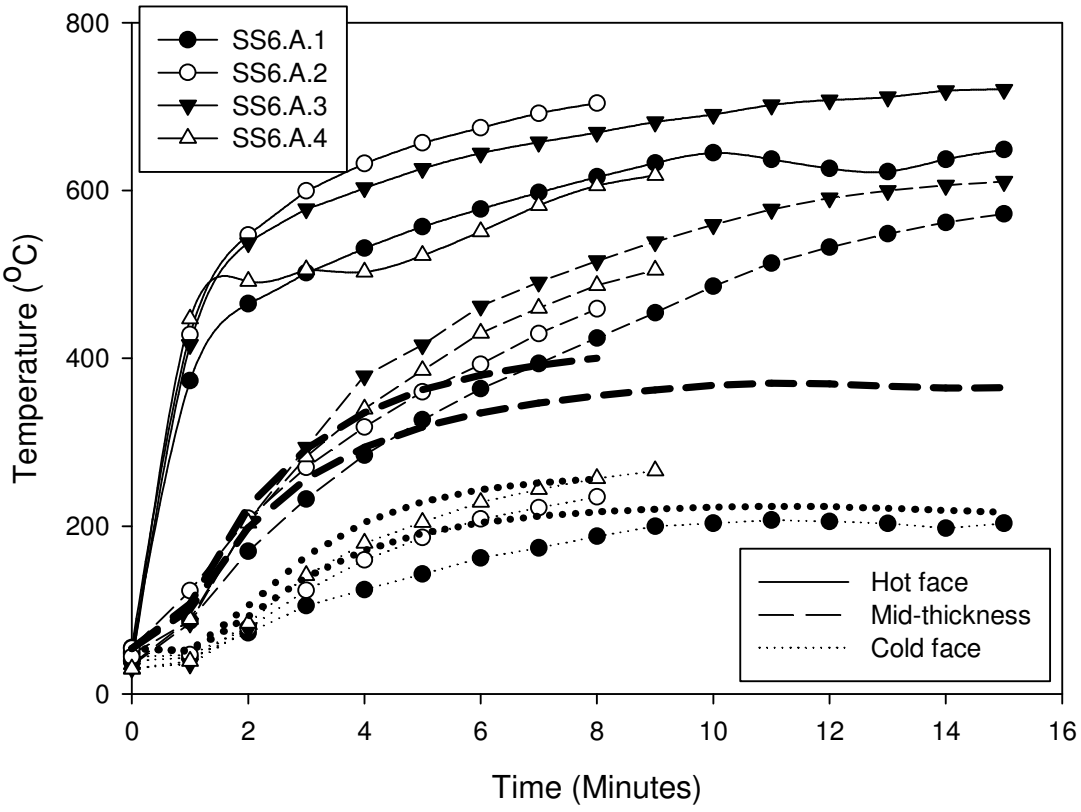

Figure 4.13: Comparison between predicted temperatures and temperatures recorded from experimentation for SS6 panels under heating rate A. The bold dashed and dotted lines represent the predicted mid-thickness and cold face temperatures respectively.

The hot face temperature profiles were input into the heat transfer program [Krysl, Ramroth et al. 2004] using the constants shown in Table 4.7. Initially the cold face heat transfer coefficient was set to 1 W/m^2-K as was used in the validation performed in Krysl et al. [2004], assuming a fully insulated cold face. It was found that with this condition the output temperatures on the cold face were much higher than the

experimental results. With a heat transfer coefficient set to 50 W/m^2-K on the cold face the predicted results fall within the range of experimental data as can be seen in Figure 4.13.

The results at mid-thickness match the predictions initially but then continue to increase where the predicted temperatures level off. The increasing temperatures recorded from the mid-thickness thermocouple do not display the characteristics of a decomposing composite as described in much of the literature. In this 'ideal' composite, as described in the literature, it becomes more insulating as it degrades due to the decomposition endotherm, the convection of volatile gasses and the lower thermal conductivity of the degraded material. The behaviour shown here does correlate with the findings in Dodds et al. [2000] where it was stated that the Henderson model is less accurate for laminates less than 10mm thick. It was proposed that the reason for the difference, particularly it would appear near to the hot surface, is that: as the resin degrades the layers become more permeable to the hot gasses from the fire, which is not reflected in the modelling. Another factor that could explain the difference in the accuracy in this case compared with the results shown in Henderson et al. [1985] is the heating source. In the experiments conducted by Henderson et al. the heat source was a radiant heater, which would not be expected to produce the same level of erosion that a flame would provide. The flame in these experiments fired directly on to the panels at a velocity of 0.003-0.008 m^3/s.

The following graphs show the temperature recordings from the single skin panels tested under the cellulosic fire curve. In each case the experimental results are compared with predicted temperatures at each thermocouple location. The experimental results are shown by the solid lines and the predicted results by the dashed lines. A full set of the graphs and predictions are shown in Appendix B.3.

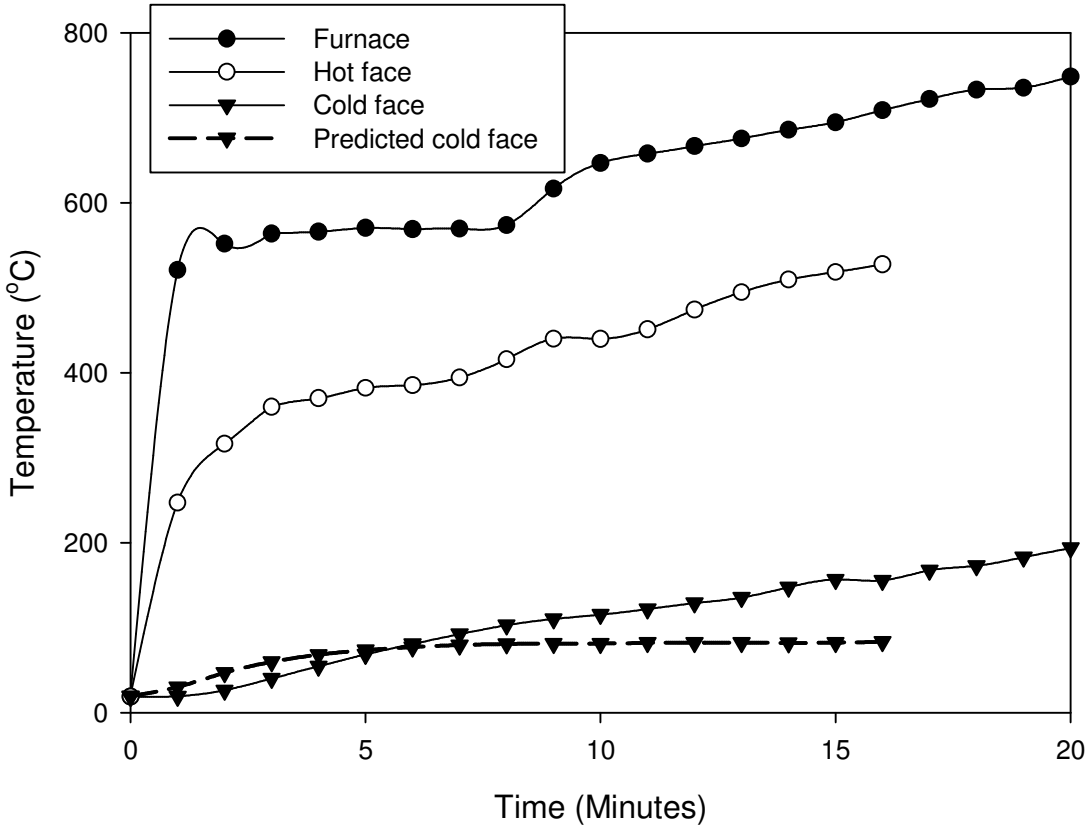

Figure 4.14: Comparison of predicted cold face temperature with experimental results for panel SS 1C.1 under cellulosic fire curve

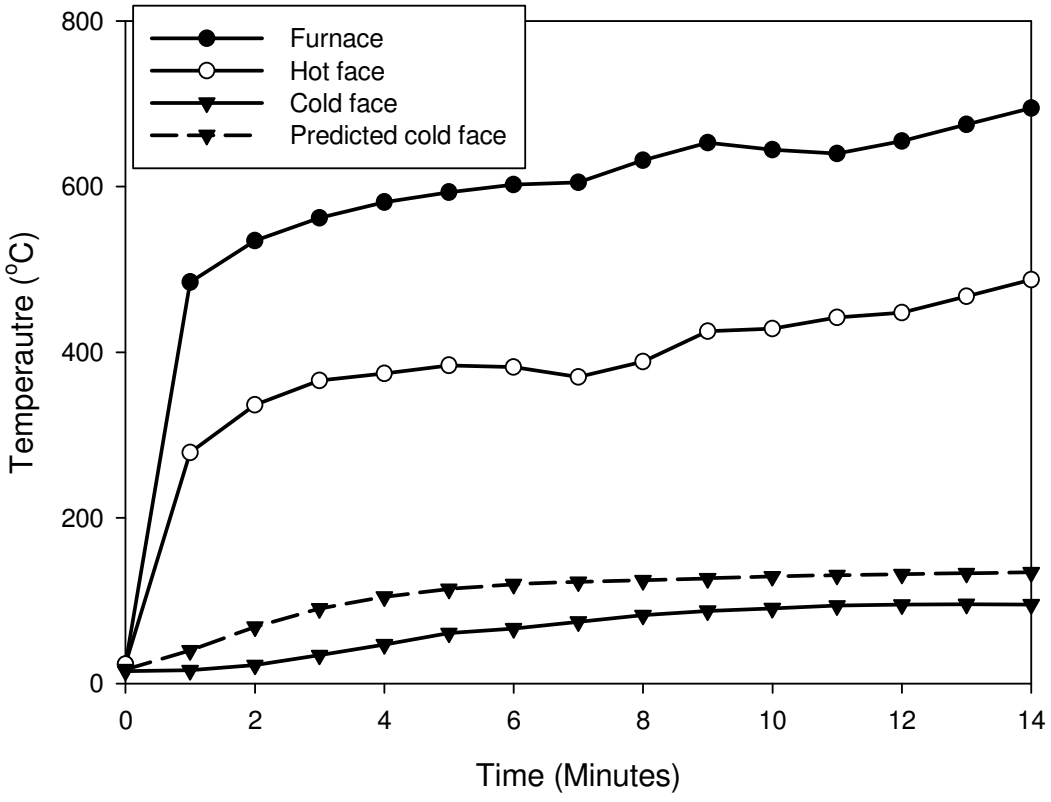

Figure 4.15: Comparison of predicted cold face temperature with experimental results for panel SS 2.C.1 under cellulosic fire curve.

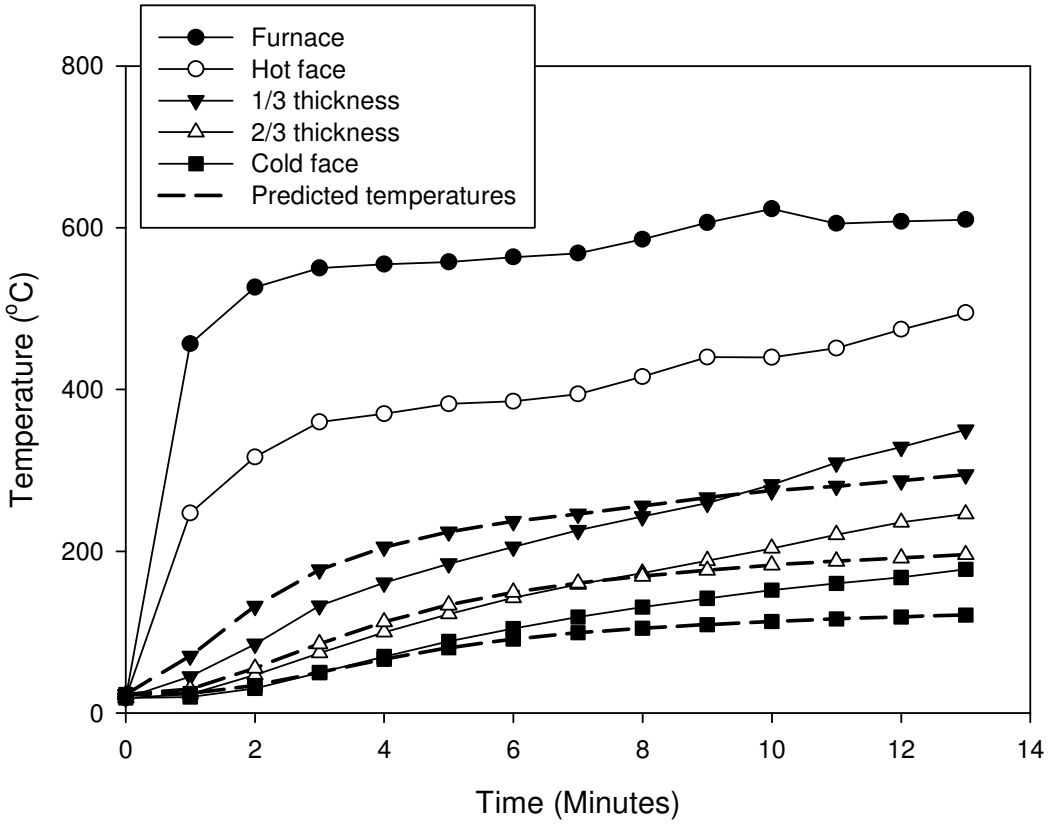

Figure 4.16: Comparison of predicted cold face temperature with experimental results for panel SS 1.C.2 under cellulosic fire curve.

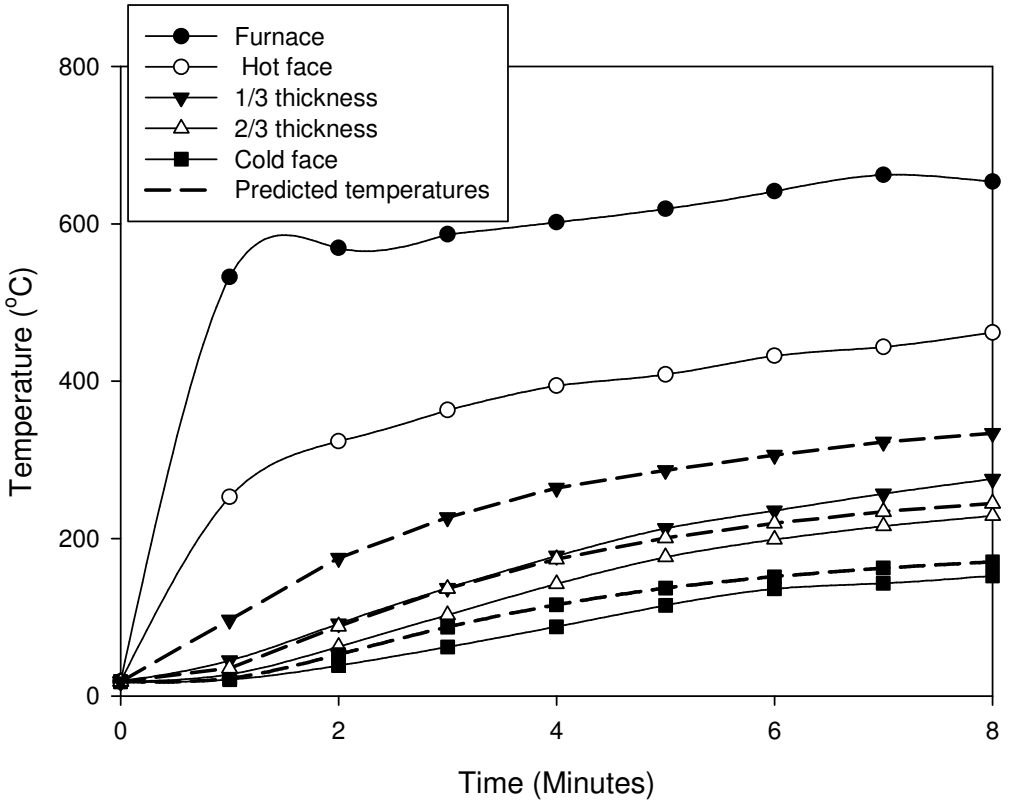

Figure 4.17: Comparison of predicted cold face temperature with experimental results for panel SS 6.C.1 under cellulosic fire curve.

Test id	Duration (mm:ss)	Thickness (mm)	Mean temp difference (^{o}C)
SS 1.C.1	20:06	11.8	23
SS 1.C.2	8:20	10.7	25
SS 2.C.1	14:30	10.9	42
SS 2.C.2	12:16	11.6	21
SS 3.C.1	08:00	11	21
SS 4.C.1	10:00	8.8	15
SS 4.C.2	12:00	9.12	28
SS 5.C.1	08:54	8.8	26
SS 6.C.1	08:24	9.1	35

Table 4.8: Summary of fire resistance tests on single skin panels under cellulosic fire curve

Under the cellulosic conditions there is a reasonable correlation between the experimental and predicted cold face temperatures and the results from Table 4.8 show the mean differences to be in line with the differences quoted by previous authors. These were quoted to be 29.66^{o}C in Looyeh et al. [1997] and 21.41^{o}C in Looyeh et al. [1998] where temperature dependent properties were used.

The following graphs show the temperatures recorded from the thermocouples in the sandwich panel experiments and again the solid lines represent the recorded temperatures and the dashed lines represent the predicted temperatures.

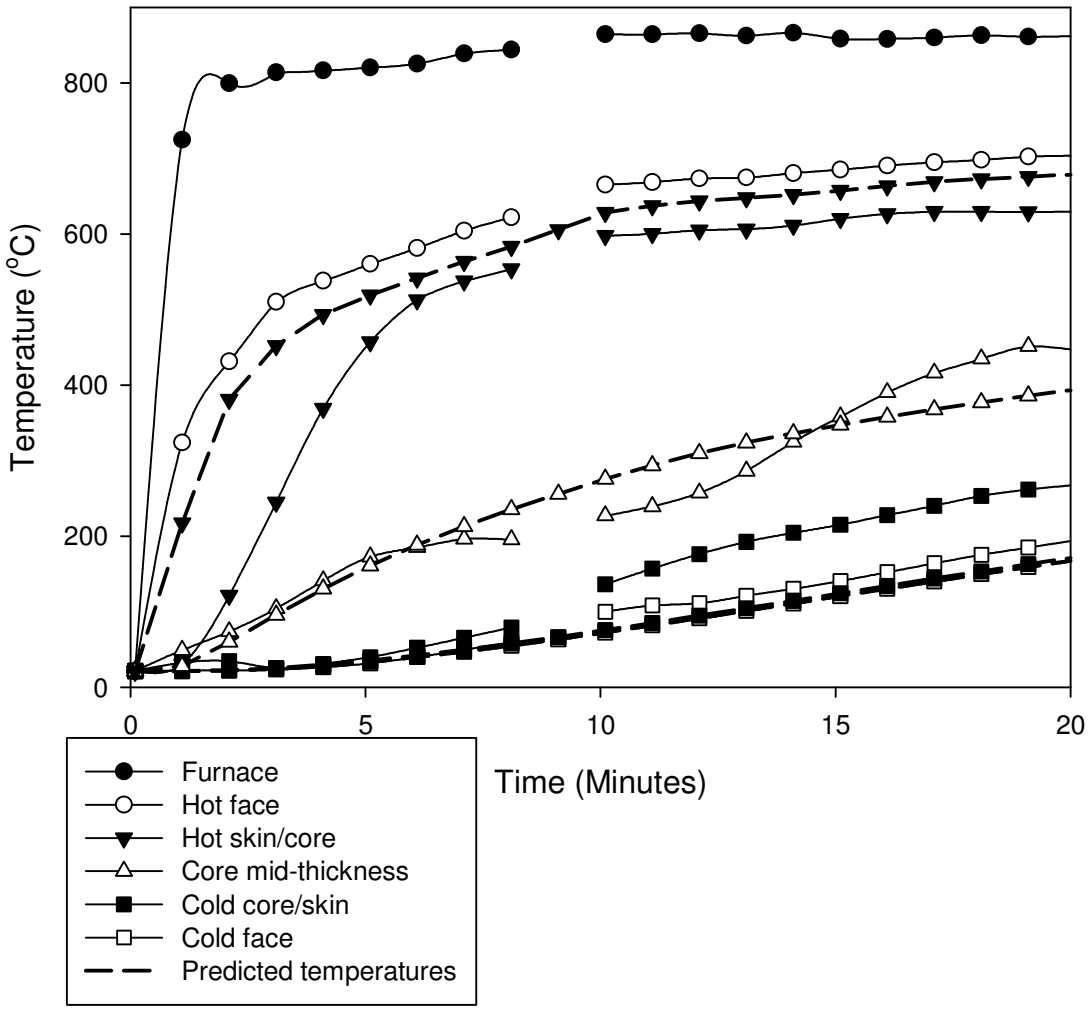

Figure 4.18: Comparison of predicted temperatures with experimental results for panel SW 1.A.1 under cellulosic fire curve.

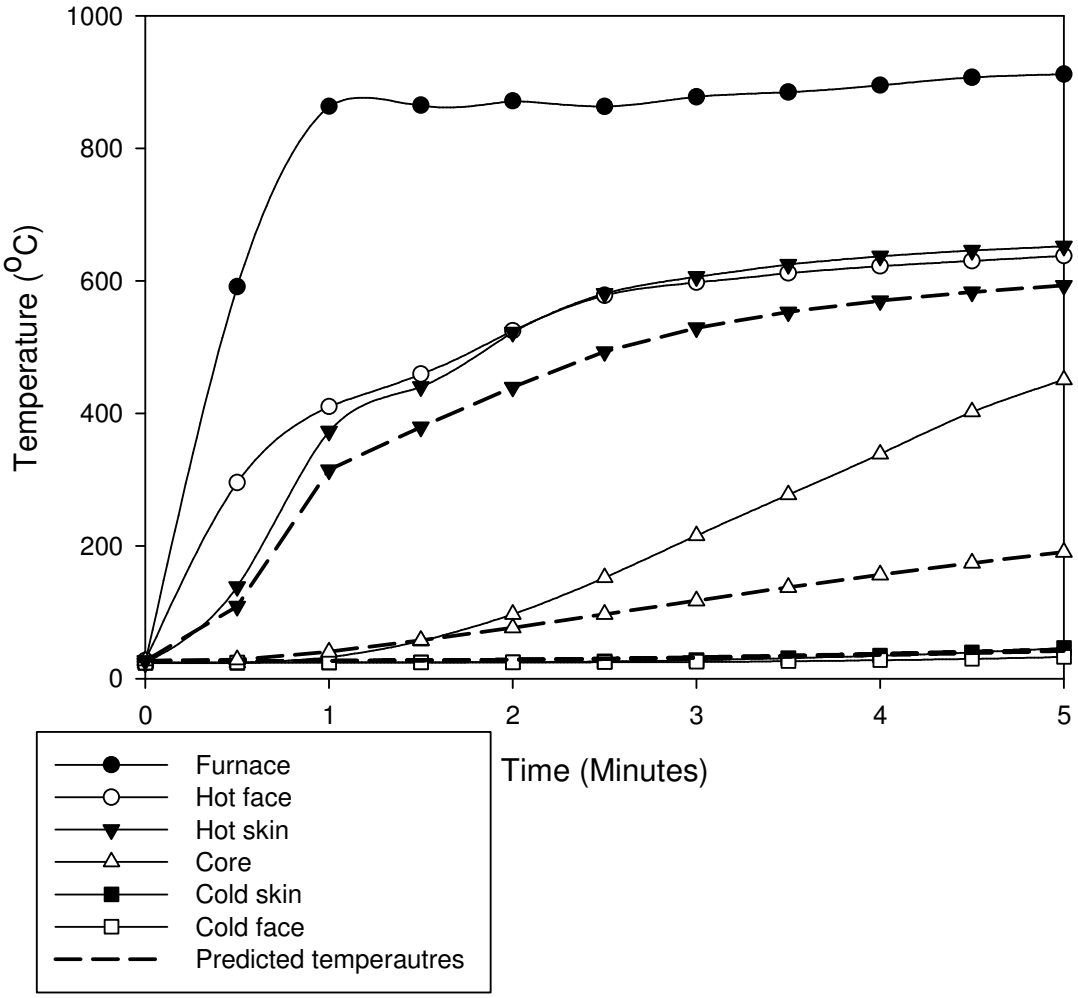

Figure 4.19: Comparison of predicted temperatures with experimental results for panel SW 1.A.2 under cellulosic fire curve.

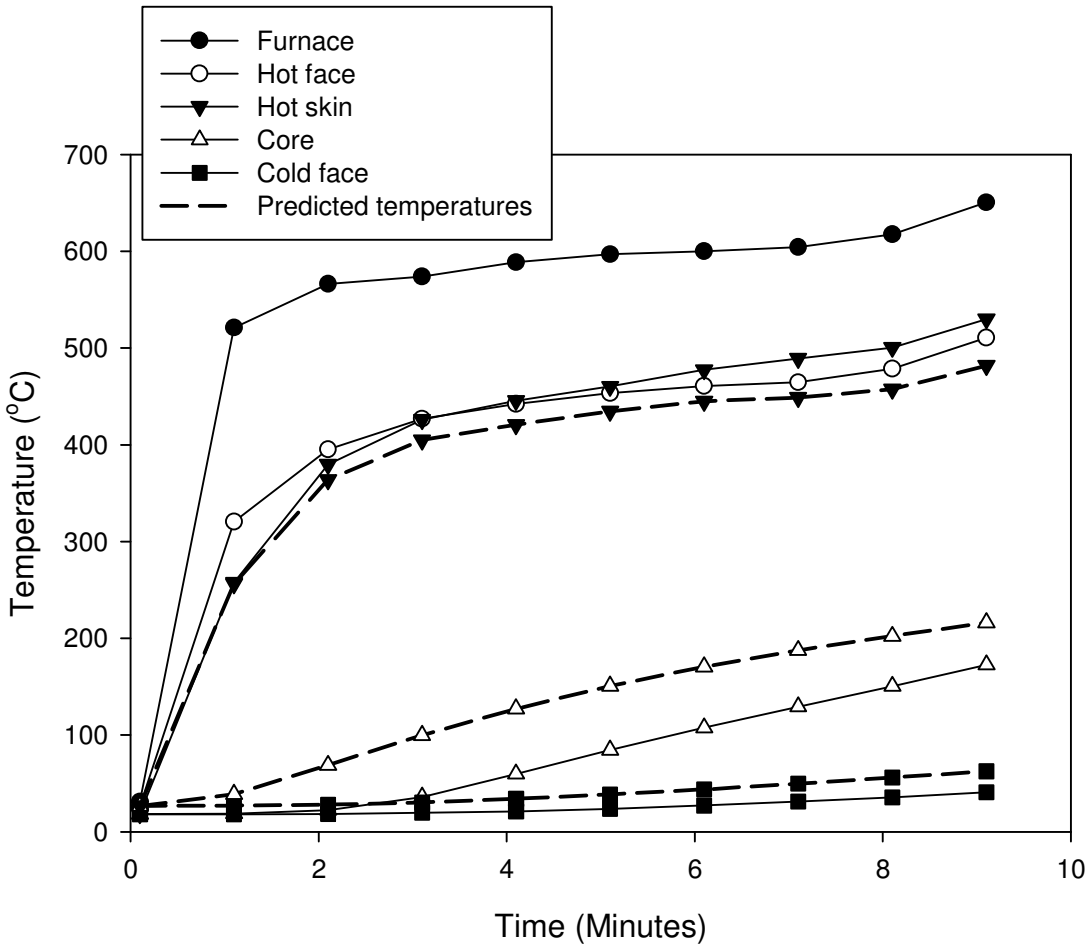

Figure 4.20: Comparison of predicted temperatures with experimental results for panel SW 1.C.1 under cellulosic fire curve.

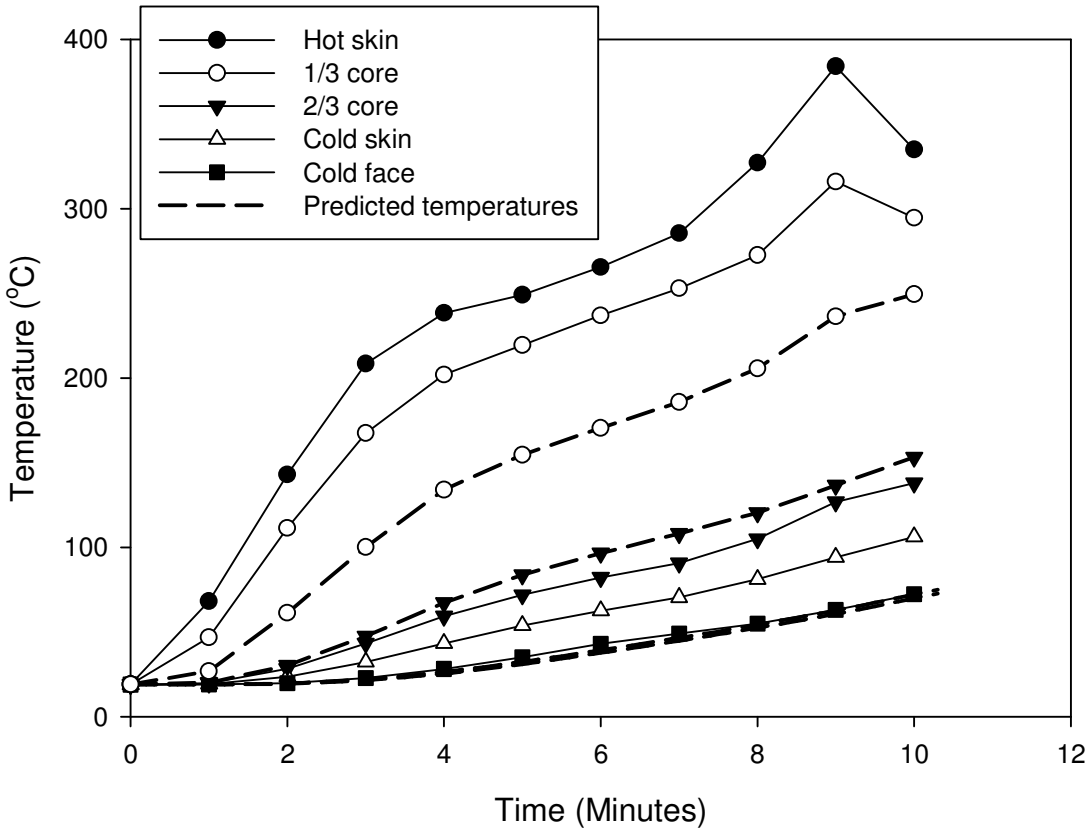

Figure 4.21: Comparison of predicted temperatures with experimental results for panel SW 2.C.2 under cellulosic fire curve.

Test id	Duration (mm:ss)	Mean temp difference (°C)	Fire curve
SW 1.A.1	21:06	42	Rate A
SW 1.A.2	05:00	39	Rate A
SW 1.C.1	09:36	31	Cellulosic
SW 1.C.2	08:36	61	Cellulosic
SW 2.C.1	13:12	18	Cellulosic
SW 2.C.2	10:18	22	Cellulosic

Table 4.9: Summary of fire resistance tests on sandwich panels

The predictions shown in Figure 4.18 to Figure 4.21 were all compiled using the heat transfer program, which assumes a non-decomposing core. The mean temperature differences were only slightly higher than the differences recorded in the single skin

panels, indicating that in the early stages of a cellulosic fire heat transfer through the core is linear.

The temperature difference between the hot and cold faces at 10 minutes into the test were recorded and then normalised with respect to the panel thickness and density. The average values for single skin and the two sandwich panel types are shown in Table 4.10. Here it is possible to compare the merits of each type of panel with respect to their insulating properties. The single skin panels perform best with respect to the panel thickness with an average temperature difference of 30 ^{o}C/mm between the hot and cold faces. In terms of the best insulating panel type with respect to the density the thick sandwich panel performs best with an average temperature difference of 1.2 ^{o}C/(kg/m^{3}), which is 7 times more insulating than the single skin panels per unit density.

Panel type	**Temperature drop per unit thickness (^{o}C/mm)**	**Temperature drop per unit density (^{o}C/(kg/m^{3}))**
Single skin panels	30	0.17
Sandwich 25mm core 1.5mm skins	21	1.2
Sandwich 15 mm core 1.5mm skins	13	0.6

Table 4.10: Average temperature difference between hot and cold face recorded temperatures for test panels over 10 minutes under Cellulosic fire curve

Very little experimental work has been conducted on foam cored sandwich materials subjected to fire. Davies et al. [Davies, Wang et al.] attempted to look at sandwich panels with 35kg/m^{3} phenolic foam cores. The tests were not completed as the foam burned too quickly. A numerical model was used to predict the cold face temperatures of sandwich panels with mineral wool cores and the results showed a maximum of 18^{o}C difference after 2 hours.

The results taken from the strain gauges showed no correlation and more work needs to be done in order to find an effective method of measuring strain at high temperatures.

4.6 Conclusion

The objective in this chapter was to predict and compare the thermal effects of fire on composite structures. This has been achieved by the development of a specific fire testing apparatus, the testing conducted with the apparatus and the verification with numerical models.

The apparatus that has been developed has been shown to be capable of subjecting small composite test panels to conditions representative of the full scale fire tests. The measured temperatures inside the furnace followed the standard BS 476 cellulosic fire curve for the first 30 minutes within the allowable limits. This will allow future users to compare the insulating performance of different materials in a fire at small scale in a fast and economical manner. It will also give an indication to the fire rating of different materials for use in ship structures.

It was discovered that the heat transfer through the sandwich core was near linear for a duration of up to 20 minutes in a cellulosic fire. In addition it was also discovered that the heat flow is very small in the transverse direction in both the single skin and sandwich panels. This meant that whilst subjecting the centre of the panels to fire the adjacent areas around the edges were relatively unaffected. Results from TGA and the fire resistance tests indicated that the PVC foam undergoes 3 stages of thermal decomposition. These results have all aided in furthering the understanding of composite materials in fire.

The heat transfer model developed by Krysl et al. [2004] has been shown to accurately model the heat flow within a single skin composite subjected to fire. The average temperature difference measured from all of the sample thermocouples was 26^{o}C, which is very close to the level of accuracy found by other authors using similar models.

The modelling of heat flow through sandwich panels was less accurate and an average temperature difference of 36^{o}C was found between predicted temperatures and the recorded values. The most effective method of modelling the sandwich panels was to assume linear heat flow through the core and model the skins as in the single skin

panels. For longer duration tests, where the core would decompose more it is suspected that this assumption may not hold.

As indicated in the methodology the results from this chapter, both experimental and predicted will be used to create thermo-mechanical models, which are described in Chapter 6.

5 Temperature Dependent Properties of Composite Materials

5.1 Introduction

This chapter aims to devise a method for obtaining the temperature dependent mechanical properties of the constituent materials in single skin and sandwich composites. The results are also to be used in creating thermo-mechanical models detailed in Chapter 6. The work from this chapter fits into the overall methodology described in Chapter 3 in Figure 3.2, Route 1, stage 2.

Tests have been performed at discrete elevated temperatures to determine strengths and stiffness's and the results have been interpolated in between these points. Using a rule of mixtures approach [Hull and Clyne 1996] the mechanical properties of laminates and sandwich panels have been derived from room temperature up to the point at which the values become negligible. These properties will then be used to link the heat transfer model discussed in Chapter 4 to the mechanical models discussed in Chapter 6. The resulting thermo-mechanical model will be used to predict the response of samples to combined load and fire tests.

The literature review, in Chapter 2, highlighted how some thermo-mechanical models have been created by other authors. Two types of approach were used, namely; temperature dependent strength and moduli [Chen, Sun et al. 1985; Griffis, Nemes et al. 1986; Dao and Asaro 1999] and a two layer approach where the layers have been defined by temperature [Gibson, Wright et al. 2004] and by temperature and mass loss [Feih, Mathys et al. 2005]. The benefit of the of using temperature dependent material properties over the other models proposed is that it can be easily integrated in to a finite element model and it allows the response of a more complex geometry to be predicted.

The approach used here is similar to that used by Chen et al. [1985] and by Dao and Asaro [1999]. The benefit of this work is that the relationships are being derived from experimental data rather than being derived analytically as was the case in Chen et al.

[1985]. Here the relationship has been created by testing resins and core materials individually at discrete elevated temperatures. For the resin samples the testing was confined to tensile loading and for the core samples testing under shear loading was carried out.

The testing of fibres has not been carried out for two reasons. First, glass fibres are known to vary very little in strength and stiffness up to 450^{o}C [Otto 1959; Agarwal and Broutman 1980; Hull and Clyne 1996; Cerny, Glogar et al. 2007], which is at least 100^{o}C above the point at which all strength is lost in most resins [Gibson, Wright et al. 2004]. Secondly, the process of testing the strength and stiffness of fibres is a complex one in which a testing machine capable of gripping individual fibres is required. The results obtained by Cerny et al. [2007] and Otto [1959] have been used in determining the strength and stiffness of glass fibres at elevated temperatures.

5.2 Experimental Apparatus

Tensile properties of resins and shear properties of foams were tested in an Instron 8872 servo-hydraulic machine, which was adapted to allow the temperature to be controlled. The apparatus was fitted with a 10kN load cell to measure the load to a precision of 0.01N. An inbuilt transducer measured the actuator displacement to a precision of 0.001mm.

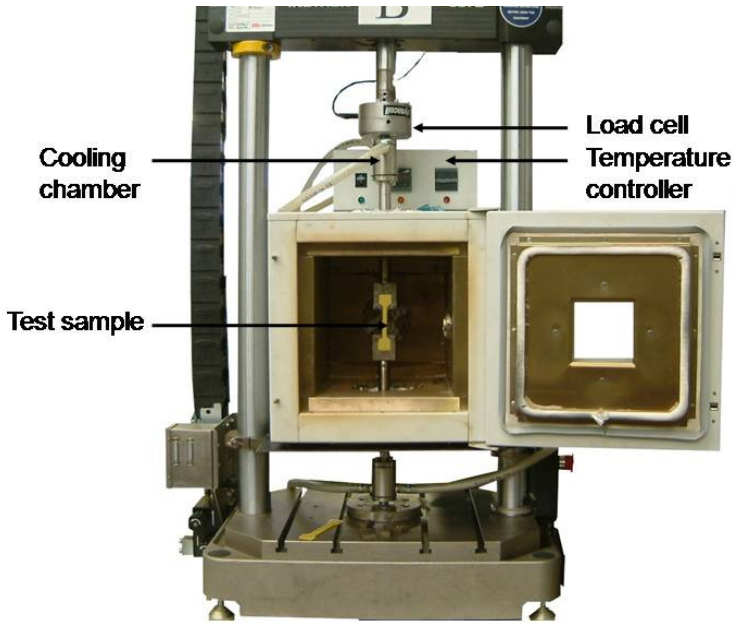

Figure 5.1: Elevated temperature tensile testing apparatus

Figure 5.1 shows the test set up; a fan assisted oven was fixed to the test machine to subject the sample to elevated temperatures. Extensions were fixed to the load cell and to the base of the test machine to allow the sample to fit inside the oven. The extensions contained hollow chambers into which cooling water was pumped to prevent the heat from the oven conducting through to the load cell. The temperature inside the oven was controlled by a Eurotherm 2416 temperature controller. This is a single loop PID controller with a single temperature feedback via a fibreglass insulated K-type thermocouple, which is attached to the test sample. The oven temperature was also recorded using two stainless steel sheathed k-type thermocouples located at the top and bottom of the oven. The oven was able to heat the samples at a rate of 10^{o}C per minute on average from room temperature up to a maximum temperature of 250^{o}C. The grips for the dog-bone shaped test samples were manufactured to type 1B samples as defined in ISO 527. These were 3mm thick, had a gauge length of 100mm and a gauge width of 10mm. This particular type was chosen due to the size restrictions inside the oven.

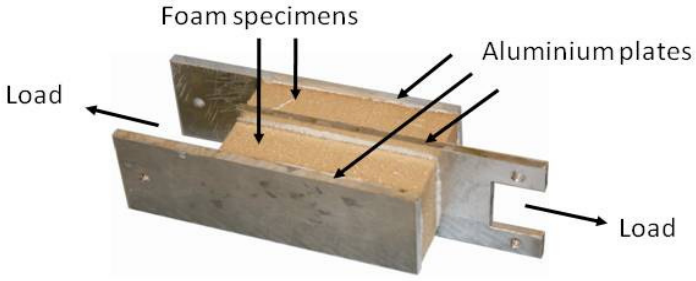

Figure 5.2: Shear test jig for foam samples

The tests on the shear properties of foam samples were conducted on the same test machine, using the jig shown in Figure 5.2. The method for shear testing was based on BS EN12090 [1997]. The foam samples, which measured 100mm long × 50mm wide × 30mm thick, were bonded to the aluminium plates with Loctite Hysol 9492; a high temperature two-part epoxy adhesive. The extensions were used again to allow the samples to be housed in the oven during the tests.

5.3 Experimental Procedure and Test Matrix

5.3.1 Resins

Two types of resin were tested; Ampreg 22 epoxy and Prime 20 epoxy. Both were manufactured by Gurit. Ampreg 22 is suited to wet lamination and Prime 20 is suited to infusion.

The samples were made by a casting process with the mixed resin poured into silicone moulds. The samples for both resins were post cured at 50°C for 16 hours, in accordance with the manufacturer's recommendations.

In each test the samples were heated to the required temperature from room temperature with no load and as soon as the test temperature had been reached a tensile load was applied at a rate of 5mm per minute. The temperature, load and actuator displacement were recorded throughout the test at a recording rate of one Hertz, onto a PC using a Measurement Computing USB1208LS analogue to digital converter. The signal was processed on the PC using the DASYLab 4.0 software. The mass of the samples was also recorded, before and after each test.

Tests with the Ampreg 22 samples were conducted at the following temperatures, in degrees Centigrade: 20, 30, 40, 50, 60, 70, 80, 90, 110, 130, 150, 170, 190, 210, 230 and 250. For the tests up to 190°C five samples were tested at each temperature, above this only two samples were tested. This was due to the time taken to heat the samples and the lack of significance of the results at the higher temperatures. If any anomalies were encountered with the results the tests were repeated.

The Prime 20 samples were tested at the following temperatures, in degrees centigrade: 30, 50, 70, 90, 110, 130, 170, 210 and 250. Five samples were tested at temperatures up to 190 and one sample at temperatures above 190°C.

5.3.2 Core

The core material tested was Divinycell H100. This is a PVC closed cell foam with a density of 100kg/m^3 and is produced by Diabgroup. The foam is commonly used in the marine industry and is the core used in the sandwich structures found onboard the RNLI all weather lifeboats. The dimensions of the samples differed from those described in BS EN 12090:1997 due to the restrictions of the space available in the test oven. The samples were fixed to the aluminium plates using Loctite Hysol 9492, which has a quoted shear strength of 15MPa for aluminium adhesions and 1.9MPa for PVC foam adhesions.

The shear strength of the adhesive is greater than the reported shear strength of Divinycell foam, which is 1.6 MPa at room temperature this should therefore have allowed failure to occur in the foam first. Loctite Hysol 9492 also has a low temperature cure, which means there was little heat generated, which could have affected the mechanical properties of the foam. For each test the plates were scored with a coarse file to add as much friction as possible to the bond. They were then cleaned with a solvent and allowed to dry, before the foam was bonded. The plates were held together in G-clamps during the cure, which was three days at room temperature, in accordance with the manufacturer's recommendations. For each test the feedback for the temperature control was measured using a K-type thermocouple, these were held in contact with the foam by high temperature adhesive tape. In addition to this a foam block with the same dimensions was placed in the oven and a thermocouple was inserted into the centre of the block. Once the centre temperature had reached the target temperature the loading commenced at 3mm per minute in the direction indicated in Figure 5.2. One sample was tested at each of the following temperatures: 20°C, 60°C, 80 °C, 100 °C, 120 °C and 140°C.

A third piece of foam was heated for the same length of time at each temperature and the change in mass was recorded.

5.4 Results and Discussion

5.4.1 Resins

From each test the load and deflection data was recorded at a frequency of one Hertz, the stress and strain and Young's modulus were calculated in the manner described in ISO 527-1 along with the yield stress and the tensile strength, where relevant.

The results of the tests at 20°C, shown in Figure 5.3, show a linear elastic relationship between the stress and strain and a brittle failure. The brittle failure was also observed in the samples and the break occurred in the centre of the parallel section. The failure stress varies from 54 MPa to 76 MPa and strain from 4.7% to 7.3% but the Young's modulus shows little deviation from the mean value of 1.48GPa.

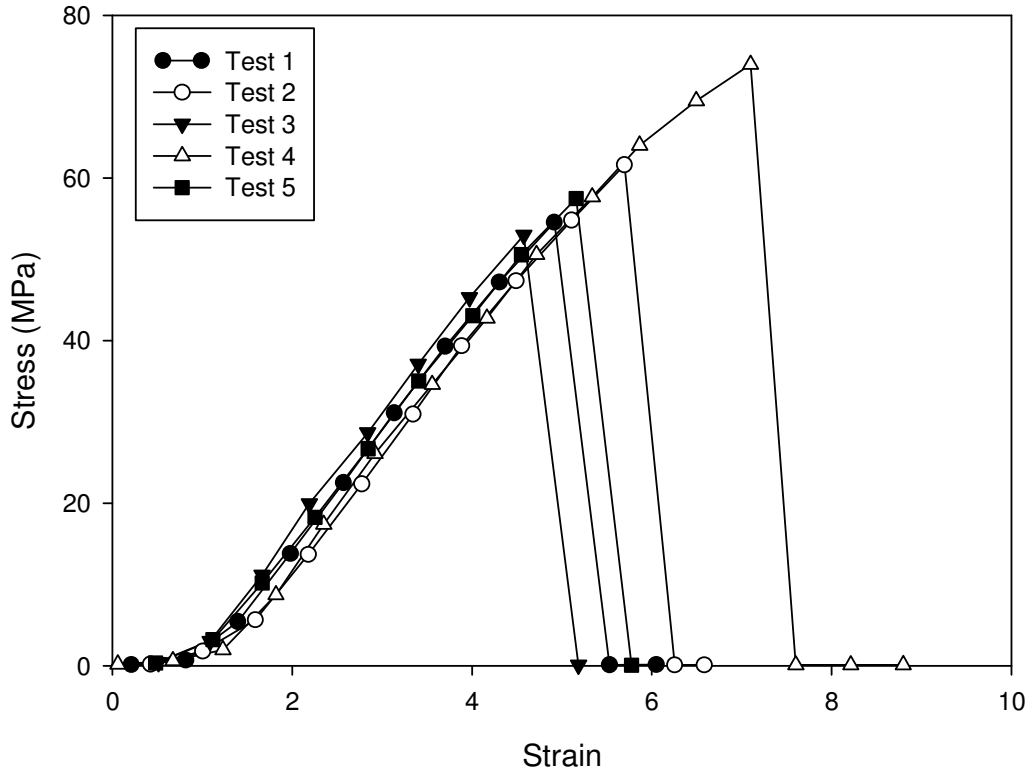

Figure 5.3: Stress vs. strain results for tensile tests of Ampreg 22 castings at 20°C

From Figure 5.4 the results of the tests at 50°C can be seen and the behaviour of the samples is less linear as the resin becomes more plastic. The maximum stress is 16% lower than that shown at 20°C, and the maximum strain is 40% higher. There is also much less variation in maximum stress at 50°C than was evident at 20°C. As was the case at 20°C there was again no necking in the samples observed during the tests and failure occurred within the parallel section. Note the change in scale on the strain axis from the previous figure.

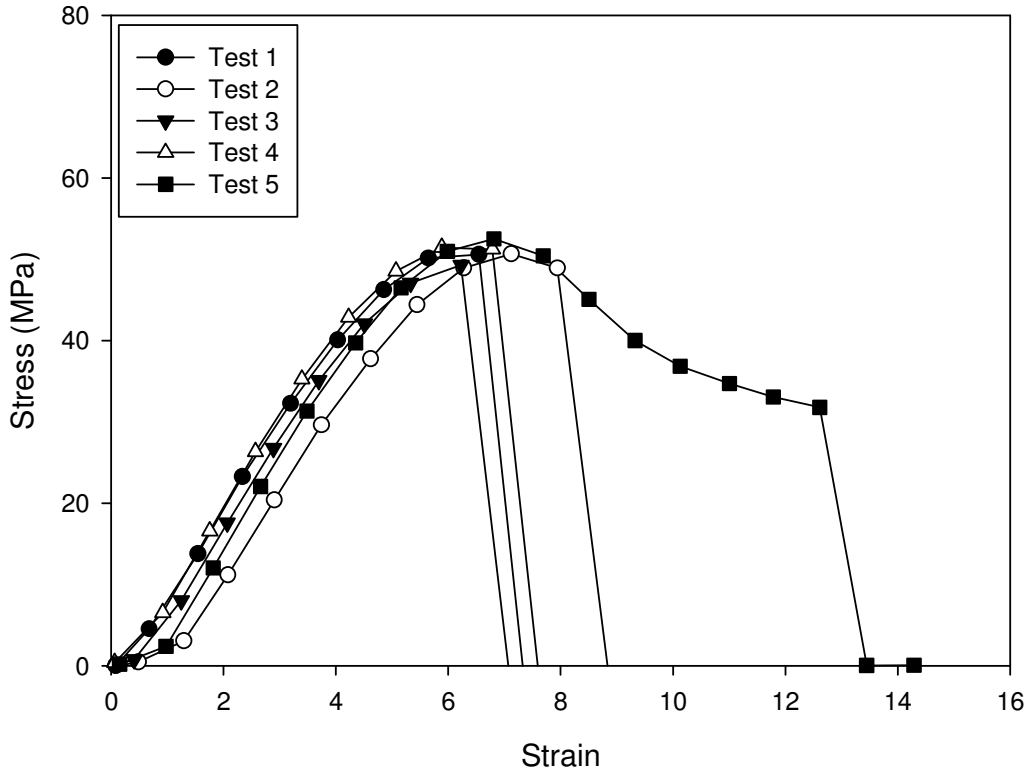

Figure 5.4: Stress vs. strain results for tensile tests of Ampreg 22 castings at 50°C

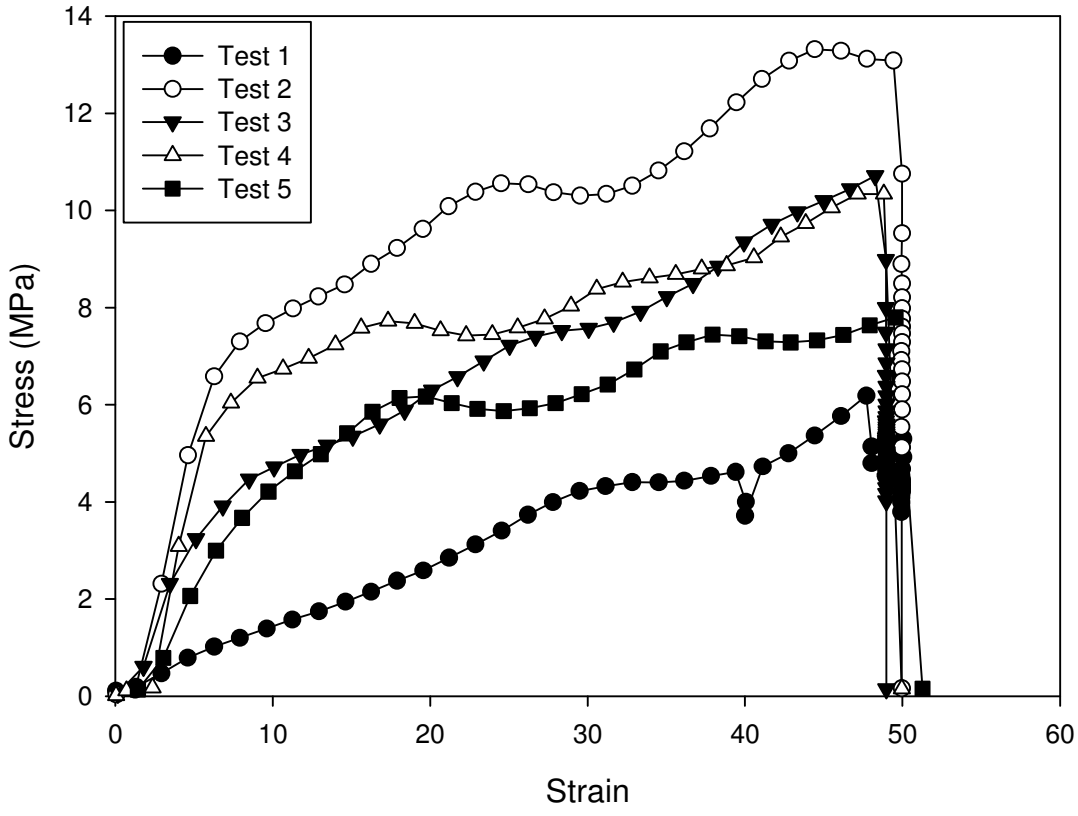

Figure 5.5: Stress vs. strain results for tensile tests of Ampreg 22 castings at 70°C

Figure 5.5 shows the results at 70°C and the first significant feature is that there is a dramatic drop in the yield stress compared to the results at 50°C and that the failure strain has also increased markedly from the previous two figures. Note the change in scale on both axes. The curves show considerable plastic deformation and a certain amount of stress relaxation before failure. There is also a greater variation of results in terms of the Young's modulus and the yield stress at 70°C. The failure strain is very consistent at around 50% though, indicating that a strain dependent failure may be dominant at this temperature.

At 70°C and above, the position of failure on the samples varied much more than below this temperature. In some cases failure was observed around the area between the parallel section of the samples and the area held in the grips. Also at very high temperatures failure occurred at both ends of the parallel section and also inside the grips.

Figure 5.6 shows the normalised strength and stiffness of the two resin types tested with respect to the average value calculated at room temperature. The theoretical fitting has been generated by taking the average value at each discrete temperature for each of the four properties.

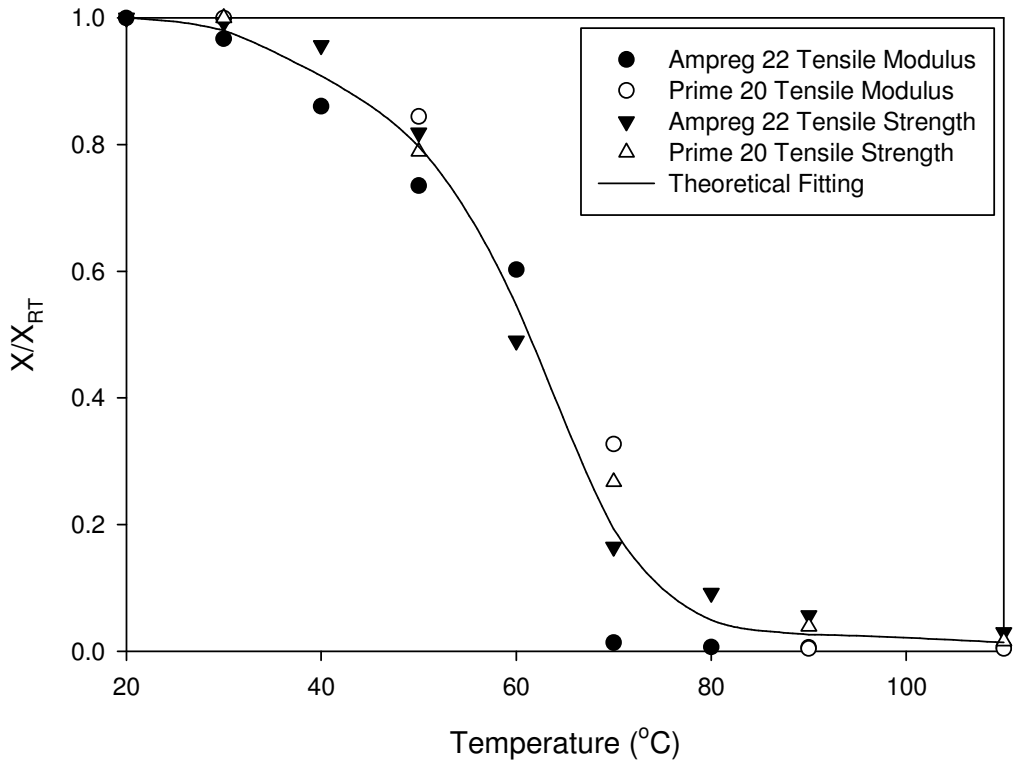

Figure 5.6: Property degradation curve; X and X_{RT} represent the strength and stiffness of the two resins tested as they depend on temperature and their initial state respectively

This shows that the degradation of strength and stiffness in both resin types follows a similar pattern, with a dramatic loss of properties between 50°C and 80°C. The manufacturers state that the heat distortion temperature for Ampreg 22 and Prime 20 are 57°C and 67°C respectively [Gurit 2007]. Whilst these values cannot be compared quantitatively with the results they do fall within the temperature range in which the properties of the resins degrade. They also back up the results in terms of showing that the Prime 20 degrades at a slightly higher temperature than Ampreg 22.

No data was available on the performance of these particular resins at elevated temperatures, however there have been some studies on other thermosetting resins at elevated temperatures. Plecnik et al. [1980] conducted compressive tests on epoxy specimens at discrete temperatures. In the study the samples were heated in an oven to the set temperatures and held for one hour. They were then taken out of the oven and loaded until failure. The results of the compressive strength are given for temperatures from room temperature up to 200°C. The results show a very similar form to that displayed in Figure 5.6 with a rapid loss of strength near to the heat distortion temperature.

Chen et al. [1985] and Dao and Asaro [1999] used temperature dependent mechanical properties to create thermo-mechanical models. In Chen et al. the strength and stiffness properties of an epoxy/graphite composite in the transverse direction were assumed to vary linearly between room temperature and the glass transition temperature, which is contrary to what has been shown here, where a non-linear relationship has been demonstrated. It is assumed that the properties in the transverse direction will be dominated by the behaviour of the resin rather than in the longitudinal direction where the fibre properties dominate. In Dao and Asaro a temperature dependent relationship is given for a woven E-glass/vinyl-ester composite. In this relationship the response is similar to that shown by the two resin types tested in this thesis.

Griffis et al. [1986] showed a near linear decrease in transverse strength and stiffness from unidirectional epoxy/graphite composites. The test method here however subjected the samples to the set temperatures for 4 seconds before loading. This short heating time may have been the reason for the difference between the results presented in this thesis and those given in Griffis et al. [1986].

Gibson and Mouritz [2006] proposed a number of relationships to model the degradation of properties of thermosetting resins. Two of these relationships are given below and these were used to fit curves to the experimental data.

$$P(T) = P_R + (P_U - P_R)exp\left(-\left(\frac{T}{T_0}\right)^m\right) \tag{5.1}$$

$$P(T) = \frac{P_U + P_R}{2} - \frac{P_U - P_R}{2}\left(1 + tanh\left(k(T - T_g)\right)\right) \tag{5.2}$$

Where:

P(T)	= property	T	= temperature (K)
T_0	= relaxation temperature (K)	k	= constant
P_U	= unrelaxed (low temperature) property	m	= constant
P_R	= relaxed (high temperature) property		

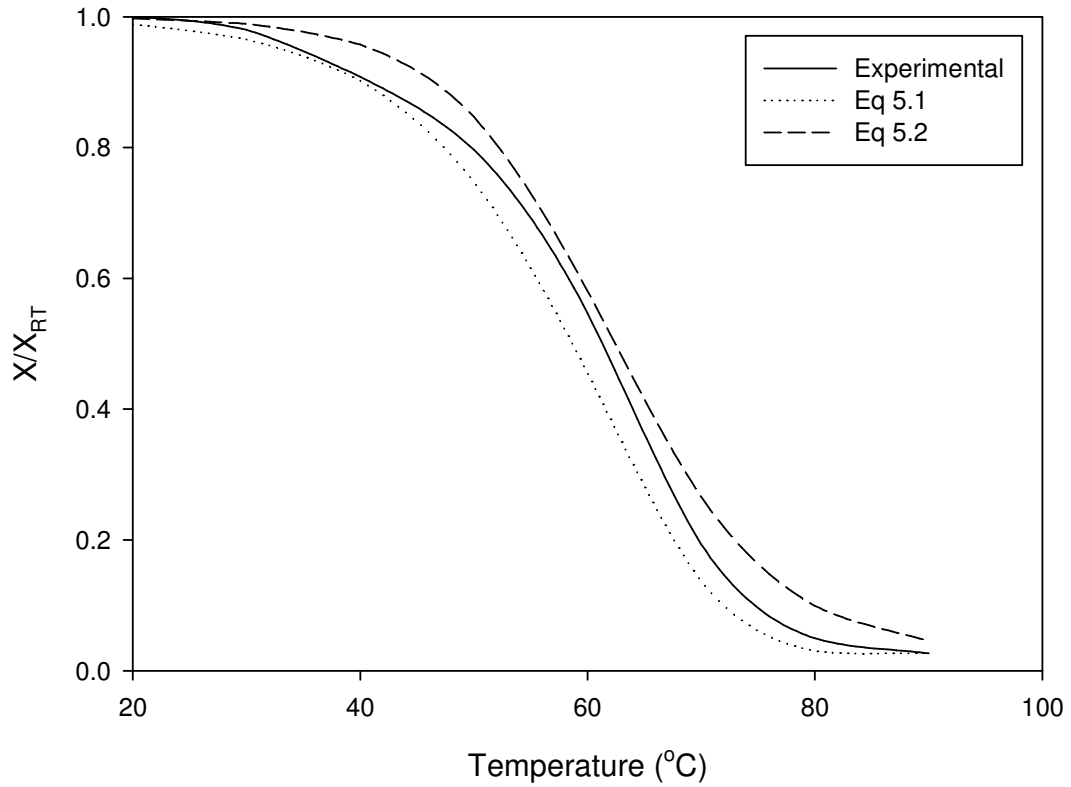

Figure 5.7: Property degradation curve; X and XRT represent the strength and stiffness of the two resins plotted with curve fit equations 5.1 and 5.2

In Figure 5.7 the two curve fit equations have been plotted with the experimental data where the constants were found to be m = 33 and k = 0.07.

Figure 5.8 shows how the average maximum strain of the samples varies over the temperature range. Again the major changes occur at around 70°C, but these occur in a much more instantaneous manner than in the stress and stiffness graphs. This shows that both of the resins become highly amorphous between 70°C and 90°C. This ties in with the results shown in Figure 5.6 where the loss of strength and stiffness occurs over a similar temperature range. In the case of the strain however the change is much more instantaneous.

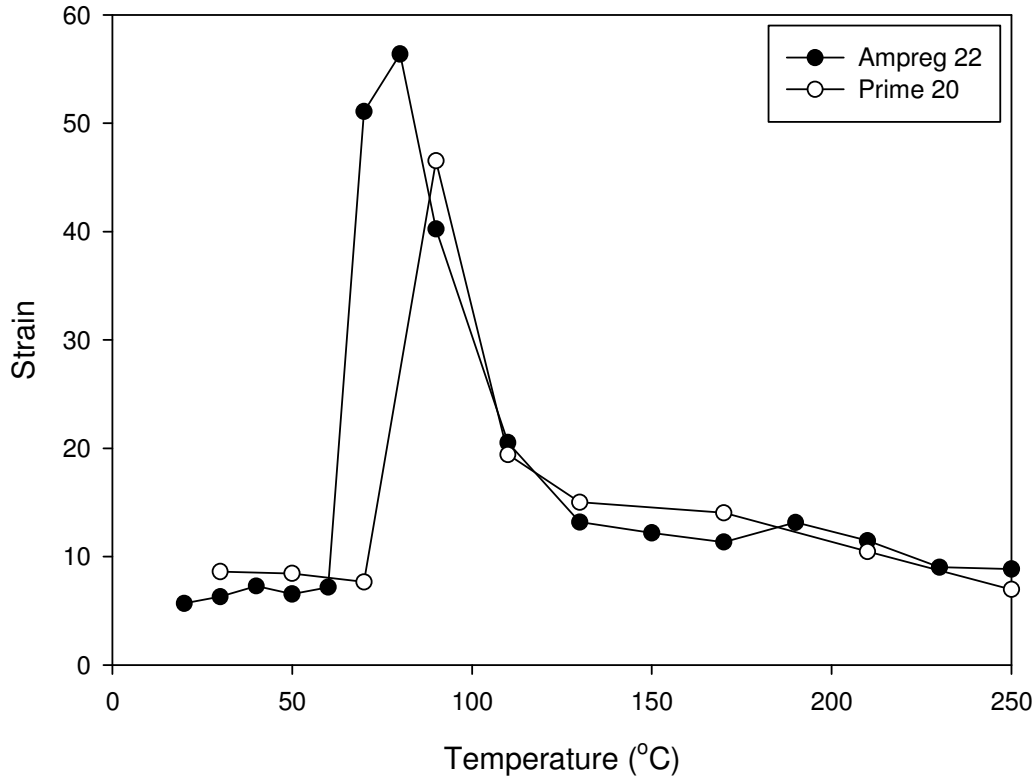

Figure 5.8: Temperature dependent failure strain of Ampreg 22 samples

Figure 5.9 shows there was a significant change in appearance of the Ampreg 22 samples after testing over the temperature range. The change in appearance does not coincide with any of the results of the mechanical properties of the samples. There is no change in the appearance of the samples until 170°C, by which point the strength and stiffness are very small in comparison to the room temperature values. It is possible that the change in appearance is reflected by corresponding changes in mechanical properties, but these would be difficult to measure with the scale of test apparatus used in these experiments.

The change in colour does however seem to relate to the mass loss recorded in the samples after testing. This is shown in Figure 5.10 in terms of the percentage mass loss.

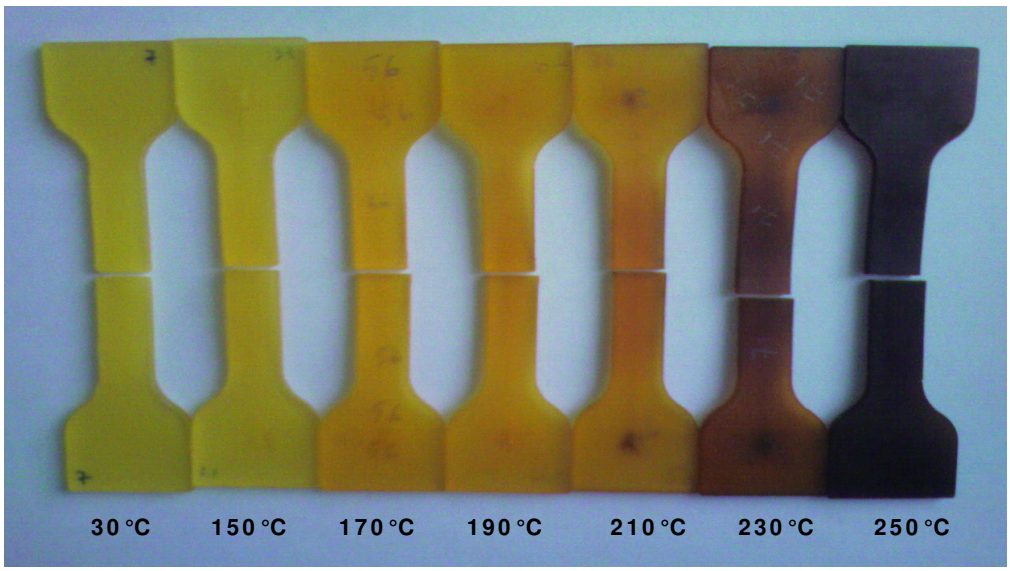

Figure 5.9: Ampreg 22 colour change from 20°C to 250°C

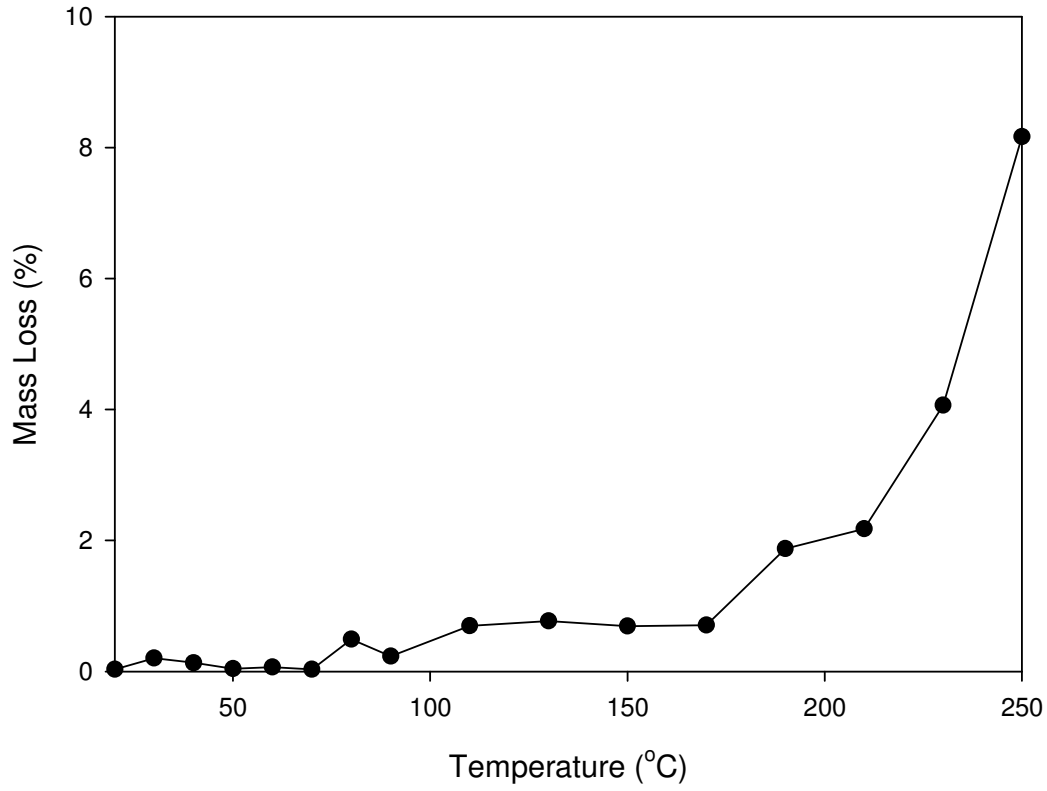

Figure 5.10: Percentage mass loss of Ampreg 22 samples after testing

The major changes in mass loss coincide with the major changes in appearance of the test samples. There is little change from 20°C to 160°C and then at 170°C there is step up and again at 230°C and at 250°C. These levels of mass loss however do not indicate that complete pyrolysis has occurred as this would result in a mass loss of

approximately 90% even when heated at a rate of 10°C/minute [Henderson, Tant et al. 1981; Gibson, Wright et al. 2004; Lattimer and Ouellette 2006].

The Poison's ratio was not measured during the tests as the devices normally used for such measurements were sensitive to a hot atmosphere. The Poisson's ratio has been assumed to vary linearly from 0.3 to 0.5 from room temperature to 70°C. These values were used by Da Silva and Adams [2005] in determining the properties of various epoxy resins at elevated temperatures.

5.4.2 Core

From each test load and deflection data was recorded at a frequency of one Hertz. Using the following equations the shear modulus and the shear strength were calculated for each test:

$$G = \frac{d \times tan\alpha}{A} \tag{5.3}$$

$$\tau = \frac{F_M}{A} \tag{5.4}$$

Where:

G	= shear modulus (Pa)	d	= specimen thickness (m)
tanα	= gradient of load vs deflection graph	A	= 2×l×b (m^2)
l	= specimen length (m)	b	= specimen width (m)
τ	= shear strength (Pa)	F_M	= maximum load (N)

Figure 5.11 shows the load and deflections recorded in the shear tests. The results show a gradual change in form of the curves from completely elastic behaviour at 20°C to a much more plastic behaviour by 120°C.

Figure 5.12 shows how the shear modulus and strength varies with temperature. The change in modulus with temperature can be described by a linear relationship from 20°C to 120°C, where the modulus approaches zero. The strength data is less linear and shows a rise in the strength at 60°C. This behaviour could be due to the way that the samples fail, which will be discussed later in this chapter.

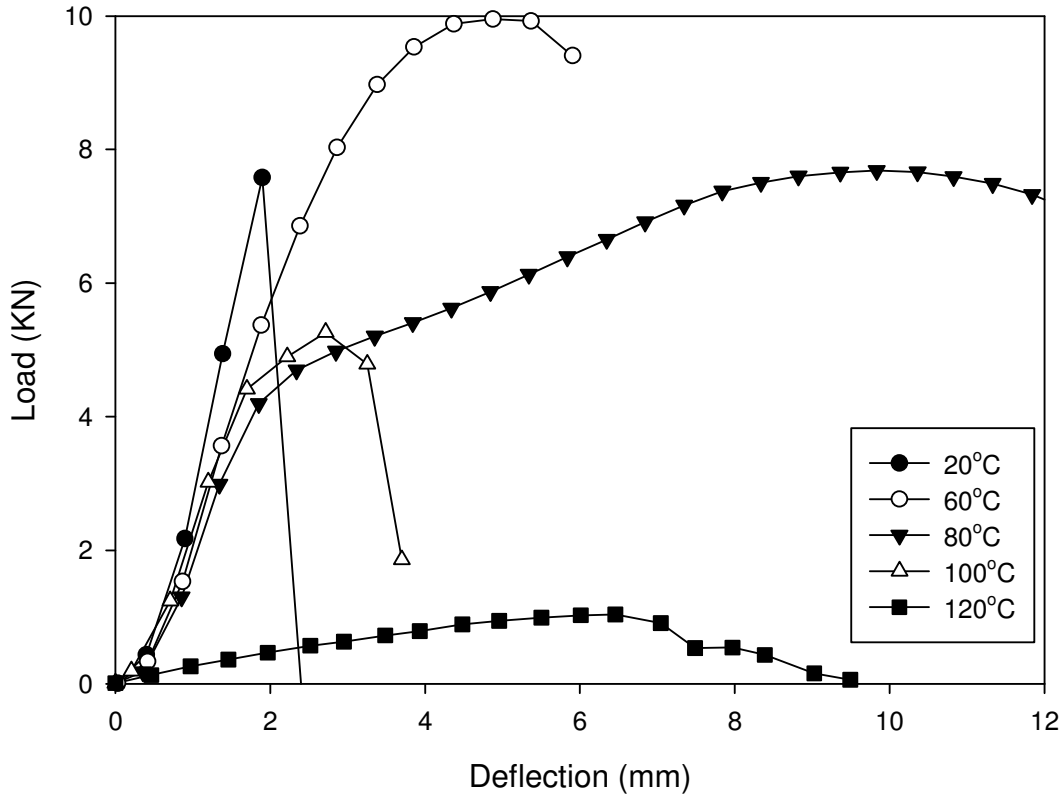

Figure 5.11: Load versus deflection curves taken from shear tests on Divinycell H100 PVC foam samples

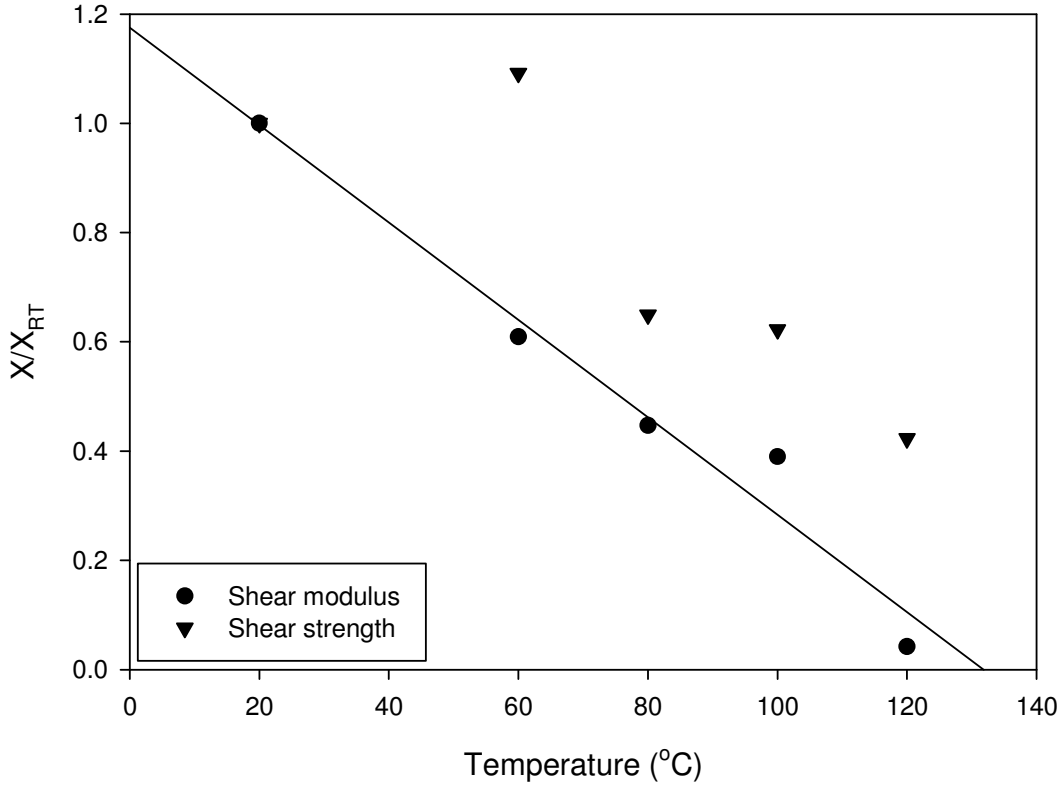

Figure 5.12: Property degradation curve; X and X_{RT} represent the shear strength and stiffness as they depend on temperature and their initial state for H100 PVC foam

The facility used to conduct this testing was damaged beyond repair and no further tests were possible to ascertain the reason for the rise in strength at 60^{o}C.

In the initial tests the failure occurred in the bond between the aluminium plates and the adhesive. The scoring of the plates prior to adhesion did improve this and caused failure to occur within the core to some extent. These results were not used in determining the relationship between the strength and temperature. Even with the scoring and cleaning of plates with acetone and holding the plates under compression during the adhesive cure, failure did occur very close to the surface of the foam and the central plate. This behaviour can be seen in Figure 5.13a. For the test at 80^{o}C the foam failed in the same manner shown in Figure 5.13b, where it can be seen that a large degree of strain has occurred as well as some separation of the foam from the plates at each end. This shows why there was such a large strain shown in Figure 5.11 at 80^{o}C. In both cases it is clear that the bond between the glue and the foam was the area of weakness and it is not clear whether the strength that has been recorded is genuinely the strength of the foam or that of the foam and glue bond.

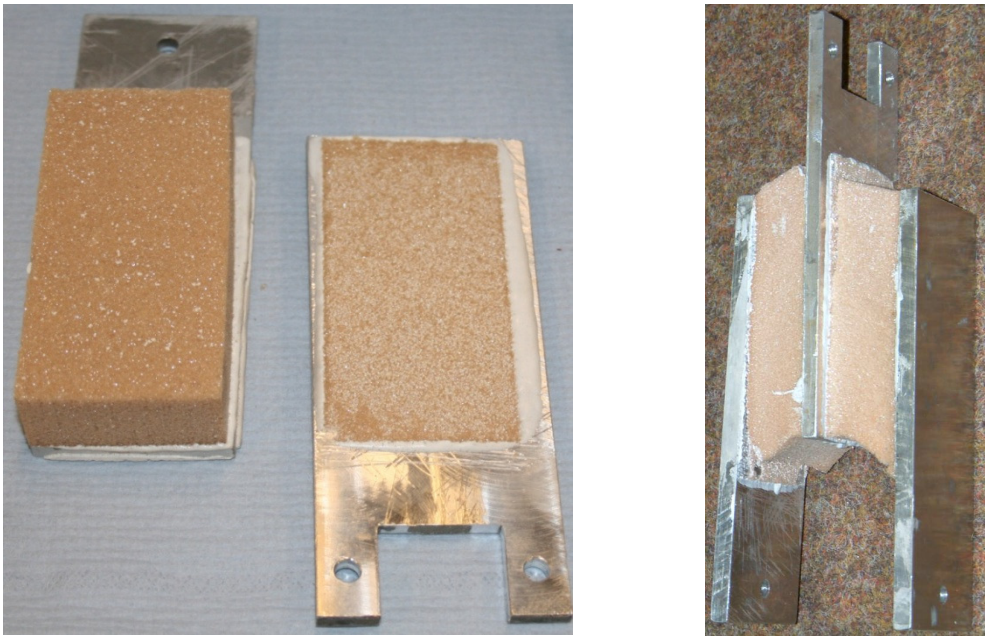

(a) (b)

Figure 5.13: Failed shear samples a) typical of all samples with the exception of 80^{o}C which is shown in b)

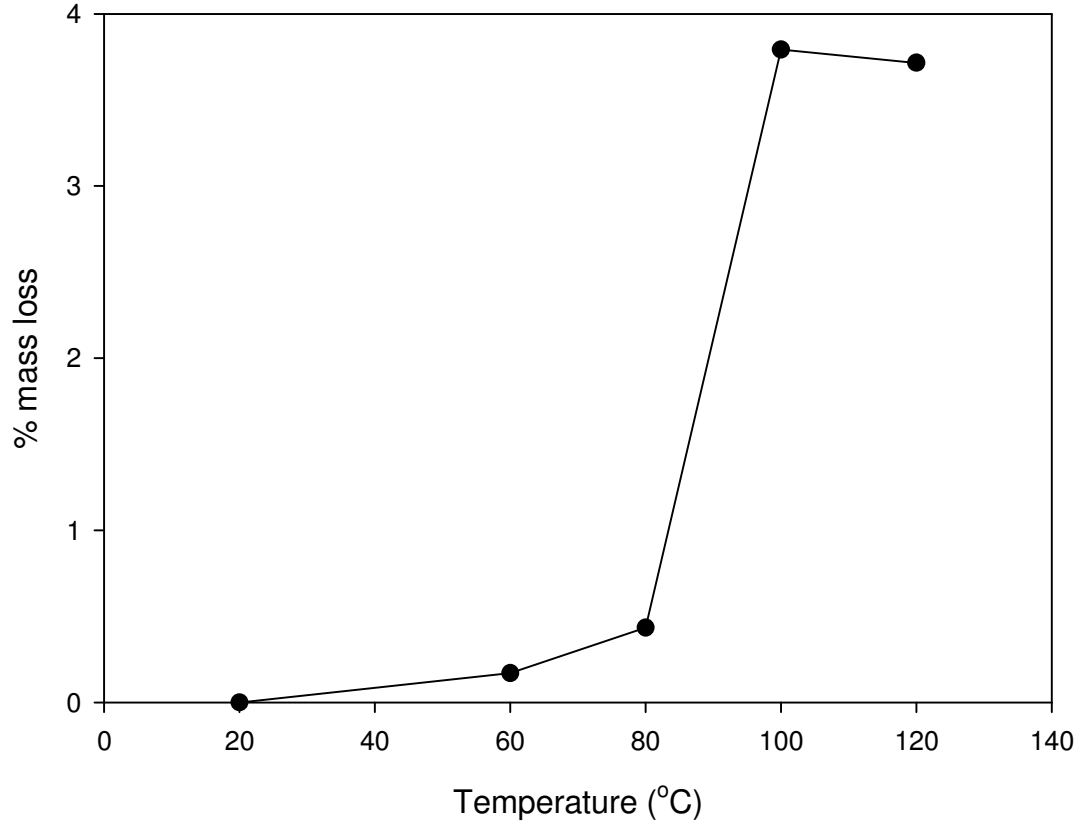

Figure 5.14: Mass loss percentage from foam after each shear test

In Farshad et al. [1997] PVC foam samples were tested under shear at temperatures from 20°C to 80°C. The results show a near linear trend in decreasing modulus, but it is not possible to compare the relative decrease in properties as they are only shown in graphical form in the paper. Lee et al. [2004] tested a PVC foam at temperatures from 20°C to 120°C under compression in this case the decrease in strength was found to be approximately 60% from room temperature and about 75% decrease in modulus. The form of the decrease in both properties was still relatively linear. The modulus at 100°C was slightly higher than a linear trend line would suggest, which matches the form found in this thesis shown in Figure 5.12.

5.4.3 Fibres

No testing of fibres was conducted; results from published research are reported here. Otto [1959] reported that the tensile strength of e-glass fibres decreased in a near linear manner from room temperature up to 650°C, which was the highest temperature they tested at. Over this range the strength decreased by approximately 65%. They also tested at 50% humidity and found that at room temperature the dry strength is 15% higher than the 50% humidity strength.

The fibre modulus remained constant up to about 200°C after which there was a gradual decrease to approximately 4% less than the room temperature value at 650°C.

Cerny et al. [2007] showed that the tensile modulus of e-glass fibres is unaffected by temperature up to 400°C. At this temperature they reported a 3-4% loss and an 8-10% loss at 450°C. These values seem to agree with each other and the values for strength and stiffness have been taken as an average of the results presented. Above 650°C it has been assumed that the results continue to vary in a linear form.

The creep properties of e-glass fibres under constant load at increasing temperatures were also investigated. The strain was negligible until a temperature of 400°C, where the fibres shrink slightly. Unlimited elongation (creep) occurred at around 700°C.

5.4.4 Laminate Properties

As previously mentioned, the mechanical properties of the resin, fibre and core found in this chapter have been used to create laminate material properties at discrete temperatures using the rule of mixtures approach [Hull and Clyne 1996]. These properties have been input into a finite element model where the values at any given temperature are interpolated, this is discussed further in Chapter 6.

The properties of the laminates at room temperature were determined through tensile coupon tests. The coupons were cut from the test panels with all fibres aligned parallel to each other. The details of these tests are given in Appendix C. This gave the elastic properties of the composite as a whole at room temperature. The properties of the resin at room temperature were known through the testing conducted in this chapter. It was then possible to derive the elastic properties of the fibres through the following equation:

$$E_{11} = V_f E_f + V_m E_m \tag{5.5}$$

Where:

E_{11} = Young's modulus in x dir'n (GPa)
E_f = Young's modulus of fibres (GPa)
E_m = Young's modulus of matrix (GPa)
V_f = volume fraction of fibres
V_m = volume fraction of matrix

The value of E_{11} was determined from the coupon tests and the volume fractions were determined by the density measurement method [Curtis 1998]. E_m was taken as the value of the Young's modulus of Ampreg 22 at 20°C and the value of the Young's modulus of the fibres was calculated to be 28.3GPa. The properties of the laminate were then calculated at set temperatures using the following series of equations:

$$
\begin{aligned}
E_{11} &= V_f E_f + V_m E_m \\
E_{22} &= E_m \left(\frac{1 + 2\eta_1 V_f}{1 - \eta_1 V_f} \right) \quad where \quad \eta_1 = \frac{\left(E_{22f} / E_m \right) - 1}{\left(E_{22f} / E_m \right) + 2} \\
E_{33} &= E_{22} \\
G_{12} &= G_m \left(\frac{1 + \eta_2 V_f}{1 - \eta_2 V_f} \right) \quad where \quad G_m = \frac{E_m}{2\left(1 + v_m\right)} \quad and \quad \eta_2 = \frac{\left(G_{12f} / G_m \right) - 1}{\left(G_{12f} / G_m \right) + 1} \\
G_{13} &= G_{12} \\
G_{23} &= \frac{G_m}{1 - V_f \left(1 - \frac{G_m}{G_{12f}} \right)}
\end{aligned}
\tag{5.6}
$$

Where:

G	= shear modulus (GPa)	X_{22}	= properties in y dir'n
X_{33}	= properties in z dir'n	X_{23}	= properties in YZ plane
X_{12}	= properties in XY plane		

E_{22f}, the transverse Young's modulus of the fibres was assumed to be the same as the axial value since glass can be treated as a homogeneous fibre [Morley 1987]. E-glass fibres have been assumed to be isotropic and the in-plane shear modulus, G_{12f}, has been calculated using the following equation:

$$
G_{12f} = \frac{E_f}{2\left(1 + v_f\right)} \tag{5.7}
$$

v_f was been taken to be 0.22 for e glass fibres [Callister 2000].

To calculate the strengths of the laminate the following equations were used:

$$
\begin{aligned}
S_{11}(T) &= \left(V_f \frac{E_m V_m}{E_{11f}} \right) S_{11f}(T) \\
S_{22}(T) &= \left[1 - \left(\sqrt{V_f} - V_f \right) \left(1 - E_m / E_{22f} \right) \right] S_m(T) \\
S_{33}(T) &= S_{22}(T) \\
S_{11}(C) &= (2S_{12m})^{2/3} (E_{11})^{1/3} \\
S_{22}(C) &= \frac{2S_{22}(T) \sin 2\varphi}{(1+v_{12})(1-\cos 2\varphi)} \quad where \quad \varphi = 30^\circ \\
S_{33}(C) &= 2S_m(C) \quad where \quad S_m(C) = \frac{0.077 G_m}{1 - v_m} \\
S_{12} &= \left[1 - \left(\sqrt{V_f} - V_f \right) \left(1 - G_m / G_{12f} \right) \right] S_{12m} \\
S_{13} &= S_{12} \\
S_{23} &= \frac{G_{23}}{G_{13}} S_{12m}
\end{aligned}
\tag{5.8}
$$

Where:

S = strength (GPa) (T) = in tension

(C) = in compression v_{12} = Poisson's ratio

The values of S_m were taken from the experimental data and the values of S_{12m} were estimated to be $0.5S_m$ [Oberg 1992].

Temperature (^oC)	**Properties**							
	E_{11} (GPa)	**E_{22} (GPa)**	**G_{12} (GPa)**	**S_{11}(T) (MPa)**	**S_{11}(C) (MPa)**	**S_{22}(T) (MPa)**	**S_{22}(C) (MPa)**	**S_{12} (MPa)**
20	14.9	4.8	0.2	1263	385	50	133	25
50	14.7	3.7	0.1	1209	337	41	109	20
70	14.2	0.1	0.002	1141	112	8	21	4
80	14.2	0.04	0.001	1128	71	4	11	2
400	14.2	0	0	744	0	0	0	0
700	12.7	0	0	360	0	0	0	0

Table 5.1: Uni-directional ply properties at elevated temperatures

Table 5.1 shows the calculated properties of a ply of UTE 800/Ampreg 22 (e-glass/epoxy) at selected temperatures. It is immediately obvious, from the first two

columns that the effect of the fibres plays a major role in the overall stiffness. In the longitudinal direction the stiffness does not change appreciably over the temperature range. In the transverse direction, where the resin properties are dominant, the stiffness decreases to a negligible value by 80°C. In shear, the effect is even more pronounced and the stiffness is negligible by 50°C. In terms of the strength, the fibre properties dominate again and the tensile strength in the longitudinal direction remains high until 400°C by which point it is just over half of the room temperature strength. It is clear that temperature has a greater effect on the strength than the stiffness in the longitudinal direction though. In compression the resin properties again dominate and the strength is reduced to a negligible value by 80°C.

5.5 Conclusion

The aim of chapter 5 was to devise a method for obtaining the temperature dependent mechanical properties of the constituent products of single skin and sandwich materials. This has been done through a test program using a servo-hydraulic testing machine with a heating chamber to apply the necessary temperature conditions. Data has also been collected for the materials used in the fire tests described in this thesis which will be used to link the temperature profiles generated in Chapter 4 to thermo-mechanical models which will be described in Chapter 6.

The results from chapter 6 have shown the strength and stiffness of two different resins to decrease sharply at around the quoted glass transition temperature (70°C-80°C). The reduction of the strength and stiffness at elevated temperatures for both resins follow a similar form when normalised against the room temperature values. This form is in line with results from other epoxies found in the literature and a curve has been fitted to the data, which can be used in the thermo-mechanical modelling to determine material properties with respect to temperature.

The ply properties calculated at elevated temperatures using the results from this chapter have predicted that the stiffness and strength of laminates can rapidly reduce with exposure to heat. This is most evident in transverse shear loading where the resin properties dominate over the fibre properties. In the fibre direction the reduction in stiffness is small but it must be borne in mind that this will only be the case in the tensile direction. In compression, once the resin has ceased to provide any stiffness the

composite as a whole will also have negligible stiffness. This decrease in mechanical properties was shown to be unrelated to mass loss and any change in appearance. No significant mass loss was recorded until 190^{o}C, by which time the resin had very little strength and stiffness. The resin did darken in colour with increasing temperature from 190^{o}C upwards and the change in colour seemed to be related to the mass loss.

The core properties have been shown to degrade with increasing temperature in a more gradual manner with the shear modulus approaching zero at around 120^{o}C. The testing was limited to a maximum of 120^{o}C due to apparatus restrictions and therefore results at higher temperatures were not possible. The form of the results found here match the trends shown in the two papers found in the literature in terms of the decrease in shear modulus although the particular foam tested here was shown to decrease at a higher rate with respect to the temperature.

6 Thermo-Mechanical Testing and Modelling

6.1 Introduction

The aim of the work described in this chapter was to create methods to predict the thermo-mechanical response of composite panels subjected to fire and mechanical load. This work fits into the overall methodology of the thesis described in Chapter 3 in Figure 3.2 Route 1, Stage 3 and Route 2, stage 3.

The development of a new test method for composite panels subjected to combined fire and mechanical load has been developed. The fire testing conducted in Chapter 4 is taken to the next stage by introducing a mechanical load during the tests.

A new method has also been developed to predict the performance of single skin and sandwich composite panels when subjected to fire and load in the apparatus. A numerical model has been written using the ANSYS finite element software. The model uses the temperature profiles generated in Chapter 4 and the results for the temperature dependent material properties generated in Chapter 5 to predict the response of composite panels to load and fire.

To assess the new test method proposed here and to validate the numerical models described in this chapter a series of composite panels were tested under fire and load in the apparatus. The performance of a series of single skin panels of varying lay-ups and thicknesses were compared with a sandwich panel.

The results of these tests are analysed and an empirical relationship has been derived from them to predict the response of composite panels at a larger scale to fire and load.

6.2 Test Apparatus and Loading Scenario

The equipment used to validate the numerical modelling is shown in Figure 6.1 and is part of the Vulcan fire testing apparatus, which was introduced in Chapter 4. The loading module was attached onto the front plate of the furnace by 8 off 12mm bolts.

The front plate was a 10mm thick piece of mild steel and was bolted onto the furnace by 6 off 12mm bolts. The furnace provided the extra stiffness to prevent the front plate bending during loading. The load system support structure was also made from mild steel sections between 8mm and 10mm thick. The test panels were loaded by a Powerjacks 50kN translating mechanical actuator and a 1.5kW BALDOR DC motor was used to power the actuator. The decision to use a mechanical motor was taken for two reasons. First, the standard hydraulic actuators commonly used in materials testing present a potential fire hazard and therefore were ruled out. Secondly, with a mechanical motor the system was also portable and only required 240 V ac mains electricity to operate. The supporting structure was designed and refined using the ANSYS finite element software to ensure adequate stiffness under maximum loads. The whole module including the supporting structure weighed approximately 40kg. To support this weight a supporting structure was manufactured, which also allowed the loading module to be moved in and out of the fume cupboard.

The out of plane load is applied by a square steel contact piece, which was located in the centre of the panel. For the single skin panels the contact piece used had an area of 40mm × 40mm, but with sandwich panels this was too small a loading area and it caused the panel to puncture rather than bend. In this instance the contact piece used was 80mm × 80mm. In order to prevent the load becoming concentrated at the corners of the contact piece and puncturing the panel a 5mm thick rubber pad with a density of 1291kg/m^3 was attached to the end of the contact piece. This minimised the effect of the load being concentrated on the corners of the loading area. An insulating Teflon disc was fixed in between the actuator and the contact piece to reduce the heat conduction back to the load cell and displacement transducer.

The load cell was made from mild steel cylindrical section, which screwed into the actuator with a steel pin through the connection to prevent any twisting. A full Wheatstone bridge was bonded around the load cell and fed into a RS components strain gauge amplifier V7412.

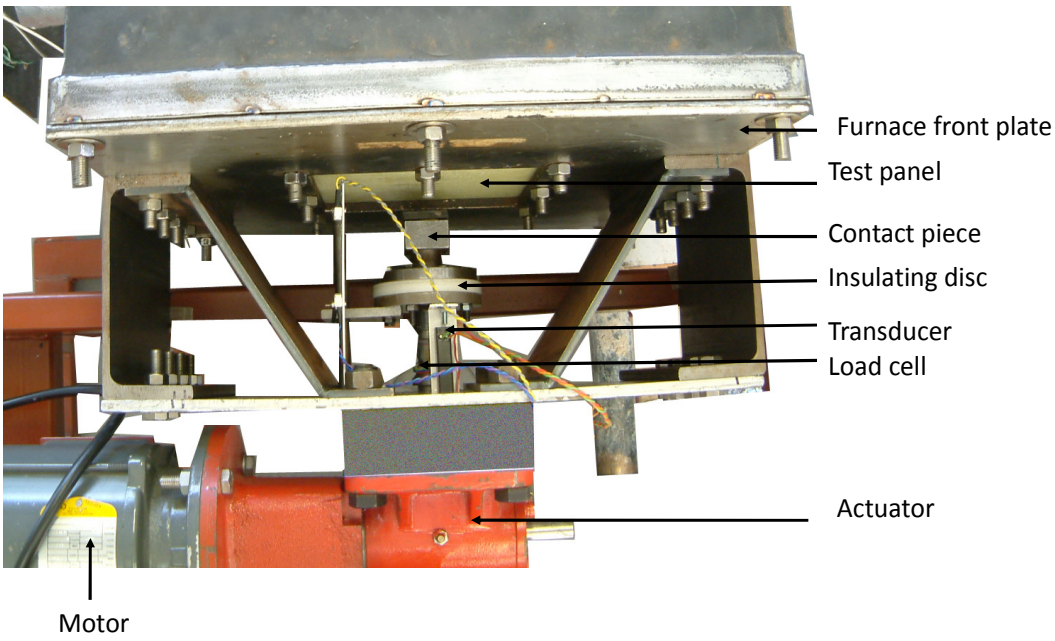

Figure 6.1: Vulcan loading system viewed from above

The load system was controlled through a Sprint Electric 1600i control board via an analogue to digital converter from a PC using the DASYlab 8.0 software package. The board employed a closed loop control of both armature current and feedback voltage to give precise control of the motor torque and speed. The DASYlab software was able to take inputs from the load cell amplifier and displacement transducer and output a voltage, which corresponds to a specific torque on the motor. Figure 6.2 indicates where each component links into the system.

The displacement transducer was calibrated using digital veneers with a precision of ±0.01mm. The load cell, with the insulating disc and rubber pad attached, was calibrated using an Instron servo hydraulic test machine. The displacement induced in the load system during calibration was recorded, most of which was thought to be due to the compression of the rubber. A curve was fitted to the load versus deflection curve to account for the compression in the load system. This was then subtracted from the recoded deflection values during testing to give the true panel deflection.

The panels were all 240mm × 240mm and clamped at all four edges by a frame held over the panel as shown in Figure 6.3. The frame was held in place by 9 off 12mm bolts, which were tightened to a torque of 40Nm.

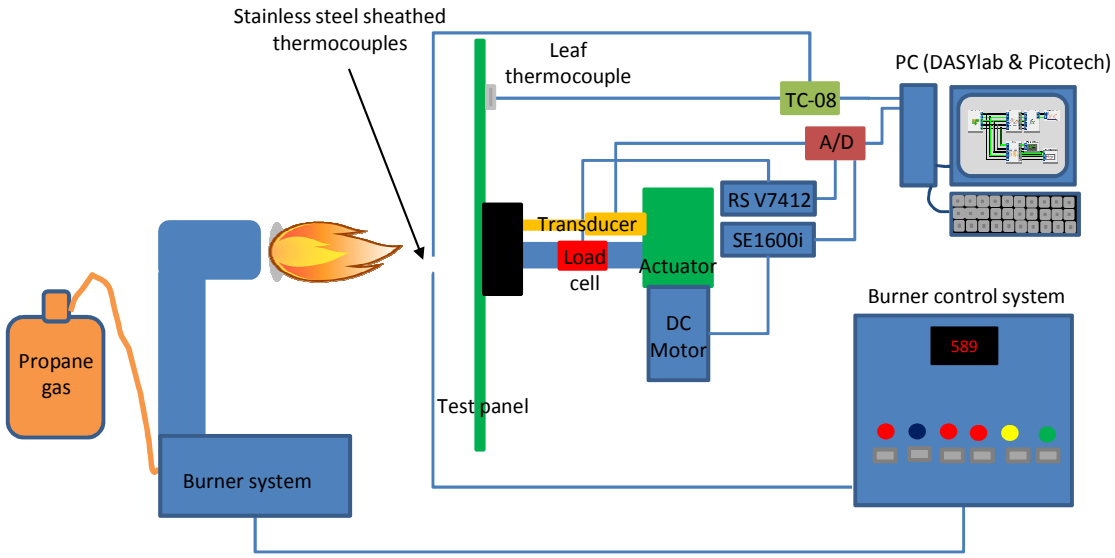

Figure 6.2: Vulcan fire and load testing apparatus system diagram

The frame clamped over the outer 20mm on each side of the panel leaving an effective panel area of 200mm × 200mm.

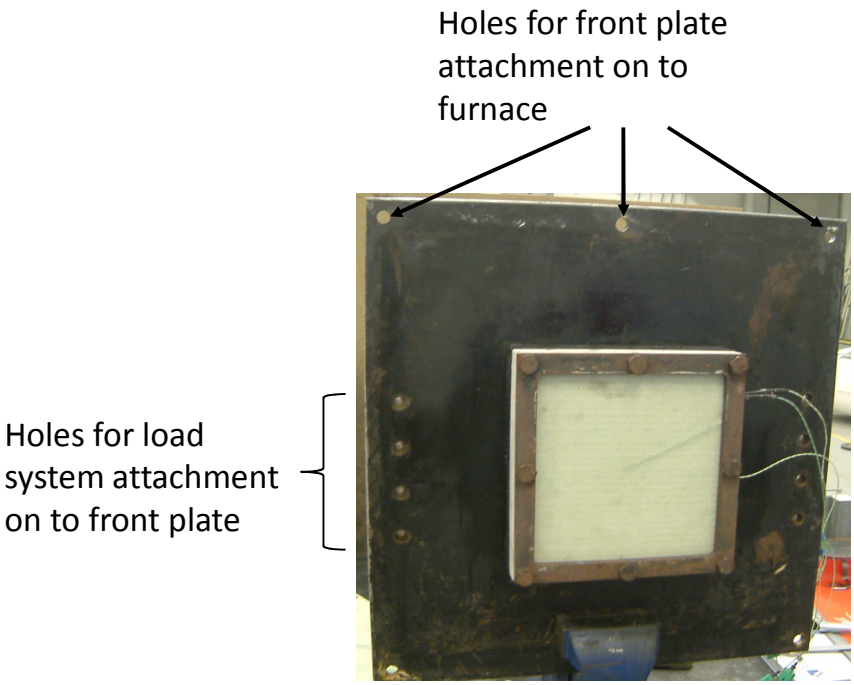

Figure 6.3: Furnace front plate, viewed from the furnace side with test panel secured in the loading frame

In each case the load was applied first and held at a constant value before the fire was started. The applied loads were relatively small in comparison to the panel strengths; this was done for two reasons. At low loads the panels can be expected to behave in a

linear manner, which simplifies the modelling. Secondly, the aim of the research was to determine the performance of composite structures in a real life scenario, where design loads are typically significantly lower than failure loads.

6.3 Thermo-Mechanical Models

The loading scenario described had a relatively simple geometry, which could have been solved analytically. Finite element modelling using a commercial software package was chosen to perform the analysis as this allowed greater flexibility in modelling more complex geometries in the future.

Two different methods were carried out in order to predict the response of the test panels subjected to combined fire and load. These methods were dictated by the options available using the layered elements within the ANSYS software.

In Chapter 4 the temperature profiles across the hot and cold faces of selected panels were measured. These showed that there was a definite temperature gradient across the surface of the panels with the centre being hotter, in general, than the edges. In view of this, it was deemed necessary to create a two dimensional thermo-mechanical model to predict the response of the panels to combine fire and load within the Vulcan fire test apparatus.

The most straightforward and time efficient method of modelling composites within ANSYS is to use shell elements. These can be used to model single skin and sandwich structures and can produce solutions with fewer elements than solid elements thus reducing the computing time. The application of temperatures to layered shell elements is done at the interface of each layer, therefore allowing a steep temperature gradient to be modelled through the thickness of the panel. The disadvantage of the elements currently available is that it is only possible to apply temperature loads to whole layers. This means that a temperature gradient across a layer cannot be modelled, limiting the temperature modelling to one dimension.

There are some solid elements available with the capability of modelling layered structures. These have the advantage of allowing temperatures to be defined at individual nodes thus allowing a temperature gradient to be modelled in three

dimensions. The method by which the solid models are treated in ANSYS is different to the shell elements and the temperatures are applied to the nodes rather than the layers. In order to create a temperature profile through the thickness of the panel, with the same level of detail that is possible using shell elements, a node is needed at the interface of each layer through the thickness. As the panels were relatively thin in comparison to their length and breadth, a very large number of elements would be required to mesh a panel with each layer being represented by a layer of elements. This is due in part to the fact that there is an aspect ratio limit of 1:20 with elements in ANSYS.

To summarise, the layered elements allow a high level of detail in terms of the through thickness temperature profile but do not allow any variation in temperature across the panels. The solid elements allow temperature variations to be defined in any direction but do not allow the level of detail in temperature gradient through the thickness without very long computing times.

Both solid element and shell element models were created to assess the most effective method of predicting the thermo-mechanical response of the panels.

In both sets of models the temperature profile through the panel needed to be input along with the temperature dependent material properties.

In order to generate the thermal profile through the panels a hot face temperature needed to be defined for each of the combined fire and load tests. This was not measured during the fire and load tests as it required holes to be drilled into the panels to insert the thermocouples, which it was thought would affect the strength and stiffness of the panels. An average value of the hot face temperatures taken from the fire tests discussed in Chapter 4 was used to model the temperature profile through each panel. This decision was justified as the same programmed fire curve and the same material at the hot surface was used in each case. The heat transfer results were then determined by inputting the volume fraction, density and thickness of each panel as described in chapter 4. Due to the way the temperatures had to be input into the ANSYS model it was necessary to define the temperature in between every layer for each time step. A time step of 30 seconds was chosen as it took a considerable time to compute the results at a much shorter period.

The material properties were then calculated at a series of set temperatures. For the single skin panels and sandwich skins the properties were calculated outside ANSYS in order to reduce the workload within the ANSYS program and allow as fast a computation time as possible. The rule of mixture laminate equations given in Chapter 5 were used to generate ply properties at set temperatures. It was found that the resin modulus could not be assumed to be zero above the glass transition temperature as this caused ANSYS to predict very large deflections. The resin modulus, which was recorded up to 250^{o}C by experiment in Chapter 5, was used and above that temperature it was assumed to carry on decreasing linearly up to 350^{o}C. This was the temperature shown in the TGA results to be the point at which pyrolysis occurs. From 350^{o}C until 450^{o}C, which was the temperature at which pyrolysis was shown to be complete, the resin modulus was assumed to decrease linearly to a nominally small value, as a value of zero Young's modulus caused problems in solving the simulation.

The Divinycell H100 foam moduli were taken from the values determined in Chapter 5 up to 120^{o}C. Above this temperature it was assumed that the modulus remained constant until 250^{o}C, when TGA results indicated pyrolysis commenced. From 250^{o}C up to 400^{o}C the modulus was assumed to decrease linearly to a nominally small value.

The orthotropic ply properties were uploaded at set temperatures and a built-in function in ANSYS interpolated the properties linearly in between these temperatures.

6.3.1 Method 1- Solid Elements

ANSYS element SOLID185 Layered Solid was used to model the single skin and sandwich structures. The element was defined by eight nodes having three degrees of freedom at each node: translations in the nodal x, y, and z directions. It allowed up to 250 layers to be defined, which were defined by material type, thickness and orientation. The model was meshed with a user defined number of elements, irrespective of the number of layers, and the element stiffness was calculated from the stiffness matrix derived from the layered input by ANSYS.

As previously mentioned the model was able to take account of the temperature gradient across the face of the panel as well as through the thickness. It was possible to model

the panels as quarter plates due to the symmetry involved, which reduced the computing time by a factor of four for each simulation. Using the data collected in Chapter 4 the panels were divided up into three layers of nodes in the thickness direction and three regions across the surface.

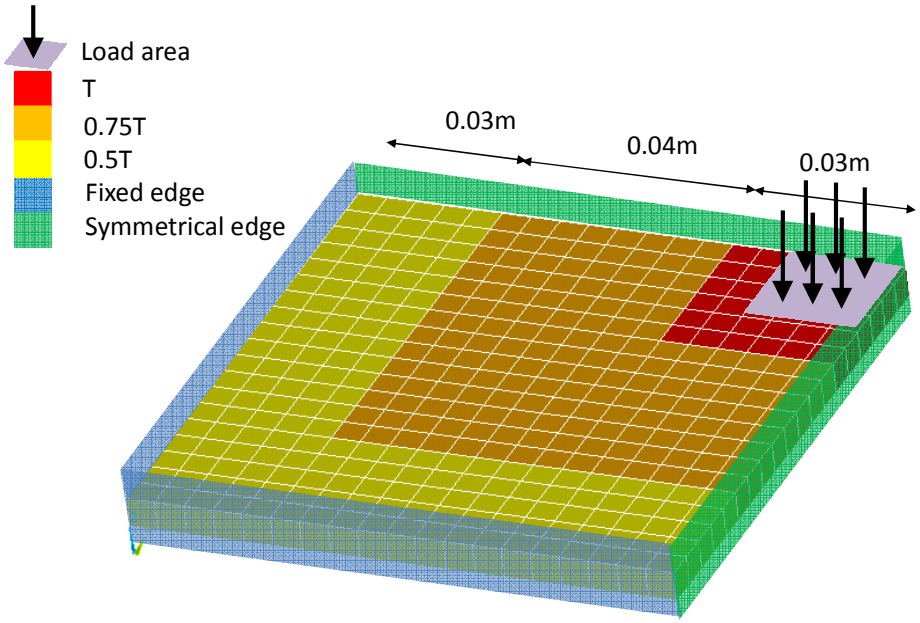

Figure 6.4: Finite element model of laminated plate subjected to fire and load, showing areas of constant temperature

Figure 6.4 shows the temperature regions across the surface of the panel and where the loading and constraints were applied. It also indicates the relative temperature decreases from the centre of the panel towards the edges. By dividing the panel up into three layers of nodes and hence two layers of elements it was possible to keep the element aspect ratio at one.

The sandwich panels were formed by creating three volumes, with coincident nodes at the interfaces. The skins were meshed with one element through the thickness and the core was meshed with three elements through the thickness. This caused the skin elements to have an aspect ratio of 3. This was slightly higher than the ideal aspect ratio of one [ANSYS 2007], but was deemed preferable to keeping all the elements at an aspect ratio of one and increasing the number of elements required from 2,000 to 43,000.

The models were written in the ANSYS Parametric Design Language (APDL), which is based on the FORTRAN language. The full scripts for both the single skin and

sandwich programs are given in Appendix D. The programs are summarised in the flowchart shown in Figure 6.5.

The model was created in ANSYS as a static structural model, with each time step being solved on its own. The temperatures, which were applied to the individual nodes, were calculated using the Krysl et al. [2004] program described in Chapter 4. The material properties of the single skin and sandwich panels were calculated outside of the ANSYS program in order to speed up the modelling process. The stiffness properties of each of the panels therefore differed according to the lay-up, the thickness and the fibre volume fraction.

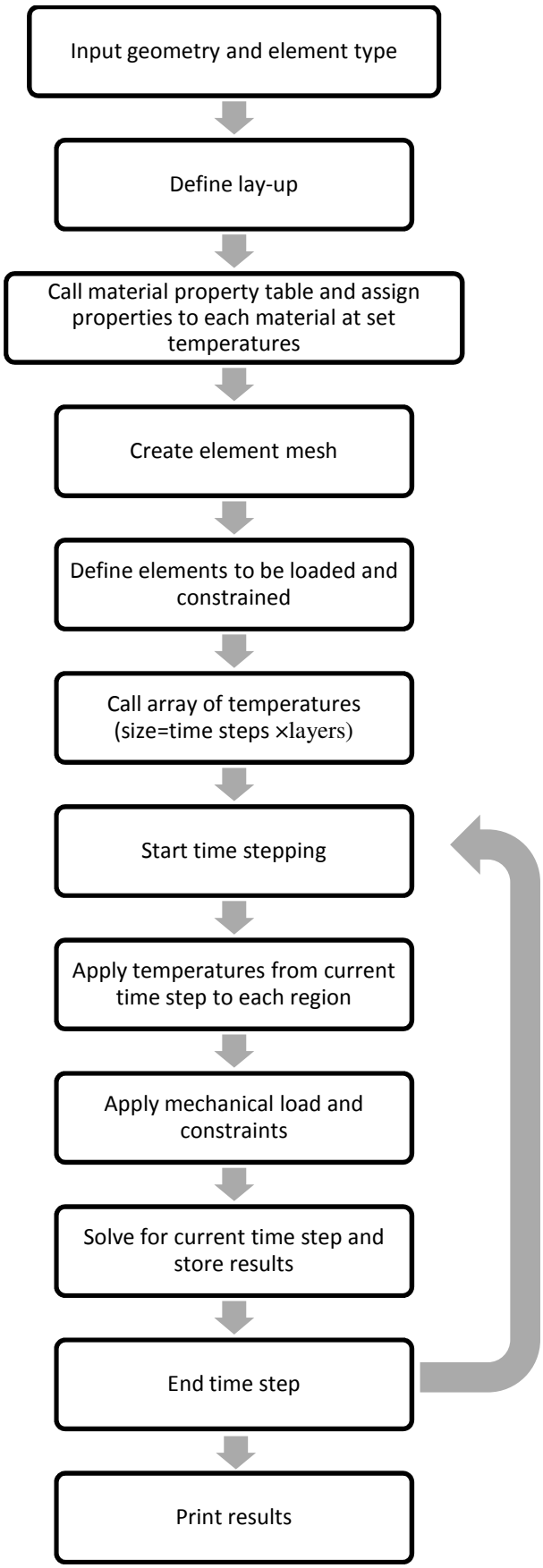

Figure 6.5: ANSYS thermo-mechanical flowchart

6.3.2 Method 2- Shell Elements

As previously mentioned the layered shell elements available in ANSYS allowed a multi-layered structure to be modelled using far fewer elements than solid elements. SHELL91 was used to model the single skin panels; this was a non-linear layered structural shell. It had four corner nodes and four mid-side nodes. The element had six degrees of freedom at each node; translations in the x, y and z directions and rotations about the x, y and z axes.

The element allowed for individual layers to be defined with individual thicknesses, angles of direction and orthotropic material properties. Temperatures were defined in between each layer and temperature dependent material properties were defined for each of the material types using this element.

For sandwich panels a solid element core was used. This was because it was only possible to apply temperatures at the interfaces of the layers between the skins and the core using shell elements. In this case SOLID186 was used. This was a 20 noded brick element with each node having 3 degrees of freedom; translations in the x, y and z directions. The element could also be used in a shell type form and be used as a layered solid. In this form it was possible to define several identical layers within the core in order to apply different temperatures through the core thickness.

The model was formed by creating a volume for the core and meshing that volume. The areas where the skins were to be adhered were selected and the area was re-meshed using SHELL91 with the properties of the skins. The nodes for the skins were offset to the outermost surface of the element.

The program was written in a manner very similar to that using the solid elements. The main difference was that the temperatures were applied at each layer as opposed to the nodes and that they were constant in the plane of the layers. The programs are given in Appendix D for both the single skin and sandwich models.

6.4 Experimental Procedure and Test Matrix

To assess the new test method proposed here and to validate the numerical models described in this chapter a series of composite panels were tested under fire and load in the Vulcan fire test apparatus. The recorded load and deflection data was compared with results produced from the thermo-mechanical finite element models.

In each case a panel was secured into the apparatus in the manner described in section 6.2. The out-of-plane load was applied and held at a constant value. When the panel had reached the set load, the furnace was started and the motor was held at a constant torque. The furnace temperature in each case was programmed to follow the cellulosic fire curve, as in the fire tests conducted in Chapter 4. In each experiment the load, actuator displacement, furnace temperature and panel cold face temperatures were recorded at a rate of 1 Hertz. Strain data was also recorded from the cold face of some of the panels. In each case four strain gauges were attached to the panels. Two were bonded to the panel at 90^{o} to each other using Vishay M-Bond 600 high temperature adhesive. The other two were attached as close as possible and in the same orientation, but with a high temperature adhesive sticky tape over the top of the gauge. The theory was that the gauges attached by tape would be subjected to temperature only and the signal from these could be subtracted from the signal obtained from bonded gauges. The details of the tested panels are given in Table 6.1.

Panel	layup	Fibre volume fraction	Thickness (mm)	Pressure (MPa)	Duration (mm:ss)
SS 1.1	$[0]_{16}$	0.41	10.7	4.4	08:10
SS 1.2	$[0]_{16}$	0.31	11.1	2.5	12:18
SS 2.1	$[0/90]_{8S}$	0.45	10.9	4.4	07:04
SS 3.1	$[\pm45]_{8S}$	0.33	12.2	4.4	07:41
SS 4.1	$[0]_{12}$	0.35	9.12	1.9	09:07
SS 5.1	$[0/90]_{6S}$	0.39	8.8	3.1	08:54
SS 6.1	$[\pm45]_{13}$	0.44	9.36	2.5	09:33
SS 6.2	$[\pm45]_{13}$	0.46	9.24	5.0	06:05
SW 2.1	QE600/QE1200/H100(15mm)/QE1200/QE600	0.50	19.1	3.1	10:12

Table 6.1: Test matrix for fire and load testing in Vulcan apparatus

6.5 Results and Discussion

The following section shows the results of the combined fire and load testing. In the predictions for each experiment four simulations were run:

1. SHELL91 constant load:
   - Using SHELL91 and taking the load to be the same in each load step at the initial recorded load as the fire was started.
   - Temperatures applied evenly across the interface of each layer.

2. SHELL91 experimental load:
   - Using SHELL91 and taking the load recorded by the load cell at each time step during the experiments.
   - Temperatures applied evenly across the interface of each layer.

3. SOLID185 constant load:
   - Using SOLID185 and taking the load to be the same in each load step at the initial recorded load as the fire was started.
   - Temperature gradient applied in the plane of the panel as well as through the thickness.

4. SOLID185 experimental load:
   - Using SOLID185 and taking the load recorded by the load cell at each time step during the experiments.
   - Temperature gradient applied in the plane of the panel as well as through the thickness.

The models were tested for convergence to find the optimum element mesh density in order to minimise computing time. The results of this are given in Appendix D.4.

With the loading module attached to the front of the furnace it was not possible to directly view the panel during the test. The motor driving the actuator was also relatively noisy and added to the noise generated by the fans in the extraction system and burner system. This meant that it was not possible to clearly hear any cracking in

the panels as a result of ply or matrix failure. The loading of the panels did not appreciably change the levels of smoke produced during the tests in comparison to the tests conducted in Chapter 4, this however was only an observation and could not be measured. As in the testing described in Chapter 4 the levels of smoke rose significantly after 50 seconds in each test.

The strain data collected during the tests was deemed inconsistent and seemed to be adversely affected by the temperature in such a way that could not be accounted for. In future work different methods of strain measurement could be looked at. Digital Image Correlation [Dulieu-Barton 2008] is a method that could be used, if the test set up were to be adapted, to measure strain in the test samples.

Figures 6.6 to 6.9 show photographs of the panels having been subjected to fire and load along with the associated deflection versus time graphs. Included in these graphs are the four predicted deflection curves. The results for all the tested panels are given in Appendix D.4.

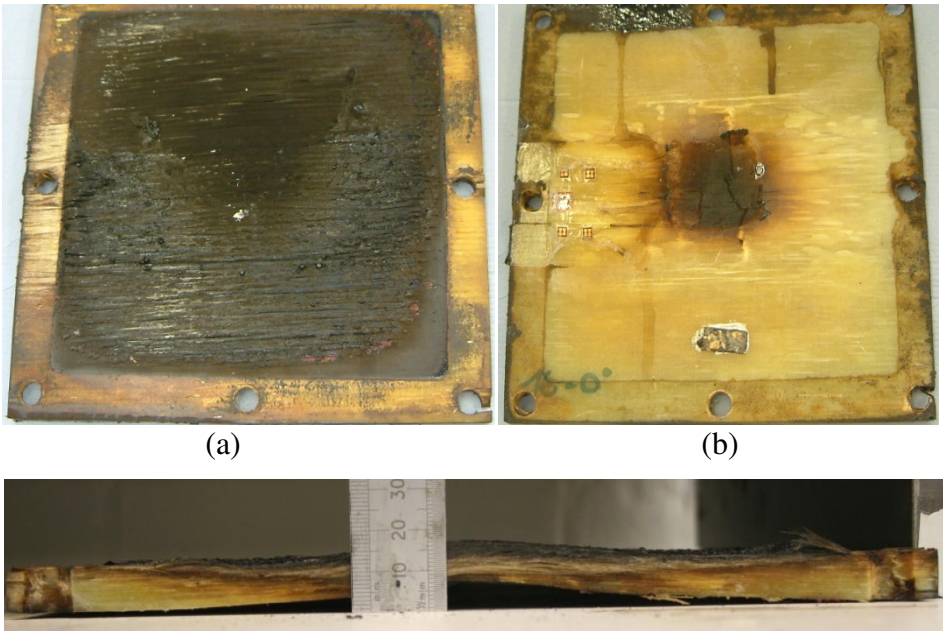

(a) (b)

(c)

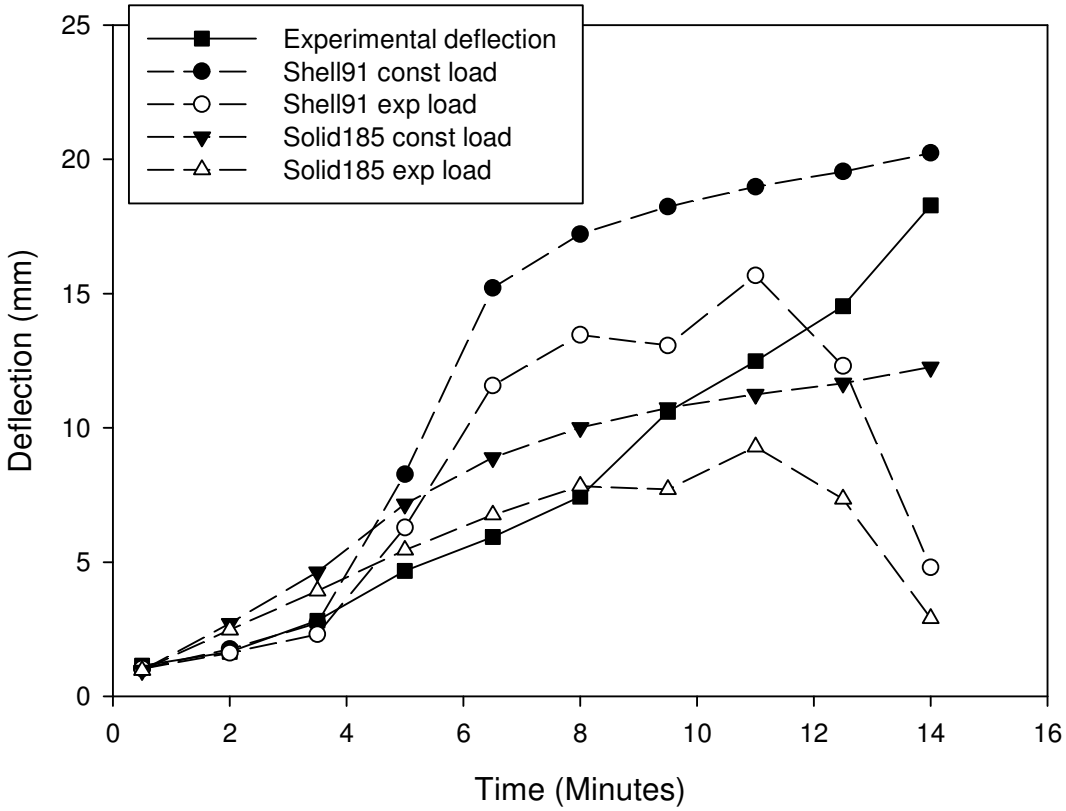

Figure 6.6: Test panel SS 1.2 $[0]_{16}$ hot(a) and cold(b) face and cross section (c) after fire and load testing and deflection data under the cellulosic fire curve at 2.5MPa for 12mins 18sec

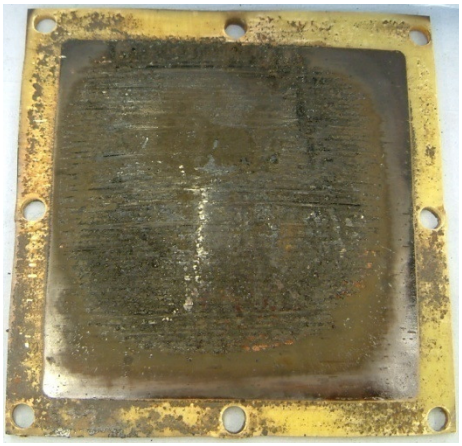

(a)

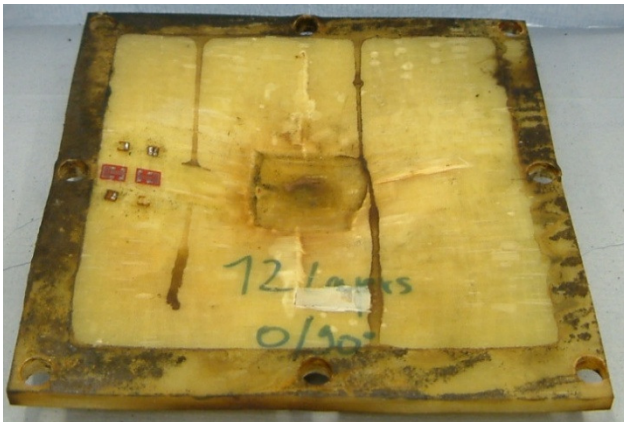

(b)

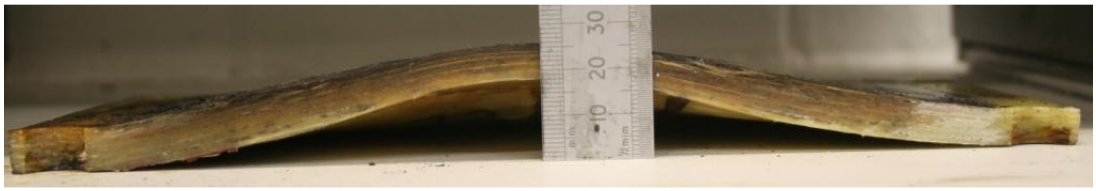

(c)

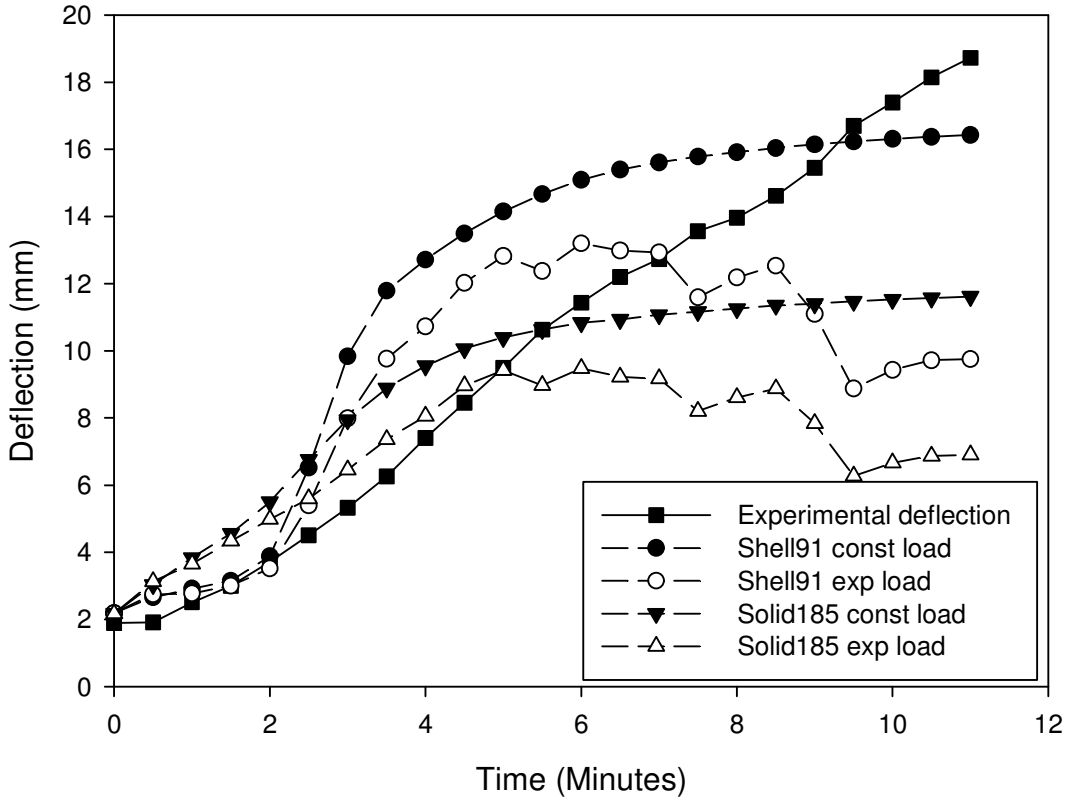

Figure 6.7: Test panel SS5 $[0/90]_6$ hot(a) and cold(b) face and cross section (c) after fire and load testing and deflection data under the cellulosic fire curve at 3.1MPa for 8mins 54sec

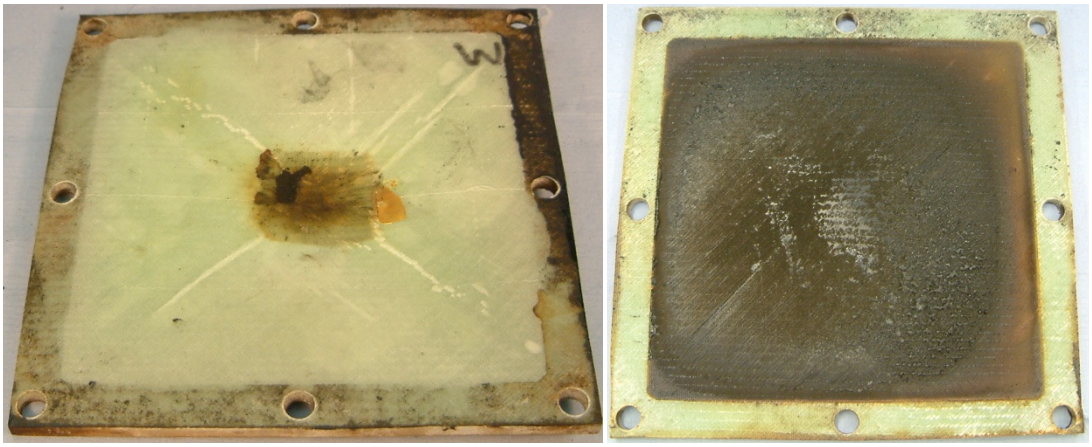

(a) (b)

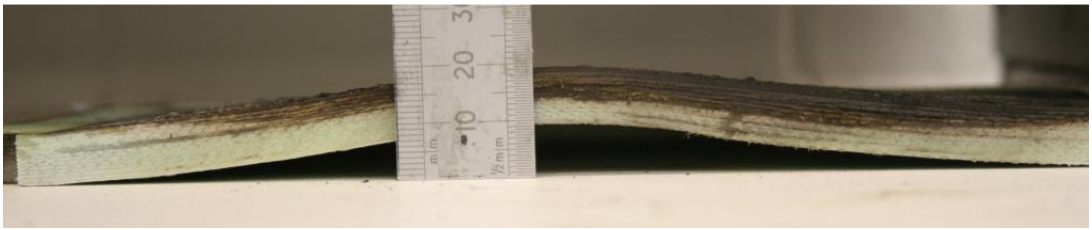

(c)

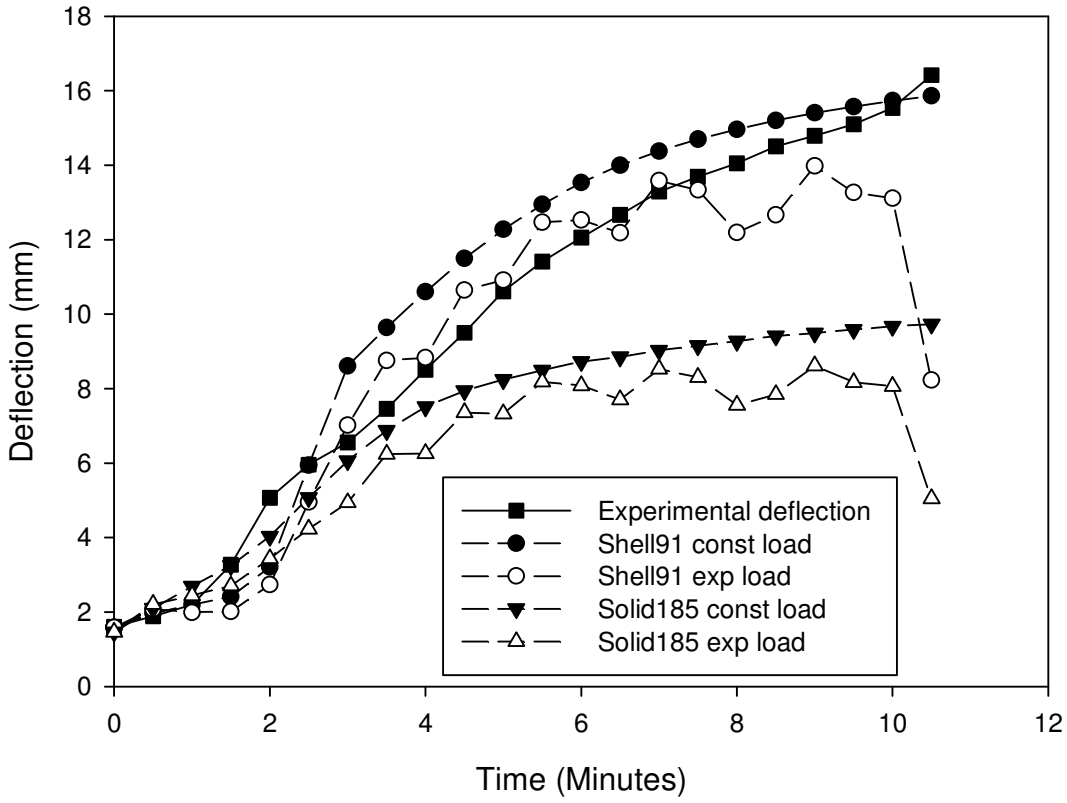

Figure 6.8: Test panel SS6.1 $[\pm 45]_{13}$ hot(a) and cold(b) face and cross section (c) after fire and load testing and deflection data under the cellulosic fire curve at 2.5MPa for 9mins 33sec

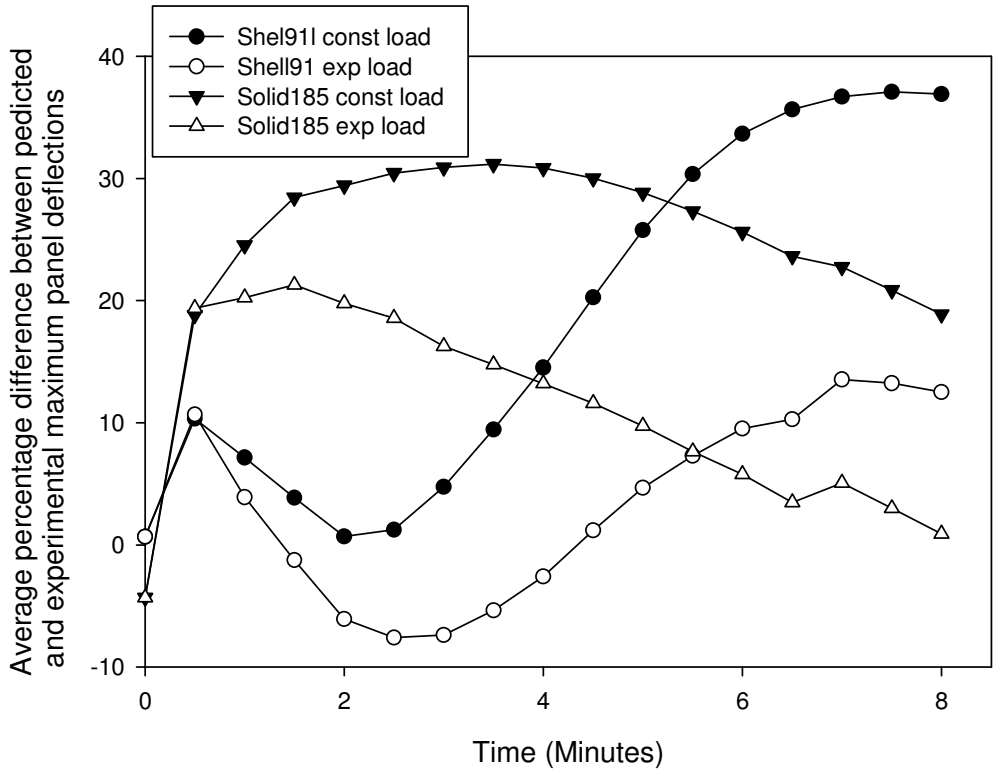

Figure 6.9: Average percentage difference between predicted and maximum panel deflections from each predictive method

The post experiment photographs show the hot and cold surfaces as well as a cross-sectional view taken at the centre of the panel. On the cold surface of each of the panels there is some discolouration in the centre where the loading pad was positioned, which looks to have been induced by the heat transfer. The reason the loaded area on the cold surfaces looks more affected by the heat is possibly that it is in the centre of the panel where it is suspected that the temperature is highest. Another contributing factor, however, it is due to the influence of the loading pad. In the unloaded area the heat can radiate away from the panel and is dissipated, which allows the panel to cool. The loading pad was made from rubber, which is a good insulator; this means that the heat was not be able to be conducted away from the panel surface over the loaded area as efficiently as it could radiate away from the unloaded area. Some delamination is evident in each of the panels on the cold surfaces along the direction of the fibres.

The hot surface of each panel has been completely charred and it is possible to see a large degree of delamination in Figure 6.6 and Figure 6.7 in particular. The edges of the panels where the support frame clamped the panels in place do not appear to have been significantly affected by the fire. This indicates that the heat transfer across the plane of

the panel is significantly less than through the thickness. The deflected shapes of the panels can be seen in the cross sectional views shown. It is possible in each case to see that the charred layer is not an even thickness across the panel. It appears that the charred region is thicker in the centre of the panel than at the edge. It is probable that this is due to the heat source being directed at the centre of the panel and causing the centre to heat up before the edges. It can also be seen that there is not a clear distinction between the virgin panel and the charred region in Figure 6.6 and Figure 6.7 when looking at the cross sections.

The graphs show the comparison between the predicted and experimental deflections. The general trend in the experimental results is a near linear increase in deflection with time. The predictions using element SHELL91, which assumed a constant temperature across each layer, show a non-linear response with a sharp rise in deflection occurring between two and four minutes in the cases shown above. This ties in with the behaviour of epoxy resin at elevated temperature discovered in Chapter 5, where a dramatic decrease in stiffness occurred at the glass transition temperature. Taking the temperature profiles that were input into the thermo-mechanical models, which are given in Appendix E.3, it can be seen that the sharp rise in deflection which occurs in each of the tests coincides with the cold face of the panels reaching 70^{o}C-80^{o}C. This trend was not matched in the experimental results. A possible reason for this discrepancy could have been the method of obtaining the material properties. In testing the properties of the epoxy resin at elevated temperatures a heating rate of 10^{o}C per minute was used. In the experiments the hot surface was being heated at a maximum rate of approximately 300^{o}C per minute. The higher heating rate would be expected to cause the glass transition temperature to occur at a higher temperature and this could account for the difference between the experimental results and the predictions.

In the predictions using the element SOLID185, which accounted for the in plane temperature gradient, the increase in deflection was more gradual and there was not a clear step in the curves at the point at which the cold face temperature reached the resin glass transition temperature.

Figure 6.9 shows the average percentage difference in maximum panel deflection between the predicted and experimental results in half minute intervals for all of the

single skin panels tested. The data has been calculated in a cumulative manner such that the difference given at a set time has been calculated as the difference from the start of the test until that time. The negative values indicate the predicted values were lower than the experimental values. Looking at the result from the solid element modelling it is clear there is a phenomenon occurring within the first minute of the tests which is not being accounted for. Before the fire was started the solid models under predict the deflections by 4%. After one minute the predictions are over predicting the results by 19% and the initial deviation in the first minute the results the solid element predictions become more accurate with time.

The shell element predictions show a good correlation with the experimental result up to three and a half minutes, at which point the constant load predictions begin to overestimate the deflection by a large degree.

Over the course of all of the experiments, it would appear, using SHELL91 with the experimentally recorded load that it predicts the deflection most accurately. Using the experimental load in both cases seems to give more accurate result indicating that the recorded load was the actual applied load and further work needs to be done refining the control system in order that a constant load can be held as the panel becomes more ductile.

The results of the sandwich panel test are shown in Figure 6.10. The photographs show a large degree of delamination on the cold face emanating from the loaded region outwards. The hot surface shows a similar form to the single skin panels in that it is completely charred and delaminated. The cross section photograph shows a large amount of core compression occurring in the area where the panel was loaded. The graph indicates that the deflection of the panel increases in three distinct steps, which appear to occur at three, five and eight minutes. This is thought to be due to the way the panel is formed of three different layers.

The predictions using SHELL91 and SOLID186 in a one dimensional heat flow thermo-mechanical simulation fluctuate either on or slightly above the experimental curve in Figure 6.10. There is an initial deviation between two and three minutes, where the predictions overestimate the deflection. This could be due to the compression of the

core, which is not accounted for in models. The three step form is also seen in the constant load prediction although the increase in deflection from the initial step is more pronounced than in the experimental result.

The predictions made using the SOLID185 and SOLID185 model do not appear to accurately model sandwich structures. This could be due to the way the element behaves. SOLID185 does not allow rotations and this could affect the way the skins in sandwich structures are modelled. Normal practise in modelling sandwich structures is to assume the skins undergo bending only while the core undergoes shear only. It is possible that it is the lack of rotations allowed at the nodes which is preventing the model from producing the expected result.

The predictions made by the thermo-mechanical models here can be seen to be in the correct order of magnitude as the experimental results and in some cases match the results to a reasonable degree. They can provide an indication of the behaviour of composites subjected to fire and load. The predictive models are not however at a stage where they should be used as a design tool and relied on to predict behaviour. Further work is needed in validating and refining the models.

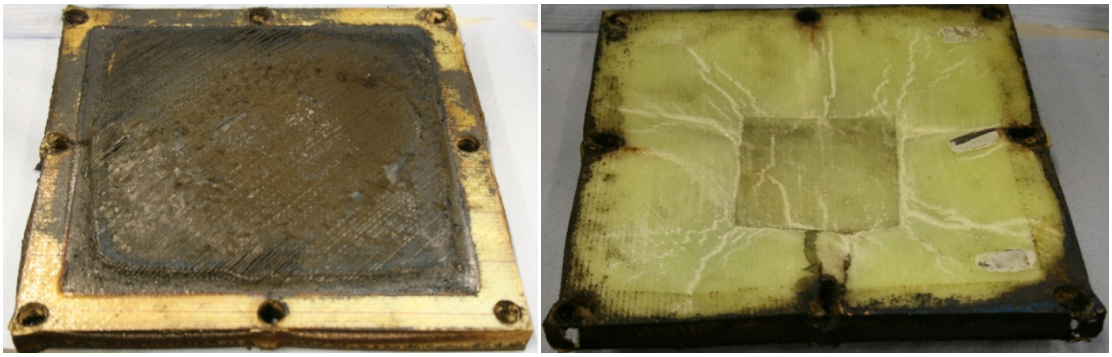

(a) (b)

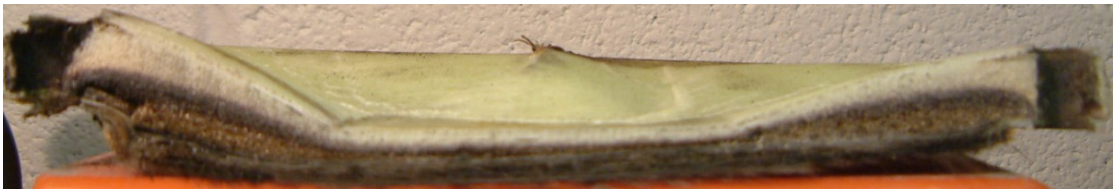

(c)

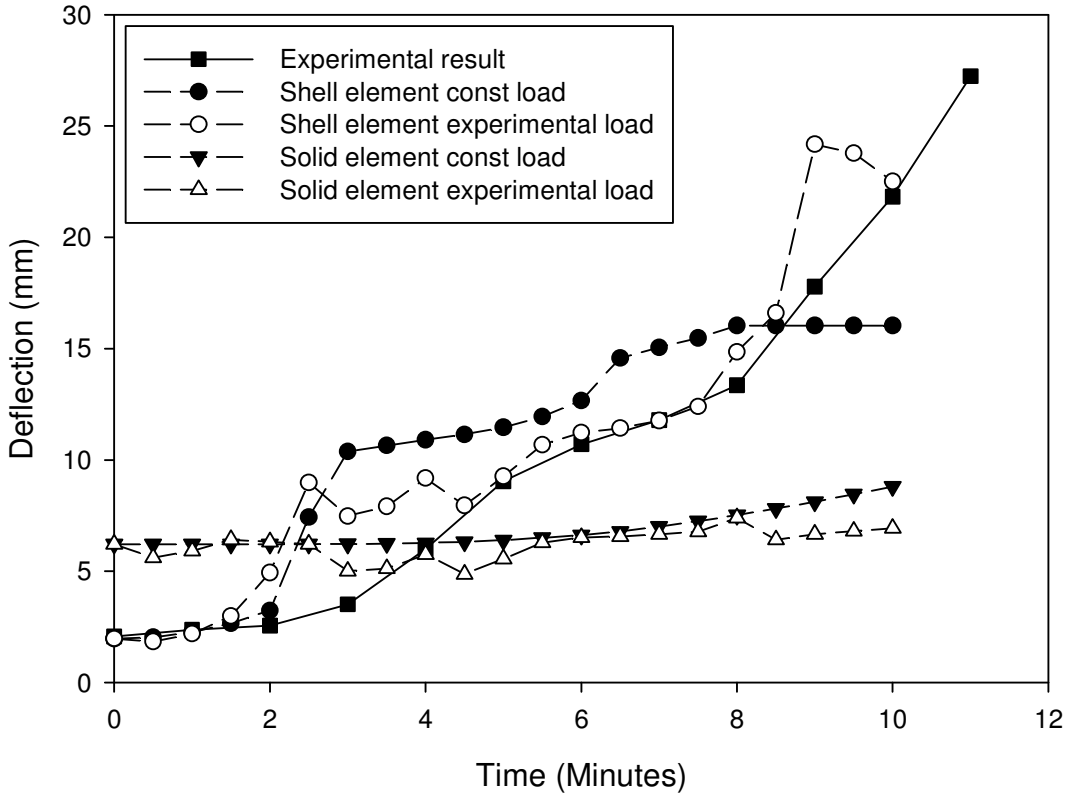

Figure 6.10: Test panel SW2 hot(a) and cold(b) face and cross section (c) after fire and load testing and deflection data under the cellulosic fire curve at 3.1MPa for 10mins 12sec

6.5.1 Analysis of Results

In order to assess the relative performance of each of the panels, whilst being subjected to a cellulosic fire and load, the percentage change in stiffness has been calculated.

The SHELL91 ANSYS finite element model created in this chapter was adapted to calculate the effective isotropic stiffness of each panel at thirty second intervals throughout the tests. The normalised decrease in stiffness was then calculated and is shown in Figure 6.11.

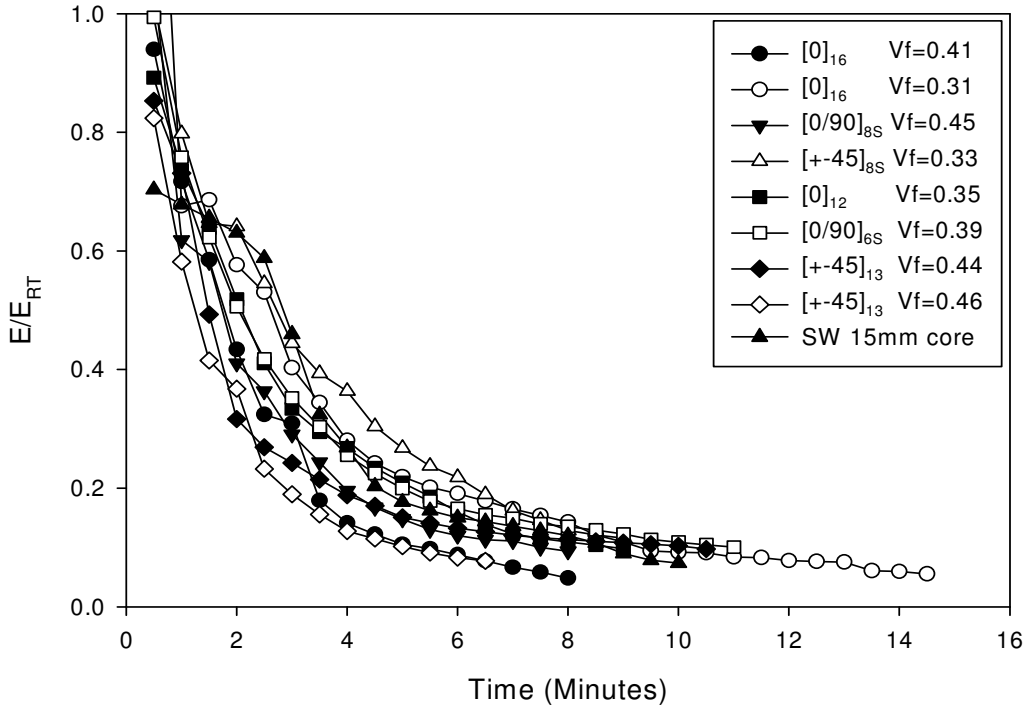

Figure 6.11: Normalised decrease in stiffness over time of composite panels subjected to combined load and cellulosic fire curve, E and E_{RT} represent the effective isotropic panel stiffness during the test and at room temperature

It is evident that there is a definite trend here, which applies to all of the panels including the sandwich panel. There is dramatic decrease very soon after the fire is started, with a 50% decrease on average after two minutes and a 75% decrease on average by four minutes. There is no clear difference in the performance of the different panels with different lay-ups, thickness or fibre volume fraction.

The form of the sandwich panel curve does differ slightly from the single skin panels in that there seems to be a more stepped decrease in stiffness than in the single skin panels

where the curves are smoother. The initial decrease in stiffness after 30 seconds, of the sandwich panel is 30%, which is considerably higher than the single skin panels. The decrease after 2 minutes is then 40% which is at the lower end of the results. By four minutes into the test the stiffness decrease is close to the average value for all of the panels.

The stiffness of a panel subjected to fire at any given time will be a function of the temperature profile through the panel. The temperature profile through the panel under a given fire curve will be a function of the panel thickness, assuming all other panel properties remain constant. Therefore in order to scale the results from a thin panel tested in the Vulcan apparatus to a large scale panel a scale factor would need to be applied. However the results shown in Figure 6.11 indicate that the percentage reduction in stiffness versus time is not sensitive to the panel thickness.

The reason for this similarity may be due to the process by which the load is supported by the fibres in a tensile net. Initially as the load is applied the loaded (cold) face will be under compression and the unloaded (hot) face will be in tension. As the panel is heated and the resin degrades the load begins to be supported by the fibres alone. As this occurs the loaded face will no longer be in compression but part of a tensile net. The net is held in place by the intact composite around the edges of the panel. Once this process has occurred it is proposed here that there is little variation in the stiffness of the fibres at elevated temperatures and this is why the results show similar levels of degradation between each panel type.

Based on the above assumption a relationship has been derived from the results shown in Figure 6.11 to relate the non-dimensional loss of stiffness in a composite panel during a cellulosic fire test to the elapsed time. The exponential decay equation shown below has been fitted to the results given in this chapter.

$$E_t/E_{RT} = A \cdot exp^{\frac{B}{t+C}} \quad (6.1)$$

Where:

E_t = effective isotropic Young's modulus of the panel at time t (GPa)

E_{RT} = Young's modulus at room temperature (GPa)

A = 0.0155 B = 28.9 C = 6.48

t = elapsed time (minutes)

Using Equation 6.1 the stiffness of a panel can be generated throughout a standard fire test. This equation has been incorporated into an ANSYS program, which has been written to output the maximum panel deflection over the course of a cellulosic fire test. The program requires the panel dimensions, loading conditions and initial panel stiffness as input parameters and is given in Appendix D.5.

The results presented in this chapter have shown that sandwich panels offer a similar level of performance to single skin panels when subjected to fire and an out of plane mechanical load. Work conducted by Mouritz and Gardiner [2002] on the post fire compression properties of sandwich beams during fire showed a similar trend in the decrease of stiffness. A beam with 2.8mm thick glass reinforced vinyl ester skins and a 30mm PVC core In these tests a heat flux of 50kW/m^2 was used, this is equivalent to a constant furnace temperature of approximately 600^{o}C [Mouritz; Feih, Mathys et al. 2005]. This is close to the conditions experienced in the tests conducted in this chapter. The results indicated that the stiffness had decreased by approximately 50% after two minutes. A similar sandwich with a phenolic foam core shows a decrease of stiffness of 30% after 2 minutes.

Gibson et al. [2004] conducted flexural tests on single skin coupon samples while subjecting them to a heat flux of 50kW/m^2. For glass reinforced polyester laminates the results indicate that by 2 minutes the stiffness had decreased by 50%. For a glass reinforced phenolic laminate the results show the stiffness to have decreased by approximately 20%.

The results from previous authors' work on similar materials agree well with the results presented here. The form of loading differs in each case but the rate at which the stiffness of single skin and sandwich materials decrease in a given fire seem to correlate.

The two methods for predicting the structural response of composite panels described here provide a different approach to previous composite fire and load investigations. In previous works the emphasis has been on conducting coupon tests under tensile or

compressive loading whilst being subjected to a constant heat flux. [Gibson, Wright et al. 2004; Feih, Mathys et al. 2005]. These investigations have concentrated on determining the strength of the given materials. The experimental results and methods given here concentrate on the stiffness of the panels under constant load and a standard temperature time curve. This will prove very useful to designers needing to predict the effect of fire and mechanical load during service and during a regulatory fire resistance test.

6.6 Conclusion

The aim of this chapter was to create a method for predicting the thermo-mechanical response of single skin and sandwich panels to fire. This has been achieved with the creation of finite element models and an empirical relationship to predict the change in stiffness of single skin and sandwich panels during a fire and load test.

A new test method has been developed here, which is capable of subjecting single skin and sandwich panels to combined fire and load. The results from the testing indicate a good level of consistency although there is room for more work to develop the apparatus further.

Of the four different methods of modelling the deflection, using the shell elements, assuming a constant temperature profile across the panels and the recorded load was found to match the predicted results with the greatest accuracy. The average difference between the predicted and recorded results was within ±14% using this method.

The results from the testing have shown that both single skin and sandwich panels undergo a rapid loss of stiffness whilst being subjected to a cellulosic fire. A decrease in stiffness of 50% occurs within the first two minutes and 75% within four minutes. Both the single skin and sandwich panels follow the same pattern of loss of stiffness which has been modelled by an exponential decay equation. This non-dimensionalised equation will be able to predict the loss of stiffness of a composite panel at a large scale and hence the deflection throughout a standard cellulosic fire resistance test. This will allow a prediction to be made for the fire rating of a panel in flexure with just knowledge of the initial equivalent isotropic stiffness.

Whilst the modelling using element SHELL91 proved to match the experimental results most accurately it would be preferable to have the ability to model heat flow in three dimensions with layered structures. This is not currently possible using ANSYS but would be particularly important when looking to develop the model for predicting the response of more complex structures outside of a laboratory environment. In order to develop the model further a progressive failure routine could also be incorporated. The work done in Padhi et al. [1997] showed how a progressive failure routine for composites can be incorporated into a finite element model using the ABAQUS software.

7 Application of Predictive Methods to Full Scale Structures

7.1 Introduction

The aim of this chapter is to verify the methods proposed in Chapter 6 for predicting the thermo-mechanical response of a full scale lifeboat deck sandwich panel under fire and mechanical load.

In this chapter the numerical models and the empirical relationship formed in the preceding chapters to predict the response of panels subjected to load and fire on a small scale were used to make predictions on a larger scale. One of the objectives of this thesis was to produce a method of predicting the response of a full scale composite panel in a fire resistance test. This chapter brings that objective to conclusion and uses the methods described in previous chapters in order to achieve this.

A fire resistance test was conducted at the Building Research Establishment (BRE) at a scale similar to that defined by IMO regulations and the results have been compared with the predictions. The test subjected a sandwich panel of the same lay-up that has been tested at small scale in this thesis to the cellulosic fire curve and a constant load.

7.2 Large Scale Fire Resistance Test Method

The fire resistance test was carried out at BRE in Watford using a furnace which measured 1.5m × 1.5m. The test panel used, which was representative of a RNLI all weather lifeboat deck, was SW 1 as used in Chapter 4 and the lay-up s given below:

QE600/QE1200/H100/QE1200/QE1200

The resin used was Ampreg 22 and the panel was made by wet lay-up with vacuum consolidation. The H100 Divinycell core was 25mm think and the skins were 1.5mm thick each, making the panel 28mm thick. The panel measured 1.8m × 1.8m and weighed 26.28kg.

The panel was attached horizontally on top of the furnace shown in Figure 7.1 and clamped along the edges as shown in Figure 7.9. The outer 0.15m around the panel rested on the furnace leaving an area of 1.5m × 1.5m exposed to the fire.

Figure 7.1: 1.5m × 1.5m fire resistance furnace

The loading was applied over a central area of 0.5m × 0.5m by four columns of weights each weighing 34.95kg and a connecting steel stud weighing 1kg giving a total weight of 140.8kg and a load of 1.38kN. Each column of weights was supported on four 15mm diameter foot prints so as to minimise the effect of the weights on the heat transfer from the cold surface of the panel.

The particular loading scenario was chosen for two reasons; first, with clamped edges and a central patch load it broadly replicated the testing conducted in the small scale experiments. Secondly, the size, boundary conditions and loads were chosen to simulate a scenario aboard a lifeboat with two people standing in the middle of a section of deck.

The furnace temperature was measured by four bare-wire chrome/alumel thermocouples arranged symmetrically in the furnace so the measuring junctions were 100mm below the surface of the test panel. The furnace temperature followed the cellulosic fire curve as specified in IMO Resolution A.754 (18). The pressure inside the furnace was

monitored by a transducer located 100mm below the test panel and the pressure was maintained in accordance with Section 8.3.2 of the IMO resolution.

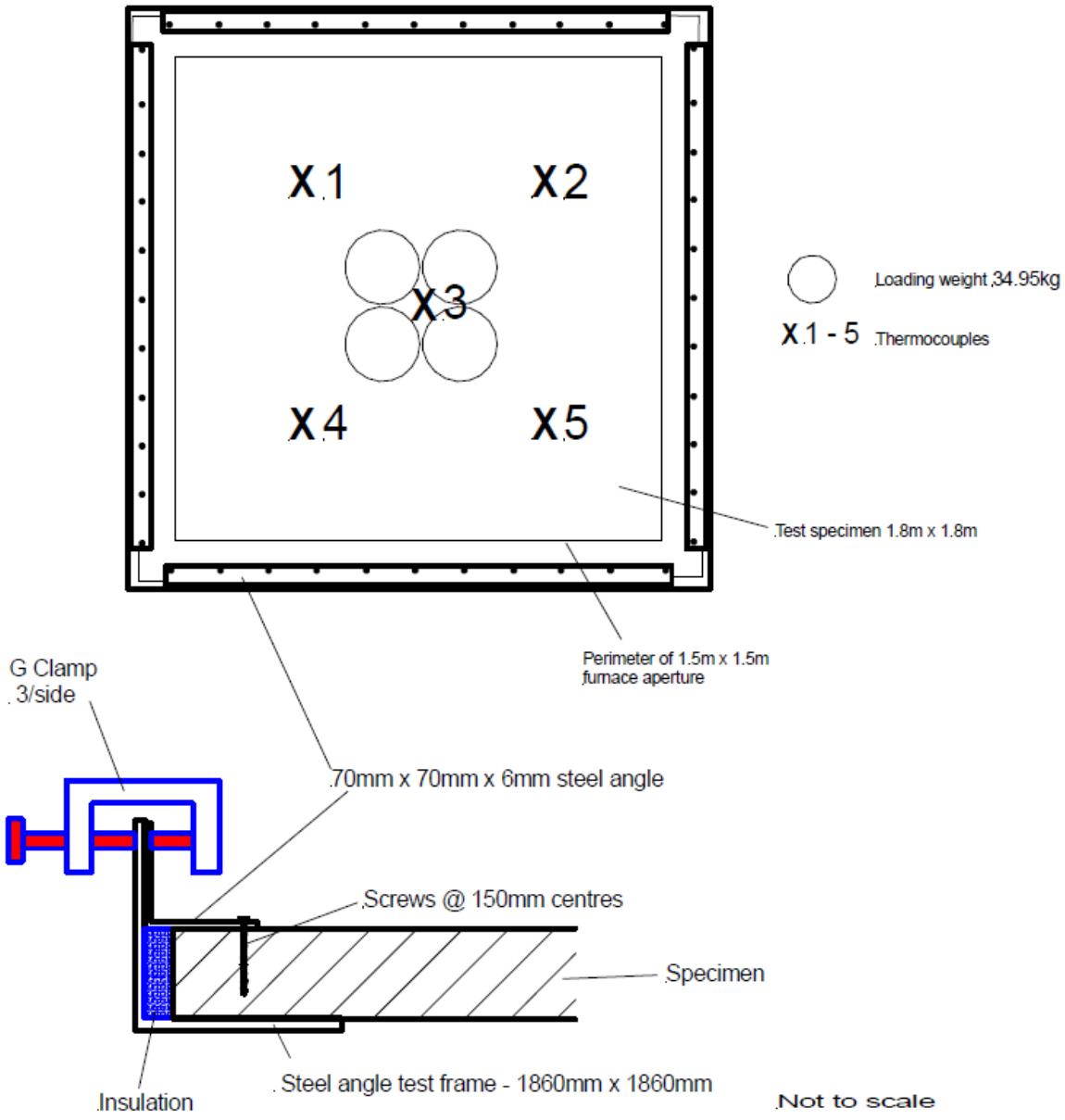

Figure 7.2: Clamping method for BRE fire resistance test

The panel cold surface temperatures were measured by five chromel/alumel thermocouples each soldered to a copper disc and covered by an insulation pad. The thermocouples were arranged as shown in the figure above with one in the centre of the panel and the other four in the centre of each quarter section.

The vertical deflection of the panel was monitored throughout the test by a displacement transducer connected via a steel wire to the centre of the unexposed face of the panel. All recordings were taken at 30 second intervals.

The test panel measured 1.8m × 1.8m and was fixed at the edges leaving an area of 1.5 × 1.5m exposed to the fire. The furnace heating curve and appropriate procedures and criteria of IMO Resolution A.754 (18) were utilised for the test. A load of 1.4kN was applied over a central area of 0.5m × 0.5m for the duration of the test.

7.3 Predictions

The prediction of the response of the fire resistance test will be dealt with in two stages, first, the temperature on the cold surface of the panel will be predicted and, secondly, the central deflection of the panel will be predicted.

7.3.1 Thermal Prediction

According to the IMO regulations the panel will be deemed to have failed if the average cold face temperature rises by 140^{o}C above the original temperature or if one thermocouple records a rise of 180^{o}C above the original temperature.

Two methods were trialled in order to predict the cold face temperature recorded during the test and hence the time to failure. Method 1 used the heat transfer program described in Chapter 4, assuming a linear heat transfer through the core. In method 2 the predicted cold face temperature was taken directly from the recorded temperatures in the fire resistance tests conducted using the Vulcan small scale testing apparatus using the same sandwich material. The use of the heat transfer program was described in Chapter 4 and will not be repeated here.

7.3.2 Thermo-Mechanical Prediction

As the test was not conducted as laid out in the IMO resolution the failure criteria given do not apply. The IMO test details are given in Appendix E.1 for reference. However, using the two methods described in Chapter 6, to predict the response of a panel under fire and load, a prediction of the failure time of the sandwich panel has been made.

Two methods were again adopted to determine the response of the panel to the combined fire and load. The first method used adopted the finite element program described in Chapter 6 with SHELL91 skins and SOLID185 core. The second method used the empirical relationship derived in Chapter 6 to relate the decrease in panel stiffness to the elapsed time.

7.4 Results

The test was filmed and still photographs were taken from a viewpoint above the furnace when conditions allowed. A series of observations were recorded by BRE and are given in Appendix E.2. Figures 7.3 to 7.6 show photographs of the state of the panel at specified points throughout the test. The time to various failure criteria are listed below in Table 7.1.

Time (minutes)	**Event**
13	Insulation failure- Thermocouples X4 and X5 exceed 180^{o}C rise
14	Insulation failure- Average cold face temperature rise exceeds 140^{o}C rise
50	Failure of panel integrity- sustained flaming on unexposed face

Table 7.1: Times of panel failure

The recorded cold face temperatures are shown in Figure 7.7 and the recorded deflection is shown in Figure 7.9 along with the results of the two predictive methods.

Figure 7.3: Unexposed face of the panel with loading weights in place before the fire was started

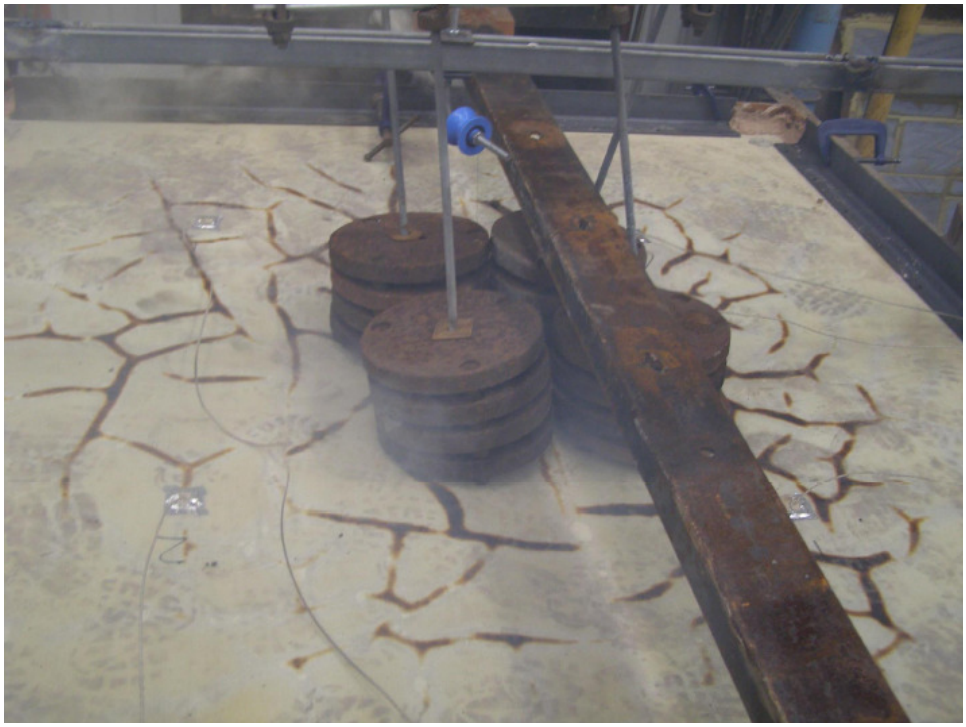

Figure 7.4: Unexposed face of test panel after approx. 14 minutes showing discolouration of surface and smoke

Figure 7.5: Unexposed face of panel after approx. 39 minutes showing darkening of surface and dense smoke

Figure 7.6: Unexposed face of panel after approx. 51 minutes showing flames protruding through hole

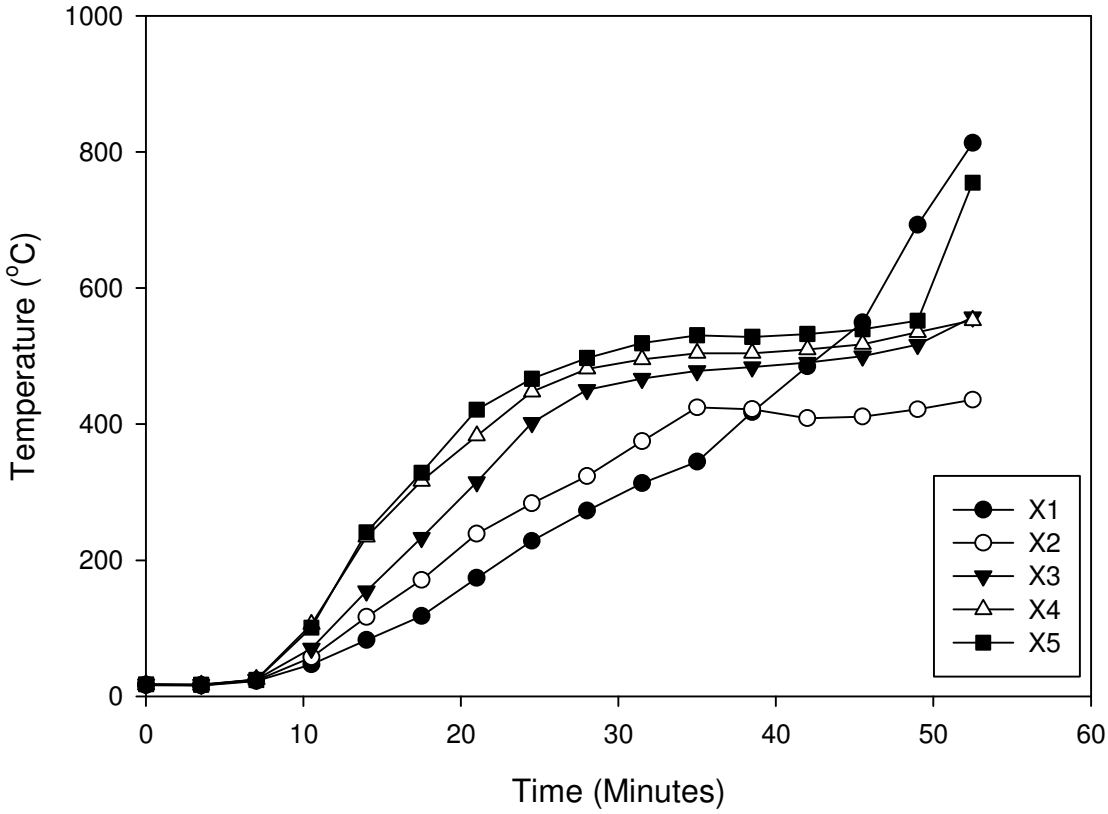

Figure 7.7: Cold surface thermocouple measurements, legend refers to positions shown in Figure 7.2

The insulation failure criteria were both met within 15 minutes, which would give the panel an A-0 rating in accordance with the IMO resolution code. The integrity of the panel was maintained until 50 minutes which would prevent the panel from attaining an A class rating in accordance with the resolution. The loading of the panel was not in line with the regulations as such it is not possible to determine at what point the panel would be deemed to have failed in accordance with the deflection limits. The resolution states, however, that the rating is determined by the first mode of failure, so the insulation failure would determine the rating in this case. These results would not necessarily represent the results of an official lifeboat deck fire resistance test as there are certain mitigating factors. In an official test the panel would be expected to be coated with the paints that would be used in service and the loading would be as described in Appendix E.1. In the case of the lifeboat deck the coatings include an intumescent paint which would be expected to have an effect on the fire resistance of the panel. In order to attain an A class rating the panel is required to prevent the passage of flame for one hour. In this test that ability would have been affected by the load applied.

The temperature results illustrated in Figure 7.2 show a large variation in the readings from the different thermocouples at any given time. During the middle period of the test there is a range of 240^{o}C between the thermocouple readings. This illustrates the uncertainty in the results of composite fire testing, even during a test conducted by an official testing body. The cause of the large difference could be the variation of the temperature within the furnace. The furnace recorded temperatures, shown in Appendix E.3, illustrate however that the difference is not as pronounced around the same period. It is possible that the difference is caused in part by the manner in which the foam core degrades. It can be seen in Figure 7.4 that the resin degradation on the cold surface is forming in a segmented manner with interconnecting brown lines. It is possible that the foam recedes on heating leaving pockets of air forming areas of low heat transfer and areas where the foam is more densely concentrated allowing heat to conduct through the panel more readily. A full field temperature measuring technique such as infrared thermography would allow a clearer picture of the temperature distribution to be monitored.

Figure 7.6, at the end of the test, shows the edge of the panel, which is not exposed to the fire, to be unaffected by the heat. This mimics the results seen from the Vulcan fire tests and shows that the heat transfer is very low in the plane of the panel during a fire test.

On the hot face of the panel it was possible to see the sheets of glass reinforcement hanging down into the furnace during the latter stages of the test. The sheets were hanging down in large sections indicating that they were full width of the sheets that the panel was laid up with. It is suspected that the glass reinforcement provides the majority of the stiffness and strength of the panel at high temperatures. This in part comes from the fact that the fibres are continuous and are clamped at the edges. The use of plies, which do not stretch the length of the panel, will reduce the ability of the panel to support a load once the resin has fully decomposed. The use of woven fibres in composite structures may help reduce the effects of this problem. These would continue to hold together after the resin had been depleted and provide a greater panel stiffness.

Figure 7.9 shows the results of the recorded deflection from the fire test on the sandwich panel along with the two sets of predicted deflections. At 4 minutes there is a

large jump in the recorded deflection, which occurs over one logging period. It is suspected that this may be due to the displacement transducer slipping during the testing or panel slipping in the test frame. The results have been offset by 14mm to account for the possible slippage of the transducer and this is indicated by the dashed line in Figure 7.9.

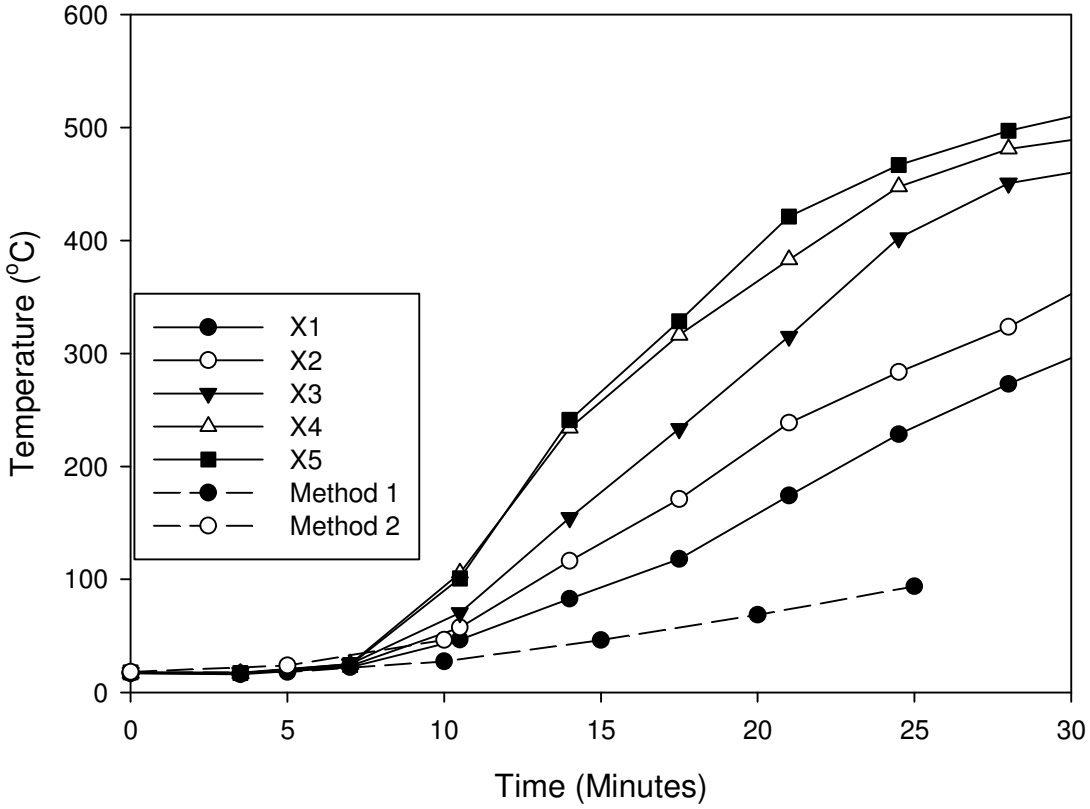

Figure 7.8: Comparison of recorded and predicted cold face temperatures

Figure 7.8 shows a comparison of the recorded temperatures from the cold face during the test and the two predicted temperatures. Method 1 took the results from the heat transfer program described in Chapter 4 assuming a linear heat transfer through the core. It can be seen that this underestimates the temperatures by a large degree. This can be explained in a two ways. It is possible that either the core becomes more conductive as it is heated or that the hot face temperature used as input into the model is lower than the actual hot face temperature of the panel tested here.

Method 2 took the cold face temperature directly from a panel of identical lay-up, which was tested in the Vulcan fire test apparatus. In this case, due to malfunction of the

burner system results were not available beyond 10 minutes. In the first 10 minutes however the result lies within the recorded temperatures.

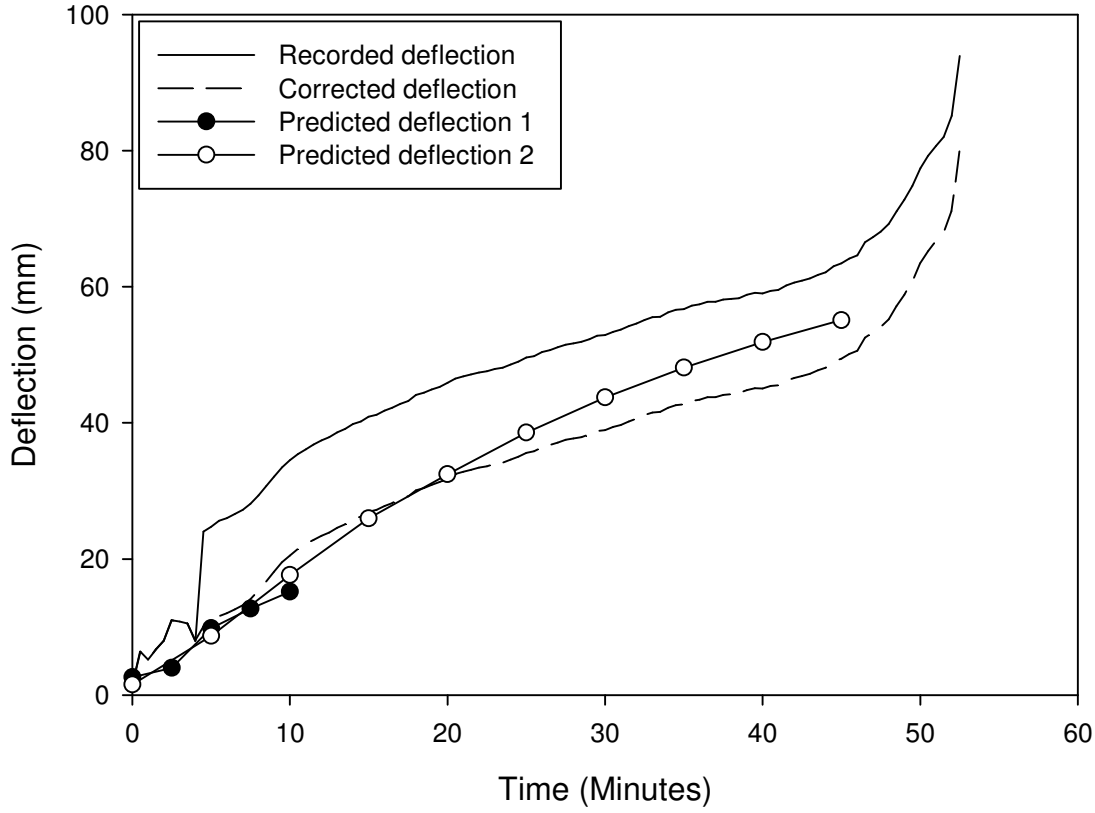

Figure 7.9: Comparison of recorded panel maximum deflection with predicted deflection

In calculating the first predicted deflection results seen in Figure 7.9 the temperatures from method 2 as described in the preceding paragraph were used. The temperature dependent material properties used were the same as derived for the sandwich panel modelling in Chapter 5. The finite element model was made using ANSYS and the panel was constructed using SHELL91 elements for the skins and SOLID185 elements for the core. The code was the same as used in the sandwich model described in Chapter 6, which is shown in Appendix D.3. The test only lasted for 10 minutes and therefore the temperature profile was not available to predict the deflections for any longer period.

The second predicted deflection was calculated using the empirical relationship developed in Chapter 6 to relate the loss of panel stiffness to the elapsed time.

Neither of the predictions match the recorded deflection with any accuracy after the first 4 minutes. This adds to the suspicion that there was an error in the recording equipment. Both the predictive curves follow a similar line, which matches the corrected deflection. The first method stops at 10 minutes, due to the lack of temperature data available. The second method appears to match the corrected deflection very well with a maximum difference of 7mm at 41 minutes into the test.

Method 2 shows a remarkable similarity to the corrected deflection in the test up until the point the panel lost structural integrity. The relationship used to model the deflection will need to be compared with further large scale experimental results but current results show that it would be able to predict the time to failure in terms of the failure criteria set in the IMO resolution.

Method 1 showed promising signs of matching the deflection. This method is more versatile than method 2 as it will allow more complex geometries to be modelled along with different temperature inputs. Further work in acquiring temperature profiles from small scale testing and heat transfer modelling will allow the method to be scrutinised further. This method should also allow a prediction of the failure time for a fire resistance test to be made.

The results shown here support the findings from earlier chapters regarding the insulating properties and the panel stiffness. The stiffness reduction seen in the panel followed the trends seen in Chapter 6 as well as the trends documented in Mouritz [Mouritz].

The insulating properties of the panel match the values found from the small scale testing for a panel with the same lay-up.

7.5 Conclusion

The aim of this chapter was to verify the thermo-mechanical models produced earlier in the thesis for a large scale sandwich structure exposed to fire and mechanical load. The cold face temperatures were successfully predicted for the initial period of a full scale fire test using small scale experimental data. Deflections were also successfully

predicted using numerical modelling and an empirical relationship derived from small scale testing.

The fire resistance test showed the panel to lose stiffness rapidly with a 70% decrease occurring in the first 30 seconds. The integrity of the panel was intact for 50 minutes before smoke and flame penetrated through the cold face. The stiffness and integrity retained in the panel is in all probability due to the fibres being supported at the edges. The edges of the panel which were not exposed to the furnace remained relatively undamaged, highlighting the very one dimensional nature of the heat flow. The continuous fibres that were used were held in the intact matrix from the undamaged edges while in the centre of the panel the load put the fibres in tension. This phenomenon of the largely one dimensional nature of the heat flow in composites could be put to good effect by designers of composite structures wishing to minimise the risk of structural catastrophe in the event of a fire.

The measured temperatures on the cold surface of the panel show a great deal of variation. This highlights the inexact nature of composite testing in fire and therefore the difficulty in predicting the response. This result from a certified IMO testing facility shows the Vulcan fire test apparatus in a good light, where the temperature difference across the hot and cold surface were relatively small.

The cold face temperature predictions showed some promising results. The temperature results taken from the small scale testing matched the recorded results up to 10 minutes. The results generated by the heat transfer finite element model under predicted the results. This indicates the possibility that as the core material decomposes a more thermally conductive structure is formed. Further work is needed in specifically modelling the decomposition of foam core materials is necessary in order to predict the temperature profile through sandwich structures.

The predictions made for the maximum deflection of the panel showed a very good correlation with the corrected recorded results. It is not known for sure why there is a sudden jump in the results, but if it is assumed that this is due to the panel or the transducer slipping then the predictions correlate very well. Both methods of prediction could prove to be an invaluable tool in determining the outcome of the standard tests

and the response of real structures subjected to fire. Further experimental work is necessary in order to validate these predictive theories further.

The small scale testing approach to predicting either the insulating properties or the structural properties has been shown to have some distinct advantages over the modelling approach. A complete self contained solution to predict the response of panels in full scale tests has been developed. No knowledge of material properties is required and no other testing is necessary. The drawback is the range of scenarios that can be predicted is limited. The fire curves which can be modelled are limited to what the burner can be programmed to do and the loading scenario is fixed.

The Numerical modelling approach could provide a more versatile solution to predicting the response of complex fire situations. These could involve different geometries and loading situations or temperature inputs. One of the limitations is that it is dependent on the material properties put into the model. As was seen in Chapter 4 a long list of properties is required needing specialist equipment to measure them. The benefit of these models over the small scale experimental approach is the versatility they can offer in terms of modelling different structures. The only drawback currently is the lack of appropriate elements within the ANSYS software.

8 Conclusion

8.1 Overview

The aim of this thesis was to develop methods for assessing the thermal and mechanical effects of fire on single skin and sandwich composite structures. This has been achieved in this thesis through the completion of each of the objectives originally stated in Chapter 1:

1. To understand the behaviour of single skin and sandwich structures under fire and mechanical loading.
2. To outline approaches to allow for scaling of experimental results from laboratory bench to full scale panels.
3. To develop predictive models for predicting the behaviour of single skin and sandwich panels under fire and mechanical loading.

In Chapter 4 the purely thermal effects were studied and a better understanding of how composites react in a fire resistance test was derived. The heat transfer through the PVC foam core was seen to be near linear for up to 20 minutes and the core was seen to decompose in a three stage process. The heat flow through both single skin and sandwich materials was found to be very small in the transverse direction. A method was outlined for a small scale fire resistance test and single skin and sandwich panels were tested. The results of the test compared well with the heat transfer model based on the Henderson equation.

In Chapter 5 a method was proposed to determine the temperature dependent mechanical properties of the constituent products of single skin and sandwich materials. This method was used to generate laminate properties of single skin and sandwich panels at a range of temperatures. The data generated was then used in the development of thermo-mechanical models.

In Chapter 6 composite panels were subjected to combined fire and load in the small scale test apparatus that was developed. A rapid loss of stiffness was witnessed in both

single skin and sandwich panels and all of the panels tested followed the same relationship in the rate at which the stiffness was lost.

In Chapter 7 a large sandwich panel was tested under fire and load. The results showed a similar behaviour to the small scale test results. There was a rapid loss of stiffness under fire and load and the rate of the stiffness degradation was similar to that found in the small scale tests. There was also a large variation in the rate of heat transfer through the panel.

8.2 Original Contributions

A new apparatus has been developed with the ability to subject single skin and sandwich panels to fire and mechanical load. The results from the testing conducted have shown a high level of consistency in both the fire and fire and load testing. This approach can now be used to compare the merits of different materials with regards to their fire resistance. There is currently no generally accepted method of comparing the fire resistance of composites without conducting large scale and expensive tests.

A new method for predicting the response of full scale fire resistance tests has been developed. The results from both the fire and the fire and load testing were scaled up to predict the response of a large scale fire resistance test. In both cases the predictions matched the experimental results very closely. This approach to predicting either the insulating properties or the structural properties has been shown to have some distinct advantages over a modelling approach. A complete self contained solution to predicting the response of panels in full scale tests has been developed. No knowledge of material properties is required and no other testing is necessary. This method has been shown to provide a very practical and economical solution to the need to be able to compare different materials' fire resistance properties and to predict the results of full scale fire tests.

A new thermo-mechanical model has been developed using the ANSYS software and a version of the Henderson model for heat transfer has been used to model the response of composite panels subjected to fire. The heat transfer model produced adequate results in line with the experimental results. The thermo-mechanical model was used to predict the response of the small scale fire and load testing as well as the large scale test. It was

shown to be able to predict the deflections in the small scale tests to within ±14%. In the large scale test the model showed promising results during the initial phase of the fire, matching the recorded deflections well within the first 10 minutes. The benefit of these models over the small scale experimental approach is the versatility they can offer in terms of modelling different structures.

8.3 Further Work

1. The heat transfer through sandwich panels with decomposing cores is still not understood and further work is required in order to be able to model the decomposition effectively.

2. The thermo-mechanical numerical model is currently limited by the choice of elements available to allow for layered structures and 3 dimensional heat flow. The current method for modelling sandwich structures requires a vast number of elements to be used, which is not practical.

3. One of the areas of uncertainty regarding the modelling approach was the rate dependency of the material properties at elevated temperatures. Further experimental work in this area would allow this uncertainty to be quantified.

4. Each of the predictive methods presented in this thesis have had some success in matching the experimental results but further experimental work is needed to improve the confidence in the predictions

5. The small scale fire testing apparatus was shown to be limited in some areas and there are some refinements which could be made to improve the consistency of the testing. A more precise load control system would help a constant load to be kept throughout a test. The burner system was at times unreliable, which resulted in tests stopping before the intended time.

6. A method of measuring the strain at high temperatures would also aid the understanding of the response of composite materials to fire.

7. Lastly the next logical step in predicting the response of composites in fire would be to look at the strength. It would be possible to test panels to failure in the Vulcan apparatus and this would be of great interest to composite designers and operators of composite structures.

Appendix A

A.1 The Orkla Disaster

The Royal Navy of Norway composite mine hunter "Orkla" fire in 2002 did much to publicise the perceived weaknesses of composite boats. The vessel was largely constructed using sandwich materials with PVC cores and glass reinforced plastic skins. The fire, which started due to an oil leak resulting from a shaft failure, burnt for 24 hours before the boat capsized. The official report into the accident [RNoN TEG Report 2003] and Høyning [2003] give an insight into the causes of the fire.

The Orkla was sailing in calm seas, with very little wind, at a speed of 21-22 knots. At 0653 a loud band was heard. At 0654 a fire was discovered in the port side lift fan room. By 0656 the fire had escalated and 4 metre high flames could be seen on the outside of the vessel. All 5 of the fire hoses lost water pressure after 30 seconds and by 0659 the bridge was on fire. The ship was abandoned apart from a small team of crew fire fighting. At 0720 the wheelhouse collapsed and the fire spread throughout the ship.

At 1010 the fire fighting team left the ship and efforts to extinguish the fire from other vessels continued until 1730 without success. The ship then capsized at 0826 the next day.

The causes of the fire according to the report [RNoN TEG Report 2003] are numerous and involve design flaws, inadequate training, lack of risk assessments and a poor culture of safety within the organisation.

The direct cause of the fire initially was the failure of the cardan shaft connecting the engine to the lift fan on the port side. This tore off a hydraulic hose and sprayed hydraulic oil under pressure into the lift fan room, which ignited immediately. The reason for the shaft failure was said to be down to inadequate lubrication of the bearings. A similar incident had occurred in a sister vessel in 1997 but no fire was caused. However no action was taken after the original incident to prevent similar occurrences.

It was estimated that 2.5 litres of hydraulic oil were sprayed onto a red-hot bearing which started the fire. The fuel is estimated to have burned for 30 seconds with an average heat release of 2.7MW.

In the lift fan room, sound absorbing material lined the housing. This material was described as self extinguishing according to ASTM DI 1692. This does not necessarily mean that the material was non-flammable and no testing of the material was done to verify this. The material ignited immediately and it was calculated that it would have taken 2 minutes for all the material to burn with an average heat release of 6MW.

Figure A.1 shows the estimated heat release from the materials in the lift fan room. It can be seen that there is relatively little heat release from the initial hydraulic oil. The contribution from the GRP structure however is much greater and the long period of time it burned for will have contributed to the further spread of the fire. The graph shows the effect that the sound absorbing material had in providing the energy for the fire to start consuming the GRP structure. Without the insulation it is unlikely that the temperatures would have been high enough to ignite the GRP.

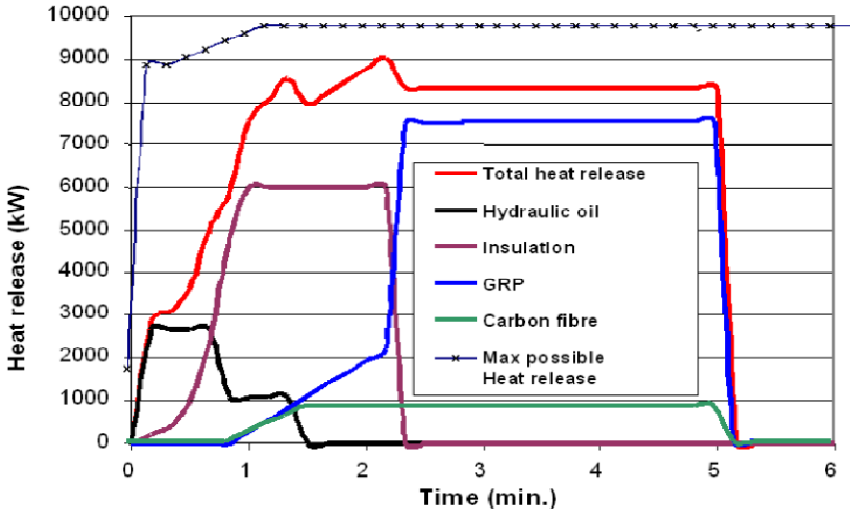

Figure A.1:Heat release from the combustible materials in the lift fan room. Source [RNoN TEG Report 2003]

No sprinkler systems were in place in the lift fan room as fire was not considered as a hazard. This also had some bearing on the reason why the sound absorbing material was not fully fire tested.

The failure of the cardan shaft resulted in a 40 cm diameter hole into the engine room. In addition the fire spread into the engine room through the hole and began to consume the GRP structure. A standard fire test was conducted for the GRP sandwich material used for the deck. The material failed the test but this was said to be due to insufficient curing of the laminates. No fire protective coatings were in place on either the underside of the decks or the bulkheads in the engine room. A risk assessment during the design stage stated that fire retardant paint was recommended for the interior structure and bulkheads. It was reported that the recommended thickness of fire retardant paint would have protected the structure from burning in the first ten minutes of the fire.

The wheelhouse which was made from a composite sandwich construction collapsed during the fire allowing the fire to spread into the rest of the vessel. Once one of the laminate skins of the sandwich construction failed, the global strength of the structure rapidly decreased and resulted in its collapse. The report states that the wheelhouse had no built in structural redundancy and the weight of the mast on the wheelhouse could not be supported when one of the laminate skins failed. However it had been recommended that internal stiffeners be used to support the wheelhouse roof and bulkheads to provide structural redundancy if one of the skins were to fail.

The fire spread further through the internal structure of the vessel once the wheelhouse had collapsed. It was stated that the doors in the vessel had passed recommended fire restriction tests, but no evidence of the testing was found. It was suspected that none of the doors, or ducts for cables and pipes had been tested.

In terms of fire fighting the crew were reported to have responded in the correct manner for which they had been trained. The training however was standard for all RNoN vessels and no special training was given for composite boats. As the lift fan room was not considered a fire hazard no sprinkler systems had been installed and the crew were not aware that a fire may start tin that location. If the crew had been trained differently it was claimed that they may have tackled the lift fan fire in a different manner and would have had some success in extinguishing it.

The water pumps failed after 30 seconds and all water pressure was lost. It was reported that it was known that the pumps had problems from experience on similar vessels, but

such problems were not documented. It was also stated that the pumps were only ever tested before the vessel was in service, whilst it was moored and in calm conditions. The report stated that these conditions were too ideal and in future the pumps should be tested in service on a weekly basis.

The fire and eventual loss of the Orkla cannot be put down to one single cause. The use of composite materials alone were not to blame for the loss of the vessel. It is clear that the real cause of the fire was a general lack of regard for safety in all stages of design and operation within the organisation.

It can be concluded from the report that composite boats are not intrinsically unsafe and should be able to withstand a fire given the correct preventative measures. Careful risk assessment and a culture of reporting problems and acting on them is needed to ensure the safety of any vessel. The fact that the Orkla was a military vessel meant that it did not have to comply with the IMO fire regulations. Following these regulations could have reduced the severity of the fire and prevented the loss of the vessel.

A.2 Fire Resistance Modelling

Research into the heat transfer through decomposing materials started with Bamford et al. [1946] who studied the one dimensional heat transfer through wood subjected to an intense heat source. The model predicted the heat transfer using the one dimensional transient heat conduction equation with an extra term to account for the decomposition reaction. The decomposition term was modelled using a first order Arrhenius equation and constant thermal material properties were used. A finite difference method was been used to solve the equations.

Research into the effects of fire on composite structures appears to have started in the early 1980s. This work generally comes from an aerospace background and as such concentrates on graphite/epoxy laminates. Pering et al. [1980] looked at the post fire strength and modulus and related this to the mass loss in the laminate. The heat transfer model proposed was based upon the transient heat conduction equation and accounts for the chemical reactions that take place in a decomposing composite by employing an n^{th} order Arrhenius equation. The format of the model in this case differs from most in that the heat source was been applied equally at both boundaries.

Chen et al. [1985] made the assumption that material was removed once it had undergone the charring reaction with a moving coordinate system used to account for the receding surface. This method was reported to overestimate the temperatures within the composite by about 15% initially, with increasing error over time. The error could be due to the very rapid heating to which the samples were subjected. The rate of temperature increase has a bearing on the reactions which occur within polymers, so the method of obtaining the temperature dependant properties needs to reflect the test conditions.

A.3 Reaction to Fire Tests

Ignitability is the ease with which a material can be ignited from a heat or flame source of a given size. This can be tested in a cone calorimeter and is measured as the time taken for flaming to start at a particular irradiation.

Non-combustibility involves heating a sample up to a temperature of around 750°C for 30 minutes using a radiant heat source. For a material to be classified as non-combustible there are limits on the allowable temperature rise of the sample above the set furnace temperature and also limits on the allowable weight loss of a sample.

Heat release is the amount of heat emitted by a material when it is subjected to a given heat or flame source. This is considered by some as the most important property of a material when categorising it with regards to fire [Babrauskas and Peacock 1992; Gibson and Mouritz 2006]. As such regulatory bodies have stringent limits on the allowable test results. These tests can also be conducted in a cone calorimeter.

Smoke toxicity and density are two properties which are also measured in a cone calorimeter. The density and toxicity are measured for given levels of irradiance on a sample. With regards to the loss of life through fire in the UK in 2004 over 53% of fatalities were due to being overcome by smoke [Office of The Deputy Prime Minister 2004].

A.4 Sensitivity of Material Properties

Krysl et al. [2004] conducted a parametric study of input variables to determine the relative effect of each property on the result of the temperature calculation. Figure A.2 shows the relative change needed in the given input variables to produce a change in the temperature of 50°C or 100°C.

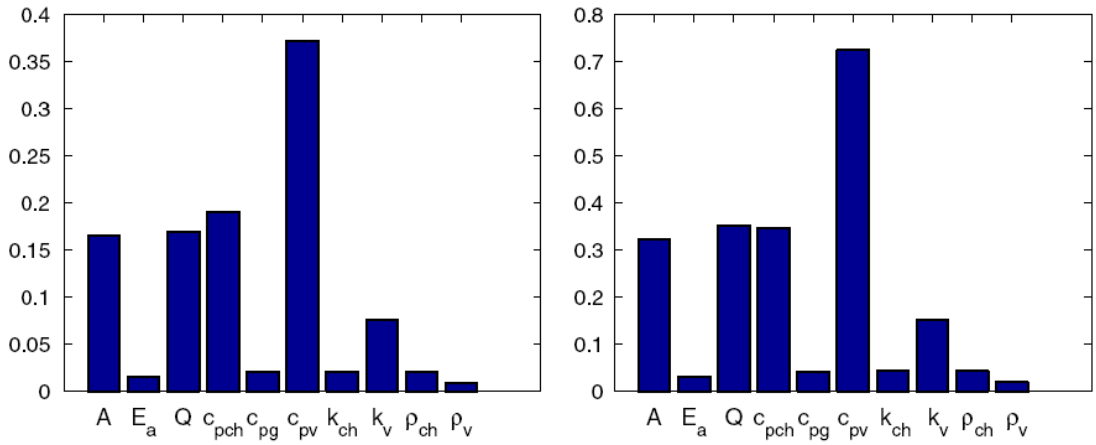

Figure A.2: Relative perturbations required to produce given variation of temperature. Left: variation of 50°C; right variation of 100°C. Source [Krysl, Ramroth et al. 2004]

From the results it can be seen that the most sensitive properties and therefore the properties which should be studied in greatest detail are the activation energy (E_a), the specific heat capacity of gas (Cp_g), the char thermal conductivity (K_{ch}) and the mass densities of the char and virgin material (ρ_{ch} and ρ_v). It should be noted however that the particular heating rate will have a bearing on these results. In a lower temperature test it would be expected that the properties of the virgin material would have a greater bearing on the results than the properties of the char material and the kinetic properties. The same must also be true in the initial stages of a high temperature test before the material has undergone pyrolysis. In Ramroth et al. [2006] this issue was addressed and the local sensitivity of each input variable with respect to time was studied to the calculated cold face temperature using the results from Wu et al. [1993]. An analysis of the uncertainty in the thermal output from a defined set of uncertain input data is also estimated. This has allowed the authors to estimate the variability in the model output and to see which parameter is having the largest effect on the output. Figure A.3 shows the normalised local sensitivity coefficients; the positive values indicate that increasing the input parameter results in an increase in the output (cold face temperature) and the

negative values indicate the reverse. For each parameter the sensitivity with respect to time is indicated by the varying shade from left to right. The rank order of the sensitivity of input values at a given time is shown in Figure A.4. What these two graphs show which could not be determined from Figure A.2 is the relative importance of each input property at any given time during fire exposure. This is particularly relevant when modelling the thermomechanical response of samples when failure can occur relatively quickly. Gibson et al. [2004] however, claims that the resin type has very little effect when it comes to modelling the mechanical failure of a laminate in an intense fire. The fibre volume fraction will also have an influence on the overall properties of any given material. The fibres tend to be more conductive than the resin so advanced composites with a higher fibre volume fraction would be expected to have a higher thermal conductivity.

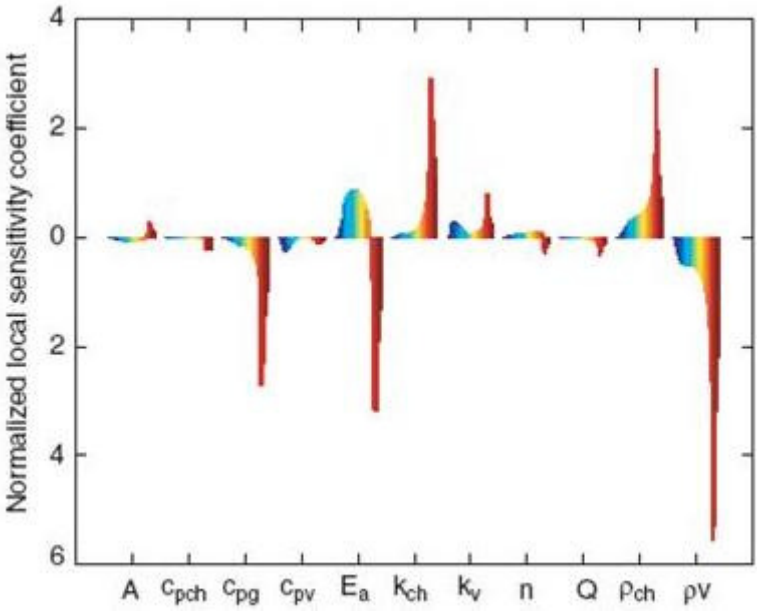

Figure A.3: Normalised local sensitivity coefficients. Source [Ramroth, Krysl et al. 2006]

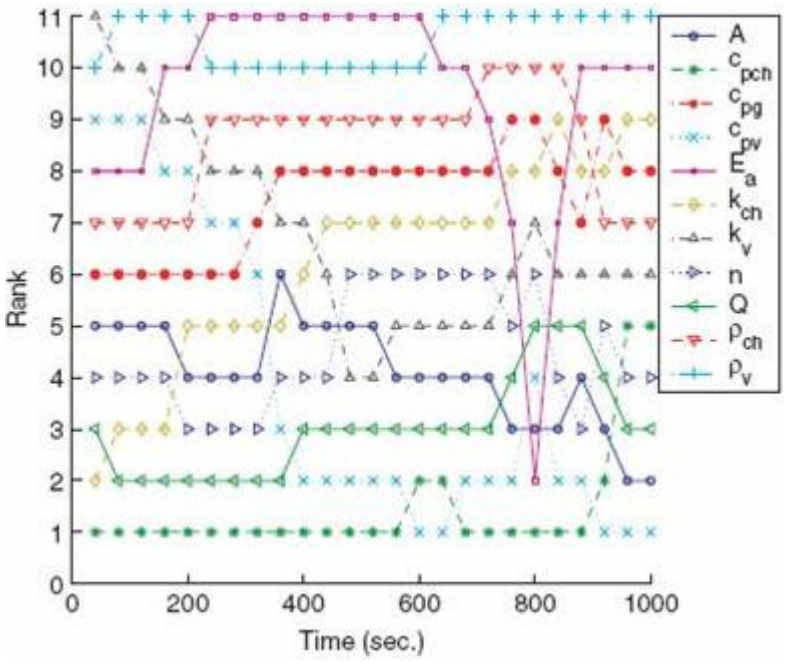

Figure A.4: Rank order of material property sensitivity with time. Source [Ramroth, Krysl et al. 2006]

Time period	**Positive effect**	**Neutral effect**	**Negative effect**
Early stages	E_a, K_v		C_{pv}, ρ_v
Mid stage	C_{pg}, ρ_v	E_a	K_{ch}, ρ_{ch}
Later stages	C_{pg}, E_a, ρ_v		K_{ch}, k_v, ρ_{ch}

Table A.1: Summary of effects of input parameters from Ramroth et al. [2006]

Table A.1 shows which properties have a significant impact on the output at different stages of the simulation conducted by Ramroth et al. [2006]. A, C_{pch}, n and Q have very little effect on the output during any period of this simulation and have been omitted from the table. During the mid-stage of the simulation the effect of E_a starts off having a positive effect and then switches to a negative one. This analysis has limitations since it is specific to this particular test on a 10.9mm thick glass/polyester laminate subjected to a hydrocarbon fire curve. Other limiting factors are that the properties used in this instance are not temperature dependant. If temperature dependant properties were used it is expected that the results may be different. It must also be borne in mind that the output to which the effects are judged is the temperature of the cold face. If one were to be linking a thermal and mechanical model by means of the temperatures within the composite or the thickness of the char layer then these results may not be relevant.

A.5 Test Methods for the Thermal Properties of Composites

The specific heat capacity is the energy required to raise the temperature of a body by a specific amount. It is usually measured in J/kg-K. Plastics typically have high specific heats compared with metals; stainless steel has a specific heat of 500 J/kg-K [Callister 2000] and for an E-glass/vinyl ester composite the specific heat is around 1100 J/kg-K [Lattimer and Ouellette 2006]. These values are highly temperature dependant and in the case of plastics they will also change after the material has decomposed.

Measurement of the specific heat capacity is carried out using a differential scanning calorimeter (DSC). This is a piece of apparatus which heats two samples; the material for which the specific heat capacity is required and a reference sample for which the specific heat capacity is known. The two samples are kept at the same temperature and the differential energy required to heat each sample is recorded. With the specific heat capacity of the reference sample known the energy input can be calculated and the specific heat capacity of the unknown sample can be calculated from Equation (A.1) as stated in the standard [ISO11357-4 2005]

$$C_p(T) = \frac{dq/dt}{m\,dT/dt} \tag{A.1}$$

Where:

dq/dt = Measured differential heat input (J/s)

dT/dt =Heating rate (°C/s)

m = Mass of the sample (kg)

Complications arise however when a material looses mass and also when a reaction occurs. In the case of most organic materials the experiment would be conducted in an inert atmosphere so that no combustion takes place. In order to account for these factors investigators [Henderson, Tant et al. 1981; Henderson, Wiebelt et al. 1982; Lattimer and Ouellette 2006] have proposed a method whereby the virgin material is heated past the temperature at which the pyrolysis reaction occurs and then a second test is conducted where a fully charred sample is heated from room temperature to the upper limit of the apparatus. In a separate experiment involving a thermogravimetric analyser

(TGA) the mass loss of a sample at the same heating rate is recorded. This information is used to correct the data from the DSC, to calculate the specific heat capacity of the sample from room temperature, past the decomposition temperature and up to around 900°C for most DSC apparatus.

The determination of specific heat capacity of decomposition gas is an area which seems to be untouched by investigators. Values have been given [Henderson, Wiebelt et al. 1985; Looyeh, Bettess et al. 1997] but there is no indication on how these figures have been reached.

The heat of decomposition is the amount of energy consumed by the material during the decomposition reaction, above the energy required to heat the material. This value can be calculated using a DSC by taking a virgin sample and heating it until the decomposition reaction has finished. Complications arise, however since the value is mass specific and mass is being lost during the reaction. Henderson et al. [1982] propose a method however where mass loss data recorded from TGA run at the same heating rate as the DSC tests is used to correct the values.

Thermal conductivity is the measure of the heat transmitted through a material. It is usually measured in W/m-K and is calculated by Equation (A.2).

$$k = \frac{Q}{t} \cdot \frac{L}{A \cdot \Delta T} \tag{A.2}$$

Where:

Q	= heat (J)	t	= time period (s)
L	= thickness of the material (m)	A	= surface area (m^2)
ΔT	= temperature difference in the time period and through the thickness stated (°C)		

Thermal conductivity cannot be calculated directly and is a derived quantity. It can either be calculated for a particular temperature in steady state or over a temperature range in transient state.

The standard method for steady state thermal conductivity is to use the guarded hot plate method [BS874] where two identical disc shaped samples sandwich a heating plate. Either side of the samples two water cooled plates are kept at a constant temperature and the apparatus is enclosed by insulation to prevent heat loss. The temperatures of each of the surfaces of the samples are measured along with the heat output from the hot plate and are used to calculate the thermal conductivity. For transient thermal conductivity the same apparatus can be used but the temperature measurements need to be taken at set time intervals.

These methods are limited by the heat which can be generated by a hot plate and because there is a risk of combustion of organic materials at high temperatures.

Lattimer and Ouellette [2006] present their method for determining the thermal conductivity of virgin and charred composite panels using a heat flux meter to record the heat that the panel was exposed to. They subjected composite panels to a heat source from one side and insulated the other side. They found that for steady state conductivity thicker panels of around 6mm were most effective in achieving a reasonable temperature drop over the thickness (20°C). For the transient experiments the temperature ideally needs to be constant through the thickness of the sample. For this reason 3mm thick samples were used. It was reported that a temperature ramp of 3°C per minute was needed in order to prevent a significant temperature drop across the sample.

Henderson et al. [1983] report on their method for deriving the thermal conductivity using the line source technique. A cylindrical sample is heated using a wire running axially through its centre. Thermocouples are located at varying depths through the sample. The sample, fitted with thermocouples and the heater wire was put into an atmosphere of nitrogen to prevent combustion. The ends of sample were insulated to try and reduce temperature gradients, but it was reported that at temperatures of 500^{o}C and above it took four hours to reach steady state.

It is not possible to say which method is the most valid for determining the thermal conductivity since the principals in each of the methods are identical. Composites

clearly provide a challenge in this area especially when obtaining the conductivity at high temperatures.

The kinetic properties are those used in the Arrhenius equation to model the decomposition reaction, given in Equation (A.3)

$$\frac{\partial \rho}{\partial t} = -A\left[\frac{(\rho_v - \rho_{ch})}{\rho_v}\right]^n e^{(-E_a/RT)} \qquad \text{(A.3)}$$

Where:

E_a = activation energy (kJ/mol-kg)

A = pre exponential factor (s^{-1})

n = order of reaction

The activation energy is the minimum energy input required to cause the decomposition reaction to occur. The pre-exponential factor is a constant specific to the reaction. The order of the reaction is the power to which the instantaneous density is raised in Equation (A.3).

The accepted method for calculating the kinetic parameters is TGA. This involves heating a sample of a few milligrams at a specified heating rate whilst measuring the change in mass on a precision balance. The sample is kept in an inert atmosphere to avoid any combustion taking place. The method used by investigators [Henderson, Tant et al. 1981; Lattimer and Ouellette 2006] to obtain the kinetic parameters involves subjecting samples to a range of heating rates and taking the average values of the kinetic properties.

The enthalpy has been calculated, in all the numerical models discussed, by the following relationship:

$$h = \int_{T_0}^{T} C_p dT \qquad \text{(A.4)}$$

This relationship has been used to calculate enthalpies of solid material and decomposition gas.

Emissivity is a ratio of the energy radiated to a body and the energy absorbed by that body. A 'black body' is assumed to have an emissivity of 1, although in reality the highest emissivity achievable is around 0.94 which is that of a mat black surface. A highly polished metal surface will have an emissivity of around 0.03. The surface of a typical unpainted polymer composite will have an emissivity of around 0.8-0.9 [Callister 2000].

The surface heat transfer coefficient is an experimentally determined property which is dependent on surface geometry, the nature of the fluid motion i.e. the airflow across the surface and the properties of the fluid. This value can be determined by simple laboratory experiments where a sample is heated to a known temperature and the change in the ambient temperature is used to calculate the appropriate value. For free convection of gasses the value is somewhere between 2-25 W/m^2 [Çengel 1998]. Whilst most of the literature cites the following relationship between the heat flux and the surface temperature, it is unclear whether it is used in any of the numerical models. The determination of an accurate value of the heat transfer coefficient makes the problem a difficult one to solve.

$$Q = h(T)\left[T_s - T_c\right] + \sigma\left[\varepsilon_s T_s^4 + \varepsilon_c T_c^4\right] \tag{A.5}$$

Where:

Q = heat loss to the surroundings (W/m^2)

h(T) = surface heat transfer coefficient (W/m^2-K)

σ = stefan-Boltzman constant (5.67×10^8 W/m^2-K^4).

subscripts s and c are those of the surroundings and of the composite respectively.

These properties have generally been ignored by the heat transfer models already discussed here. Most investigators have used a prescribed heat flux or surface temperature at the exposed boundary and have assumed a fully insulated unexposed boundary.

Appendix B

B.1 Fire Curve Calculation

The British Standard BS 476-20 specifies the following temperature/time relationship for a cellulosic fire curve:

$$T = 345log_{10}(8t + 1) + 20 \quad \text{(B.1)}$$

The allowable limits for deviation from this curve are described as follows:

The per cent deviation d in the area of the curve of the average temperature recorded by the specified furnace thermocouples versus time from the area of the standard heating curve should be within:

(i)	± 15%	from t = 0 to t = 10
(ii)	± 15-0.5(t-10)%	from 10 < t ≤ 30
(iii)	± 5 – 0.083(t-30)%	from 30 < t ≤ 60
(iv)	± 2.5%	From t = 60 and above

where:

d = (A – A_S) x 1/A_S x 100, and

A is the rea under the actual average furnace time-temperature curve

A_S is the area under the standard time-temperature curve

All areas should be computed by the same method, i.e. by the summation of areas at intervals not exceeding 1 min for (i), 2 min for (ii), and 5 min for (iii) and (iv).

At any time after the first 10 min of test, the temperature recorded by any thermocouple should not differ from the corresponding temperature of the standard time-temperature curve by more than ± 100°C.

To calculate the area under the curve Equation A.1 was integrated to give:

$$Area = \frac{345(-8x-1)}{8Ln(10)} + 20x + \frac{345(8x+1)Ln(8x+1)}{8Ln(10)} \quad \text{(B.2)}$$

The areas under the recorded temperature curve were recorded by the trapezium rule.

Time (Minutes)	BS 476 temp (°C)	Area under BS 476 Curve	Test furnace temp (°C)	Area under furnace curve	% difference
0	20		30		
1	349	222	611	321	
2	445	402	619	615	
3	502	475	631	625	
4	544	524	637	634	
5	576	561	646	642	
6	603	590	650	648	
7	626	615	656	653	
8	645	636	657	657	
9	663	654	664	661	
10	678	671	673	669	14.4
11	693	686	689	681	0.7
12	705	699	697	693	0.9
13	717	711	712	705	1.0
14	728	723	723	718	0.7
15	739	733	730	727	1.0
16	748	743	742	736	1.0
17	757	753	750	746	0.9
18	766	761	758	754	1.0
19	774	770	760	759	1.4
20	781	778	770	765	1.6
21	789	785	775	773	1.6
22	796	792	797	786	0.8
23	802	799	785	791	1.0
24	809	805	791	788	2.2
25	815	812	794	793	2.4
26	820	818	797	796	2.7
27	826	823	800	799	3.0
28	832	829	802	801	3.4
29	837	834	806	804	3.6
30	842	839	809	808	3.8

Table B.1: BS 476 fire curve validation data

B.2 Thermogravimetric Analysis Calculations

The mass loss results were normalised with respect to the initial mass and are shown in Figure B.1 for Ampreg 22 resin.

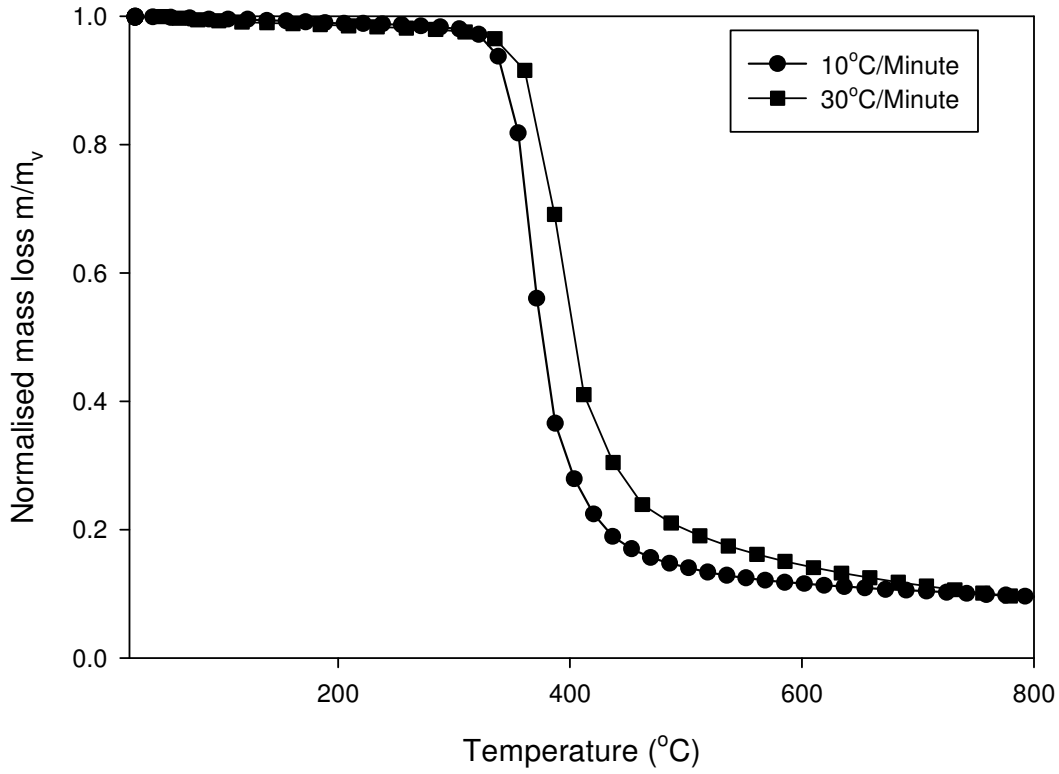

Figure B.1: TGA mass loss curves for Ampreg 22 resin with extra slow hardener in powder form

From Figure B.1 it can be seen that decomposition of the resin starts at around 350°C and by 400°C 70% of the resin has decomposed. It is also noticeable that decomposition occurs at a higher temperature for the higher heating rate. The final stages of the decomposition from 400°C to 700°C are much slower, leaving a char material which is about 10% of the initial mass. This char appears to remain, even at very high temperatures.

Figure B.2 shows that the decomposition process for foam is not single step in nature as in the resin. Firstly the material undergoes a reaction at around 250°C where around 30% of the mass is lost almost instantaneously. There then follows a much slower reaction which causes the material to lose a further 60% of the mass over a 500°C range. Again around 10% of the mass remains after the decomposition process has finished.

The results from the foam test seem to have a large amount of scatter and this is thought to be due to the light weight of the foam which causes the balance readings to be more affected by gas fluctuations in the TGA.

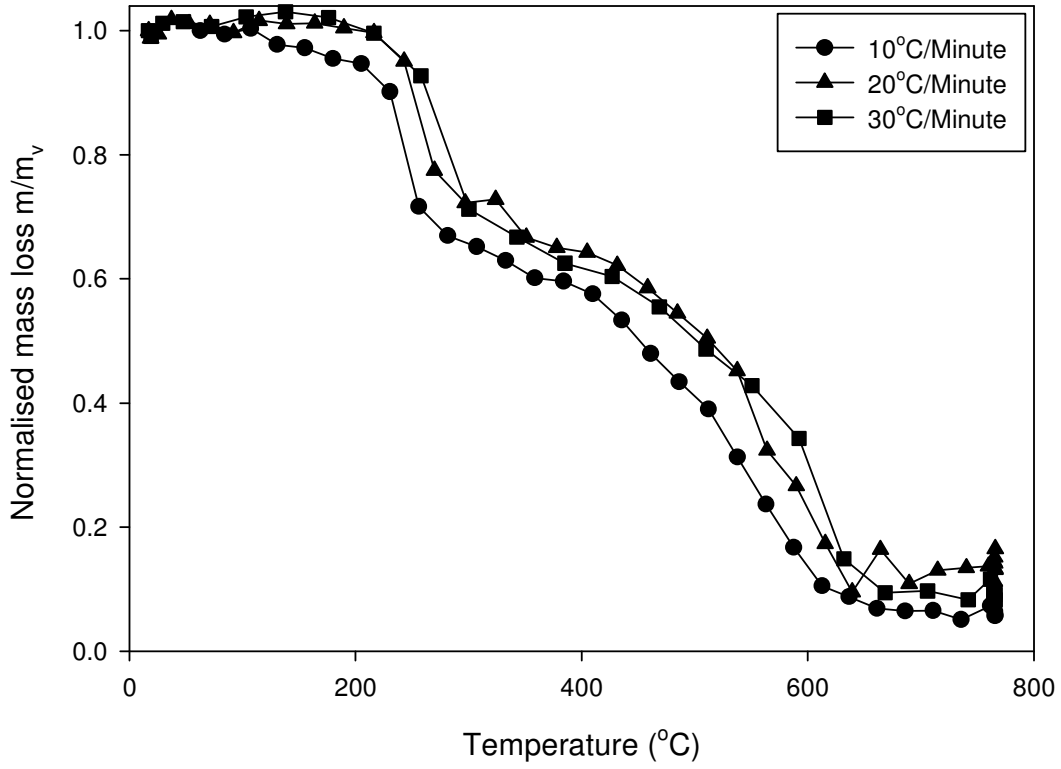

Figure B.2: TGA mass loss curve for 100kg/m^3 Divinycell H foam - 10°C/min curve corrected for initial mass loss

The data from the TGA apparatus shows the instantaneous sample mass and temperature with respect to time for the given heating rate. The following section will summarise Friedman's method [Henderson, Tant et al. 1981] to obtain the kinetic properties from that data.

TGA tests are run at various heating rates on each material and from the mass and temperature data the following relationship is obtained for each experiment:

$$\ln\left(-\frac{1}{m_v}\frac{\partial m}{\partial t}\right) = f\left(\frac{1}{T}\right) \tag{B.3}$$

For values of m/m_v the term on the left hand side of Equation (A.3) is plotted against 1/T for different heating rates as shown in Figure B.3 for the resin.

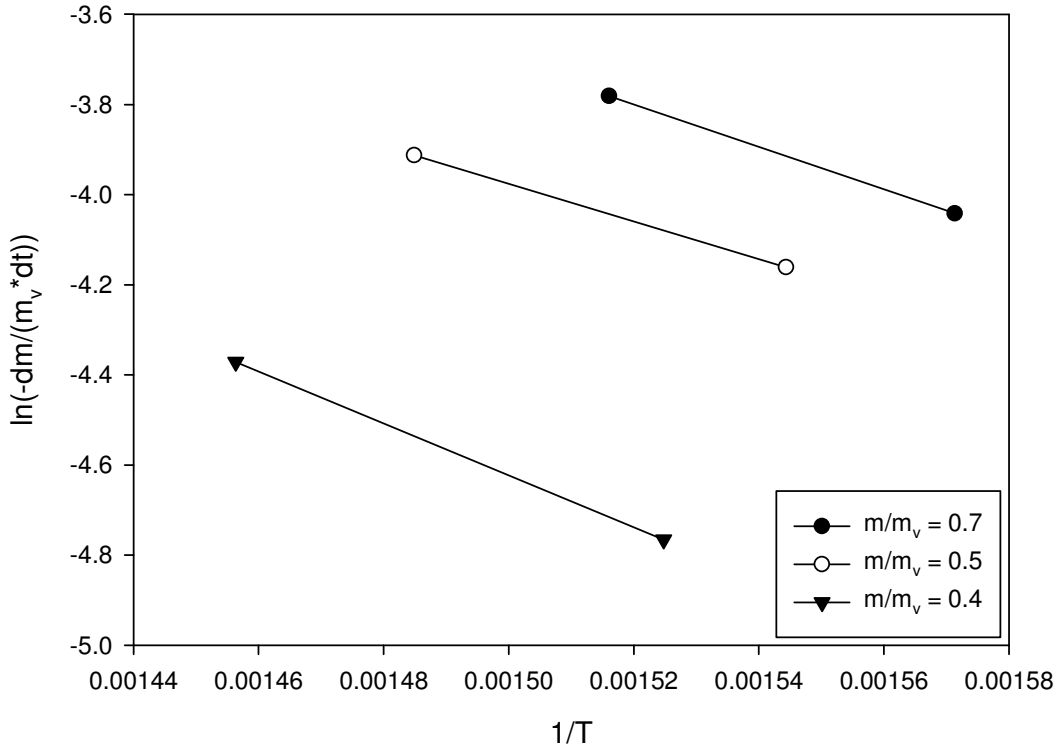

Figure B.3: Curves derived from TGA data to extrapolate activation energy for Ampreg 22 resin

If the activation energy is the same in each sample tested the lines should be parallel.

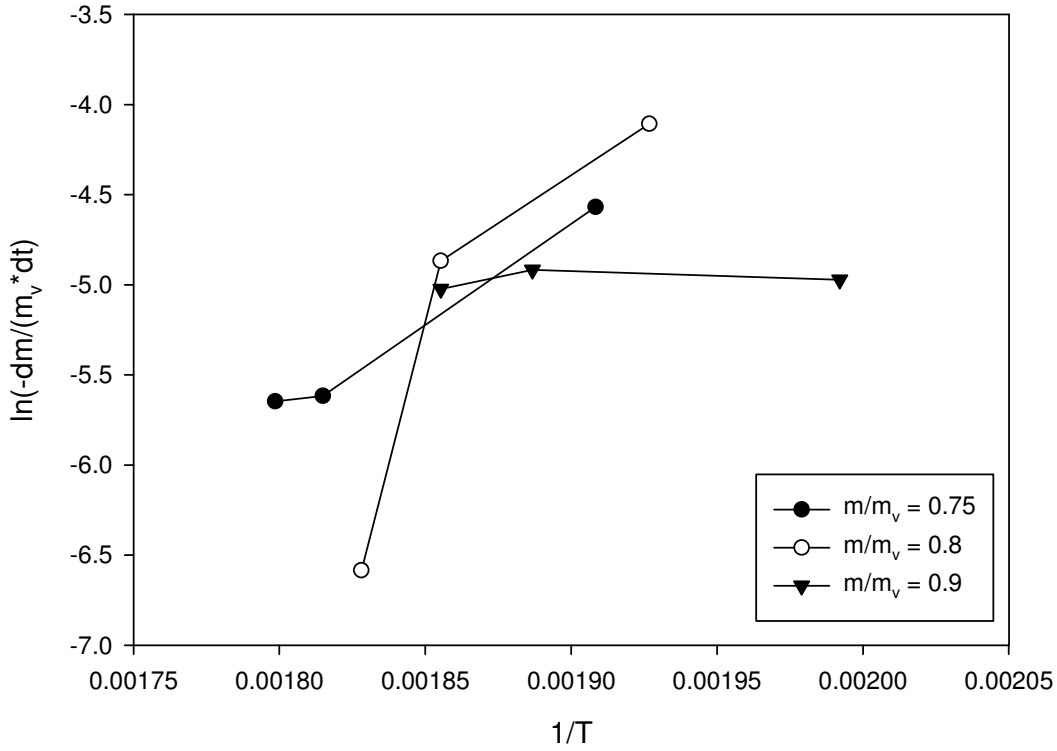

Figure B.4: Curves derived from TGA data to extrapolate activation energy for Divinycell H100

Figure B.4 shows the results from the foam tests. The m/m_v values were all taken from the first reaction which can be seen in Figure B.2 at around 350°C. The first aspect of the results to note is that the slopes of the curves are all positive, which would indicate a negative activation energy. Aside from the fact that the results indicate a negative activation energy there is also little correlation between each of the curves, which should be parallel if the activation energy is the same in each sample. The errors encountered are thought to be due to fluctuations in the mass readings from the TGA balance. The part of the curves from Figure B.2 where the first reaction occurs have therefore been plotted separately and dm/dt calculated by a best-fit line as shown in Figure B.5.

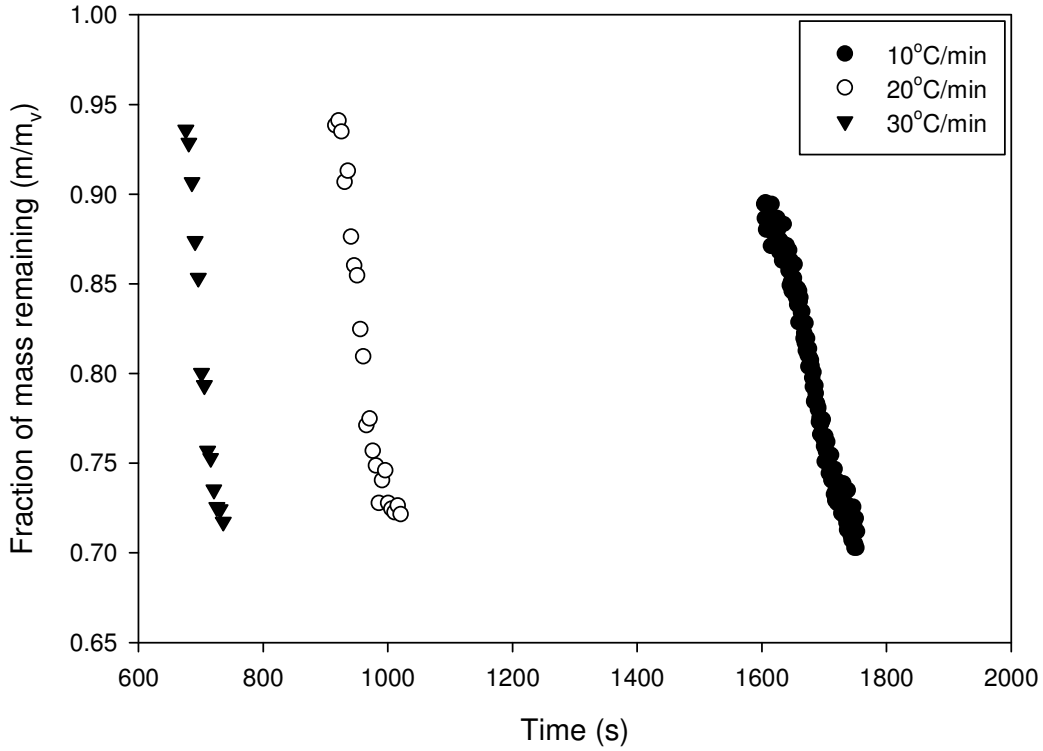

Figure B.5: TGA Mass loss rate curves from PVC samples for first stage reaction

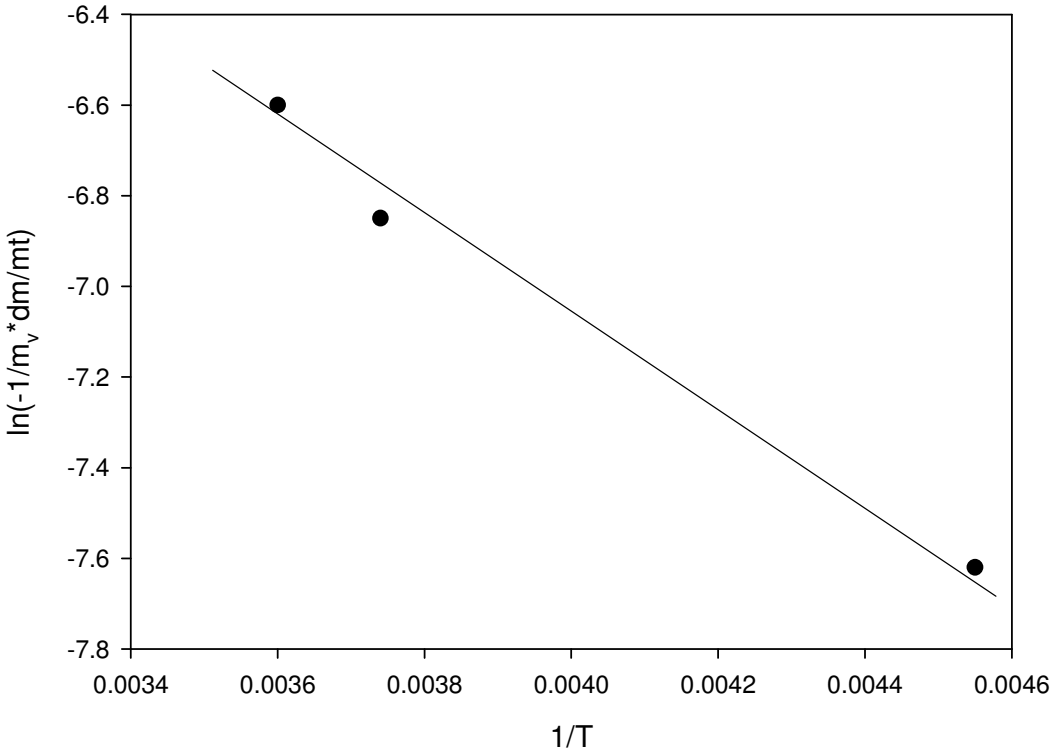

Figure B.6: Curves derived from TGA data to extrapolate activation energy for Divinycell H100 using best fit line during reaction period

The values of dm/dt have then been used to plot the curve shown in Figure B.6.

As the values of dm/dt were constant from the data obtained from Figure B.5 it is only necessary to plot one set of data. The results show good agreement between the tests and indicate that the activation energy was relatively constant in each of the different tests.

The activation energy is calculated from the equation of the line:

$$y = mx + c \tag{A.4}$$

So that:

$$E_a = -R\,m \tag{A.5}$$

Where R is the gas constant, 8.31455 J/mol. Where the lines are not parallel an average value of m is taken.

To calculate the pre-exponential factor and the order of the reaction the following equation is used:

$$c = \ln(A) + n\ln(m - m_{ch})\,m_v \tag{A.6}$$

Where c is the intercept from the curves in Figure B.3, m is the instantaneous mass, m_v is the initial mass and m_{ch} is the final mass. This equation is solved simultaneously using different values of m/m_v.

Material	E_a, J/mol	n	A, s^{-1}
Ampreg 22	0.406×10^5	2.78	115
Divinycell H100	0.997×10^5	0.626	1.15×10^6

Table B.2: Kinetic constants determined from TGA experiments

B.3 Fire Resistance Test Results

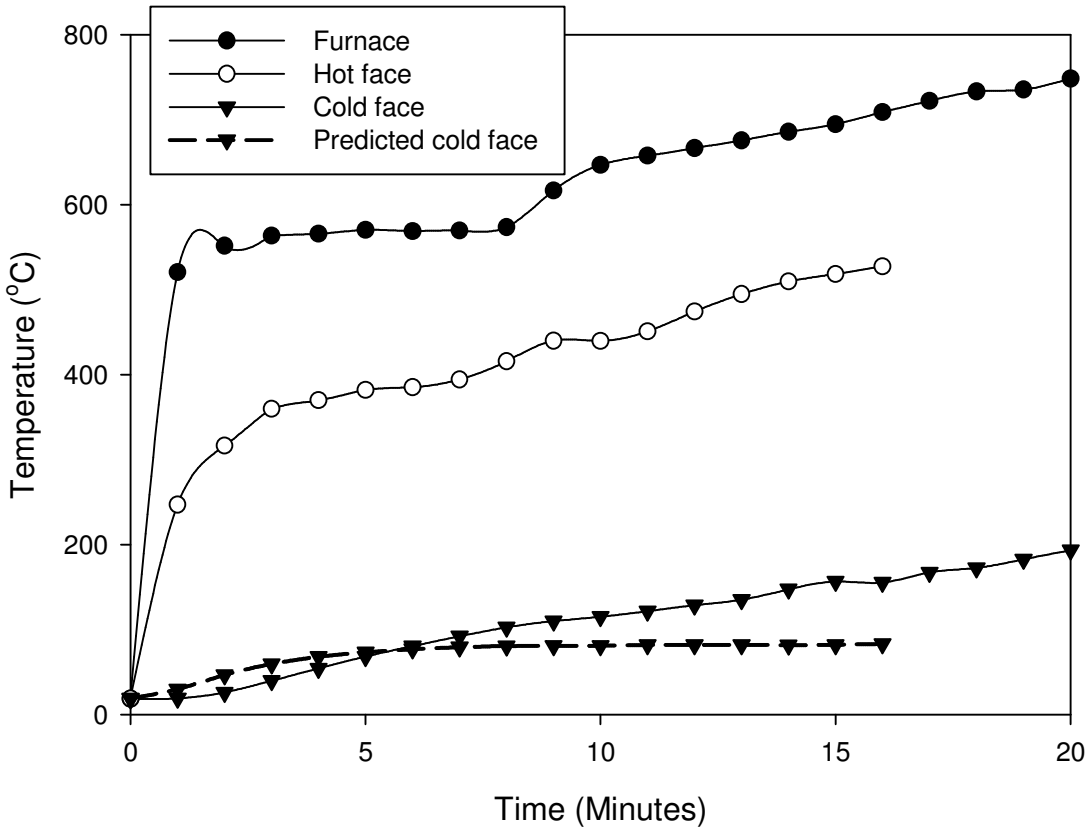

Figure B.7: Comparison of predicted cold face temperature with experimental results for panel SS 1C.1 under cellulosic fire curve.

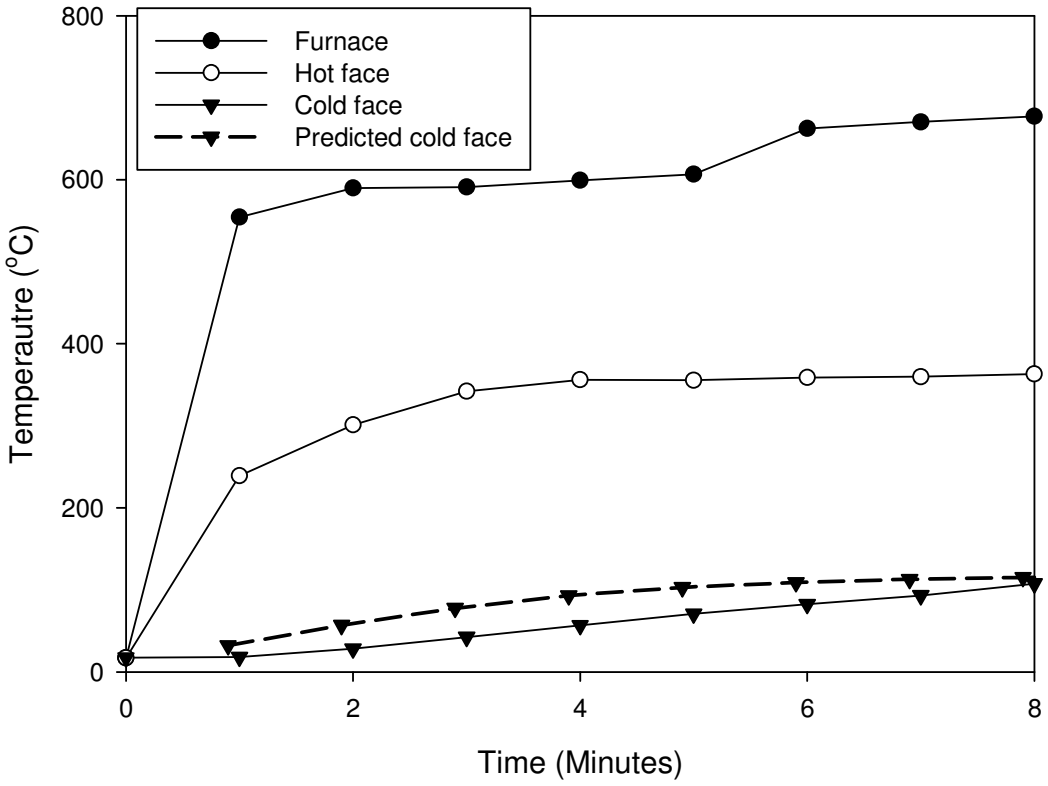

Figure B.8: Comparison of predicted cold face temperature with experimental results for panel SS 1C.2 under cellulosic fire curve.

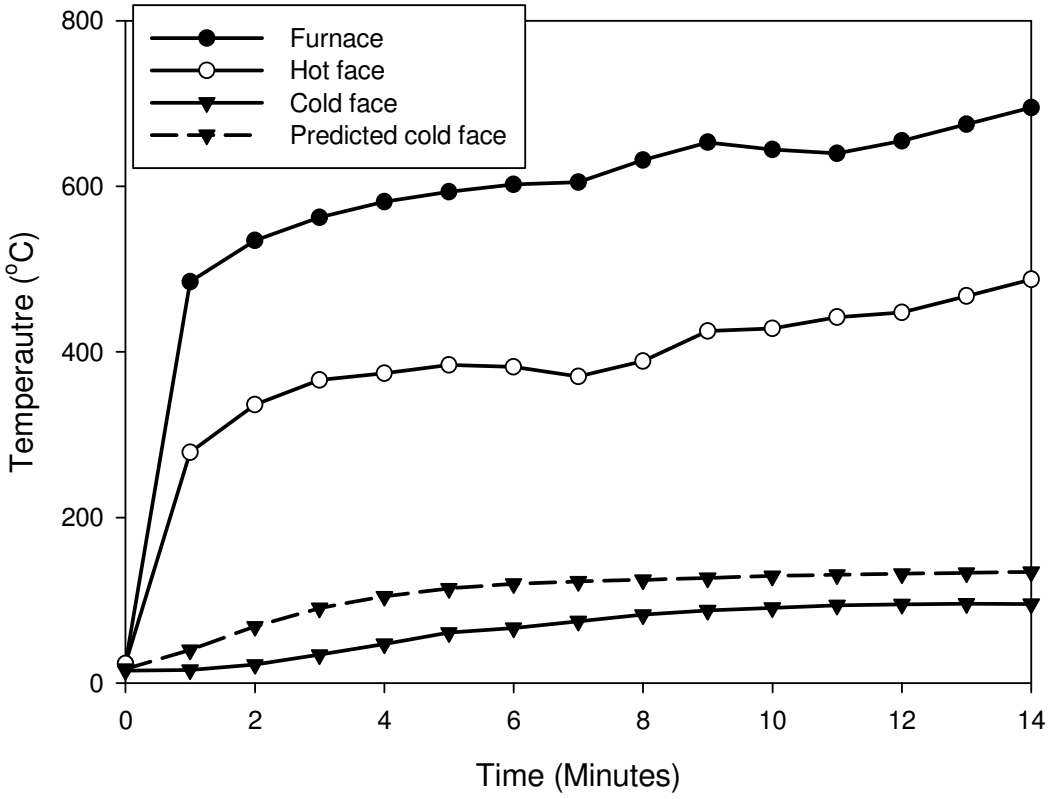

Figure B.9: Comparison of predicted cold face temperature with experimental results for panel SS 2.C.1 under cellulosic fire curve.

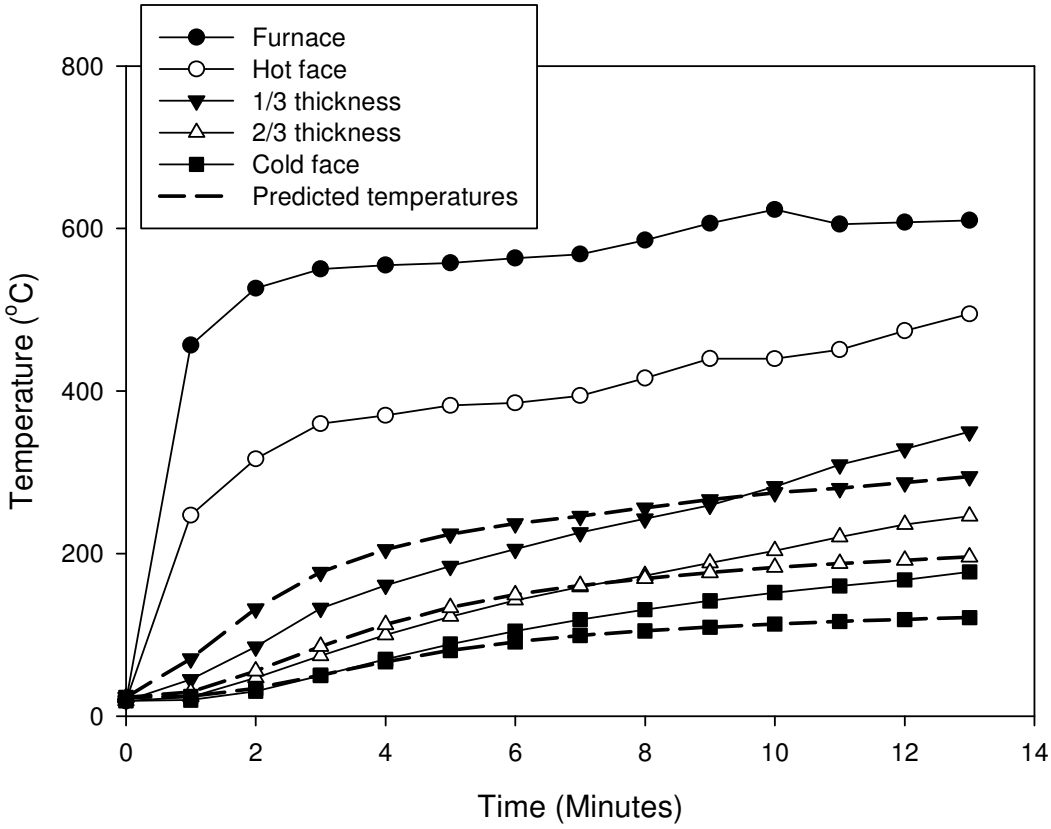

Figure B.10: Comparison of predicted cold face temperature with experimental results for panel SS 1.C.2 under cellulosic fire curve.

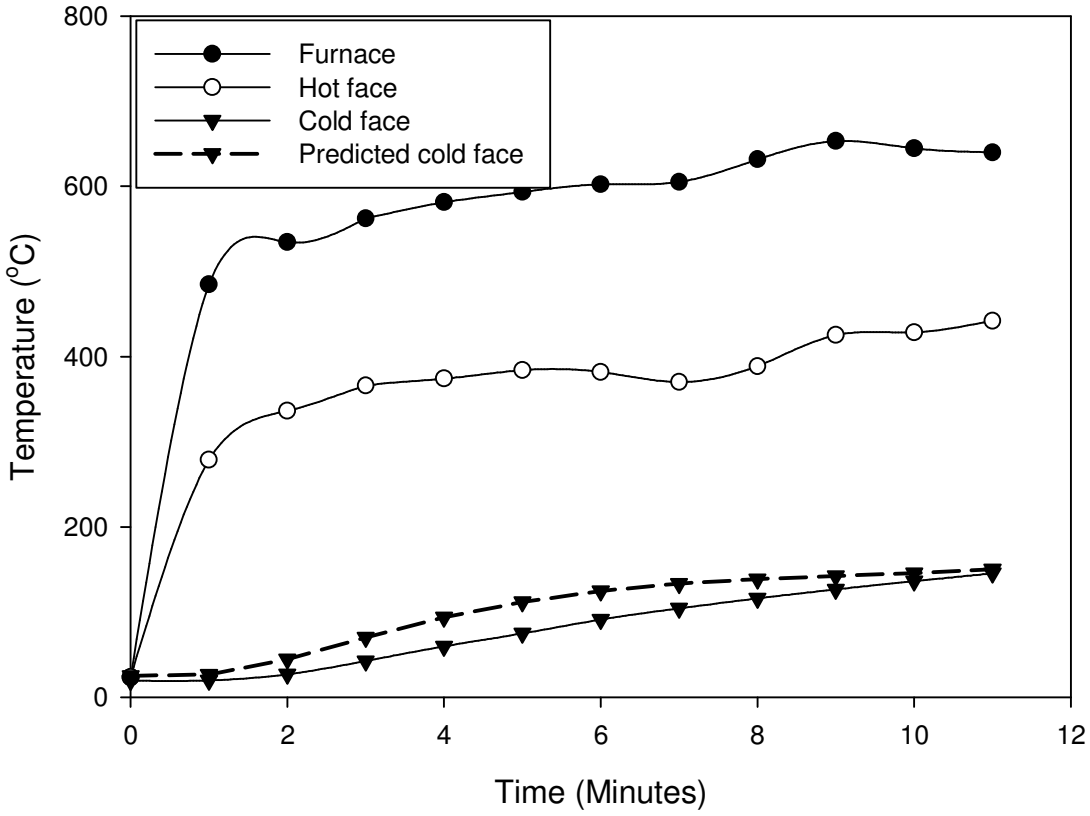

Figure B.11: Comparison of predicted cold face temperature with experimental results for panel SS 3.C.1under cellulosic fire curve.

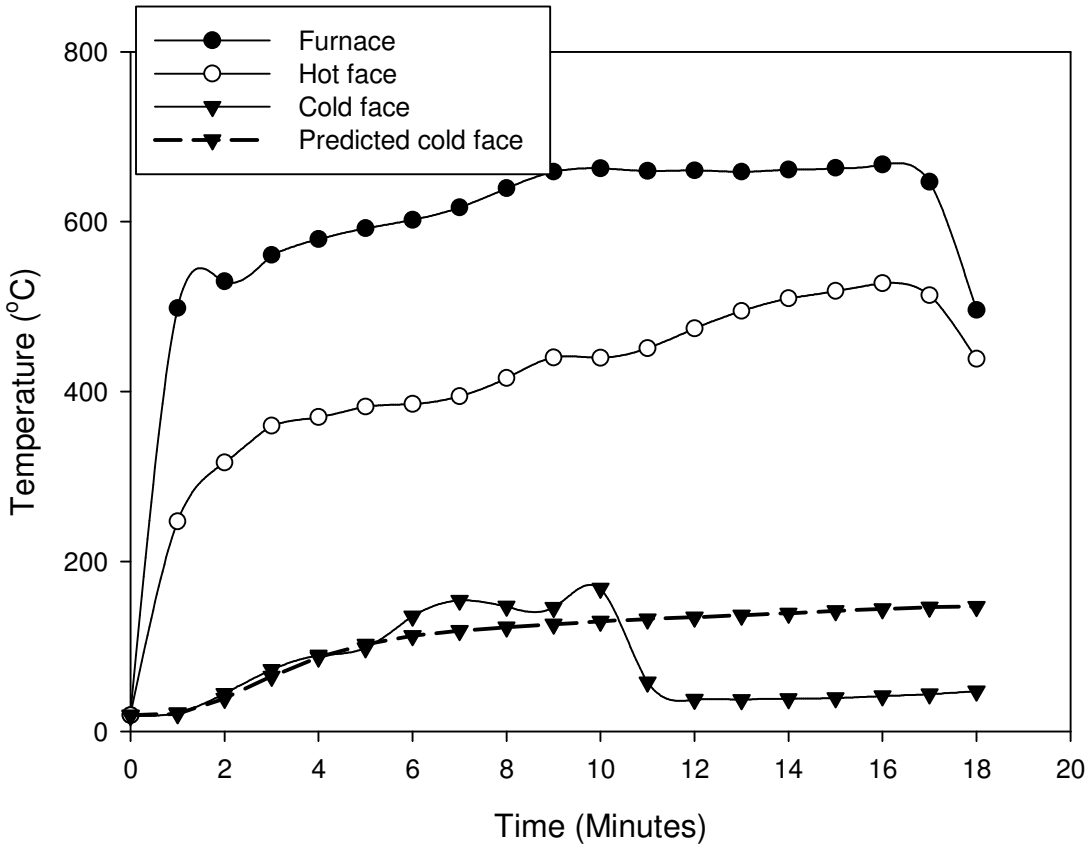

Figure B.12: Comparison of predicted cold face temperature with experimental results for panel SS 4.C.1 under cellulosic fire curve.

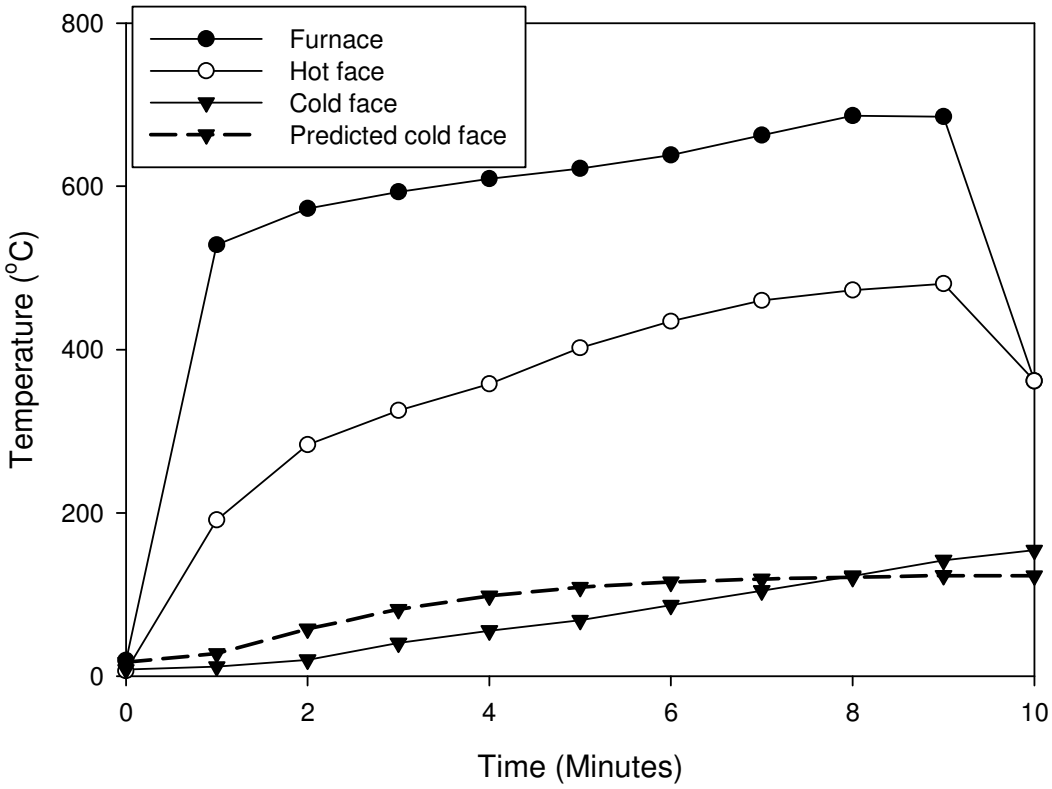

Figure B.13: Comparison of predicted cold face temperature with experimental results for panel SS 4.C.2 under cellulosic fire curve.

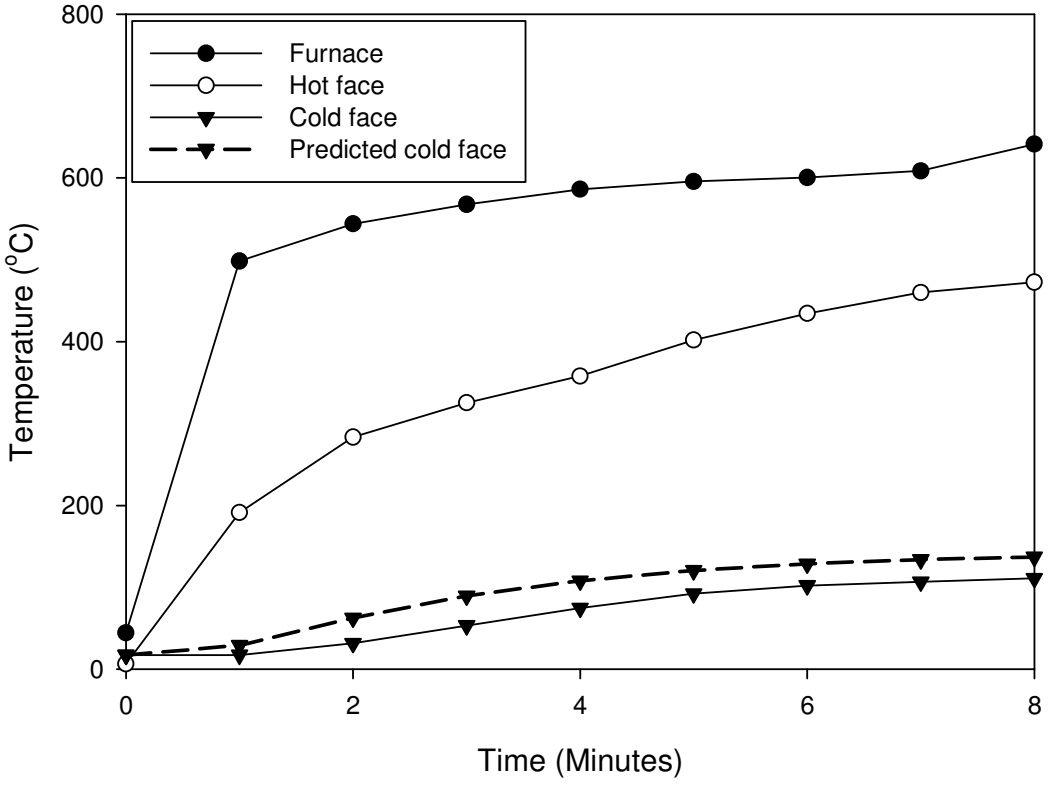

Figure B.14: Comparison of predicted cold face temperature with experimental results for panel SS 5.C.1 under cellulosic fire curve.

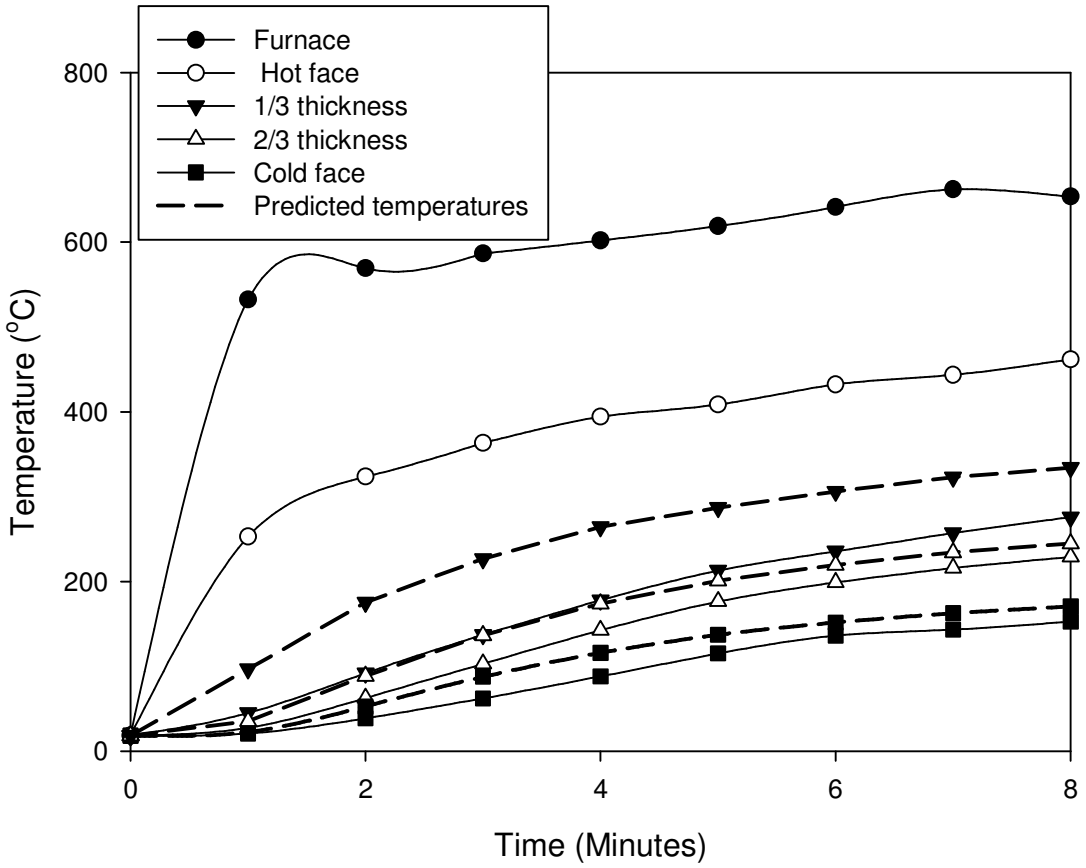

Figure B.15: Comparison of predicted cold face temperature with experimental results for panel SS 6.C.1 under cellulosic fire curve.

Test id	Duration (mm:ss)	Thickness (mm)	Mean temperature difference (°C)
SS 1.C.1	20:06	11.8	23
SS 1.C.2	8:20	10.7	25
SS 2.C.1	14:30	10.9	42
SS 2.C.2	12:16	11.6	21
SS 3.C.1	08:00	11	21
SS 4.C.1	10:00	8.8	15
SS 4.C.2	12:00	9.12	28
SS 5.C.1	08:54	8.8	26
SS 6.C.1	08:24	9.1	35

Table B.2: Summary of fire resistance tests on single skin panels under cellulosic fire curve

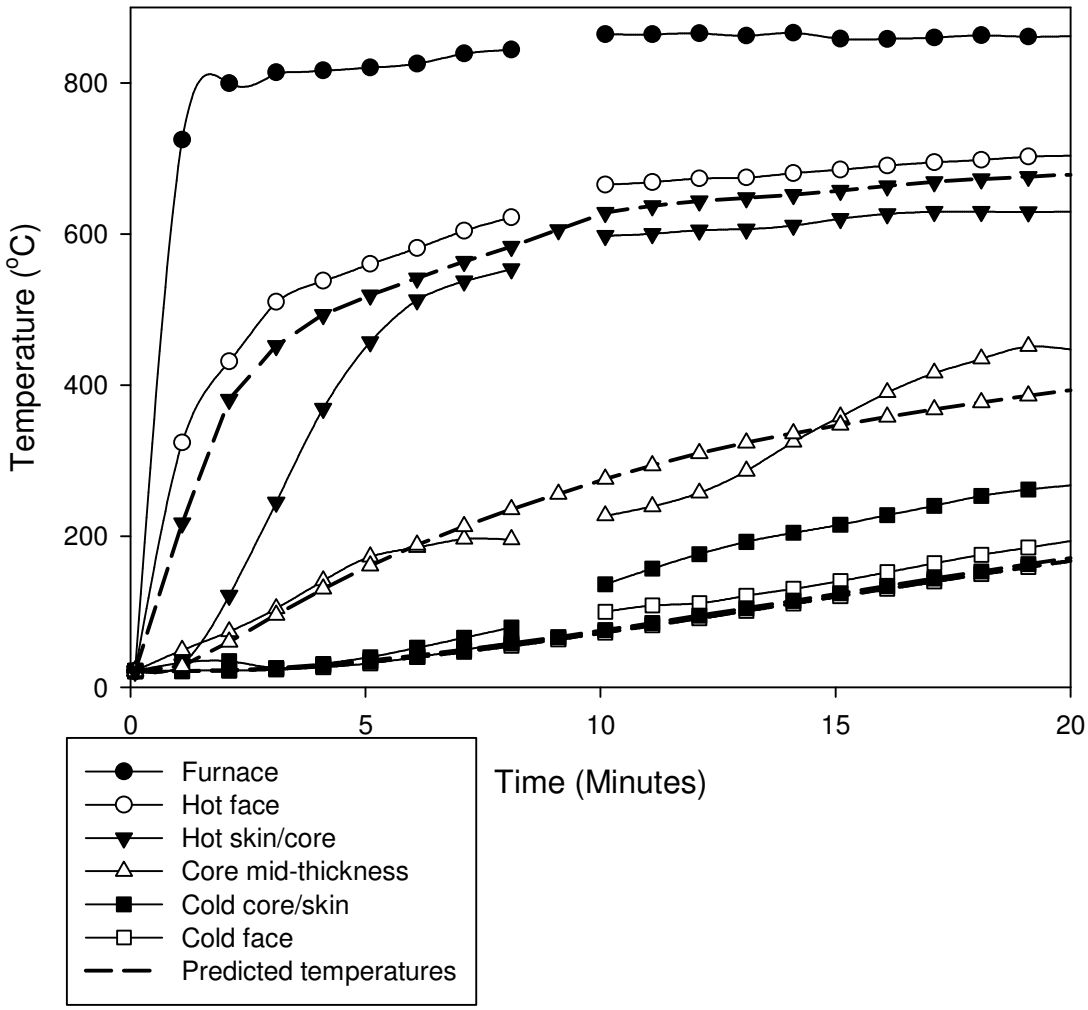

Figure B.16: Comparison of predicted temperatures with experimental results for panel SW 1.A.1 under cellulosic fire curve.

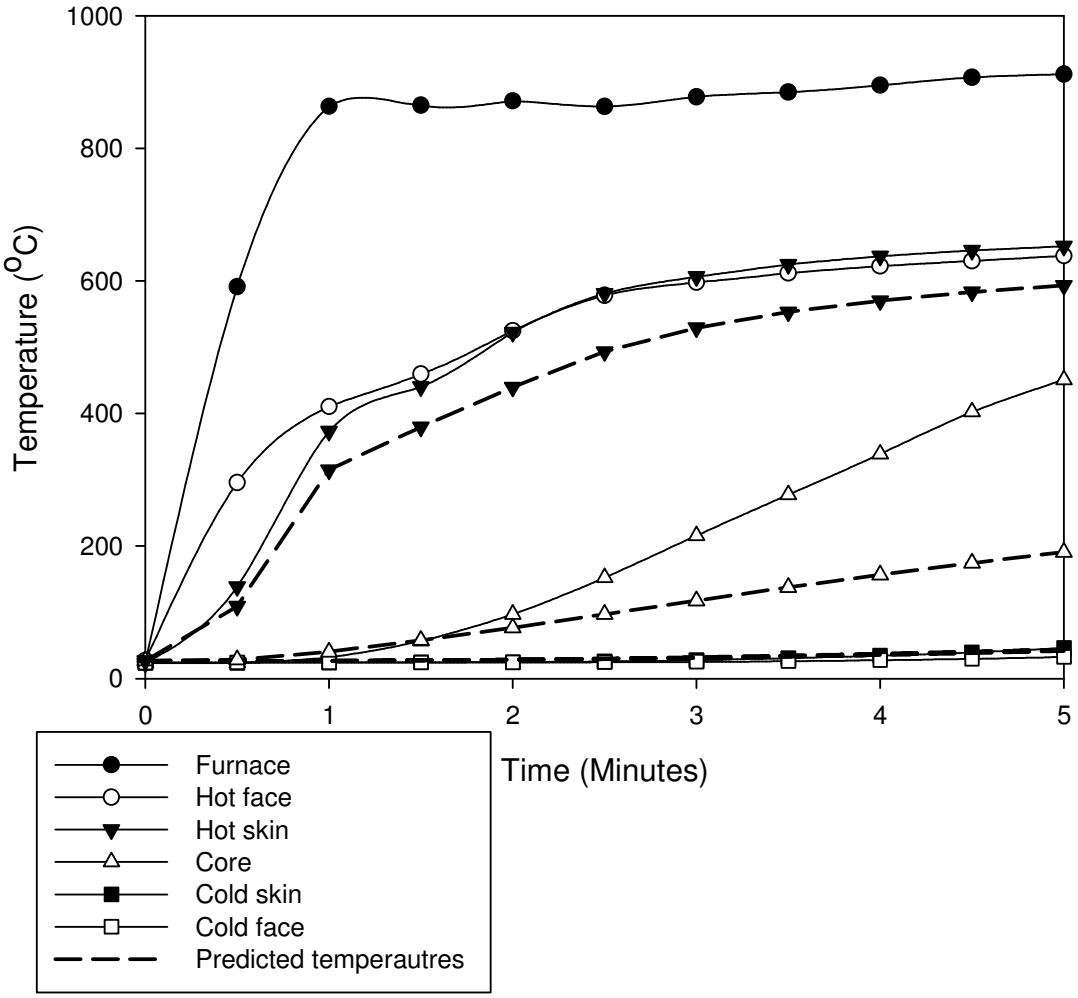

Figure B.17: Comparison of predicted temperatures with experimental results for panel SW 1.A.2 under cellulosic fire curve.

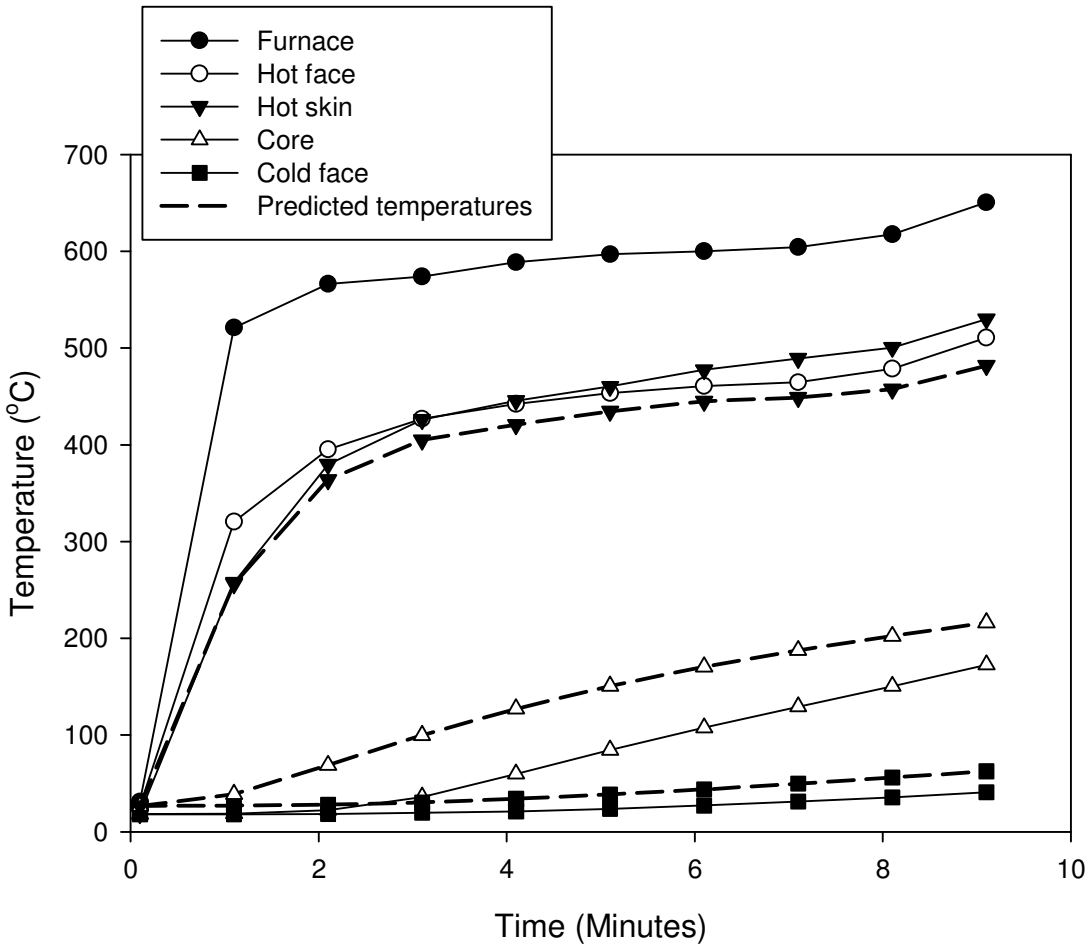

Figure B.18: Comparison of predicted temperatures with experimental results for panel SW 1.C.1 under cellulosic fire curve.

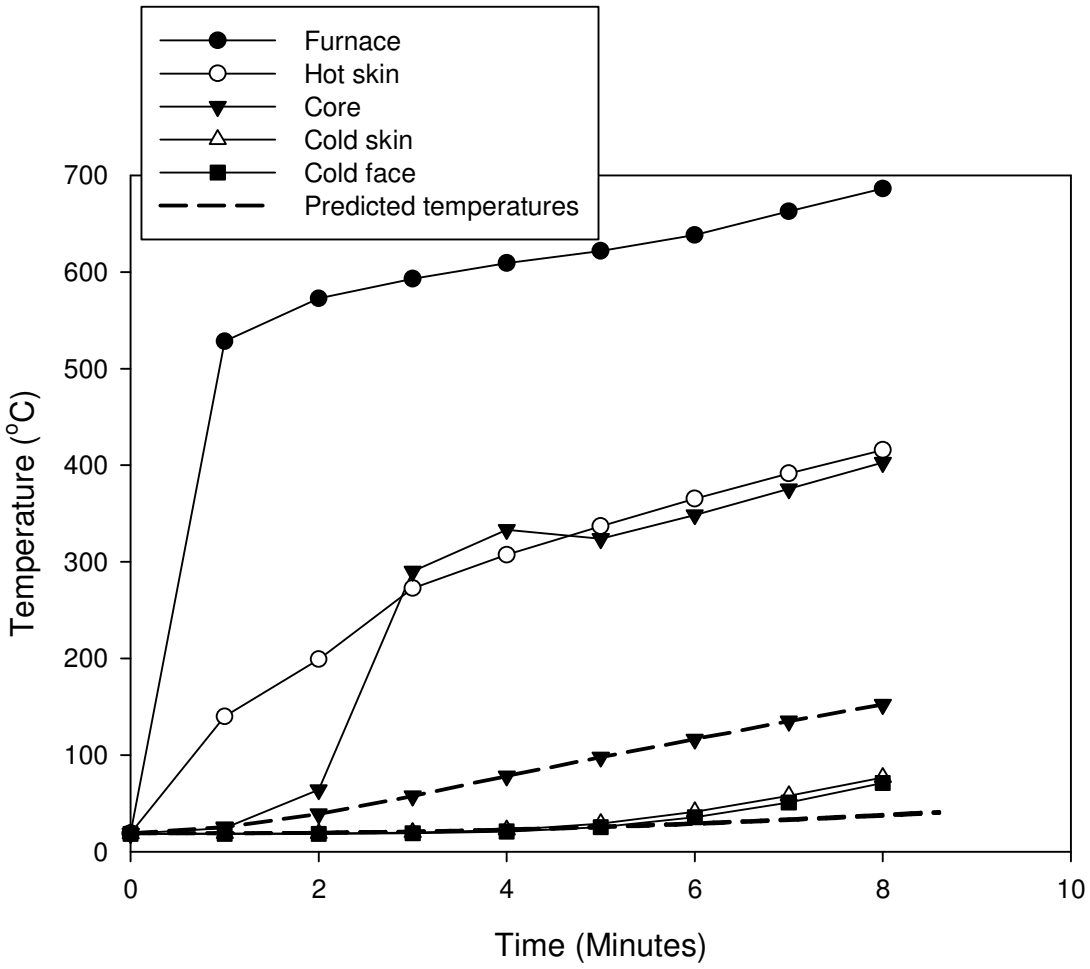

Figure B.19: Comparison of predicted temperatures with experimental results for panel SW 1.C.2 under cellulosic fire curve.

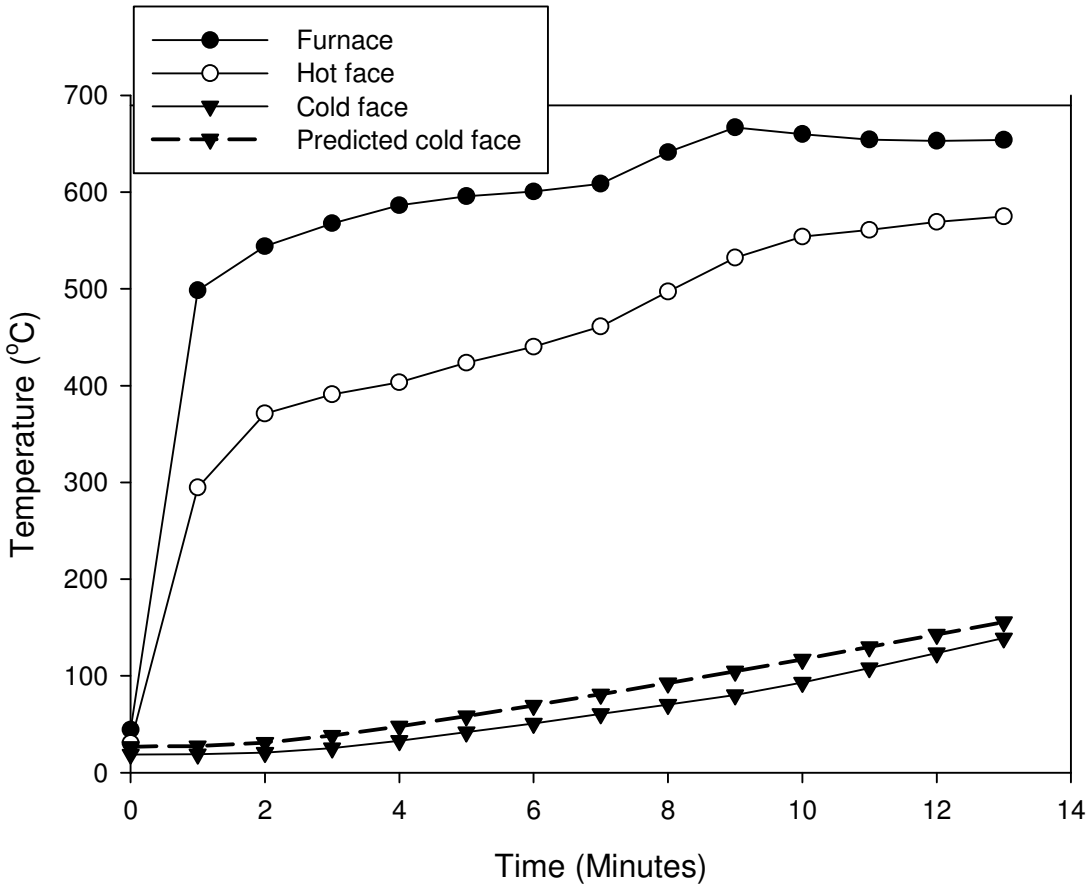

Figure B.20: Comparison of predicted temperatures with experimental results for panel SW 2.C.1 under cellulosic fire curve.

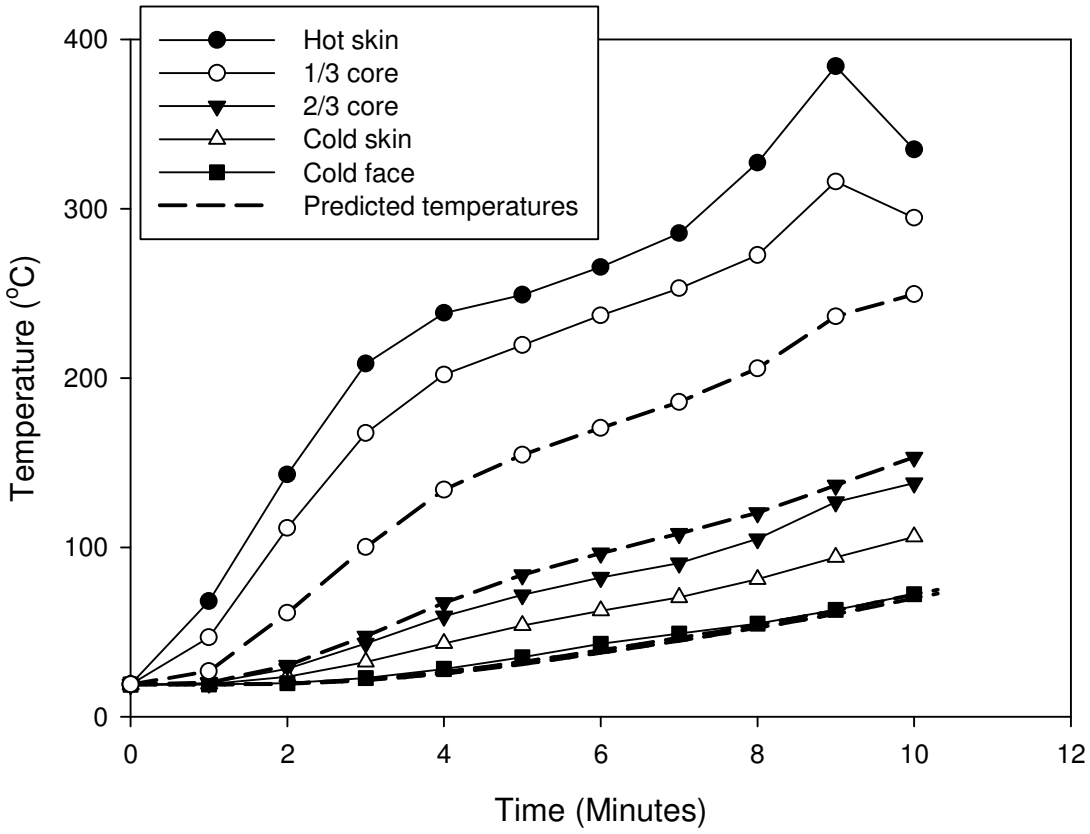

Figure B.21: Comparison of predicted temperatures with experimental results for panel SW 2.C.2 under cellulosic fire curve.

Test id	Duration (mm:ss)	Mean temp difference (°C)	Fire curve
SW 1.A.1	21:06	42	Rate A
SW 1.A.2	05:00	39	Rate A
SW 1.C.1	09:36	31	Cellulosic
SW 1.C.2	08:36	61	Cellulosic
SW 2.C.1	13:12	18	Cellulosic
SW 2.C.2	10:18	22	Cellulosic

Table B.3: Summary of fire resistance tests on sandwich panels

Appendix C

C.1 Tensile Tests

Length (mm)	Width (mm)	Thickness (mm)	Volume (m^3)	Weight (kg)	Layers	Fibre weight (kg)	Resin weight (kg)	Resin volume (m^3)	Vf	Vr	E11 (GPa)	Ef (GPa)
276	25	9	6.21E-05	0.105	12	0.0627	0.0423	4.04E-05	0.35	0.65	12.42	32.8
276	25	9	6.21E-05	0.101	12	0.0627	0.0383	3.66E-05	0.41	0.59	12.98	29.5
276	25	9	6.21E-05	0.109	12	0.0627	0.0463	4.42E-05	0.29	0.71	13.22	42.3
276	25	8	5.52E-05	0.095	12	0.0627	0.0323	3.09E-05	0.44	0.56	12.40	26.2
276	25	9	6.21E-05	0.101	12	0.0627	0.0383	3.66E-05	0.41	0.59	11.82	26.6
270	25	11	7.43E-05	0.128	16	0.0818	0.0462	4.41E-05	0.41	0.59	11.43	26.0
270	27	11	8.02E-05	0.143	16	0.0884	0.0546	5.22E-05	0.35	0.65	12.77	33.9
270	25	10	6.75E-05	0.115	16	0.0818	0.0332	3.17E-05	0.53	0.47	11.49	20.4
270	25	11	7.43E-05	0.125	16	0.0818	0.0432	4.13E-05	0.44	0.56	11.37	23.8

270	25	11	7.43E-05	0.122	16	0.0818	0.0402	3.84E-05	0.48	0.52	11.18	21.6
											Average	**28.3**

Table C.1: Results from tensile tests on unidirectional coupons with calculations for determining the room temperature fibre modulus

Fibre density	0.7576	kg/m2
Resin density	1046	kg/m3
Resin RT mod	1.48	GPa
Resin shear mod	0.568	GPa
N	-1.00	
G12f	27.6	GPa
Sm	61.9	

Table C.2: Values used in the calculation of room temperature fibre modulus

Appendix D

D.1 SHELL91 Single Skin Input File

```
/filname,shell91tmechSS1_1,1
/TITLE,thermal mechanical plate bending
/COM,shell91 tmech
C*** USING SHELL91
/prep7
! record start time
~eui, 'set fid [open "start.txt" w]'
~eui, 'puts $fid [clock format [clock seconds] -format "%c"]'
~eui, 'close $fid'
et,1,shell91                ! set element shell91
keyopt,1,1,16               ! 16 layers symmetrical stacking
width=0.2/2                 ! 1/2 width
length=0.2/2                ! 1/2 length
lwidth=0.04                 ! width of area over which load is applied
llength=0.04                ! length of area over which load is applied
thick=10.72e-3              ! panel thickness
layers=16                   ! No of lyers
plythk=thick/layers         ! thickness of each ply
elsize=0.1/36               ! element size
telno=17                    ! No of temperature layers
area=lwidth*llength         ! load area
step=30                                 ! Time PERIOD
ti= 17                      ! No of time steps
immed,off                   ! Toggle graphics
!*****************lay-up***************************************
R,1,layers,1,,,,                ! No of layers, symmetrical
RMORE,,,,,,
RMORE,1,0,plythk,plythk,plythk,plythk   ! mat, theta, tk(i), tk(j), tk(k), tk(l)
RMORE,1,0,plythk,plythk,plythk,plythk   ! mat, theta, tk(i), tk(j), tk(k), tk(l)
RMORE,1,0,plythk,plythk,plythk,plythk   ! mat, theta, tk(i), tk(j), tk(k), tk(l)
RMORE,1,0,plythk,plythk,plythk,plythk   ! mat, theta, tk(i), tk(j), tk(k), tk(l)
RMORE,1,0,plythk,plythk,plythk,plythk   ! mat, theta, tk(i), tk(j), tk(k), tk(l)
RMORE,1,0,plythk,plythk,plythk,plythk   ! mat, theta, tk(i), tk(j), tk(k), tk(l)
RMORE,1,0,plythk,plythk,plythk,plythk   ! mat, theta, tk(i), tk(j), tk(k), tk(l)
RMORE,1,0,plythk,plythk,plythk,plythk   ! mat, theta, tk(i), tk(j), tk(k), tk(l)

!*****************GEOMETRY****************************************
rectng,0,length,0,width             ! create rectangle
!*****************MATERIAL
PROPERTIES*******************************
!******upload material properties file*******
mptable=
mptab=
*DIM,mptable,table,7,12       ! create table for mp
```

```
*DIM,mptab,array,7,12          ! create array for temperatures
*TREAD,mptable,mpss1-1,csv     ! input temperatures from data file into table
*MFUN,mptab,COPY,mptable       ! copy table into an array
MPTEMP,,,,,,,,
MPTEMP,1,mptab(1,1)
MPTEMP,2,mptab(1,2)
MPTEMP,3,mptab(1,3)
MPTEMP,4,mptab(1,4)
MPTEMP,5,mptab(1,5)
MPTEMP,6,mptab(1,6)
MPTEMP,7,mptab(1,7)
MPTEMP,8,mptab(1,8)
MPTEMP,9,mptab(1,9)
MPTEMP,10,mptab(1,10)
MPTEMP,11,mptab(1,11)
MPTEMP,12,mptab(1,12)

MPDATA,EX,1,,mptab(2,1)
MPDATA,EX,1,,mptab(2,2)
MPDATA,EX,1,,mptab(2,3)
MPDATA,EX,1,,mptab(2,4)
MPDATA,EX,1,,mptab(2,5)
MPDATA,EX,1,,mptab(2,6)
MPDATA,EX,1,,mptab(2,7)
MPDATA,EX,1,,mptab(2,8)
MPDATA,EX,1,,mptab(2,9)
MPDATA,EX,1,,mptab(2,10)
MPDATA,EX,1,,mptab(2,11)
MPDATA,EX,1,,mptab(2,12)

MPDATA,EY,1,,mptab(3,1)
MPDATA,EY,1,,mptab(3,2)
MPDATA,EY,1,,mptab(3,3)
MPDATA,EY,1,,mptab(3,4)
MPDATA,EY,1,,mptab(3,5)
MPDATA,EY,1,,mptab(3,6)
MPDATA,EY,1,,mptab(3,7)
MPDATA,EY,1,,mptab(3,8)
MPDATA,EY,1,,mptab(3,9)
MPDATA,EY,1,,mptab(3,10)
MPDATA,EY,1,,mptab(3,11)
MPDATA,EY,1,,mptab(3,12)

MPDATA,EZ,1,,mptab(4,1)
MPDATA,EZ,1,,mptab(4,2)
MPDATA,EZ,1,,mptab(4,3)
MPDATA,EZ,1,,mptab(4,4)
MPDATA,EZ,1,,mptab(4,5)
MPDATA,EZ,1,,mptab(4,6)
MPDATA,EZ,1,,mptab(4,7)
MPDATA,EZ,1,,mptab(4,8)
```

```
MPDATA,EZ,1,,mptab(4,9)
MPDATA,EZ,1,,mptab(4,10)
MPDATA,EZ,1,,mptab(4,11)
MPDATA,EZ,1,,mptab(4,12)

MPDATA,PRXY,1,,0.3
MPDATA,PRXY,1,,0.2
MPDATA,PRXY,1,,0.15
MPDATA,PRXY,1,,0.1
MPDATA,PRXY,1,,0.05
MPDATA,PRXY,1,,0.01
MPDATA,PRXY,1,,0.001
MPDATA,PRXY,1,,0.001
MPDATA,PRXY,1,,0.001
MPDATA,PRXY,1,,0.001
MPDATA,PRXY,1,,0.001
MPDATA,PRXY,1,,0.001

MPDATA,PRYZ,1,,0.3
MPDATA,PRYZ,1,,0.2
MPDATA,PRYZ,1,,0.15
MPDATA,PRYZ,1,,0.1
MPDATA,PRYZ,1,,0.05
MPDATA,PRYZ,1,,0.01
MPDATA,PRYZ,1,,0.001
MPDATA,PRYZ,1,,0.001
MPDATA,PRYZ,1,,0.001
MPDATA,PRYZ,1,,0.001
MPDATA,PRYZ,1,,0.001
MPDATA,PRYZ,1,,0.001

MPDATA,PRXZ,1,,0.3
MPDATA,PRXZ,1,,0.2
MPDATA,PRXZ,1,,0.15
MPDATA,PRXZ,1,,0.1
MPDATA,PRXZ,1,,0.05
MPDATA,PRXZ,1,,0.01
MPDATA,PRXZ,1,,0.001
MPDATA,PRXZ,1,,0.001
MPDATA,PRXZ,1,,0.001
MPDATA,PRXZ,1,,0.001
MPDATA,PRXZ,1,,0.001
MPDATA,PRXZ,1,,0.001

MPDATA,GXY,1,,mptab(5,1)
MPDATA,GXY,1,,mptab(5,2)
MPDATA,GXY,1,,mptab(5,3)
MPDATA,GXY,1,,mptab(5,4)
MPDATA,GXY,1,,mptab(5,5)
MPDATA,GXY,1,,mptab(5,6)
MPDATA,GXY,1,,mptab(5,7)
```

```
MPDATA,GXY,1,,mptab(5,8)
MPDATA,GXY,1,,mptab(5,9)
MPDATA,GXY,1,,mptab(5,10)
MPDATA,GXY,1,,mptab(5,11)
MPDATA,GXY,1,,mptab(5,12)

MPDATA,GYZ,1,,mptab(6,1)
MPDATA,GYZ,1,,mptab(6,2)
MPDATA,GYZ,1,,mptab(6,3)
MPDATA,GYZ,1,,mptab(6,4)
MPDATA,GYZ,1,,mptab(6,5)
MPDATA,GYZ,1,,mptab(6,6)
MPDATA,GYZ,1,,mptab(6,7)
MPDATA,GYZ,1,,mptab(6,8)
MPDATA,GYZ,1,,mptab(6,9)
MPDATA,GYZ,1,,mptab(6,10)
MPDATA,GYZ,1,,mptab(6,11)
MPDATA,GYZ,1,,mptab(6,12)

MPDATA,GXZ,1,,mptab(7,1)
MPDATA,GXZ,1,,mptab(7,2)
MPDATA,GXZ,1,,mptab(7,3)
MPDATA,GXZ,1,,mptab(7,4)
MPDATA,GXZ,1,,mptab(7,5)
MPDATA,GXZ,1,,mptab(7,6)
MPDATA,GXZ,1,,mptab(7,7)
MPDATA,GXZ,1,,mptab(7,8)
MPDATA,GXZ,1,,mptab(7,9)
MPDATA,GXZ,1,,mptab(7,10)
MPDATA,GXZ,1,,mptab(7,11)
MPDATA,GXZ,1,,mptab(7,12)
!*****************************Meshing*********************************
****
lsel,s,line,,1,4,,0                              ! Select all lines
cm,l1xy,line
lesize,l1xy,elsize,,                             ! set size of element
asel,s,,,1,,,
amesh,1
allsel,all,all
!************constraint and mechanical load**************************
nsel,s,loc,x,0,                ! select all edges
nsel,a,loc,y,0,
cm,edges,node                    ! label edges
allsel,all,node
nsel,s,loc,x,width-(lwidth*0.5),width        ! select central square region
nsel,r,loc,y,width-(lwidth*0.5),width
cm,loadarea,node                           ! label load area
!**************upload temperature file**********************
temptable=
temptab=
*DIM,temptable,table,17,telno+1      ! create table for temperatures
```

```
*DIM,temptab,array,17,telno+1        ! create array for temperatures
*TREAD,temptable,tempoutss1,csv      ! input temps from data file into table
*MFUN,temptab,COPY,temptable         ! copy table into an array
!*******************loading and constraints*****************************
/SOLU
ANTYPE,0
*Do,i,1,ti,1
TIME,i

!****apply temperatures to layers******
BFE,all,temp,1,temptab(i,1),temptab(i,2),temptab(i,3),temptab(i,4)
BFE,all,temp,5,temptab(i,5),temptab(i,6),temptab(i,7),temptab(i,8)
BFE,all,temp,9,temptab(i,9),temptab(i,10),temptab(i,11),temptab(i,12)
BFE,all,temp,13,temptab(i,13),temptab(i,14),temptab(i,15),temptab(i,16)
BFE,all,temp,17,temptab(i,17)
allsel,all,all
load=1000*temptab(i,telno+1)
pressure=load/area
allsel,all,all
NSEL,S,LOC,X,length        ! symmetry along x=length
DSYM,SYMM,X
allsel,all,all
NSEL,S,LOC,Y,width         ! symmetry along y=width
DSYM,SYMM,Y
allsel,all,all
D,edges,all,0              ! apply clamped condition to edges
allsel,all,all
SF,loadarea,pres,pressure, ! apply pressure to load area
lswrite                    ! write loadstep to file
*enddo
allsel,all,all
lssolve,1,ti,1             ! solve all load steps
!**********************writing                                          results
file************************************
/POST1
*dim,table,,ti,3                      ! create table with ti rows and 3 cols
*do,i,1,ti,1
set,i


ASEL,ALL,NODE                          ! reselects all the nodes
nSORT,U,Z,1,1,,SELECT                            ! selects uz for all nodes
*GET,d,SORT,,MAX                               ! sorts the values
Deflection=ABS(d)                      ! outputs the max value of uz
allsel,all,all                        ! selects the minimum value of
nsel,s,node,,loadarea                  ! deflection in the load area
nsort,u,z,0,1,,SELECT
*get,dmin,sort,,min
deflection_min=abs(dmin)
table(i,1)=(i-1)*step
table(i,2)=deflection_min*1000
```

```
table(i,3)=Deflection*1000
*enddo
*CREATE,ansuitmp
*CFOPEN,'resultsshellexp','csv',
*VWRITE,table(1,1),table(1,2),table(1,3), , , , , , ,
(F6.0,',',F20.10,',',F20.10)
*CFCLOS
*END
/INPUT,ansuitmp
!get end time
~eui, 'set fid [open "end.txt" w]'
~eui, 'puts $fid [clock format [clock seconds] -format "%c"]'
~eui, 'close $fid'
finish
```

D.2 SOLID185 Single Skin Input File

```
/filname,solid185tmechSS1-1,1
/TITLE,2D thermal mechanical plate bending
/COM,solid185 tmech
C*** USING SHELL91
/prep7
!**********record start time*********************
~eui, 'set fid [open "start.txt" w]'
~eui, 'puts $fid [clock format [clock seconds] -format "%c"]'
~eui, 'close $fid'
et,1,solid185
keyopt,1,3,1                    ! layered option
width=0.2/2                     ! panel width
length=0.2/2
lwidth=0.04                     ! width of area over which load is applied
llength=0.04
thick=10.72e-3                  ! panel thickness
layers=16                       ! no. of layers
plythk=thick/layers             ! ply thickness
elsize=thick/2                  ! element size through thickness
telno=3                         ! No of temperature layers
area=lwidth*llength             ! area over which load is applied
step=30                                 ! Time step
ti= 17                          ! No of time steps
! ****temperature layer 1 areas****
r11= 0.03    ! central region for highest temperature
r12= 0.07    ! region 2 for next temp decrease
TD11= 1      ! temperature drop % for region 1
TD12= 0.75   ! temperature drop % for region 2
TD13= 0.5    ! temperature drop % for region 3
! ****temperature layer 2 areas****
r21=0.03
r22=0.07
TD21=1
TD22=0.75
TD23=0.5
! ****temperature layer 3 areas****
r31= 0.03
r32= 0.07
TD31= 1
TD32= 0.75
TD33= 0.5
immed,off     ! toggle graphics
!*******************lay-up*****************************************
SECTYPE,1,SHELL
SECDATA,plythk,1,0        ! LAYER 1:  THK, THETA 0
SECDATA,plythk,1,0        ! LAYER 2:  THK, THETA 0
SECDATA,plythk,1,0        ! LAYER 3:  THK, THETA 0
SECDATA,plythk,1,0        ! LAYER 4:  THK, THETA 0
```

```
SECDATA,plythk,1,0        ! LAYER 5:  THK, THETA 0
SECDATA,plythk,1,0        ! LAYER 6:  THK, THETA 0
SECDATA,plythk,1,0        ! LAYER 7:  THK, THETA 0
SECDATA,plythk,1,0        ! LAYER 8:  THK, THETA 0
SECDATA,plythk,1,0        ! LAYER 9:  THK, THETA 0
SECDATA,plythk,1,0        ! LAYER 10: THK, THETA 0
SECDATA,plythk,1,0        ! LAYER 11: THK, THETA 0
SECDATA,plythk,1,0        ! LAYER 12: THK, THETA 0
SECDATA,plythk,1,0        ! LAYER 13: THK, THETA 0
SECDATA,plythk,1,0        ! LAYER 14: THK, THETA 0
SECDATA,plythk,1,0        ! LAYER 15: THK, THETA 0
SECDATA,plythk,1,0        ! LAYER 16: THK, THETA 0
!***************input parameters************************************
layer1=  thick/3    ! thickness of 1st layer for const temp
layer2=   2*layer1  ! z cooord of 2nd layer for const temp
layer3=   3*layer1  ! z coord of 3rd layer for const temp
!******************GEOMETRY*************************************
block,0,length,0,width,0,thick            ! create block
!*****************MATERIAL PROPERTIES************************
mptable=
mptab=
*DIM,mptable,table,7,12       ! create table for mp
*DIM,mptab,array,7,12         ! create array for temperatures
*TREAD,mptable,mpss1-1,csv    ! input temperatures from data file into table
*MFUN,mptab,COPY,mptable      ! copy table into an array
MPTEMP,,,,,,,,
MPTEMP,1,mptab(1,1)
MPTEMP,2,mptab(1,2)
MPTEMP,3,mptab(1,3)
MPTEMP,4,mptab(1,4)
MPTEMP,5,mptab(1,5)
MPTEMP,6,mptab(1,6)
MPTEMP,7,mptab(1,7)
MPTEMP,8,mptab(1,8)
MPTEMP,9,mptab(1,9)
MPTEMP,10,mptab(1,10)
MPTEMP,11,mptab(1,11)
MPTEMP,12,mptab(1,12)

MPDATA,EX,1,,mptab(2,1)
MPDATA,EX,1,,mptab(2,2)
MPDATA,EX,1,,mptab(2,3)
MPDATA,EX,1,,mptab(2,4)
MPDATA,EX,1,,mptab(2,5)
MPDATA,EX,1,,mptab(2,6)
MPDATA,EX,1,,mptab(2,7)
MPDATA,EX,1,,mptab(2,8)
MPDATA,EX,1,,mptab(2,9)
MPDATA,EX,1,,mptab(2,10)
MPDATA,EX,1,,mptab(2,11)
MPDATA,EX,1,,mptab(2,12)
```

MPDATA,EY,1,,mptab(3,1)
MPDATA,EY,1,,mptab(3,2)
MPDATA,EY,1,,mptab(3,3)
MPDATA,EY,1,,mptab(3,4)
MPDATA,EY,1,,mptab(3,5)
MPDATA,EY,1,,mptab(3,6)
MPDATA,EY,1,,mptab(3,7)
MPDATA,EY,1,,mptab(3,8)
MPDATA,EY,1,,mptab(3,9)
MPDATA,EY,1,,mptab(3,10)
MPDATA,EY,1,,mptab(3,11)
MPDATA,EY,1,,mptab(3,12)

MPDATA,EZ,1,,mptab(4,1)
MPDATA,EZ,1,,mptab(4,2)
MPDATA,EZ,1,,mptab(4,3)
MPDATA,EZ,1,,mptab(4,4)
MPDATA,EZ,1,,mptab(4,5)
MPDATA,EZ,1,,mptab(4,6)
MPDATA,EZ,1,,mptab(4,7)
MPDATA,EZ,1,,mptab(4,8)
MPDATA,EZ,1,,mptab(4,9)
MPDATA,EZ,1,,mptab(4,10)
MPDATA,EZ,1,,mptab(4,11)
MPDATA,EZ,1,,mptab(4,12)

MPDATA,PRXY,1,,0.3
MPDATA,PRXY,1,,0.2
MPDATA,PRXY,1,,0.15
MPDATA,PRXY,1,,0.1
MPDATA,PRXY,1,,0.05
MPDATA,PRXY,1,,0.01
MPDATA,PRXY,1,,0.001
MPDATA,PRXY,1,,0.001
MPDATA,PRXY,1,,0.001
MPDATA,PRXY,1,,0.001
MPDATA,PRXY,1,,0.001
MPDATA,PRXY,1,,0.001

MPDATA,PRYZ,1,,0.3
MPDATA,PRYZ,1,,0.2
MPDATA,PRYZ,1,,0.15
MPDATA,PRYZ,1,,0.1
MPDATA,PRYZ,1,,0.05
MPDATA,PRYZ,1,,0.01
MPDATA,PRYZ,1,,0.001
MPDATA,PRYZ,1,,0.001
MPDATA,PRYZ,1,,0.001
MPDATA,PRYZ,1,,0.001
MPDATA,PRYZ,1,,0.001

```
MPDATA,PRYZ,1,,0.001

MPDATA,PRXZ,1,,0.3
MPDATA,PRXZ,1,,0.2
MPDATA,PRXZ,1,,0.15
MPDATA,PRXZ,1,,0.1
MPDATA,PRXZ,1,,0.05
MPDATA,PRXZ,1,,0.01
MPDATA,PRXZ,1,,0.001
MPDATA,PRXZ,1,,0.001
MPDATA,PRXZ,1,,0.001
MPDATA,PRXZ,1,,0.001
MPDATA,PRXZ,1,,0.001
MPDATA,PRXZ,1,,0.001

MPDATA,GXY,1,,mptab(5,1)
MPDATA,GXY,1,,mptab(5,2)
MPDATA,GXY,1,,mptab(5,3)
MPDATA,GXY,1,,mptab(5,4)
MPDATA,GXY,1,,mptab(5,5)
MPDATA,GXY,1,,mptab(5,6)
MPDATA,GXY,1,,mptab(5,7)
MPDATA,GXY,1,,mptab(5,8)
MPDATA,GXY,1,,mptab(5,9)
MPDATA,GXY,1,,mptab(5,10)
MPDATA,GXY,1,,mptab(5,11)
MPDATA,GXY,1,,mptab(5,12)

MPDATA,GYZ,1,,mptab(6,1)
MPDATA,GYZ,1,,mptab(6,2)
MPDATA,GYZ,1,,mptab(6,3)
MPDATA,GYZ,1,,mptab(6,4)
MPDATA,GYZ,1,,mptab(6,5)
MPDATA,GYZ,1,,mptab(6,6)
MPDATA,GYZ,1,,mptab(6,7)
MPDATA,GYZ,1,,mptab(6,8)
MPDATA,GYZ,1,,mptab(6,9)
MPDATA,GYZ,1,,mptab(6,10)
MPDATA,GYZ,1,,mptab(6,11)
MPDATA,GYZ,1,,mptab(6,12)

MPDATA,GXZ,1,,mptab(7,1)
MPDATA,GXZ,1,,mptab(7,2)
MPDATA,GXZ,1,,mptab(7,3)
MPDATA,GXZ,1,,mptab(7,4)
MPDATA,GXZ,1,,mptab(7,5)
MPDATA,GXZ,1,,mptab(7,6)
MPDATA,GXZ,1,,mptab(7,7)
MPDATA,GXZ,1,,mptab(7,8)
MPDATA,GXZ,1,,mptab(7,9)
MPDATA,GXZ,1,,mptab(7,10)
```

```
MPDATA,GXZ,1,,mptab(7,11)
MPDATA,GXZ,1,,mptab(7,12)
!*****************************Meshing************************
lsel,s,line,,1,8,,0                          ! Element size in xy plane
cm,l1xy,line
lesize,l1xy,elsize/2,,
lsel,s,line,,9,12,,0
cm,l1z,line
lesize,l1z,elsize,,                          ! Element size in z direction
vsel,s,,,1,,,                          ! Meshing volume 1
veorient,1,line,9
vmesh,1
allsel,all,all

!************ select edges for constraint and loading area***************
nsel,s,loc,x,0,                          ! select all edges for constraint
nsel,a,loc,y,0,
cm,edges,node                          ! label edges
allsel,all,node                          ! select all nodes again
nsel,s,ext                          ! select exterior nodes
nsel,r,loc,z,thick,
nsel,r,loc,x,width-(lwidth*0.5),width       ! select central square region
nsel,r,loc,y,width-(lwidth*0.5),width       ! select central square region
cm,loadarea,node                          ! label load area
!************************temperature loads**************************
allsel,all,all
!****layer 1****
NSEL,s,loc,z,0,layer1
nsel,r,loc,x,0.1 - r11,0.1 + r11
nsel,r,loc,y,0.1 - r11,0.1 + r11    ! select region 1 on layer 1
CM,layer1r1,node
allsel,all,all
NSEL,s,loc,z,0,layer1
nsel,r,loc,x,0.1-r12,0.1+r12
nsel,r,loc,y,0.1-r12,0.1+r12
nsel,u,,,layer1r1                ! select region 2 on layer 1
CM,layer1r2,node
allsel,all,all
nsel,s,loc,z,0,layer1
nsel,u,,,layer1r2
nsel,u,,,layer1r1
CM,layer1r3,node                  ! select region 3 on layer 1
!**** layer 2****
allsel,all,all
Nsel,s,loc,z,layer1,layer2
nsel,r,loc,x,0.1 - r21,0.1 + r21
nsel,r,loc,y,0.1 - r21,0.1 + r21    ! select region 1 on layer 2
CM,layer2r1,node
allsel,all,all
NSEL,s,loc,z,layer1,layer2
nsel,r,loc,x,0.1-r22,0.1+r22
```

```
nsel,r,loc,y,0.1-r22,0.1+r22
nsel,u,,,layer2r1                ! select region 2 on layer 2
CM,layer2r2,node
allsel,all,all
nsel,s,loc,z,layer1,layer2
nsel,u,,,layer2r2
nsel,u,,,layer2r1
CM,layer2r3,node                 ! select region 3 on layer 2
!**** layer 3****
allsel,all,all
Nsel,s,loc,z,layer2,layer3
nsel,r,loc,x,0.1 - r31,0.1 + r31
nsel,r,loc,y,0.1 - r31,0.1 + r31    ! select region 1 on layer 3
CM,layer3r1,node
allsel,all,all
NSEL,s,loc,z,layer2,layer3
nsel,r,loc,x,0.1-r32,0.1+r32
nsel,r,loc,y,0.1-r32,0.1+r32
nsel,u,,,layer3r1                ! select region 2 on layer 3
CM,layer3r2,node
allsel,all,all
nsel,s,loc,z,layer2,layer3
nsel,u,,,layer3r2
nsel,u,,,layer3r1
CM,layer3r3,node                 ! select region 3 on layer 3
!**************upload temperature file**********************
temptable=
temptab=
*DIM,temptable,table,17,telno+1      ! create table for temperatures
*DIM,temptab,array,17,telno+1        ! create array for temperatures
*TREAD,temptable,tempoutss1solid,csv ! input temperatures from data file
*MFUN,temptab,COPY,temptable         ! copy table into an array
!********************loading and constraints*****************************
/SOLU
ANTYPE,0
*Do,i,1,ti,1
Tini=temptab(1,1)   !initial temperature
 !************apply temperature loads**********
!******1st layer*****************
allsel,all,all
T1=temptab(i,1)
BF,layer1r1,temp,T1
allsel,all,all
TD12a=TD12*T1               ! reduce temperature in middle region
*if,TD12a,LE,Tini,THEN       ! if reduced temperature is less than initial
TD12a=Tini                  ! temperature reset to initial temperature
*endif
BF,layer1r2,temp,TD12a       ! Apply temperature to selected nodes
allsel,all,all
TD13a=TD13*T1
*if,TD13a,LE,Tini,THEN
```

```
TD13a=Tini
*endif
BF,layer1r3,temp,TD13a
allsel,all,all
!**********2nd layer***************
T2=temptab(i,2)
BF,layer2r1,temp,T2
allsel,all,all
TD22a=TD22*T2
*if,TD22a,LE,Tini,THEN
TD22a=Tini
*endif
BF,layer2r2,temp,TD22a
allsel,all,all
TD23a=TD23*T2
*if,TD23a,LE,Tini,THEN
TD23a=Tini
*endif
BF,layer2r3,temp,TD23a
allsel,all,all
!********3rd layer****************
T3=temptab(i,3)
BF,layer3r1,temp,T3
allsel,all,all
TD32a=TD32*T3
*if,TD32a,LE,Tini,THEN
TD32a=Tini
*endif
BF,layer3r2,temp,TD32a
allsel,all,all
TD33a=TD33*T3
*if,TD33a,LE,Tini,THEN
TD33a=Tini
*endif
BF,layer3r3,temp,TD33a
allsel,all,all
!***************apply structural load and constraints**********
load=1000*temptab(i,4)
pressure=load/area
allsel,all,all
NSEL,S,LOC,X,width            ! symmetry along x=width
DSYM,SYMM,X
NSEL,S,LOC,Y,width            ! symmetry along y=width
DSYM,SYMM,Y
allsel,all,all
D,edges,all,0                 ! fix other two edges
allsel,all,all
SF,loadarea,pres,pressure,    ! Apply pressure
allsel,all,all
lswrite                       ! Write loadsteps to file
*enddo
```

```
lssolve,1,ti,1                ! solve all loadsteps
!**********************writing results file*********************
/POST1
*dim,table,,ti,3                ! create table with nloop rows and 3 cols
*do,i,1,ti,1
set,i
NSORT,s,x,1,1,,SELECT           ! Selects the x comp of stress for all nodes
*GET,smax,SORT,,MAX                          ! sorts the values of sx
Smax=ABS(smax)                                ! selects the max value
ASEL,ALL,NODE                 ! reselects all the nodes
nSORT,U,Z,1,1,,SELECT                        ! selects uz for all nodes
*GET,d,SORT,,MAX                        ! sorts the values
Deflection=ABS(d)             ! outputs the max value of uz
allsel,all,all                ! output minimum value of uz within load area
nsel,s,node,,loadarea
nsort,u,z,0,1,,SELECT
*get,dmin,sort,,min
deflection_min=abs(dmin)
table(i,1)=(i-1)*step
table(i,2)=deflection_min*1000
table(i,3)=Deflection*1000
*enddo
*CREATE,ansuitmp
*CFOPEN,'resultssolidexp','csv'        ! output results file
*VWRITE,table(1,1),table(1,2),table(1,3), , , , , , ,
(F6.0,',',F20.10,',',F20.10)
*CFCLOS
*END
/INPUT,ansuitmp
! record end time
~eui, 'set fid [open "end.txt" w]'
~eui, 'puts $fid [clock format [clock seconds] -format "%c"]'
~eui, 'close $fid'
finish
```

D.3 SHELL91/SOLID186 Sandwich Input File

```
/TITLE,thermal mechanical plate bending quarter plate
/COM,shell91 tmech
C*** USING SHELL91
/prep7
! record time
~eui, 'set fid [open "start.txt" w]'
~eui, 'puts $fid [clock format [clock seconds] -format "%c"]'
~eui, 'close $fid'
et,1,shell91                ! element for skins
keyopt,1,1,9
et,2,solid186               ! element for core
keyopt,2,3,1
width=0.2/2                 ! panel width
length=0.2/2
lwidth=0.08                 ! width of area over which load is applied
llength=0.08                ! length of area over which load is applied
thick=1.6e-3                ! skin thickness
corethk=15e-3               ! core thickness
layers=8
plythk6=thick/6
plythck12=thick/12
elsize=corethk
telno=20                    ! No of temperature layers
area=lwidth*llength         ! area over which load is applied
step=30                             ! Time PERIOD
ti= 21                      ! No of time steps
immed,off
!*****************skin lay-up*************************************
R,1,layers,1,,,,        !all other keyoption are default
RMORE,,,,,,
RMORE,1,0,plythk6,  !mat, theta, tk(i), tk(j), tk(k), tk(l)
RMORE,1,90,plythk6,
RMORE,1,-45,plythk6,
RMORE,1,45,plythk6,  !mat, theta, tk(i), tk(j), tk(k), tk(l)
RMORE,1,45,plythk12, !mat, theta, tk(i), tk(j), tk(k), tk(l)
RMORE,1,-45,plythk12,
RMORE,1,90,plythk12,
RMORE,1,0,plythk12,
!**********core lay up*******************
SECTYPE,1,shell
SECDATA,corethk,2,0         !
SECDATA,corethk,2,0         !
SECDATA,corethk,2,0         !
!*****************GEOMETRY****************************
block,0,length,0,width,0,corethk        !thickness
!****************MATERIAL PROPERTIES*****************
!*************upload material properties file*******************
mptable=
```

```
mptab=
*DIM,mptable,table,9,12    ! create table for mp
*DIM,mptab,array,9,12      ! create array for temperatures
*TREAD,mptable,mpsw1,csv   ! input temperatures from data file into table
*MFUN,mptab,COPY,mptable   ! copy table into an array
MPTEMP,,,,,,,,
MPTEMP,1,mptab(1,1)
MPTEMP,2,mptab(1,2)
MPTEMP,3,mptab(1,3)
MPTEMP,4,mptab(1,4)
MPTEMP,5,mptab(1,5)
MPTEMP,6,mptab(1,6)
MPTEMP,7,mptab(1,7)
MPTEMP,8,mptab(1,8)
MPTEMP,9,mptab(1,9)
MPTEMP,10,mptab(1,10)
MPTEMP,11,mptab(1,11)
MPTEMP,12,mptab(1,12)
!MPTEMP,13,mptab(1,13)
!**********skin properties**********************************
MPDATA,EX,1,,mptab(2,1)
MPDATA,EX,1,,mptab(2,2)
MPDATA,EX,1,,mptab(2,3)
MPDATA,EX,1,,mptab(2,4)
MPDATA,EX,1,,mptab(2,5)
MPDATA,EX,1,,mptab(2,6)
MPDATA,EX,1,,mptab(2,7)
MPDATA,EX,1,,mptab(2,8)
MPDATA,EX,1,,mptab(2,9)
MPDATA,EX,1,,mptab(2,10)
MPDATA,EX,1,,mptab(2,11)
MPDATA,EX,1,,mptab(2,12)
!MPDATA,EX,1,,mptab(2,13)

MPDATA,EY,1,,mptab(3,1)
MPDATA,EY,1,,mptab(3,2)
MPDATA,EY,1,,mptab(3,3)
MPDATA,EY,1,,mptab(3,4)
MPDATA,EY,1,,mptab(3,5)
MPDATA,EY,1,,mptab(3,6)
MPDATA,EY,1,,mptab(3,7)
MPDATA,EY,1,,mptab(3,8)
MPDATA,EY,1,,mptab(3,9)
MPDATA,EY,1,,mptab(3,10)
MPDATA,EY,1,,mptab(3,11)
MPDATA,EY,1,,mptab(3,12)
!MPDATA,EY,1,,mptab(3,13)

MPDATA,EZ,1,,mptab(4,1)
MPDATA,EZ,1,,mptab(4,2)
MPDATA,EZ,1,,mptab(4,3)
```

```
MPDATA,EZ,1,,mptab(4,4)
MPDATA,EZ,1,,mptab(4,5)
MPDATA,EZ,1,,mptab(4,6)
MPDATA,EZ,1,,mptab(4,7)
MPDATA,EZ,1,,mptab(4,8)
MPDATA,EZ,1,,mptab(4,9)
MPDATA,EZ,1,,mptab(4,10)
MPDATA,EZ,1,,mptab(4,11)
MPDATA,EZ,1,,mptab(4,12)
!MPDATA,EZ,1,,mptab(4,13)

MPDATA,PRXY,1,,0.3
MPDATA,PRXY,1,,0.2
MPDATA,PRXY,1,,0.15
MPDATA,PRXY,1,,0.1
MPDATA,PRXY,1,,0.05
MPDATA,PRXY,1,,0.01
MPDATA,PRXY,1,,0.001
MPDATA,PRXY,1,,0.001
MPDATA,PRXY,1,,0.001
MPDATA,PRXY,1,,0.001
MPDATA,PRXY,1,,0.001
MPDATA,PRXY,1,,0.001

MPDATA,PRYZ,1,,0.3
MPDATA,PRYZ,1,,0.2
MPDATA,PRYZ,1,,0.15
MPDATA,PRYZ,1,,0.1
MPDATA,PRYZ,1,,0.05
MPDATA,PRYZ,1,,0.01
MPDATA,PRYZ,1,,0.001
MPDATA,PRYZ,1,,0.001
MPDATA,PRYZ,1,,0.001
MPDATA,PRYZ,1,,0.001
MPDATA,PRYZ,1,,0.001
MPDATA,PRYZ,1,,0.001

MPDATA,PRXZ,1,,0.3
MPDATA,PRXZ,1,,0.2
MPDATA,PRXZ,1,,0.15
MPDATA,PRXZ,1,,0.1
MPDATA,PRXZ,1,,0.05
MPDATA,PRXZ,1,,0.01
MPDATA,PRXZ,1,,0.001
MPDATA,PRXZ,1,,0.001
MPDATA,PRXZ,1,,0.001
MPDATA,PRXZ,1,,0.001
MPDATA,PRXZ,1,,0.001
MPDATA,PRXZ,1,,0.001

MPDATA,GXY,1,,mptab(5,1)
```

```
MPDATA,GXY,1,,mptab(5,2)
MPDATA,GXY,1,,mptab(5,3)
MPDATA,GXY,1,,mptab(5,4)
MPDATA,GXY,1,,mptab(5,5)
MPDATA,GXY,1,,mptab(5,6)
MPDATA,GXY,1,,mptab(5,7)
MPDATA,GXY,1,,mptab(5,8)
MPDATA,GXY,1,,mptab(5,9)
MPDATA,GXY,1,,mptab(5,10)
MPDATA,GXY,1,,mptab(5,11)
MPDATA,GXY,1,,mptab(5,12)
!MPDATA,GXY,1,,mptab(5,13)

MPDATA,GYZ,1,,mptab(6,1)
MPDATA,GYZ,1,,mptab(6,2)
MPDATA,GYZ,1,,mptab(6,3)
MPDATA,GYZ,1,,mptab(6,4)
MPDATA,GYZ,1,,mptab(6,5)
MPDATA,GYZ,1,,mptab(6,6)
MPDATA,GYZ,1,,mptab(6,7)
MPDATA,GYZ,1,,mptab(6,8)
MPDATA,GYZ,1,,mptab(6,9)
MPDATA,GYZ,1,,mptab(6,10)
MPDATA,GYZ,1,,mptab(6,11)
MPDATA,GYZ,1,,mptab(6,12)
!MPDATA,GYZ,1,,mptab(6,13)

MPDATA,GXZ,1,,mptab(7,1)
MPDATA,GXZ,1,,mptab(7,2)
MPDATA,GXZ,1,,mptab(7,3)
MPDATA,GXZ,1,,mptab(7,4)
MPDATA,GXZ,1,,mptab(7,5)
MPDATA,GXZ,1,,mptab(7,6)
MPDATA,GXZ,1,,mptab(7,7)
MPDATA,GXZ,1,,mptab(7,8)
MPDATA,GXZ,1,,mptab(7,9)
MPDATA,GXZ,1,,mptab(7,10)
MPDATA,GXZ,1,,mptab(7,11)
MPDATA,GXZ,1,,mptab(7,12)
!MPDATA,GXZ,1,,mptab(7,13)
!**********core
properties**********************************************
MPDATA,EX,2,,mptab(8,1)    !Ex
MPDATA,EX,2,,mptab(8,2)
MPDATA,EX,2,,mptab(8,3)
MPDATA,EX,2,,mptab(8,4)
MPDATA,EX,2,,mptab(8,5)
MPDATA,EX,2,,mptab(8,6)
MPDATA,EX,2,,mptab(8,7)
MPDATA,EX,2,,mptab(8,8)
MPDATA,EX,2,,mptab(8,9)
```

```
MPDATA,EX,2,,mptab(8,10)
MPDATA,EX,2,,mptab(8,11)
MPDATA,EX,2,,mptab(8,12)
!MPDATA,EX,1,,mptab(2,13)

MPDATA,PRXY,2,,0.3
MPDATA,PRXY,2,,0.2
MPDATA,PRXY,2,,0.15
MPDATA,PRXY,2,,0.1
MPDATA,PRXY,2,,0.05
MPDATA,PRXY,2,,0.01
MPDATA,PRXY,2,,0.001
MPDATA,PRXY,2,,0.001
MPDATA,PRXY,2,,0.001
MPDATA,PRXY,2,,0.001
MPDATA,PRXY,2,,0.001
MPDATA,PRXY,2,,0.001

MPDATA,GXY,2,,mptab(9,1)
MPDATA,GXY,2,,mptab(9,2)
MPDATA,GXY,2,,mptab(9,3)
MPDATA,GXY,2,,mptab(9,4)
MPDATA,GXY,2,,mptab(9,5)
MPDATA,GXY,2,,mptab(9,6)
MPDATA,GXY,2,,mptab(9,7)
MPDATA,GXY,2,,mptab(9,8)
MPDATA,GXY,2,,mptab(9,9)
MPDATA,GXY,2,,mptab(9,10)
MPDATA,GXY,2,,mptab(9,11)
MPDATA,GXY,2,,mptab(9,12)
!MPDATA,GXY,1,,mptab(5,13)
!*****************************Meshing************************
lsel,s,line,,1,12,,0                    ! layer 1 xy lines
cm,l1xy,line
lesize,l1xy,elsize,,                    ! 25mm element size in xy plane
mat,2                    ! select material 2
type,2                   ! select element type 2
vmesh,1
asel,s,,,2,,,            !select top surface
mat,1                    !use material 1
type,1                   !use element type 1
real,1                   !use real constant set 1
keyopt,1,11,2            !nodes located at top surface
amesh,2                    !mesh area 2
allsel,all,area
asel,s,,,1,,,
mat,1
type,1
real,1
keyopt,1,11,1
amesh,1
```

```
allsel,all,area
CPINTF,all,
nummrg,node
allsel,all,all
/eshape,1
eplot
!************constraint and mechanical load******************
nsel,s,loc,x,0,                ! select all edges
nsel,a,loc,y,0,
cm,edges,node                          ! label edges
allsel,all,node                        ! select all nodes again
nsel,s,loc,z,corethk
nsel,r,loc,x,width-(lwidth*0.5),width              ! select central square region
nsel,r,loc,y,width-(lwidth*0.5),width              ! select central square region
cm,loadarea,node                       ! label load area
!**************upload temperature file**********************
temptable=
temptab=
*DIM,temptable,table,21,telno+1      ! create table for temperatures
*DIM,temptab,array,21,telno+1        ! create array for temperatures
*TREAD,temptable,C:\Users\Phil\Documents\Work\Predictions\Chapter_6_predictions
\sw_250208\tempoutsw1,csv  !input temperatures from data file into table
*MFUN,temptab,COPY,temptable      ! copy table into an array
!***************select each set of temperature elements**********
allsel,all,all
nsel,s,loc,z,corethk   !top skin elements
esln,s,0, all
esel,r,type,,1
cm,topelem,elem
allsel,all,all        !bottom skin elements
nsel,s,loc,z,0
esln,s,0, all
esel,r,type,,1
cm,botelem,elem
allsel,all,all
esel,s,type,,2
cm,coreelem,elem
!*******************loading and constraints**************
/SOLU
ANTYPE,0
SOLCONTROL,ON
*Do,i,1,ti,1
time,i
allsel,all,all
! apply temperatures to hot skin
BFE,botelem,temp,1,temptab(i,1),temptab(i,2),temptab(i,3),temptab(i,4)
BFE,botelem,temp,5,temptab(i,5),temptab(i,6),temptab(i,7),temptab(i,8)
BFE,botelem,temp,9,temptab(i,9)!
! apply temperatures to core
bfe,coreelem,temp,1,temptab(i,9),temptab(i,10),temptab(i,11),temptab(i,12)
bfe,coreelem,temp,5,temptab(i,13)
```

```
! apply temperatures to cold skin
BFE,topelem,temp,1,temptab(i,13),temptab(i,14),temptab(i,15),temptab(i,16)
BFE,topelem,temp,5,temptab(i,17),temptab(i,18),temptab(i,19),temptab(i,20)
BFE,topelem,temp,9,temptab(i,20),temptab(i,21)!
allsel,all,all
load=1000*temptab(i,telno+1)
pressure=load/area
allsel,all,all
NSEL,S,LOC,X,width                    ! symmetry along x=width
DSYM,SYMM,X
NSEL,S,LOC,Y,length
DSYM,SYMM,Y                           ! symmetry along y=length
allsel,all,all
D,edges,all,0                         ! constrain edges
allsel,all,all
nsel,s,loc,z,corethk
nsel,r,loc,x,width-(lwidth*0.5),width       ! select central square region
nsel,r,loc,y,width-(lwidth*0.5),width
ESLN,s,1,all
sfe,all,2,pres,,pressure                ! apply pressure to skin elements
allsel,all,all
lswrite                               ! write load file
*enddo
lssolve,1,ti,1                        ! sove all load steps

!**********************writing results file**************************
/POST1
*dim,table,,ti,3              ! create table with nloop rows and 3 cols
*do,i,1,ti,1
set,i
NSORT,s,x,1,1,,SELECT         ! Selects the x comp of stress for all nodes
*GET,smax,SORT,,MAX                    ! sorts the values of sx
Smax=ABS(smax)                          ! selects the max value
ASEL,ALL,NODE                 ! reselects all the nodes
nSORT,U,Z,1,1,,SELECT                  ! selects uz for all nodes
*GET,d,SORT,,MAX                    ! sorts the values
Deflection=ABS(d)             ! outputs the max value of uz
allsel,all,all
nsel,s,node,,loadarea
nsort,u,z,0,1,,SELECT
*get,dmin,sort,,min
deflection_min=abs(dmin)
table(i,1)=(i-1)*step
table(i,2)=deflection_min*1000
table(i,3)=Deflection*1000
*enddo
*CREATE,ansuitmp
*CFOPEN,'results1','csv',
*VWRITE,table(1,1),table(1,2),table(1,3), , , , , , ,
(F6.0,',',F20.10,',',F20.10)
*CFCLOS
```

```
*END
/INPUT,ansuitmp
! record time
~eui, 'set fid [open "end.txt" w]'
~eui, 'puts $fid [clock format [clock seconds] -format "%c"]'
~eui, 'close $fid'
finish
```

D.4 Combined fire and load test results and input data

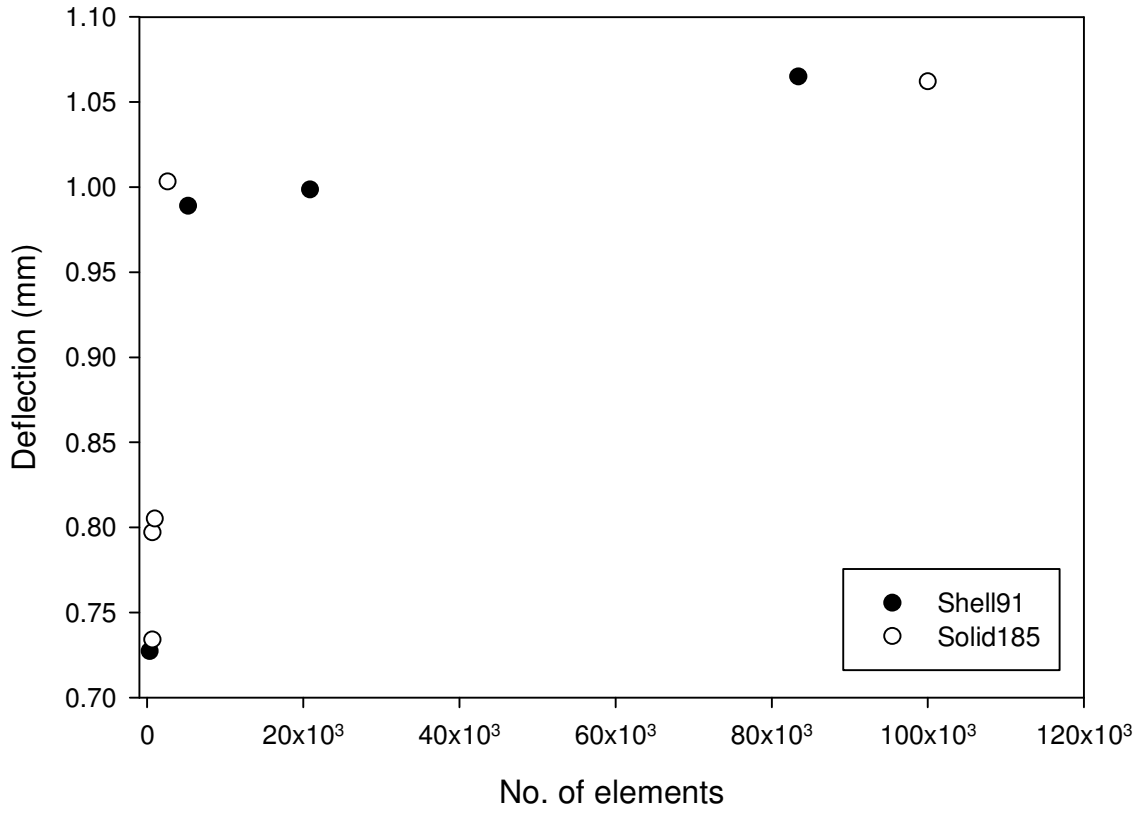

Figure D.1: Convergence of results for FE program with increasing number of elements

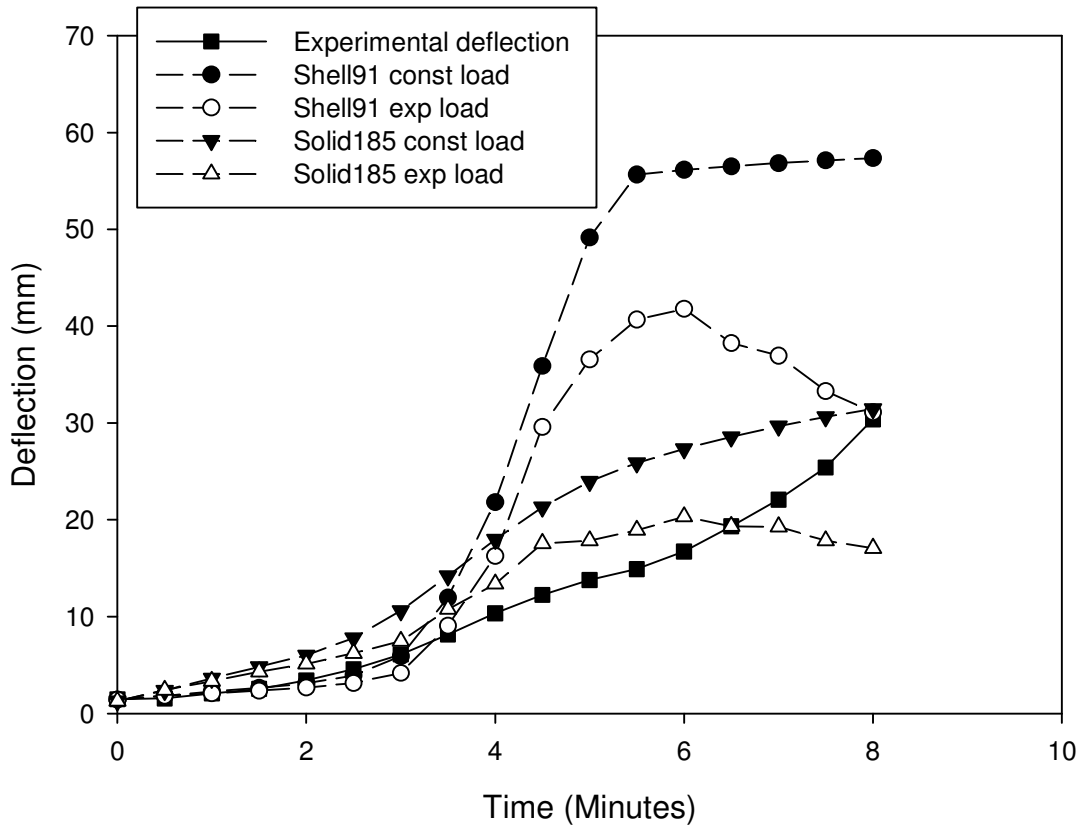

Figure D.2: Test panel SS 1.1 after fire and load testing under the cellulosic fire curve at 4.4MPa for 8mins 10sec

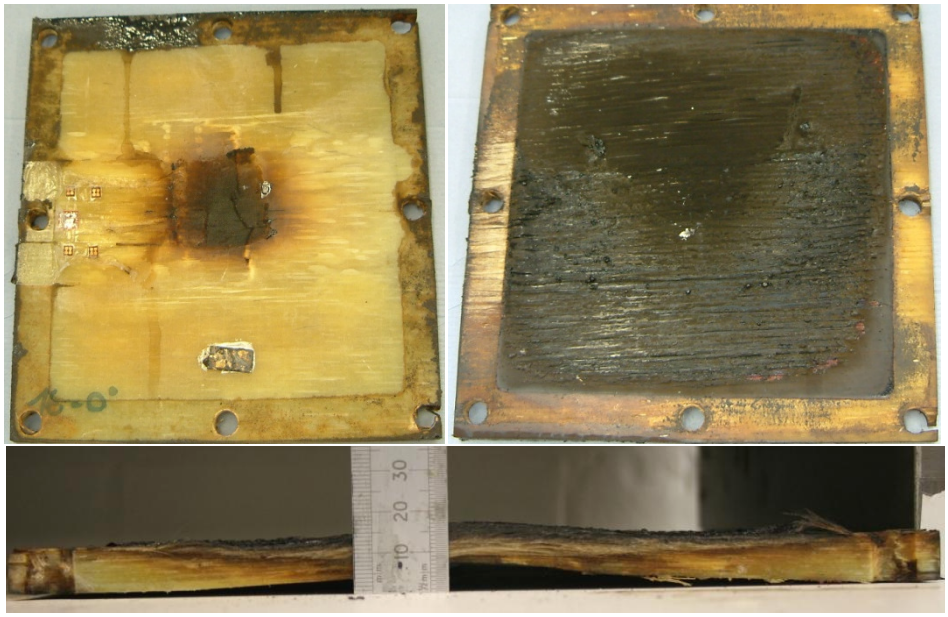

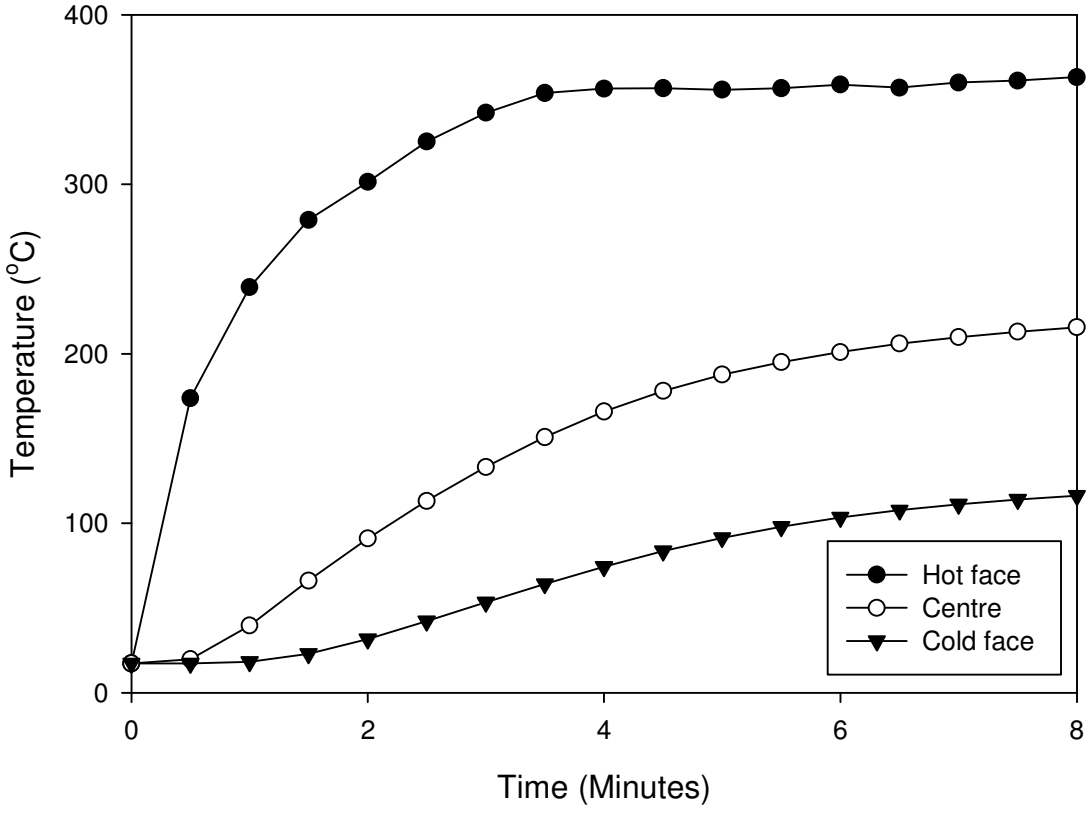

Figure D.3: Temperature profile used in thermo-mechanical model of panel SS 1.1

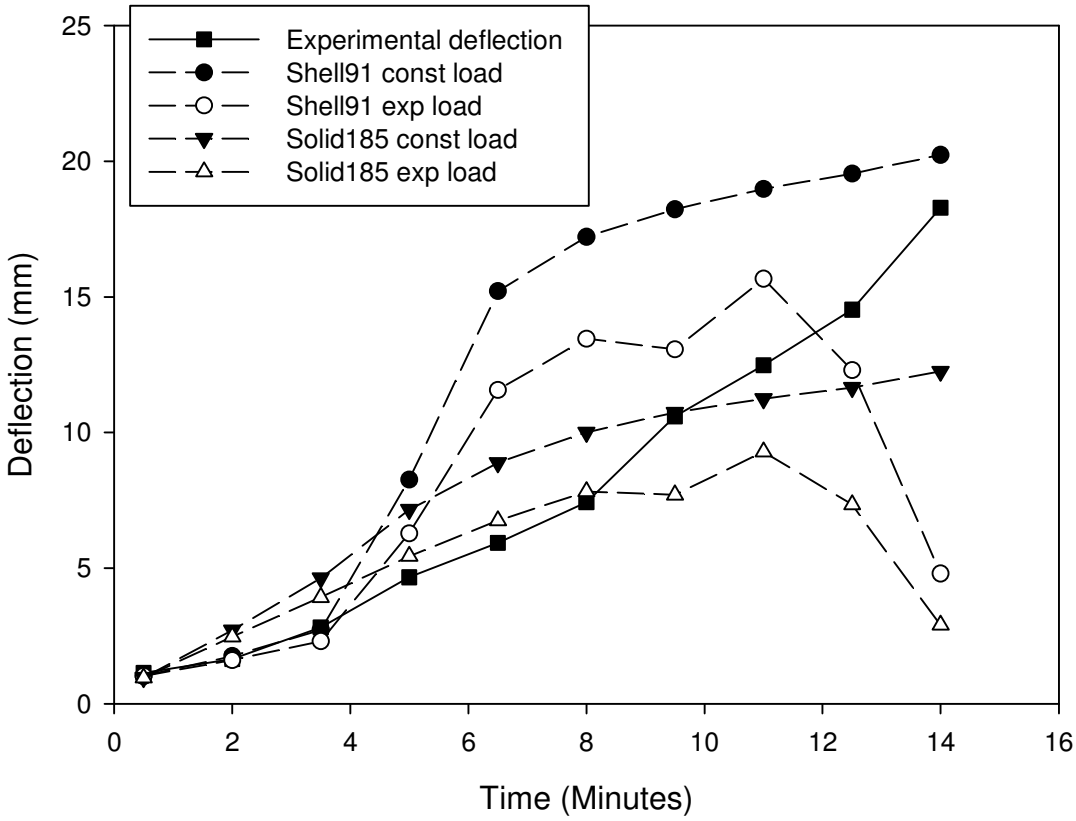

Figure D.4: Test panel SS 1.2 $[0]_{16}$ after fire and load testing under the cellulosic fire curve at 2.5MPa for 12mins 18sec

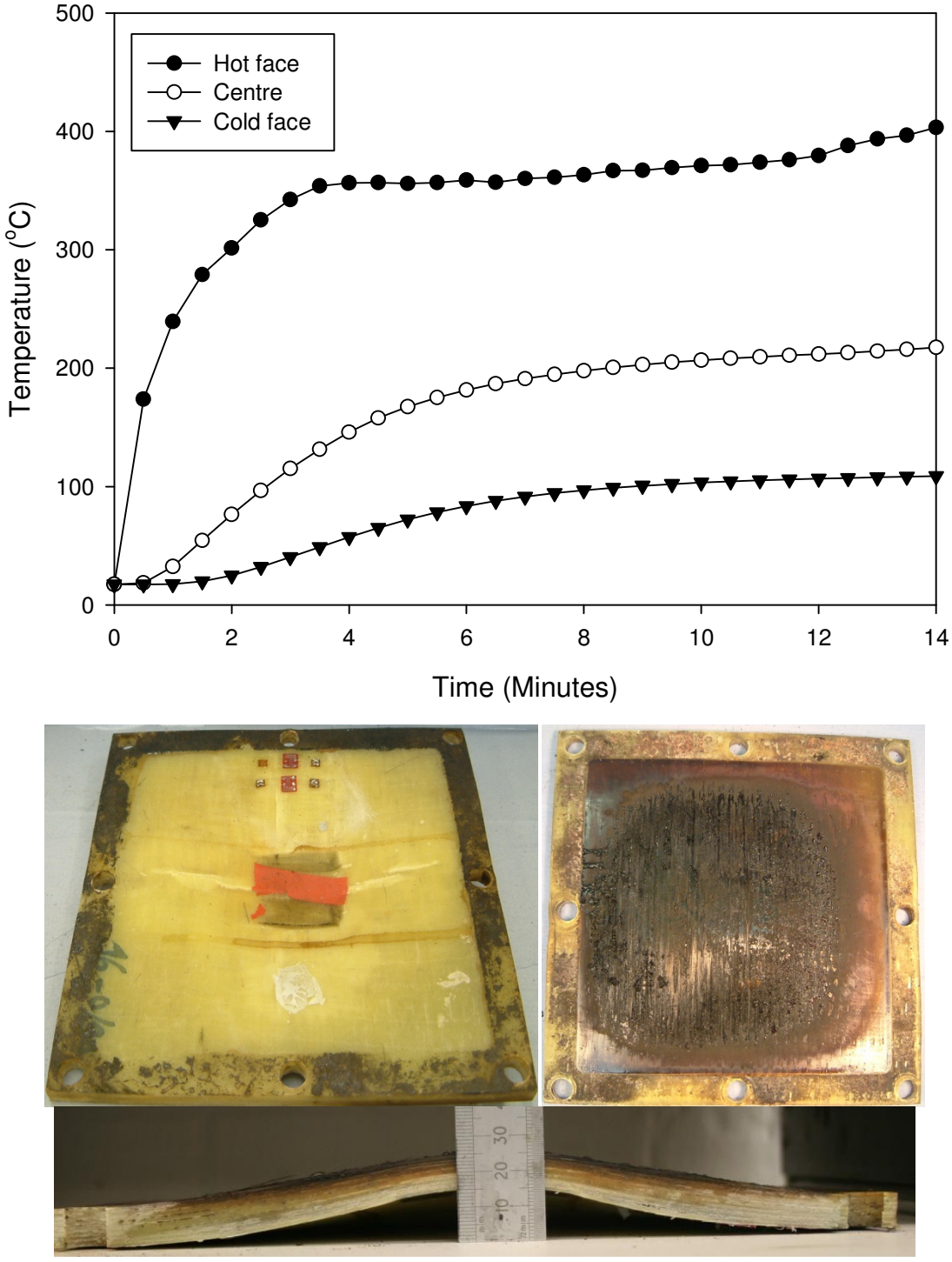

Figure D.5: Temperature profile used in thermo-mechanical model of panel SS 1.2

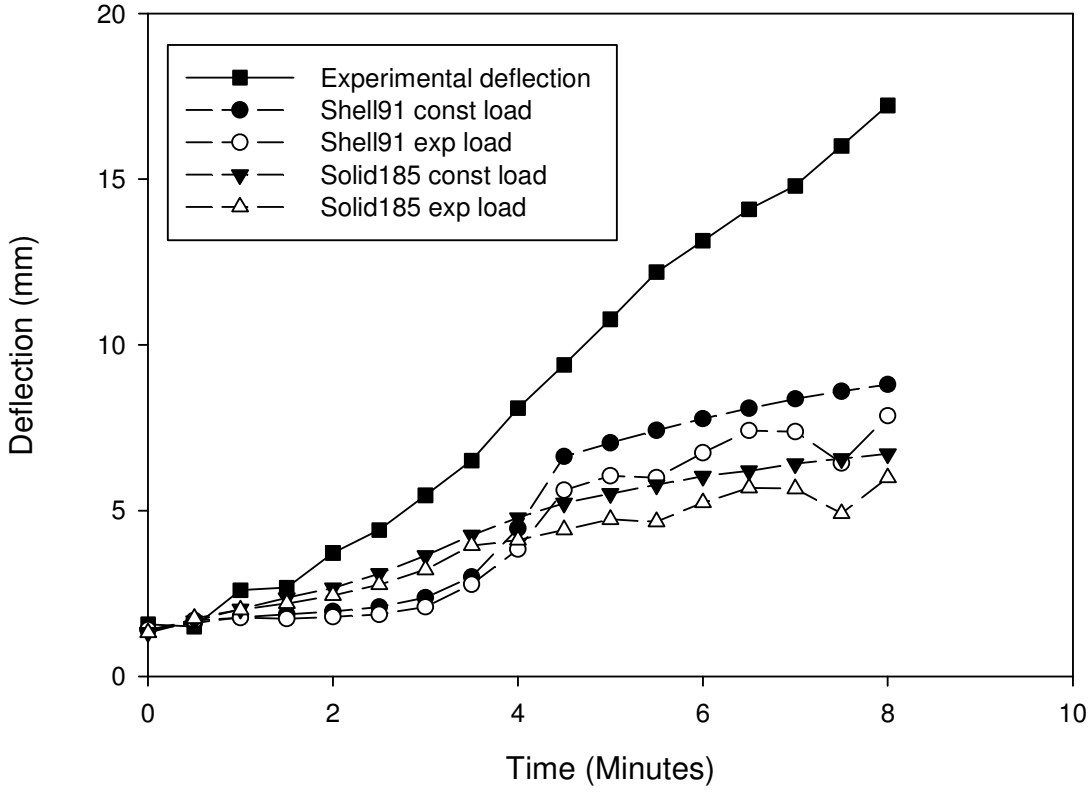

Figure D.6: Test panel SS2 after fire and load testing under the cellulosic fire curve at 4.4MPa for 7mins 4sec

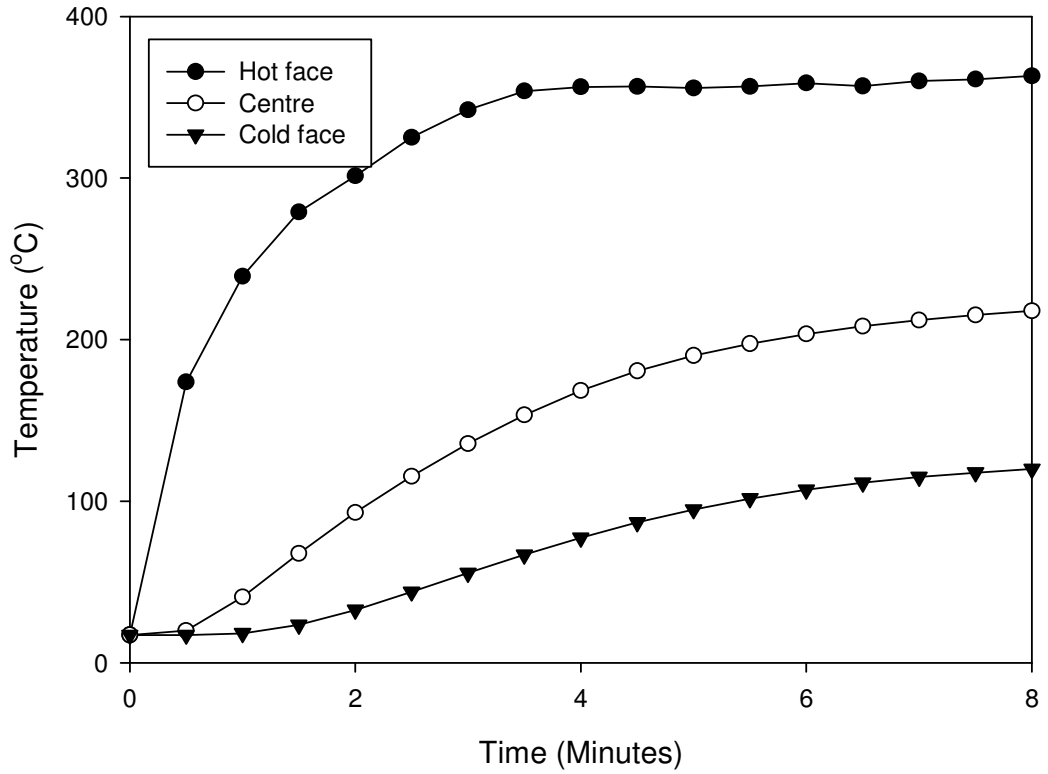

Figure D.7: Temperature profile used in thermo-mechanical model of panel SS 2

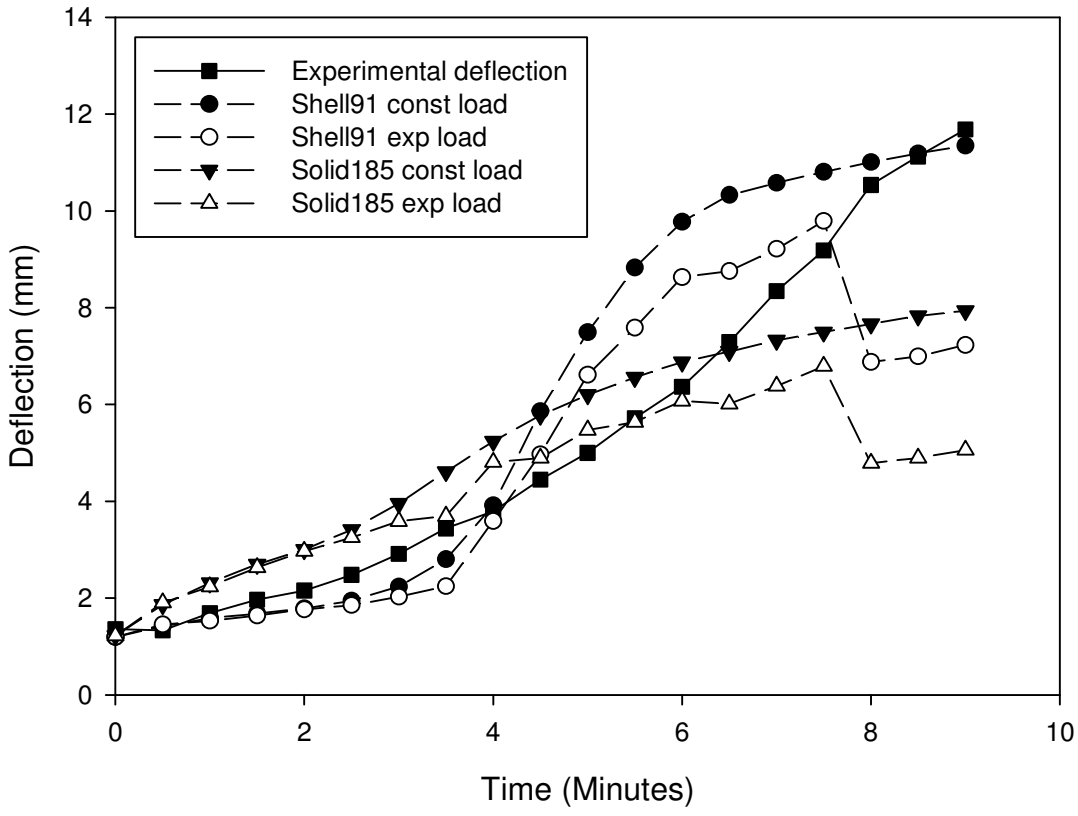

Figure D.8 Test panel SS3 after fire and load testing under the cellulosic fire curve at 4.4 MPa for 12mins 2sec

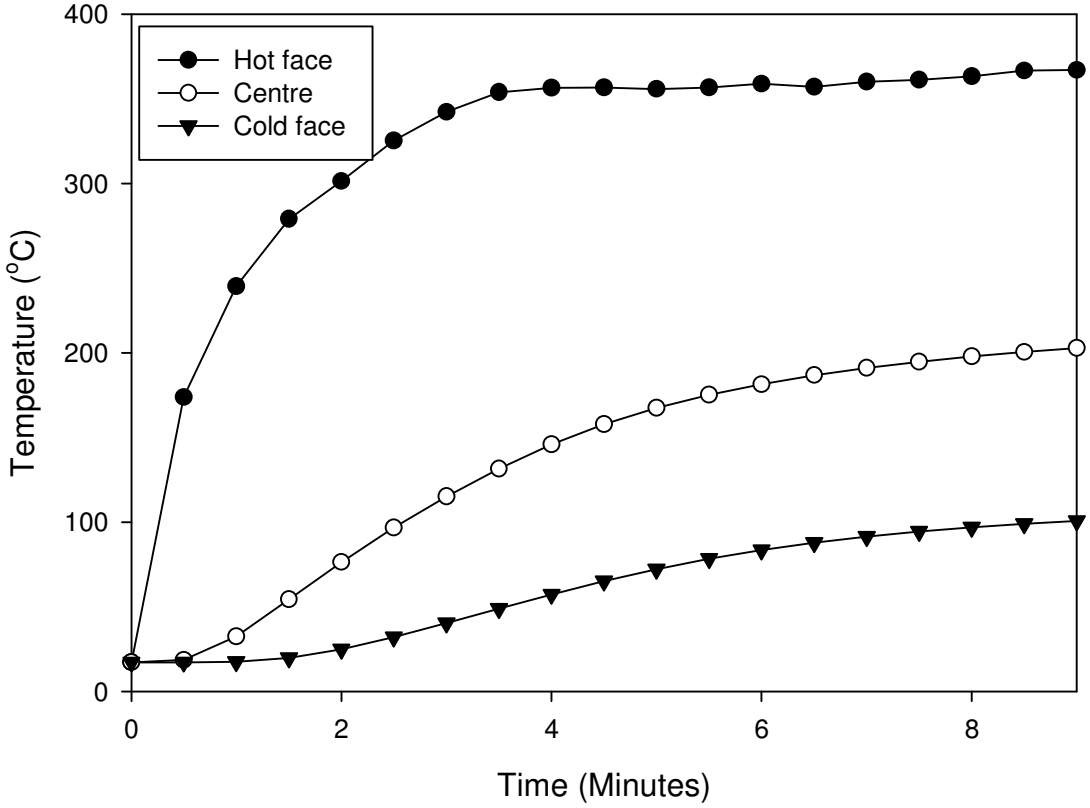

Figure D.9: Temperature profile used in thermo-mechanical model of panel SS 3

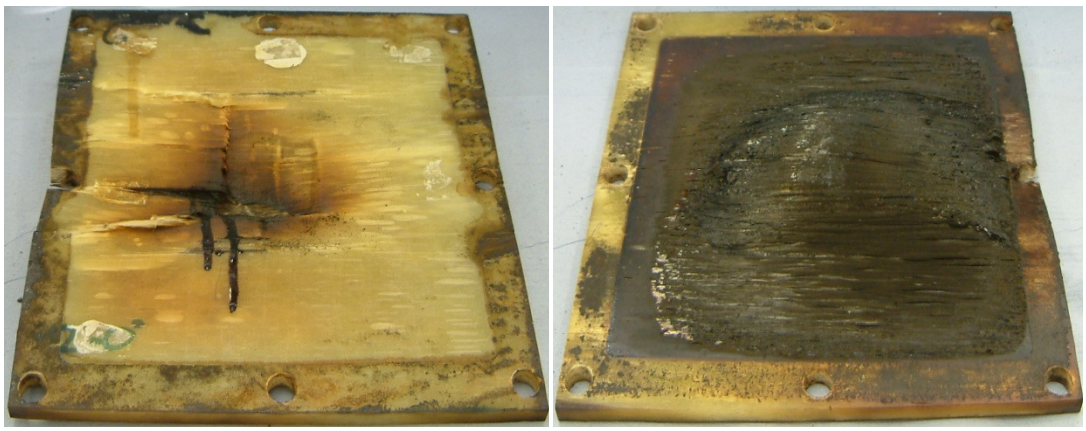

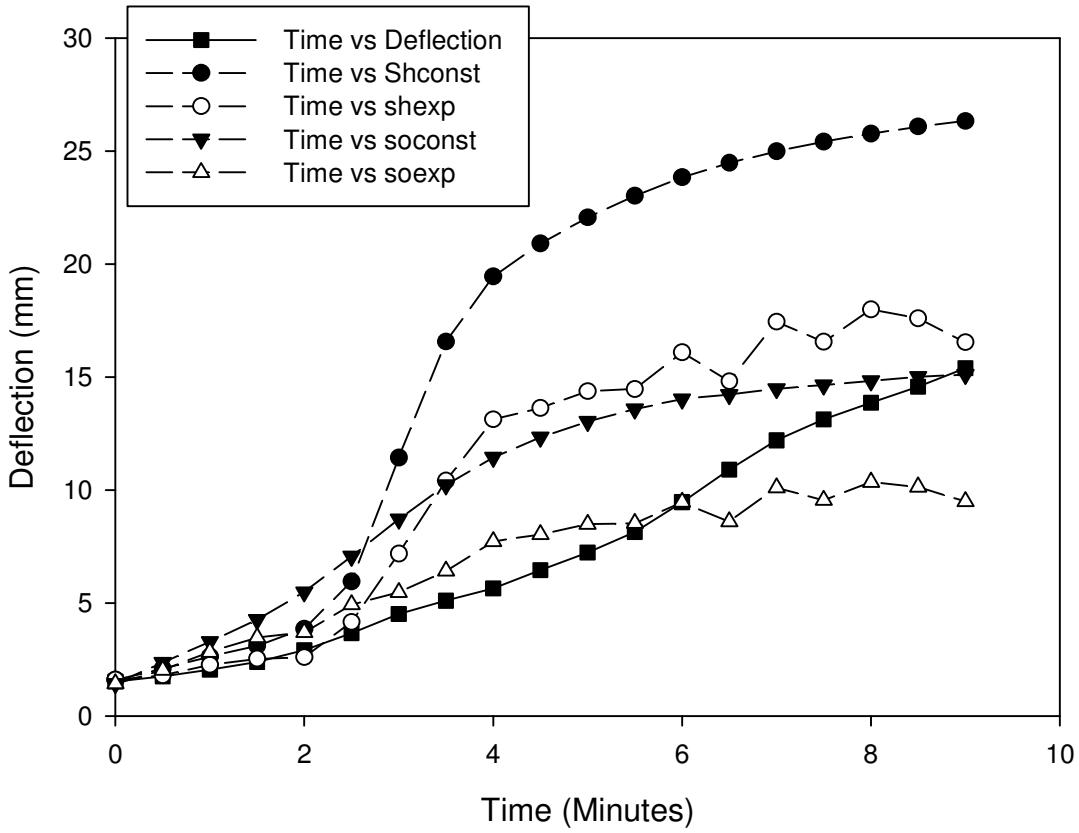

Figure D.10: Test panel SS4 after fire and load testing under the cellulosic fire curve at 1.9MPa for 9mins 7sec

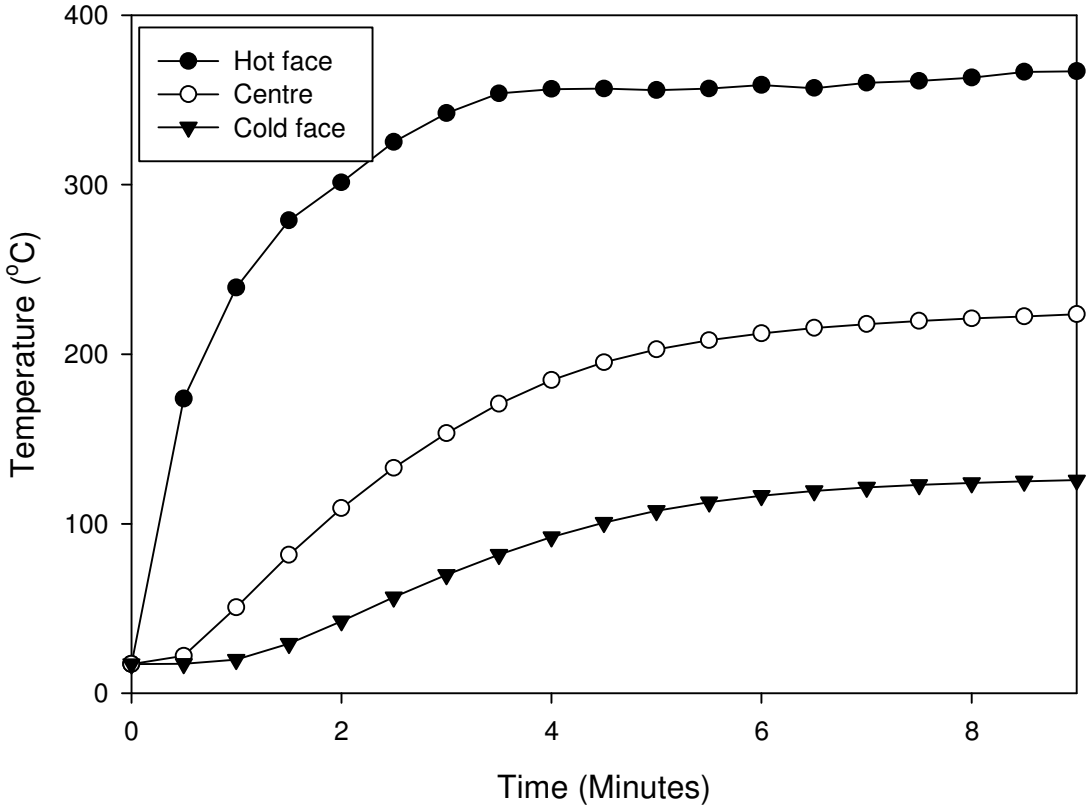

Figure D.11: Temperature profile used in thermo-mechanical model of panel SS 4

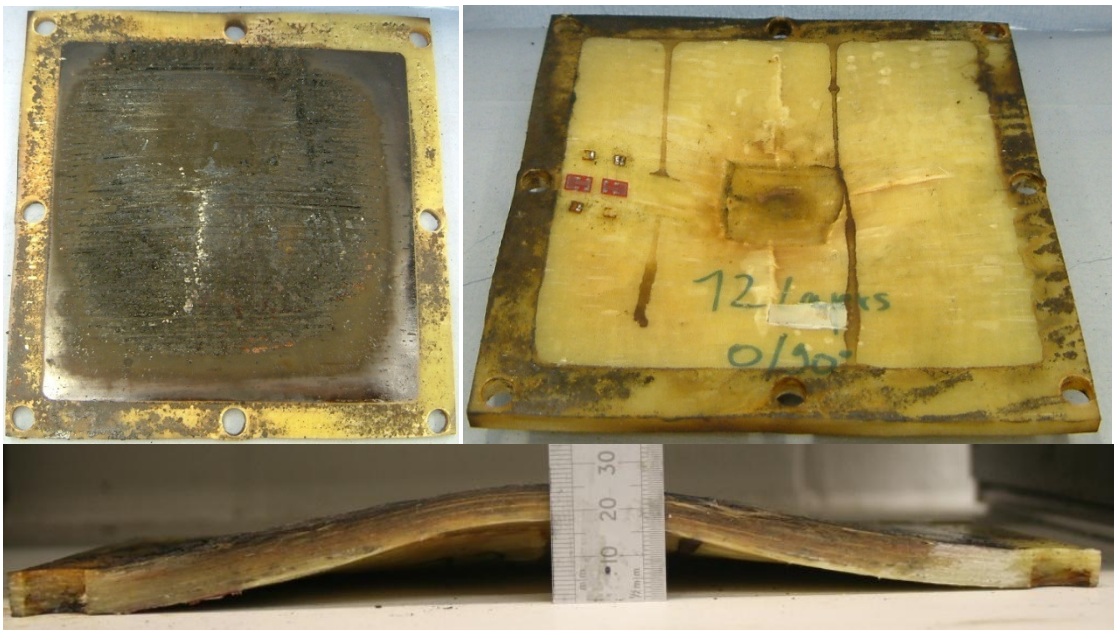

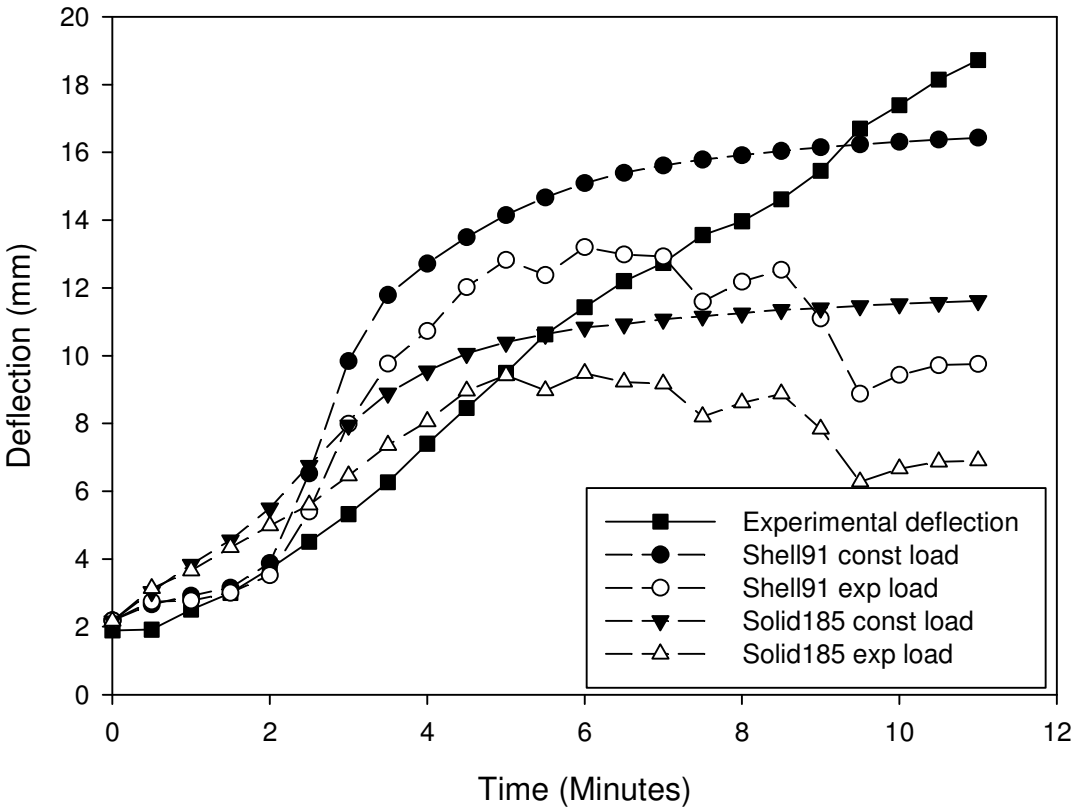

Figure D.12: Test panel SS5 after fire and load testing under the cellulosic fire curve at 3.1MPa for 8mins 54sec

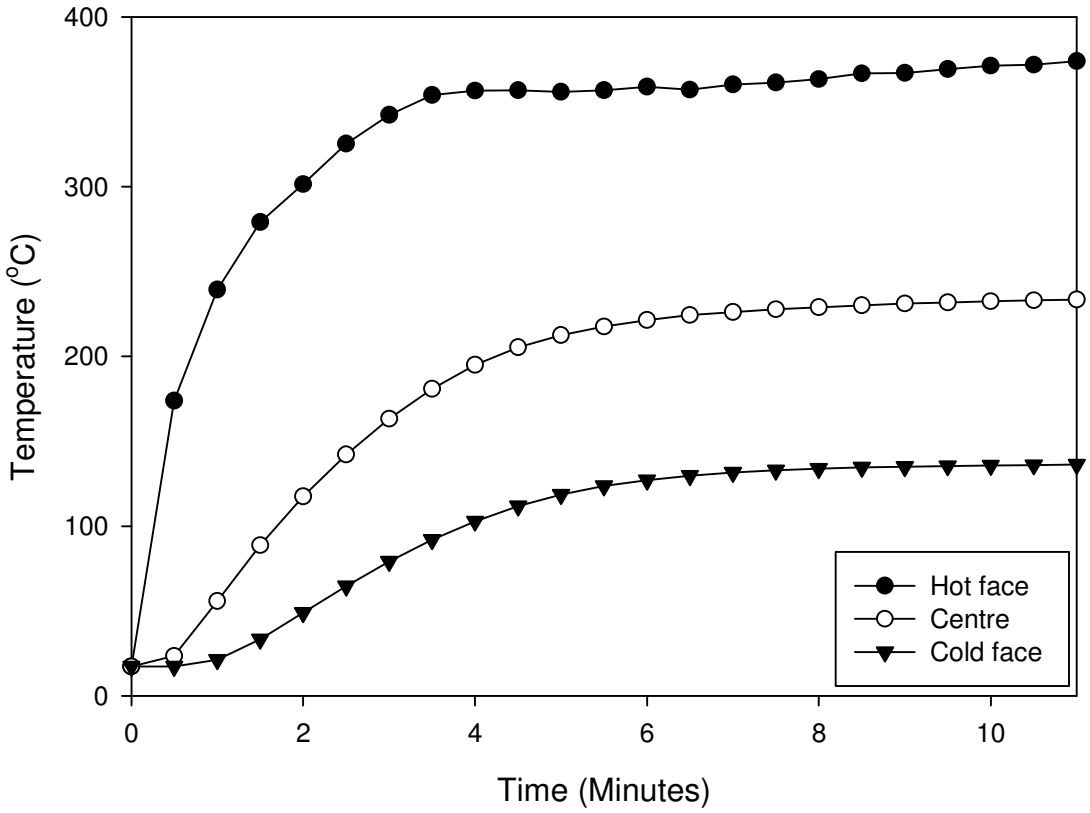

Figure D.13: Temperature profile used in thermo-mechanical model of panel SS 5

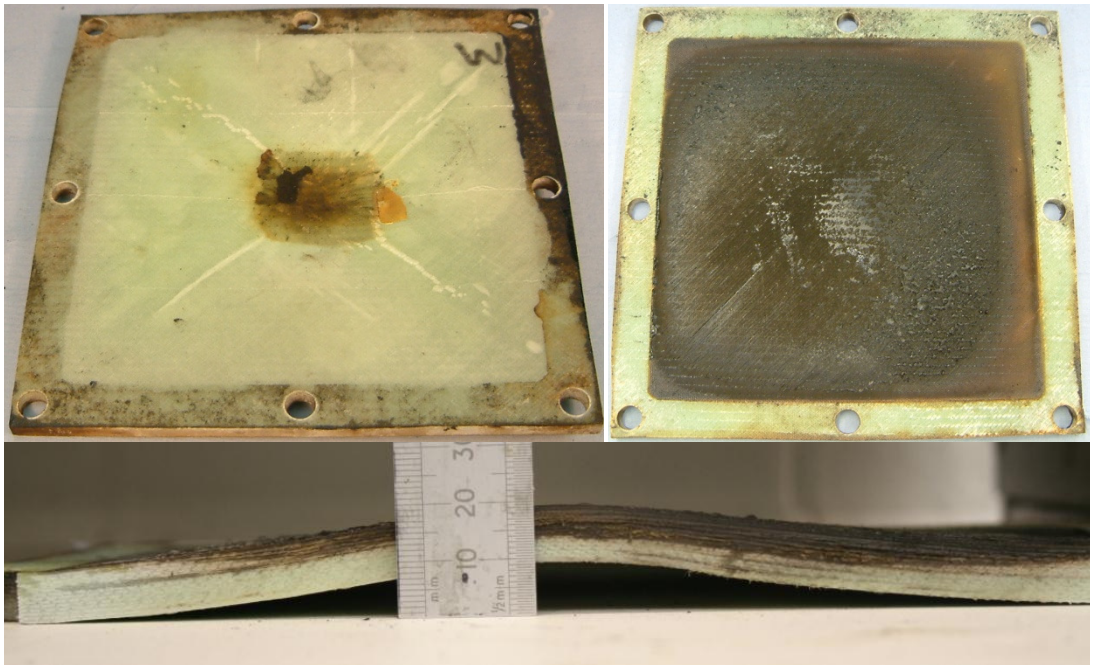

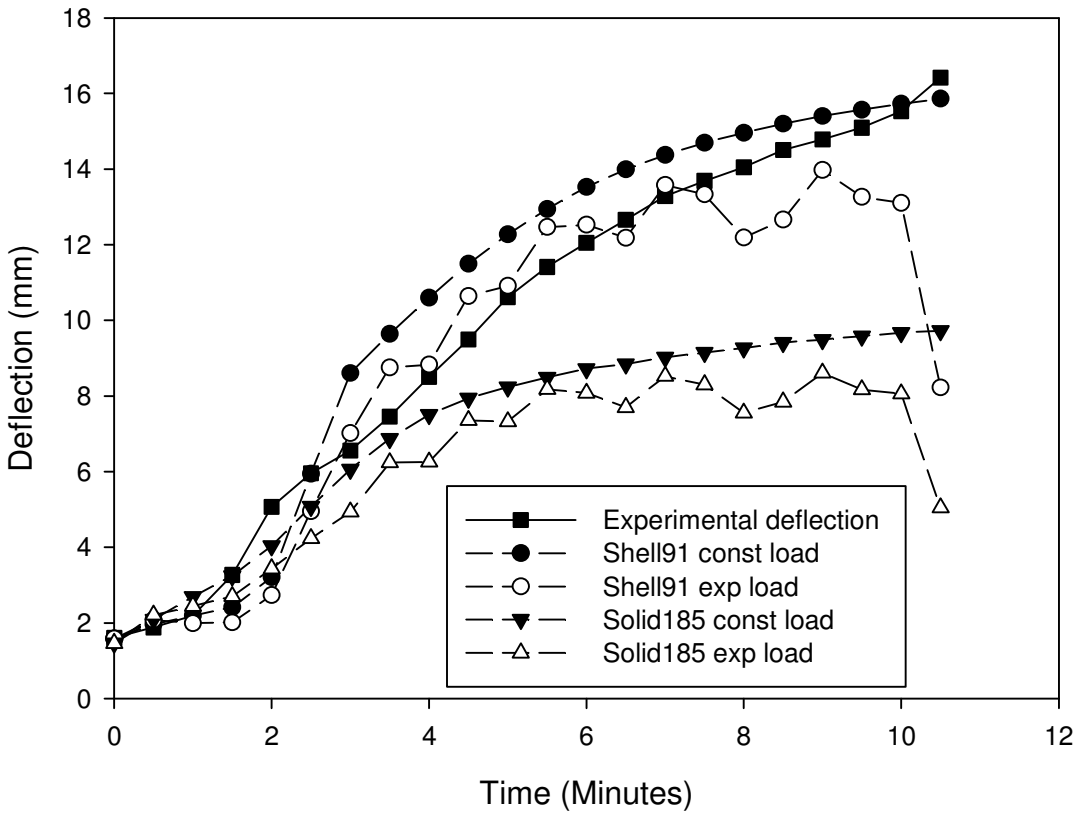

Figure D.14: Test panel SS6.1 $[\pm 45]_{13}$ after fire and load testing under the cellulosic fire curve at 2.5MPa for 9mins 33sec

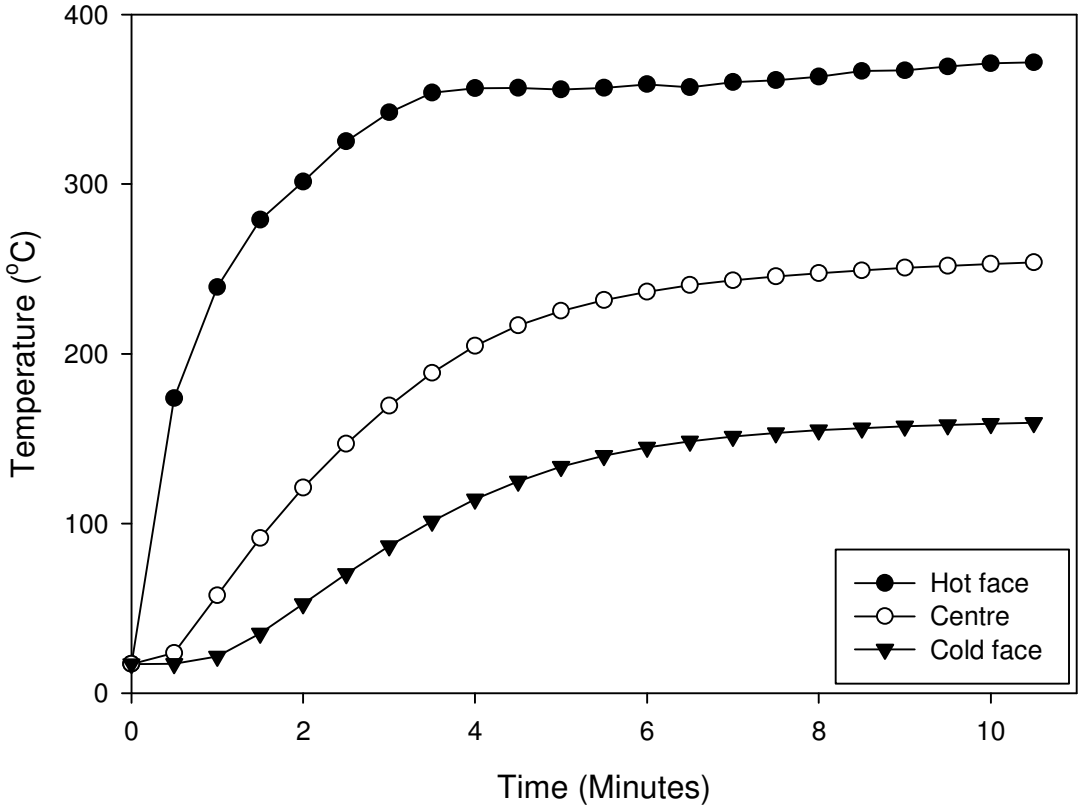

Figure D.15: Temperature profile used in thermo-mechanical model of panel SS 6.1

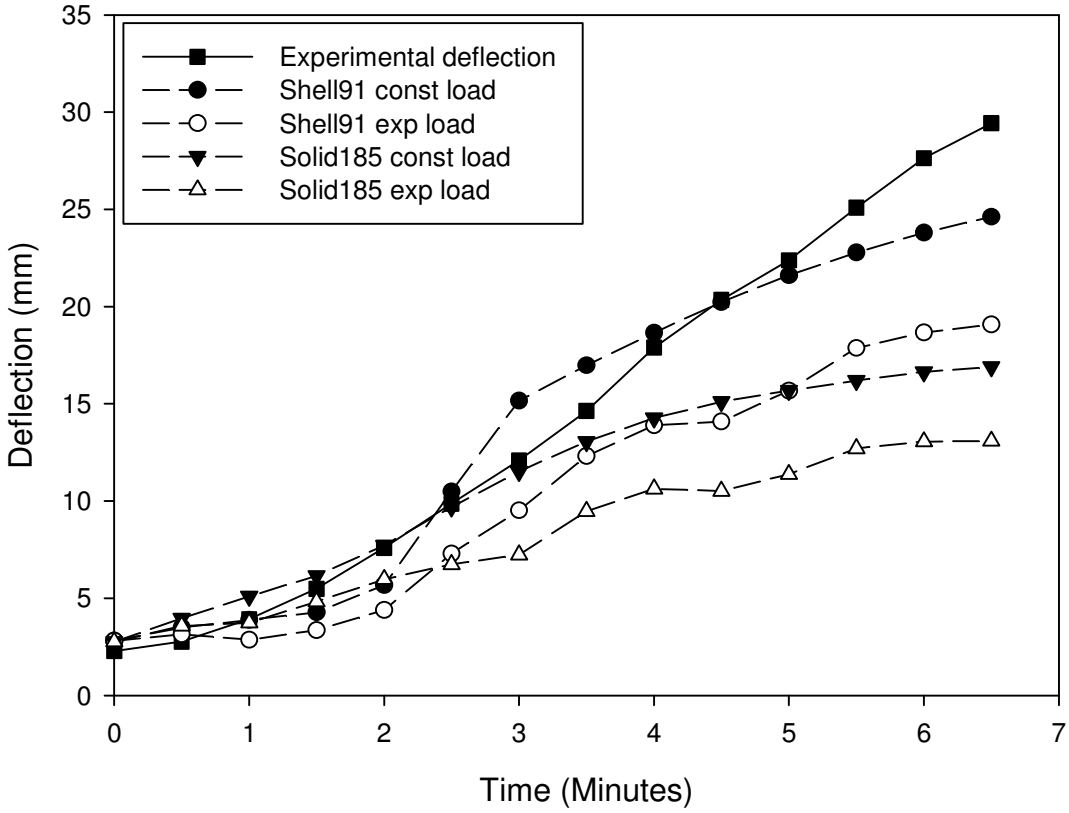

Figure D.16: Test panel SS6.2 after fire and load testing under the cellulosic fire curve at 3.1MPa for 6mins 05sec

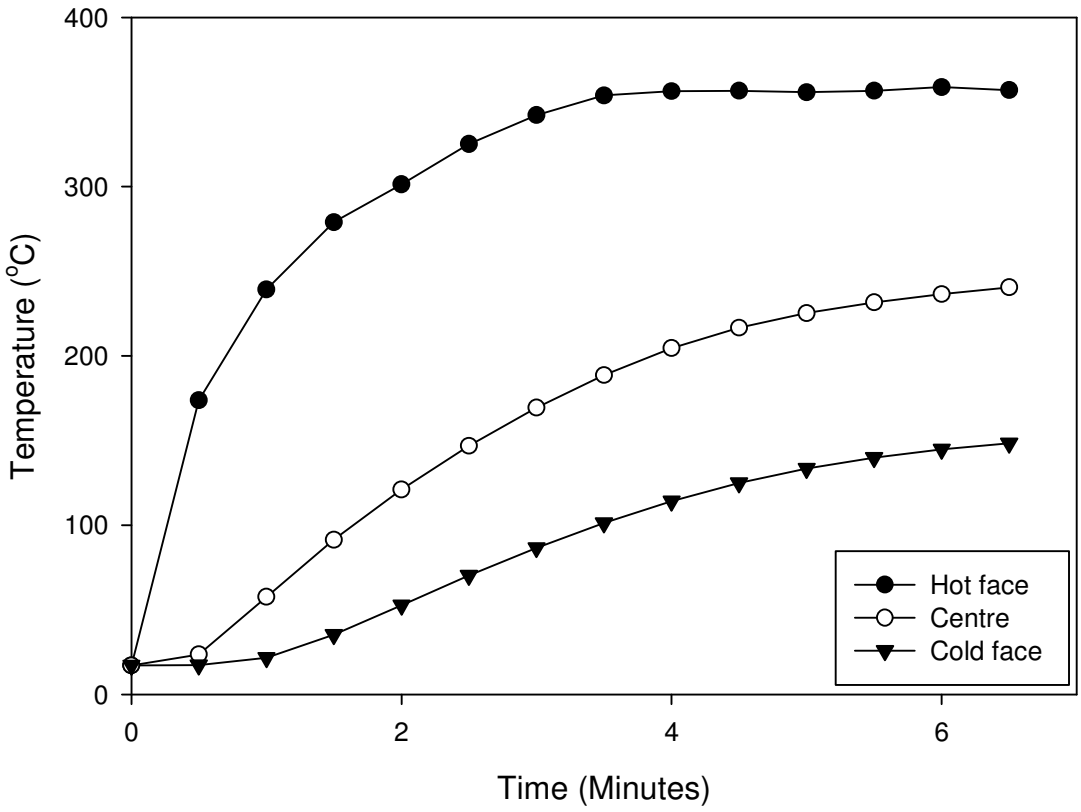

Figure D.17: Temperature profile used in thermo-mechanical model of panel SS 6.2

Appendix E

E.1 IMO Resolution A.754(18)

In the IMO resolution A.754 (18) the test procedure for load bearing divisions is described. A panel of 2.44m × 3.04m is required to be simply supported across the short sides and unsupported along the long edges. It is to be subjected to a universally distributed pressure of 3.5kN/m during the cellulosic fire curve and the failure criteria are then as follows in terms of the structural element of the test:

$$D_{fail} = \frac{2L^2}{400d} \tag{8.3}$$

$$R_{fail} = \frac{2L^2}{9000d} \tag{8.4}$$

Where:

D_{fail} = Failure threshold for maximum deflection in mm

R = Failure threshold for rate of deflection in mm/minute

L = Span in mm

d = Distance from the extreme fibre of the design compression zone to the extreme fibre of the design tension zone in mm

E.2 Large Scale Fire Resistance Test Observations

Time min	Observations
0	Test started
3	Smoke issuing from around perimeter of specimen, from gaps between test frame and furnace.
$4^1/_2$	Smoke issuing from perimeter of specimen becoming denser and increasing in quantity.
$12^1/_2$	Surface of deck is discolouring, short irregular brown lines approx 200mm long formed on surface. Discoloured patches are uniformly distributed over surface of deck in area above furnace aperture.
14	Increase in quantity of brown marks which are darkening and have scorched appearance. Smoke continues to issue from perimeter of specimen. Plate 2.
$15^1/_2$	Slight quantities of smoke issuing from darkened areas on surface. Two parallel rows of short dark lines extend across specimen at mid-width (See A in diagram above).
21	On exposed face underside of deck is flaming, flaming is brighter and more pronounced at mid-width of specimen.
25	On exposed face, underside of deck is flaming as before, some reinforcing fibres visible at centre of exposed face.
$25^1/_2$	Darkened brown marks on surface are widening and are more widespread, increase in quantities of smoke issuing from darkened areas on surface.
30	On exposed face brighter and more pronounced flaming at mid-width of specimen, reinforcing mat hanging down along mid-line across width of specimen.
31	Darkened brown marks on surface are widening and are merging giving a mottled appearance, increase in quantities of smoke issuing from darkened areas on surface. Plate 3.
37	Darkened brown marks on surface are continuing to merge. Increase in quantities of smoke issuing from darkened areas on surface . At two locations, near thermocouples 1 and 2, can see smoke rising along two lines, each approx. 200mm long (See B in diagram above); in other places smoke is issuing from small isolated points on surface.
44	Darkened brown marks on surface are continuing to merge giving a more uniform appearance. Increase in quantities of smoke issuing from central portion of deck from loaded area. At one location, near loading weights, can see smoke rising along a line, approx. 150mm long (See C in diagram above).
$46^1/_2$	Plate 5.
$47^1/_2$	On exposed face, some reduction in flaming on underside of deck, at centre of exposed face can see reinforcement hanging down and underlying core which is cracked; through cracks in core can see fibres of upper reinforcing mat.
50	Sustained flaming on unexposed face, near weights in area where smoking line was observed earlier (See C in diagram above) - Failure of integrity.
$50^1/_2$	On unexposed face, large hole (approx. 300mm x 300mm) formed in vicinity of thermocouple 5 (See D in diagram above). Remnants of top reinforcement visible around perimeter of hole.
51	Loading weights are tipping slightly towards hole. Plate 6.
$52^3/_4$	Loading weights fall through deck.
53	Test terminated.

E.3 Results From Large Scale Fire Resistance Test

Time (Minutes)	Tc1 (^{o}C)	Tc2 (^{o}C)	Tc3 (^{o}C)	Tc4 (^{o}C)	Tc5 (^{o}C)	Av. (^{o}C)	Method 1 using Krysl FE program (^{o}C)	Method 2 from Vulcan test (^{o}C)
0	516.6	17.1	17.6	17.1	17.7	17.2	17.2	18.1
0.5	15.7	16.2	16.8	16.1	16.7	16.3	17.2	18.1
1	15.8	16.3	16.9	16.2	16.8	16.4	17.2	18.1
1.5	15.8	16.2	16.9	16.2	16.8	16.4	17.2	18.4
2	15.8	16.2	16.9	16.1	16.8	16.4	17.2	18.6
2.5	15.8	16.2	16.9	16.1	16.8	16.4	17.2	18.8
3	15.9	16.3	17.0	16.3	16.9	16.5	17.3	19.6
3.5	16	16.5	17.3	16.6	17.1	16.7	17.3	20.3
4	16.4	16.9	17.7	17.0	17.5	17.1	17.4	21.1
4.5	16.9	17.4	18.3	17.7	18.1	17.7	17.6	22.2
5	17.6	18.1	19.1	18.6	18.9	18.5	17.8	23.6
5.5	18.4	18.9	20.2	19.6	19.8	19.4	18.2	25.3
6	19.4	20.0	21.4	21.0	20.9	20.5	18.7	27.2
6.5	20.7	21.4	22.9	22.7	22.4	22.0	19.3	29.4
7	22.3	23.3	24.9	25.0	24.2	23.9	20.1	31.3
7.5	24.2	25.7	27.5	28.5	26.4	26.5	21.0	33.7
8	26.5	29.1	31.2	34.5	29.9	30.2	22.1	35.7
8.5	29.3	33.3	36.1	43.2	35.5	35.5	23.2	38.4
9	32.8	38.7	42.8	54.2	44.7	42.6	24.5	40.8
9.5	36.9	45.0	51.0	67.5	57.0	51.5	25.9	43.4
10	41.5	51.6	59.0	84.9	75.7	62.5	27.4	46.3
10.5	46.6	57.4	70.4	105.6	100.8	76.2	29.0	49.9
11	51.5	65.4	83.8	127.4	128.5	91.3	30.7	
11.5	55.9	73.8	94.5	146.4	151.9	104.5	32.4	
12	61.3	82.4	106.3	165.2	173.2	117.7	34.2	
12.5	66.8	91.3	118.6	184.2	192.1	130.6	36.1	
13	72.3	99.9	130.9	202.2	208.4	142.7	38.1	
13.5	77.5	107.9	142.6	218.3	224.5	154.2	40.0	
14	82.8	116.3	154.5	234.0	241.1	165.7	42.1	
14.5	87.8	124.1	165.8	247.8	255.4	176.2	44.1	
15	92.9	131.5	177.6	260.8	268.7	186.3	46.2	
15.5	98	138.6	189.2	273.2	281.3	196.1	48.4	
16	103	145.9	200.2	284.4	293.4	205.4	50.5	
16.5	107.8	153.5	211.0	295.5	305.2	214.6	52.7	
17	112.5	161.9	222.1	306.1	316.4	223.8	54.9	
17.5	117.9	170.9	233.2	316.2	328.6	233.4	57.1	
18	123.2	180.1	244.7	325.3	342.1	243.1	59.4	

18.5	129.3	189.9	256.3	332.9	356.1	252.9	61.6	
19	136.1	199.3	268.4	339.8	369.4	262.6	63.9	
19.5	143.6	209.3	280.4	348.2	382.5	272.8	66.2	
20	152.7	219.1	293.1	358.9	395.4	283.8	68.6	
20.5	163.3	229.3	305.4	370.7	409.0	295.5	70.9	
21	174.1	238.6	315.1	382.9	421.2	306.4	73.3	
21.5	184.5	247.5	326.0	395.5	430.9	316.9	75.7	
22	193.8	255.8	338.7	407.7	439.6	327.1	78.2	
22.5	201.8	263.0	352.5	418.6	446.6	336.5	80.7	
23	209.1	269.0	366.6	427.7	451.8	344.8	83.2	
23.5	216	274.0	379.6	436.0	456.6	352.4	85.8	
24	222	278.8	391.8	442.3	461.7	359.3	88.4	
24.5	228.3	283.5	402.1	447.5	466.8	365.6	91.1	
25	234.6	287.4	411.7	453.0	471.9	371.7	93.8	
25.5	241.3	291.6	420.1	458.7	477.2	377.8	96.6	
26	247.9	295.5	428.2	464.6	482.3	383.7	99.4	
26.5	254	300.5	435.7	469.8	486.4	389.3	102.2	
27	260.6	306.4	441.9	474.5	490.0	394.7	105.1	
27.5	266.7	314.4	447.0	478.1	493.8	400.0	108.0	
28	272.9	323.4	450.7	481.0	497.2	405.0	110.9	
28.5	278.8	330.8	453.9	483.1	500.1	409.3	113.9	
29	283.6	338.6	457.1	485.2	501.7	413.2	116.9	
29.5	288.3	346.6	458.8	486.1	504.0	416.8	119.9	
30	293.2	353.4	460.0	487.6	506.9	420.2		
30.5	299.4	360.2	461.1	489.5	511.2	424.3		
31	305.9	366.9	462.5	491.0	515.1	428.3		
31.5	313.2	374.6	466.9	494.8	519.0	433.7		
32	320.4	381.9	469.8	496.5	521.5	438.0		
32.5	325.5	389.5	471.2	498.4	523.1	441.5		
33	326.5	397.8	473.4	500.8	525.4	444.8		
33.5	329.2	406.2	475.5	502.6	527.4	448.2		
34	333.8	413.5	477.3	503.6	528.8	451.4		
34.5	339.3	419.8	477.8	503.9	530.0	454.2		
35	344.9	424.4	477.9	504.2	530.6	456.4		
35.5	350.9	427.3	478.4	504.1	530.8	458.3		
36	357.8	428.5	479.3	505.2	530.6	460.3		
36.5	366.7	429.0	480.3	505.2	530.4	462.3		
37	377.6	428.1	480.7	504.9	530.0	464.3		
37.5	389.8	426.5	481.5	504.8	529.5	466.4		
38	403.1	424.4	482.4	504.7	529.0	468.7		
38.5	417.5	421.7	484.0	504.2	528.2	471.1		
39	432.5	419.2	484.4	504.5	528.2	473.8		
39.5	443.8	417.0	483.5	506.0	528.8	475.8		
40	454.3	414.3	482.6	506.4	529.0	477.3		
40.5	465.1	411.8	483.5	506.0	529.6	479.2		
41	472.5	410.3	485.5	506.0	530.5	481.0		

41.5	479.7	409.4	487.8	508.0	532.2	483.4		
42	484.8	408.5	490.3	509.6	532.5	485.1		
42.5	490.4	408.2	492.5	510.8	532.9	487.0		
43	496.9	407.7	494.6	511.0	534.5	488.9		
43.5	503.4	407.9	495.8	512.1	535.7	491.0		
44	511.6	408.3	496.4	512.2	537.3	493.2		
44.5	521.6	409.0	496.9	515.1	538.6	496.2		
45	532.5	409.7	497.4	516.4	539.7	499.1		
45.5	549	411.0	499.7	517.3	539.2	503.2		
46	565.9	411.8	502.0	518.0	539.3	507.4		
46.5	581	413.3	505.1	522.4	539.4	512.2		
47	593.6	413.9	506.3	523.3	542.7	516.0		
47.5	606.8	415.8	509.1	533.1	544.6	521.9		
48	621.7	417.8	512.0	528.1	546.1	525.1		
48.5	652.4	419.8	514.7	533.0	547.4	533.5		
49	692.7	421.5	516.7	534.9	551.9	543.5		
49.5	750	423.2	519.6	537.0	563.1	558.6		
50	792.7	425.7	523.8	539.0	581.5	572.5		
50.5	806.9	426.7	526.3	541.5	607.5	581.8		
51	803.1	428.1	525.4	544.1	632.9	586.7		
51.5	794.1	430.4	521.7	547.7	680.4	594.9		
52	796.8	433.2	532.0	551.0	725.1	607.6		
52.5	812.9	435.7	557.4	552.3	754.5	622.6		
53	794.9	438.8	813.5	556.0	748.8	670.4		
53.5	732.1	444.6	818.5	562.4	715.0	654.5		
54	631.4	437.8	718.9	553.0	653.5	598.9		
54.5	549	422.5	666.1	539.2	602.9	555.9		
55	502.1	403.7	625.8	521.6	569.1	524.5		

Table E.1: Cold face temperature measurements from large scale fire resistance test and predicted cold face temperatures

F1 (^{o}C)	F2 (^{o}C)	F3 (^{o}C)	F4 (^{o}C)	Average (^{o}C)
18	18	18	18	18
255	312	286	250	276
331	385	344	317	344
360	421	295	354	358
383	465	36	363	312
419	506	243	402	393
473	557	459	421	478
491	571	576	438	519
611	659	259	523	513
721	622	656	579	645
739	653	678	538	652
701	678	710	583	668
704	717	747	633	700

701	730	795	643	717
694	744	804	655	724
719	732	813	646	728
708	743	820	648	730
704	748	818	650	730
721	736	788	658	726
694	737	791	663	721
708	723	798	661	723
704	714	764	688	718
673	693	753	648	692
655	686	739	640	680
640	676	691	651	665
653	681	726	616	669
655	686	728	613	671
657	695	729	620	675
666	703	735	619	681
665	699	739	622	681
675	726	749	634	696
683	734	740	639	699
695	741	767	646	712
718	749	777	650	724
719	755	793	661	732
730	769	802	680	745
738	774	814	708	759
740	791	803	699	758
753	790	818	722	771
757	797	817	703	769
763	799	815	719	774
763	799	817	726	776
758	794	809	732	773
760	788	810	754	778
758	777	807	758	775
751	782	813	762	777
764	777	800	767	777
770	791	797	759	779
767	802	781	770	780
771	818	770	776	784
783	818	771	787	790
781	829	777	789	794
790	830	781	802	801
801	828	787	799	804
809	838	791	800	810
812	842	794	807	814
817	844	793	803	814
816	847	790	809	816
813	847	790	806	814

818	874	794	831	829
819	894	795	825	833
840	922	811	837	853
845	929	820	848	861
858	931	829	852	868
859	929	832	861	870
854	928	839	861	871
867	923	846	861	874
859	916	848	863	872
865	906	851	862	871
861	896	851	861	867
854	886	852	862	864
854	889	853	866	866
857	899	853	865	869
855	905	849	859	867
850	910	848	858	867
848	915	846	858	867
849	915	842	855	865
856	916	840	856	867
858	923	842	853	869
856	926	841	851	869
859	931	841	856	872
861	940	845	849	874
861	937	846	856	875
863	943	846	861	878
864	945	848	859	879
863	946	850	857	879
867	949	851	862	882
869	957	855	865	887
871	953	854	866	886
871	958	856	865	888
870	958	859	867	889
873	961	859	865	890
874	971	862	869	894
879	971	871	869	898
881	975	870	874	900
885	980	874	875	904
890	975	873	874	903
894	981	880	871	907
905	984	882	877	912
895	989	885	877	912
889	991	872	872	906
866	995	884	870	904
849	1002	914	880	911
845	1002	938	882	917
842	1004	939	877	916

845	1031	943	874	923
837	868	853	867	856
780	680	819	769	762
716	577	722	688	676
673	527	629	638	617
647	496	673	603	605

Table E.2: Recorded furnace temperatures from large scale fire resistance test

Time (Minutes)	Deflection (mm)	Corrected Deflection (mm)	Method 1 using FE model (mm)	Method 2 using Eq 6.1 (mm)
0.0	1.5	1.5	2.6	1.5
0.5	6.4	6.4		2.0
1.0	5.2	5.2		2.6
1.5	6.7	6.7		3.2
2.0	8.0	8.0		3.9
2.5	11.0	11.0	4.0	4.6
3.0	10.8	10.8		5.4
3.5	10.5	10.5		6.1
4.0	8.0	8.0		7.0
4.5	24.0	10.0		7.8
5.0	24.7	10.7	9.8	8.7
5.5	25.6	11.6		9.6
6.0	26.0	12.0		10.4
6.5	26.6	12.6		11.3
7.0	27.2	13.2		12.2
7.5	28.1	14.1	12.7	13.1
8.0	29.3	15.3		14.1
8.5	30.7	16.7		15.0
9.0	32.1	18.1		15.9
9.5	33.5	19.5		16.7
10.0	34.5	20.5	15.2	17.6
10.5	35.4	21.4		18.5
11.0	36.1	22.1		19.4
11.5	36.8	22.8		20.2
12.0	37.4	23.4		21.1
12.5	37.9	23.9		21.9
13.0	38.6	24.6		22.8
13.5	39.1	25.1		23.6
14.0	39.8	25.8		24.4
14.5	40.2	26.2		25.2
15.0	40.9	26.9		26.0
15.5	41.2	27.2		26.7
16.0	41.8	27.8		27.5
16.5	42.2	28.2		28.2
17.0	42.8	28.8		29.0
17.5	43.2	29.2		29.7
18.0	44.1	30.1		30.4
18.5	44.4	30.4		31.1
19.0	44.9	30.9		31.8
19.5	45.3	31.3		31.8
20.0	45.9	31.9		32.4
20.5	46.5	32.5		33.1
21.0	46.8	32.8		33.8
21.5	47.1	33.1		34.4

22.0	47.4	33.4		35.0
22.5	47.6	33.6		35.6
23.0	47.9	33.9		36.3
23.5	48.1	34.1		36.8
24.0	48.6	34.6		37.4
24.5	49.0	35.0		38.0
25.0	49.6	35.6		38.6
25.5	49.8	35.8		39.1
26.0	50.4	36.4		39.7
26.5	50.7	36.7		40.2
27.0	51.1	37.1		40.7
27.5	51.5	37.5		41.3
28.0	51.7	37.7		41.8
28.5	51.9	37.9		42.3
29.0	52.3	38.3		42.8
29.5	52.8	38.8		43.3
30.0	52.9	38.9		43.7
30.5	53.4	39.4		44.2
31.0	53.7	39.7		44.7
31.5	54.2	40.2		45.1
32.0	54.6	40.6		45.6
32.5	55.1	41.1		46.0
33.0	55.5	41.5		46.5
33.5	55.6	41.6		46.9
34.0	56.2	42.2		47.3
34.5	56.6	42.6		47.7
35.0	56.7	42.7		48.1
35.5	57.2	43.2		48.5
36.0	57.4	43.4		48.9
36.5	57.8	43.8		49.3
37.0	57.8	43.8		49.7
37.5	58.1	44.1		50.1
38.0	58.2	44.2		50.4
38.5	58.3	44.3		50.8
39.0	58.8	44.8		51.2
39.5	59.1	45.1		51.5
40.0	59.0	45.0		51.9
40.5	59.4	45.4		52.2
41.0	59.5	45.5		52.5
41.5	60.2	46.2		52.9
42.0	60.6	46.6		53.2
42.5	60.9	46.9		53.5
43.0	61.2	47.2		53.8
43.5	61.7	47.7		54.2
44.0	62.1	48.1		54.5
44.5	63.0	49.0		54.8
45.0	63.4	49.4		55.1

45.5	64.1	50.1		55.4
46.0	64.6	50.6		55.7
46.5	66.5	52.5		56.0
47.0	67.3	53.3		56.2
47.5	68.1	54.1		56.5
48.0	69.2	55.2		56.8
48.5	71.1	57.1		57.1
49.0	72.8	58.8		
49.5	74.8	60.8		
50.0	77.4	63.4		
50.5	79.2	65.2		
51.0	80.7	66.7		
51.5	82.0	68.0		
52.0	85.1	71.1		
52.5	93.9	79.9		

Table E.3: Recorded and predicted deflections from large scale fire resistance test

9 References

Agarwal, B. D. and L. J. Broutman (1980). Analysis and Performance of Fiber Composites. New York, Wiley-Interscience.

Asaro, R. J., P. Krysl, B. Zhu and W. T. Ramroth (2005). "rate dependent constitutive modelling of laminated FRP composites degraded by fire." Composite Structures 68: 399-408.

Babrauskas, V. and R. D. Peacock (1992). "Heat release rate. The single most important variable in fire hazard." Fire Safety Journal 18(3): 255-272.

Bamford, C. H., J. Crank and D. H. Malan (1946). "The Combustion of Wood. Part 1." Cambridge Philosophical Society Proceedings 42: 166.

Barnett, C. R. (2007). "Replacing international temperature-time curves with BFD curve." Fire Safety Journal 42(4): 321-327.

BS476-20 (1987). Fire tests on building materials and structures — Part 20: Method for determination of the fire resistance of elements of construction (general principles), British standard.

BS476-20 (1987). Fire tests on building materials and structures. Method for determination of the fire resistance of elements of construction (general principles).

BS874 Determining thermal insulating properties.

Callister, W. D. (2000). Materials Science and Engineering An Introduction John Wiley & Sons, Inc.

Çengel, Y. A. (1998). Heat Transfer, McGraw Hill.

Cerny, M., P. Glogar, V. Golias, J. Hruska, P. Jakes, Z. Sucharda and I. Vavrova (2007). "Comparison of mechanical properties and structural changes of continuous basalt and glass fibres at elevated temperatures." Ceramics - Silikaty 51(2): 82-88.

Chen, J. K., C. T. Sun and C. I. Chang (1985). "Failure Analysis of a Graphite/Epoxy Laminate Subjected to Combined Thermal and Mechanical Loading." Journal of Composite Materials 19(September): 408-423.

Costa, M. L., M. C. Rezende, J. M. F. de Paiva and E. C. Botelho (2006). "Structural carbon/epoxy prepregs properties comparison by thermal and rheological analyses." Polymer - Plastics Technology and Engineering 45(10): 1143-1153.

Curtis, P. T. (1998). Crag test methods for the measurement of the engineering properties of fibre reinforced plastics., Royal Aerospace Establishment (UK) TR 88012.

Cutter, P. A., A. W. Gillitt, G. Hilmarson and N. Mitsotakis (2004). Development of a Method for Assessing the Strength of Composite Materials in Fire, MEng Group Design Project Report, School of Engineering Sciences, Ship Science, University of Southampton.

Da Silva, L. F. M. and R. D. Adams (2005). "Measurement of the mechanical properties of structural adhesives in tension and shear over a wide range of temperatures." Journal of Adhesion Science and Technology 19(2): 109-141.

Dao, M. and R. J. Asaro (1999). "A study on failure prediction and design criteria for fiber composites under fire degradation." Composites: Part A 30: 123-131.

Davies, J. M. (1995). Performance of Sandwich Panels in Fire 1. Onshore Applications. Sandwich Construction 3, Southampton, UK, Emas.

Davies, J. M. (2001). Lightweight Sandwich Construction, Blackwell Science Ltd.

Davies, J. M., D. Dewhurst and J. McNicolas (1995). Performance of Sandwich Panels in Fire 2. Offshore Applications. Sandwich Construction 3, Southampton, UK, Emas.

Davies, J. M., D. Dewhurst, Y. C. Wang and H. B. Wang (2000). Research Studies of the Fire Performance of Composite Materials at the University of Manchester. ASCE Advanced technology in Structural Engineering Structures Congress, Philadelphia, USA.

Davies, J. M. and H. B. Wang (1996). A Numerical and Experimental heat Transfer study of GRP Panels Subject to Standard Cellulosic and Hydrocarbon Fire Tests. Interflam '96, Cambridge.

Davies, J. M., Y. C. Wang and P. M. H. Wong (2005). "Polymer composites in fire." Composites: Part A in press.

Davies, J. M., Y. C. Wang and P. M. H. Wong (2006). "Polymer composites in fire." Composites Part A: Applied Science and Manufacturing 37(8): 1131-1141.

DIAB (2007). Divnycell H Technical Manual.

Dodds, N., A. G. Gibson, D. Dewhurst and J. M. Davies (2000). "Fire behaviour of composite laminates." Compsites: Part A 31: 689-702.

Drysdale, D. (1999). An Introduction to Fire Dynamics, John Wiley & Sons.

Dulieu-Barton, J. M. (2008). Full-field experimental stress/strain analysis of sandwich structures. Advanced School on Sandwich Structures, Porto, Portugal.

EN12090:1997, B. (1997). Thermal insulating products for building applications - Determination of shear behaviour.

Fanucci, J. P. (1987). "Thermal Response of radiantly Heated Kevlar and Graphite/Epoxy Composites." Journal of Composite Materials 21(Febuary): 129-139.

Farshad, M., M. W. Wildenberg and P. Flueler (1997). "Determination of shear modulus and Poisson's ratio of polymers and foams by the anticlastic plate-bending method." Materials and Structures/Materiaux et Constructions 30(200): 377-382.

Feih, S., Z. Mathys, A. G. Gibson and A. P. Mouritz (2005). Property degradation of Fibreglass Composites in Fire. Composites in Fire 4, University of Newcastle, UK.

Feih, S., Z. Mathys, A. G. Gibson and A. P. Mouritz (2005). Property Degradation of Fibreglass Composites in Fire. Composites in Fire 4. A. G. Gibson. University of Newcastle.

Gibson, A. G. (2005). Laminate Analysis of Composites under Load in Fire. Composites in Fire 4, University of Newcastle upon Tyne.

Gibson, A. G. and A. P. Mouritz (2006). Fire Properties of Polymer Composite Materials Kluwer Academic Publishers.

Gibson, A. G., P. N. H. Wright, Y.-S. Wu, A. P. Mouritz, Z. Mathys and C. P. Gardiner (2004). "The Integrity of Polymer Composites During and After Fire." Journal of Composite Materials 38(15): 1283-1307.

Gibson, A. G., Y.-S. Wu, H. W. Chandler and J. A. D. Wilcox (1995). "A Model for the Thermal Performance of Thick Composite Laminates in Hydrocarbon Fires." Revue De L'Institut Francais Du Petrole 50(1): 69-74.

Grenier, A. T., N. A. Dembsey and J. R. Barnett (1998). "Fire Characteristics of Cored Composite Materials for Marine Use." Fire Safety Journal 30: 137-159.

Griffis, C. A., J. A. Nemes, F. R. Stonesifer and C. I. Chang (1986). "Degradation in Strength of Laminated Composites Subjected to Intense Heating and Mechanical Loading." Journal of Composite Materials 20(May): 216-235.

Gurit. (2006). "Ampreg 22 Epoxy Laminating System."

Gurit (2007). PRIME™ 20LV Epoxy Infusion System - Data Sheet.

Henderson, J. B., M. R. Tant, G. R. Moore and J. A. Wiebelt (1981). "Determination of kinetc parameters for the thermal decomposition of phenolic ablative materials by a multiple heating rate method." Thermochimica Acta 44: 253-264.

Henderson, J. B., Y. P. Verma, M. R. Tant and G. R. Moore (1983). "Measurement of the Thermal Conductivity of Polymer Composites to HIgh Temperatures Using the Line Source Technique." Polymer Composites 4(4): 219-224.

Henderson, J. B., J. A. Wiebelt and M. R. Tant (1985). "A Model for The Thermal Response of Polymer Composite Materials with Experimental Verification." Journal of Composite Materials 19(November): 579-595.

Henderson, J. B., J. A. Wiebelt, M. R. Tant and G. R. Moore (1982). "A method for the determination of the specific heat and heat of decomposition of composite materials." Thermochimica Acta 57: 161-171.

Henderson, J. B. and T. E. Wiecek (1987). "A Mathematical Model to Predict the Thermal Response of Decomposing, Expanding Polymer Composites." Journal of Composite Materials 21(April): 373-393.

Ho, T.-H., T.-S. Leu, Y.-M. Sun and J.-Y. Shieh (2006). "Thermal degradation kinetics and flame retardancy of phosphorus-containing dicyclopentadiene epoxy resins." Polymer Degradation and Stability 91(10): 2347-2356.

Høyning, B. (2003). The Fire Onboard The RNoN MCMV Composite vessel "Orkla" - The Accident and Lessons Learned. Composite in Fire, Newcastle, UK.

Hudson, F. D., I. A. Hicks and R. M. Cripps (1993). "Design and development of modern lifeboats." Proceedings of the Institution of Mechanical Engineers, Part A: Journal of Power and Energy 207(1): 3-22.

Hull, D. and T. W. Clyne (1996). An Introduction to Composite Materials. Cambridge, Cambridge University Press.

IMO (1998). FTP Code- International Code for Application of Fire Test procedures, IMO.

ISO11357-4 (2005). Plastics- Differential scanning calorimetry (DSC) - Part 4: Determination of specific heat capacity.

Jakob, M. (1959). Heat Transfer. New York, John Wiley and Sons.

Key, C. T. and J. Lua (2006). "Constituent based analysis of composite materials subjected to fire conditions." Composites Part A: Applied Science and Manufacturing 37(7): 1005-1014.

Krysl, P., W. T. Ramroth, L. K. Stewart and R. J. Asaro (2004). "Finite element modelling of fibre reinforced polymer sandwich panels exposed to heat." International Journal for Numerical Methods in Engineering 61: 49-68.

Lattimer, B. Y. and J. Ouellette (2006). "Properties of composite materials for thermal analysis involving fires." Composites Part A: Applied Science and Manufacturing 37(7): 1068-1081.

Lee, C. S., D. G. Lee and J. H. Oh (2004). "Co-cure bonding method for foam core composite sandwich manufacturing." Composite Structures 66(1-4): 231-238.

Looyeh, M. R. E. and P. Bettes (1998). "A finite element model for the fire performance of GRP panels including variable thermal properties, Finite Elements in Analysis and Design " Finite Elements in Analysis and Design 30: 313-324.

Looyeh, M. R. E., P. Bettes, A. G. Gibson and N. Dodds (1998). A Two-Dimensional Finite Element Model For The Thermal Response of GRP Panels Under Fire. Fibre Reinforced Composites 7, University of Newcastle.

Looyeh, M. R. E., P. Bettess and A. G. Gibson (1997). "A one dimensional finite element simulation for the fire-performance of GRP panels for offshore structures." International Journal of Numerical methods for Heat and Fluid Flow 7(6): 609-625.

Looyeh, M. R. E., K. Rados and P. Bettess (2001). "Thermochemical responses of sandwich panels to fire." Finite Elements in Analysis and Design 37(11): 913-927.

Lua, J., J. O'Brien, C. T. Key, Y. Wu and B. Y. Lattimer (2006). "A temperature and mass dependent thermal model for fire response prediction of marine composites." Composites Part A: Applied Science and Manufacturing 37(7): 1024-1039.

Lui, L., J. W. Holmes, G. A. Kardomateas and V. Birman (2005). Compressive Response of Composites under Combined Fire and Compression Loading. Composites in Fire 4, University of Newcastle.

MAIB (2000). "Report of an Investigation into an engine room fire on the UK registered merchant vessel Toisa Gryphon 150 miles west-south-west of the Isles of Scilly on 2 February 1999."

MAIB (2000). Report of the Investigation into an engine room fire on mv Pride of Le Havre on 18 March 1999 off the Isle of Wight.

MAIB (2000). "Report on the investigation of the engine room fire on MS St Helena 25 August 2000."

MAIB (2003). Report of investigation into a fire in the aft engine room of ro-ro ferry Norsea on 2 September 2002.

McManus, H. L. and G. S. Springer (1992). "High Temperature Thermomechanical Behaviour of Carbon-Phenolic and carbon-Carbon Composites, I. Analysis." Journal of Composite Materials 26(2): 206-229.

McManus, H. L. and G. S. Springer (1992). "High Temperature Thermomechanical Behaviour of Carbon-Phenolic and carbon-Carbon Composites, II. Results." Journal of Composite Materials 26(2): 230-255.

Morley, J. G. (1987). High-Preformance Fibre Composites. London, Academic Press.

Mouritz, A. P. (2003). "Simple models for determining the mechanical properties of burnt FRP composites." materials and Engineering A359: 237-246.

Mouritz, A. P. and C. P. Gardiner (2002). "Compression properties of fire-damaged polymer sandwich composites." Composites: Part A 33: 609-620.

Mouritz, A. P. and Z. Mathys (1999). "Post-fire mechanical properties of marine polymer composites." Composite Structures 47: 643-653.

Mouritz, A. P. and Z. Mathys (2001). "Post-fire mechanical properties of glass-reinforced polyester composites." Composites Science and technology 61: 475-490.

Mouritz, A. P., Z. Mathys and A. G. Gibson (2005). "Heat release of polymer composites in fire." Composites: Part A in press.

Mouritz, A. P., Z. Mathys and A. G. Gibson (2006). "Heat release of polymer composites in fire." Composites Part A: Applied Science and Manufacturing 37(7): 1040-1054.

Oberg, E. (1992). Machinery's handbook : a reference book for the mechanical engineer, dsigner, manufacturing engineer, draftsman, toolmaker, and machinist. New York, Industrial Press.

ODPM (2004). Fire Statistics, United Kingdom, 2004, Crown Publishing.

Otto, W. H. (1959). Properties of glass fibres at elaveted temperatures. Proceedings of Sixth Sagamore Ordinance Materials Research Conference on Composite Materials and Composite Structures, Sagamore Conference Center, Racquette Lake, New York,.

Padhi, G. S., R. A. Shenoi, S. S. J. Moy and G. L. Hawkins (1997). "Progressive failure and ultimate collapse of laminated composite plates in bending." Composite Structures 40(3-4): 277-291.

Pering, G. A., P. V. Farrell and G. S. Springer (1980). "Shear properties of Composites Exposed to Fire or High Temperature." Journal of Composite Materials 14(January): 54-68.

Plecnik, J. M., B. Bresler and J. D. Cunningham (1980). "Temperature Effects of Epoxy Adhesvies." 106(1): 99-113.

Quintiere, J. G. (1998). Principles of Fire Behavior, Delmar Publishers.

Ramroth, W. T., P. Krysl and R. J. Asaro (2005). "Sensitivity and Uncertainty analyses for FE thermal model of FRP panel exposed to fire." Composites: Part A in press.

Ramroth, W. T., P. Krysl and R. J. Asaro (2006). "Sensitivity and uncertainty analyses for FE thermal model of FRP panel exposed to fire." Composites Part A: Applied Science and Manufacturing 37(7): 1082-1091.

RNoN TEG. (2003). The fire on board the HNoMS Orkla 19th November 2002, Technical Expert Group Norwegian Defence Logistics Organisation.

Springer, G. S. (1984). "Model for Predicting the Mechanical Properties of Composites at Elevated Temperatures." Journal of Reinforced plastics and Composites 3(January): 85-95.

Staggs, J. E. J. (2002). "Estimating the thermal conductivity of chars and porous residues using thermal resistor networks." Fire Safety Journal 37(1): 107-119.

Tsai, S. W. and T. H. Hahn (1980). Introduction to Composite Materials, Technomic Publishing.

Urbas, J. and W. J. Parker (1993). "Surface temperature measurements on burning wood specimens in the cone calorimeter and the effect of grain orientation." Fire and Materials 17(5): 205-208.

Wu, Y.-S., J. A. D. Wilcox, A. G. Gibson and P. Bettes (1993). Design for Composite Panels for Mechanical and Fire Performance, Final report prepared for British gas, University of Newcastle.

Zehfuss, J. and D. Hosser (2007). "A parametric natural fire model for the structural fire design of multi-storey buildings." Fire Safety Journal 42(2): 115-126.